CANOPY STRUCTURAL AND METEOROLOGICAL INFLUENCES ON CO_2 EXCHANGE FOR MODIS PRODUCT VALIDATION IN A BOREAL JACK PINE CHRONOSEQUENCE

by

Laura Elizabeth Chasmer

A thesis submitted to the Department of Geography

In conformity with the requirements for

the degree of Doctor of Philosophy

Queen's University

Kingston, Ontario, Canada

Copyright © Laura Elizabeth Chasmer

Abstract

Previously disturbed and regenerating forests make up a significant proportion of the North American land area, and therefore play an important role in the exchanges of heat and trace gases between the terrestrial biosphere and the atmosphere. Assessment of local to global variability in CO_2 exchanges by forests requires a combination of CO_2 measurements made by eddy covariance (EC), field measurements, remote sensing data, and ecosystem models. The integration of these is problematic because of a mis-match in scale between measurement techniques. Despite the importance of regenerating forests on the global carbon balance, the processes affecting the carbon cycle within these forests is not well understood.

Airborne scanning light detection and ranging (lidar) instruments provide new opportunities to examine three-dimensional forest characteristics from the level of individual trees to ecosystems and beyond. Lidar is therefore an effective link between plot measurements, eddy covariance, and low resolution remote sensing pixels. This thesis dissertation presents new science on the use of airborne lidar for evaluating remote sensing products within heterogeneous and previously clearcut ecosystems. The goals of this thesis were to first understand the processes affecting CO_2 exchanges within a previously disturbed boreal jack pine chronosequence located in Saskatchewan, Canada and then to apply this understanding to evaluate low resolution remote sensing data products from the Moderate Resolution Imaging Spectroradiometer (MODIS) using airborne lidar.

The first objective of this dissertation examined the factors that control light use efficiency (LUE) within the jack pine chronosequence during dry and wet years. The second objective examined the importance of vegetation structure and ground surface elevation on CO_2 fluxes within a

mature jack pine forest. The third objective developed and tested a simple model of lidar fractional cover and related this to the fraction of photosynthetically active radiation absorbed by the canopy (fPAR). This was then used to evaluate the MODIS fPAR product across the lower part of a watershed. Finally, the fourth objective was to model gross primary production (GPP) from airborne lidar. Lidar estimates of GPP were then compared with those from the EC system at the jack pine chronosequence and with the MODIS GPP (Collection 5) product.

Co-Authorship

This thesis dissertation presents four original manuscripts that have been accepted or are in press within international and top quality academic journals. These manuscripts are as follows:

Title: "Investigating Light Use Efficiency (LUE) Across a Jack Pine Chronosequence During Dry and Wet Years"
Co-authors: L. Chasmer[1], H, McCaughey[1], A. Barr[2], A. Black[3], A. Shashkov[4], P. Treitz[1], and T. Zha[2]
Affiliations: [1]Dept. of Geography, Queen's University, Kingston ON K7L 3N6
[2]Climate Research Branch, Meteorological Service of Canada, Saskatoon SK S7N 3H5
[3]Faculty of Land and Food Systems, University of British Columbia, Vancouver BC V6T 1Z4
[4]Climate Research Branch, Meteorological Service of Canada, Toronto ON M3H 5T4
Journal: *Tree Physiology*. 2008 28(9):1395-1406.

Title: "Vegetation Structural and Elevation Influences on CO_2 Uptake within a Mature Jack Pine Forest in Saskatchewan, Canada"
Co-authors: L. Chasmer[1], N. Kljun[2], A. Barr[3], A. Black[4], C. Hopkinson[5], H. McCaughey[1], and P. Treitz[1]
Affiliations: [1]Dept. of Geography, Queen's University, Kingston ON K7L 3N6
[2]Dept of Geography, School of the Environment and Society, Swansea University, Singleton Park Swansea UK SA28PP
[3]Climate Research Branch, Meteorological Service of Canada, Saskatoon SK S7N 3H5
[4]Faculty of Land and Food Systems, University of British Columbia, Vancouver BC V6T 1ZA
[5]Applied Geomatics Research Group, Lawrencetown NS BOS 1M0
Journal: *Canadian Journal of Forest Research (accepted)*

Title: "A Lidar-based Hierarchical Approach to Assessing MODIS fPAR"
Co-authors: L. Chasmer[1], C. Hopkinson[2], P. Treitz[1], H. McCaughey[1], A. Barr[3], and A. Black[4],
Affiliations: [1]Dept. of Geography, Queen's University, Kingston ON K7L 3N6
[2]Applied Geomatics Research Group, Lawrencetown NS BOS 1M0
[3]Climate Research Branch, Meteorological Service of Canada, Saskatoon SK S7N 3H5
[4]Faculty of Land and Food Systems, University of British Columbia, Vancouver BC V6T 1Z4
Journal: *Remote Sensing of Environment (in press)*

Title: "Scaling and Assessment of GPP from MODIS Using a Combination of Airborne Lidar and Eddy Covariance Measurements over Jack Pine Forests"
Co-authors: L. Chasmer[1], A. Barr[2], C. Hopkinson[3], H. McCaughey[1], P. Treitz[1], A. Black[4], and A. Shashkov[5]
Affiliations: [1]Dept. of Geography, Queen's University, Kingston ON K7L 3N6
[2]Climate Research Branch, Meteorological Service of Canada, Saskatoon SK S7N 3H5
[3]Applied Geomatics Research Group, Lawrencetown NS BOS 1M0
[4]Faculty of Land and Food Systems, University of British Columbia, Vancouver BC V6T 1Z4
[5]Climate Research Branch, Meteorological Service of Canada, Toronto ON M3H 5T4
Journal: *Remote Sensing of Environment (accepted)*

Acknowledgements

I would like to express my sincere thanks to my co-advisors Dr. Paul Treitz and Dr. Harry McCaughey for giving me the opportunity to pursue a Ph.D. within the Department of Geography at Queen's University. I am grateful to Dr. Treitz for encouraging me to use remote sensing data within my thesis. I am also grateful to Dr. McCaughey for bringing me into the Fluxnet-Canada Research Network, and for allowing me to combine eddy covariance flux data and remote sensing data. Dr. McCaughey introduced me to the eddy covariance technique, and for this I am thankful. I would also like to thank both advisors for giving me the opportunity to participate in field campaigns and for encouraging me to attend conferences and scientific meetings.

I am also very grateful to the members of my thesis dissertation committee. They have provided valuable and insightful comments, which have been exceedingly important for improving the end results of the thesis. I have learned a lot in a very short period of time from this committee, and I will continue to use this knowledge to advance my future research. I would also like to thank members of the Fluxnet-Canada Research Network and the Canadian Carbon Program for their help and access to data. Special thanks to Dr. A. Barr, Dr. T.A. Black, Dr. N. Kljun, and Dr. T.S. Zha for expertise and for their comments on manuscripts and general discussion. Also, many thanks to Dr. R. Maher and the Applied Geomatics Research Group for allowing me access to computer and technological resources, including the use of the airborne lidar.

Finally, I would like to thank my husband, Chris, for introducing me to airborne lidar, and for working hard to organize the lidar data collection over the BERMS sites with limited resources. He has also been open to all questions regarding lidar and has involved me as much as possible in the process of collecting, processing, and manipulating lidar data. I dedicate my thesis to my family, Chris, Ron, Pam, Ryan, Nana and my friends for their infinite love and support, and to my dog Ailsa.

Statement of Originality

I hereby certify that all of the work described within this thesis is the original work of the author. Any published (or unpublished) ideas and/or techniques from the work of others are fully acknowledged in accordance with the standard referencing practices.

(Laura Chasmer)

(August, 2008)

Table of Contents

Abstract ii
Co-Authorship iv
Acknowledgements v
Statement of Originality vi
Table of Contents vii
List of Figures xii
List of Tables xvii
Chapter 1 Introduction 1
1.1 Background 1
1.2 Thesis Objectives 4
1.2.1 Objective 1: Investigation of LUE 4
1.2.2 Objective 2: Vegetation Structure and Ground Elevation Influences on CO_2 Exchanges 6
1.2.3 Objective 3: Using Airborne Lidar for the Assessment of MODIS fPAR 8
1.2.4 Objective 4: Validation of MODIS GPP using the EC system and airborne lidar 10
1.3 Thesis Organisation 12
1.4 References 12
Chapter 2 17
Investigating Light Use Efficiency (LUE) Across A Jack Pine Chronosequence during Dry and Wet Years 17
2.1 Abstract 17
2.2 Introduction 18
2.3 Study Area 19
2.4 Site Instrumentation 22
2.5 Methodology 24
2.5.1 Calculation of Light Use Efficiency 24
2.5.2 Statistical Analysis 28
2.6 Results 28
2.6.1 Influences of Dry, Normal and Wet Years on LUE at Individual Sites 28
2.6.2 Meteorological Influences on GPP and LUE 33
2.6.3 LUE Differences between Jack Pine Ages 38
2.6.4 Influences of Radiation on LUE at Individual Sites 39

2.6.5 A Comparison of Methods for Estimating LUE 41
2.7 Discussion 44
2.7.1 Drought and Wet Growing Season Influences on LUE 44
2.7.2 Environmental Influences on LUE 46
2.8 Conclusions 48
2.9 Acknowledgements 50
2.10 References 50
Chapter 3 56
Vegetation Structural and Ground Elevation Influences on CO_2 Uptake within a Mature Jack Pine Forest in Saskatchewan, Canada 56
3.1 Abstract 56
3.2 Introduction 57
3.3 Methods 58
3.3.1 Study Area and Site Characteristics 58
3.3.2 Canopy Structure Measurements 61
3.3.3 Flux Measurements 62
3.3.4 Lidar Data Collection and Processing 65
3.3.5 Footprint Data Analysis 67
3.3.6 Statistical Analysis 69
3.4 Results 71
3.4.1 Footprint Climatologies 71
3.4.2 Dominant Meteorological Driving Mechanisms 74
3.4.3 Within Footprint Vegetation Structural and Ground Elevation Influences on Fluxes 81
3.5 Discussion and Conclusions 87
3.6 Acknowledgements 89
3.7 References 90
Chapter 4 94
Using Airborne Lidar for the Assessment of MODIS fPAR 94
4.1 Abstract 94
4.2 Introduction 95
4.3 Methodology 98
4.3.1 Study Areas 98
4.3.2 DHP Data Collection and Analysis 99

4.3.3 Validation of DHP Using PAR Sensors 101
4.3.4 Lidar Data Collection and Processing 102
4.3.5 MODIS Data 104
4.4 Results 105
4.4.1 Validating fPAR from DHP using Radiation Sensors 105
4.4.2 Relationship between fPAR from DHP and Lidar *f*cover 106
4.4.3 Using Lidar to Assess MODIS fPAR within a Watershed 108
4.5 Discussion 113
4.6 Conclusions 115
4.7 Acknowledgements 116
4.8 References 116
Chapter 5 122
Scaling and Assessment of GPP from MODIS Using a Combination of Airborne Lidar and Eddy Covariance Measurements over Jack Pine Forests 122
5.1 Abstract 122
5.2 Introduction 123
5.3 Data Collection 126
5.3.1 Site Characteristics 126
5.3.2 Site Instrumentation 128
5.3.3 Lidar Data Collection and Analysis 130
5.3.4 MODIS GPP Product 132
5.4 Methods 132
5.4.1 Landsberg Light Response Curve Analysis and Development of GPP Model 133
5.4.2 GPP Model Assessment 134
5.4.3 Model Application and Comparison 135
5.4.4 GPP Scaling Analysis 136
5.5 Results 137
5.5.1 Comparisons between Landsberg Inputs and Canopy Structure 137
5.5.2 Comparing GPP Predicted from Height and Fractional Cover with Observed GPP 140
5.5.3 Comparing GPP_{EC} with GPP_{MODIS} and GPP_{lidar} 142
5.5.4 Assessing the Influence of Site Heterogeneity - Scaling GPP from 1m to 1000m 146

5.6 Discussion 149
5.6.1 Influence of Site Heterogeneity 149
5.6.2 Other Influences Affecting MODIS vs. EC GPP 150
5.6.3 Implications of Research 152
5.7 Conclusions 153
5.8 Acknowledgements 154
5.9 References 155
Chapter 6 163
Discussion 163
6.1 Observing LUE and the Ability of Chronosequence Jack Pine Forests to Sequester CO_2 During Dry and Wet Years 163
6.2 Investigating the Influence of Canopy Structure on CO_2 Fluxes within a Mature Jack Pine Forest 165
6.3 Using Airborne Lidar for the Assessment of MODIS fPAR 167
6.4 Modelling and Scaling GPP from Lidar in Comparison with MODIS Products 169
6.5 Future Research 170
6.5.1 Footprint Modelling, Parameterization, and Improvement within Complex Canopies 171
6.5.2 MODIS Vegetation Product Validation and Improvement 172
6.5.3 Spatial Scaling and the Influences of Vegetation Patches on MODIS Product Biases 173
6.6 References 174
Chapter 7 178
Summary and Conclusions 178
Appendix A 181
Definitions and Concepts 181
A.1 Site-Level Eddy Covariance and Meteorology Definitions and Concepts 181
A.1.1 Eddy Covariance Method 181
A.1.2 Net Ecosystem Exchange (NEE), Net Ecosystem Production (NEP) and Net Biome Production (NBP) 182
A.1.3. Gross Primary Production (GPP) and Gross Ecosystem Production 182
A.1.4 Net Primary Production (NPP) 183

A.1.5 Ecosystem Respiration (Re), Autotrophic Respiration (Ra), and Heterotrophic Respiration (Rh) 183
A.1.6 Photosynthetically Active Radiation (PAR), Absorbed PAR (APAR), the fraction of PAR absorbed by a plant canopy (fPAR), and Intercepted PAR (IPAR) 184
A.1.7 Light Use Efficiency (LUE) 185
A.1.8 Leaf Area Index (LAI), Effective LAI (LAIe), Plant Area Index (PAI), and fractional cover 185
A.2 Remote Sensing Terms 186
A.2.1 Remote Sensing 186
A.2.2 The Moderate Resolution Imaging Spectroradiometer (MODIS) 186
A.2.3 Airborne Lidar / Airborne Laser Scanning (ALS) 186
A.2.4 Pixels and Laser Returns 187

List of Figures

Figure 2.1. Cumulative precipitation measured at OJP for 2001 to 2005 illustrating dry (i.e. 2001 and 2003), and wet conditions (i.e. 2004 through 2005). 2002 may be considered normal because the cumulative precipitation approximates the 30-year normal yearly cumulative precipitation (~450 mm) measured by Environment Canada at a nearby weather station (Waskesiu, Saskatchewan). 22

Figure 2.2. Relationship (thin line) between measured total daytime APAR and modeled APAR at OJP during the four years of study (n = 488). The relationship tends to follow the 1:1 line for most days. 27

Figure 2.3. Cumulative growing season CO_2 fluxes estimated at a) OJP; b) HJP75; c) HJP94; and d) HJP02. Early spring temperatures in 2003 increased fluxes near the beginning of the growing season (June). 31

Figure 2.4. Growing season average LUE per year and average θ at each site. 32

Figure 2.5. Daily average meteorological influences on total daily GPP and average LUE at a) OJP and b) HJP75 for the 2002 to 2005 combined growing seasons (where data exist). Quadratic regression lines ($y=b_0+b_1x+b_2x^2$) are provided to illustrate relationships between driving mechanisms and GPP and LUE. 36

Figure 2.5 cont. Daily average meteorological influences on total daily GPP and average LUE at c) HJP94 and d) HJP02 for the 2002 to 2005 combined growing seasons (where data exist). 37

Figure 2.6. Box plot of daily average LUE over four growing seasons (June to September). Circle with cross hairs represent mean LUE, whereas the central line represents the median LUE. The top portion of the box is the top 75th percentile, and bottom portion of the box is the lower 25th percentile. Upper and lower whisker lines extend to the maximum and minimum limits of LUE. 39

Figure 2.7. Box plots of daily average LUE over four growing seasons (June to September) studied for a) OJP, b) HJP75, c) HJP94, and d) HJP02. Each growing season has been divided

into cloudy, partly sunny, and sunny days. Circles with cross hairs represent mean LUE, whereas the central line represents the median LUE. The top portion of the box is the top 75th percentile, and bottom portion of the box is the 25th percentile. Upper and lower whisker lines extend to the maximum and minimum limits of LUE. 41

Figure 2.8. A comparison of four separate methods commonly used to estimate LUE: a) LUE = GPP/APAR; b) LUE = GPP/IPAR; c) LUE = GPP/total intercepted solar radiation; d) LUE = 1.058 g C·MJ^{-1} IPAR linearly reduced with VPD > 2500 Pa, and T_{air} < -8°C. Each has been averaged from daily estimates per growing season per year. 43

Figure 3.1. a) Lidar measured ground surface elevation within 750 m of the flux station with removal of understory and canopy vegetation. b) Lidar measured canopy heights within 750 m of the flux station after removal of topographical influences. Blue circles represent the location of 11.3 m radius measurement plots and the red circle represents the location of the EC flux tower (centre). Laser returns have been rasterized to produce a continuous surface digital elevation model (DEM) (a) of the ground returns and a canopy height model (CHM) of the maximum z returns (b). 60

Figure 3.2. Precipitation (mm) recorded at OJP and during the growing season, 2002. Grey rectangles mark the duration of the three periods of study. Total cumulative precipitation in 2002 is ~410 mm, which is the 30-year normal precipitation for this area, but is the second consecutive drought year in western Canada (Kljun et al. 2006). 63

Figure 3.3. A schematic diagram of the distribution of laser returns within a tree and the methods used to differentiate canopy height (90th percentile), canopy base height (8th percentile), canopy depth (canopy height – canopy base height), and *f*cover within a 1 m x 1 m x z (height) column. 67

Figure 3.4. Daily 30-minute footprint extent (80% contour lines) and wind direction for the three periods of study are over-laid onto the OJP CHM (shown in Figure 3.1b) to illustrate variability in canopy height and associated footprint locations for daytime periods (0900 to 1700) (approximately 17 ½ hourly periods or 8.5 hours per day). 72

Figure 3.5. Wind roses of the percent frequency of wind directions at OJP during the year 2002 (a) and for the three periods studied (b). 73

Figure 3.6. Relationships between NEP (a, b, and c) and GEP (d, e, and f) and PAR represented by Landsberg light response curves at OJP during the three periods of study: June 10 – 15, 2002 (a and d), July 5 – 13, 2002 (b and e), and August 7 – 13, 2002 (c and f). Relationships are shown for entire days when incoming PAR exceeded 0.1 μmol m^{-2} s^{-1}..... 75

Figure 3.7. Relationships (adjusted r^2) between NEP (a, b, and c), GEP (d, e, and f), and modeled estimates of the same using Landsberg + multiple regression of the residuals presented in Table 3.6 during the three periods of study: June 10 – 15, 2002 (a and d), July 5 – 13, 2002 (b and e), and August 7 – 13, 2002 (c and f). Relationships are shown for entire days when incoming PAR exceeded 0.1 μmol m^{-2} s^{-1}..... 80

Figure 3.8. Relationships (adjusted r^2) between NEP (a, b, and c), GEP (d, e, and f), and modeled estimates of the same using Landsberg + multiple regression of the residuals presented in Table 3.6 (including fcover and elevation) during three periods of study: June 10 – 15, 2002 (a and d), July 5 – 13, 2002 (b and e), and August 7 – 13, 2002 (c and f). Relationships are shown for periods between 0900 and 1700 local time. 82

Figure 3.9. Bar graph of Pearson's r correlations between daily NEP and GEP and a) fcover and b) elevation influence (n = ~17 per day but may vary due to low u_*). Orange and yellow bars represent p-values < 0.01. In a) 13 of 22 (NEP) and 9 of 22 (GEP) days are significantly correlated with areas of increased fcover, whereas the opposite is found on 2 of 22 (NEP) and 3 of 22 (GEP) days. In b) 2 of 22 (NEP) and 3 of 22 (GEP) days are significantly correlated with areas of higher elevations, whereas 10 of 22 (NEP) and 8 of 22 (GEP) days are significantly correlated with areas of lower elevations. Increases in biomass (e.g. greater foliage) should be positively correlated with increased NEP and GEP. 86

Figure 4.1. A schematic diagram of the distribution of laser returns within a conifer tree (represented by red circles) and calculation of the *f*cover ratio within a 1 m x 1 m x z (height) column. The ratio in [2] is estimated for every 1 m x 1 m of ground area within each site. 104

Figure 4.2. Comparison of fPAR on days with high and low ratios of diffuse to direct PAR days throughout the growing season at OJP and HJP75. 105

Figure 4.3. Comparisons between lidar fcover and DHP fPAR using annulus rings 1-9 (a) and 1-5 (b)..... 108

Figure 4.4. fPAR estimated from airborne lidar using the ratio of the number of canopy returns to total returns [2], and the regression model for all species (annulus rings 1-9) at a spatial resolution of 1 m. Subset areas have been expanded to show details in the spatial heterogeneity of fPAR. These include A) OJP, B) HJP94, C) riparian zone of the White Gull River, D) HJP75, and E) fen site, also monitored by the Canadian Carbon Program (CCP). Recent clear cuts have fPAR values close to zero, whereas low-lying shrub and grass vegetation near the White Gull River have fPAR values approaching one. 110

Figure 4.5. Two image maps are illustrated in this figure. The first (illustrated in dark to light tones) shows $fPAR_{lidar}$ at 1 m resolution. Overlaid on top of the $fPAR_{lidar}$ image is the difference between average 1 km x 1 km $fPAR_{lidar}$ and $fPAR_{MODIS}$ shown as transparent pixels. Shades of green indicate that $fPAR_{MODIS}$ was overestimated when compared $fPAR_{lidar}$. Shades of red indicate $fPAR_{MODIS}$ underestimates $fPAR_{lidar}$..... 112

Figure 5.1. Landsberg model light response curves and relationships between observed 30-minute incoming PAR ($\mu mol \cdot m^{-2} \cdot s^{-1}$) and GPP ($\mu mol \cdot m^{-2} \cdot s^{-1}$) during the 2004 growing season..... 138

Figure 5.2. Site-level relationships between a) P_{max} and average measured tree height; b) I_{comp} and average measured fractional foliage cover from DHP; and c) α and average measured tree height estimated in 2004..... 139

Figure 5.3. Comparisons between GPP_{EC} and $GPP_{Landsberg}$ with the inclusion of measured canopy height and fractional cover during the growing season of 2005……...141

Figure 5.4. Eight-day cumulative average GPP comparisons between GPP_{EC}, GPP_{MODIS}, and GPP_{lidar} at a) OJP; b) HJP75; and c) HJP94. Error bars on MODIS data indicate the range of GPP recorded for eight adjacent pixels (to the centre one, nine in total). 144

Figure 5.5. Differences between GPP_{lidar} on June 16, 2005 (as an example) at 1 m resolution and a) 25 m b) 250 m; c) 500 m; and d) 1000 m pixels. Maps of GPP_{lidar} illustrate more and less productive parts within 1 km x 1 km MODIS pixel areas. Low resolution pixels were subtracted from 1 m resolution pixels at each site. Positive differences indicate that lower resolutions underestimate GPP compared with 1 m resolution, whereas negative differences indicate that lower resolutions over-estimate GPP when compared with 1 m resolution. Gray areas equal missing data due to short vegetation. 147

List of Tables

Table 2.1. Average vegetation characteristics at OJP, HJP75, and HJP94 for 22 plots. The values in parentheses represent standard deviation (stdev). 21

Table 2.2. Average vegetation characteristics at HJP02 for 200 1m x 1m plots along four transects. Average percent cover does not add up to 100% (averaged between four transects) because some plots have more or less amounts of individual coverage types. The values in parentheses represent standard deviation (stdev). 21

Table 2.3. NDVI, LAI, and the scaling constant, K. Minimum and maximum growing season average estimates are shown based on *in situ* measured LAI (Tables 2.1 and 2.2) during the last year of study (2005). 26

Table 2.4. Growing season average meteorological conditions, annual variability in canopy structure, and CO_2 flux totals per site and for up to four years of study. 30

Table 3.1. Average structural vegetation characteristics measured at eight plots surrounding the flux measurement station at the jack pine site. 59

Table 3.2. Average canopy structure and elevation characteristics surrounding the EC sensor. Source of flux areas may be influenced differently depending on wind direction, canopy structure and elevation. 73

Table 3.3. Average meteorological conditions and NEP (GEP) P_{max} during three periods studied. 76

Table 3.4. Pearson's correlation coefficients for the relationships between NEP and GEP, and PAR using the Landsberg light response curve. Dominant meteorological variables affecting the residuals of NEP and GEP after accounting for PAR are also included. The *p*-value, the percentage when NEP and GEP were not affected by driving mechanisms, is shown in brackets. Number of observations = 192 (P1); 288 (P2); and 224 (P3). 77

Table 3.5. Pearson's r correlation matrix of interacting meteorological driving mechanisms and *p-values* (in brackets). 78

Table 3.6. Landsberg and multiple regression equations used to predict NEP and GEP using meteorological variables. Relative importance of each contribution is indicated by the *p-value.* Number of observations = 111 (P1); 166 (P2); and 126 (P3). 79

Table 3.7. Multiple regression equations used to predict NEP and GEP using meteorological variables, *f*cover and elevation, added to Landsberg results (Table 3.6). Relative importance of each contribution is indicated by the *p-value.* Number of observations = 111 (P1); 166 (P2); and 126 (P3). 81

Table 3.8. NEP and GEP light response curve characteristics for four days of similar meteorological conditions when footprints originated from opposite parts of the ecosystem (high biomass vs. low biomass (fcover, tree height), and higher elevation (upland) vs. lower elevation (lowland)). 84

Table 4.1. Average vegetation characteristics at OJP, HJP75, and HJP94 for 22 plots. The values in parentheses represent standard deviation (stdev). 99

Table 4.2. Comparisons between 2005 average fPAR estimates at OJP and HJP75 from: Chen et al. (2006); diffuse and direct PAR; average fPAR measured from DHP (annulus rings 1-5 and 1-9); and average photo plot-level *f*cover from lidar. 106

Table 5.1. Average vegetation characteristics at OJP, HJP75, and HJP94 for 22 plots. The values in parentheses represent standard deviation (stdev). 128

Table 5.2. Average vegetation characteristics at HJP02 for 200 1m x 1m plots along four transects. Average percent cover does not add up to 100% (averaged between four transects) due to varying amounts of vegetation coverage per plot. 128

Table 5.3. Summary of GPP methods estimated using EC, plot measurements, airborne lidar, and MODIS. 132

Table 5.4. Parameters (P_{max}, I_{comp}, and α) used in Landsberg curves and the correlation between incoming PAR and GPP described by the Landsberg curve. Landsberg input parameters have been determined from all 30-minute periods of PAR and GPP measured during the growing season of 2004. 137

Table 5.5. Measurements of the accuracy of GPP_{EC} vs. $GPP_{Landsberg}$ (n = 122) during the growing season of 2005. *p-values* are included in brackets. Pearson's r correlation is appropriate for OJP, HJP75 and HJP94, whereas Spearman's rank correlation is appropriate for HJP02. 142

Table 5.6. Pearson's r correlations between GPP_{EC}, GPP_{lidar}, and GPP_{MODIS} including *p-values* (in brackets). Average percent differences are shown for eight-day composite periods (where data were available) over the growing season, 2005. 146

Table 5.7. Summary statistics (percent differences) between GPP estimated at 1 m spatial resolution and lower resolutions per site. Negative signs represent underestimation of GPP by lower resolution pixels. 149

Chapter 1

Introduction

1.1 Background

Forests play an important role in the global carbon cycle. The ability of forest ecosystems to use carbon dioxide (CO_2) and water for photosynthesis in parallel with the amount released to the atmosphere via ecosystem respiration is strongly dependent on stand age, management practices, species composition, meteorological conditions, and phenology (e.g. Law et al. 2002; Morgenstern et al. 2004; Arain and Restrepo-Coupe, 2005). The difference between carbon uptake (i.e., photosynthesis) and carbon release (i.e., respiration) by ecosystems has critical implications for national climate change policy on an annual basis (IPCC, 2007).

The variability of CO_2 fluxes within young and regenerating forests is not well-understood, yet regenerating forests make up a significant component of the land surface. Young forests release CO_2 into the atmosphere until a certain age is reached when more CO_2 is used for photosynthesis than is released. The contribution of CO_2 to the atmosphere by young and newly regenerating stands can be significant (e.g. Law et al. 2002). Cohen et al. (1995) suggest that more than 90% of forests within the Pacific Northwest of the United States have been replaced by young conifer plantations. The State of Canada's Forests 2005-2006 (Canadian Forestry Service http://cfs.nrcan.gc.ca/sof/sof06/for_stat_trd_e.html) show that forests occupy approximately 46% of the Canadian landmass, of which, approximately 3.4% are disturbed each year by harvesting (0.2%), forest fires (0.5%) and insect defoliation (2.7%). Therefore, understanding and quantifying nutrient cycling processes, atmospheric driving mechanisms, and disturbance types

affecting young and regenerating stands is important, especially within the context of the national carbon balance.

Fluxnet-Canada (2002-2007) and the Canadian Carbon Program (2007-2010) have, in part, focused on the effects of disturbance type and age on the carbon cycle through close examination of processes at regenerating and mature forest stands across Canada (e.g. Arain and Restrepo-Coupe, 2005; Amiro et al. 2006; Giasson et al. 2006; Humphreys et al. 2006; Peichl and Arain, 2006; Schwalm et al. 2006). Eddy covariance (EC) is often used to quantify differences in CO_2 uptake and release by measuring the concentration and direction of movement of trace gases in the atmosphere. Up to 400 EC systems measuring CO_2, H_2O and energy exchanges between ecosystems and the atmosphere have been deployed over the past 10 years, mostly in areas of fairly flat and uncomplicated terrain (http://daac.ornl.gov/FLUXNET/). The EC system measures detail ecosystem fluxes at temporal scales ranging from seconds to multiple years, and typically sample the ecosystem immediately surrounding the EC system. EC systems are also prone to measurement error, and its use is limited in areas of complex terrain and during low wind speeds (e.g. Massman and Lee, 2002; Baldocchi, 2008).

Another method for measuring changes in vegetation health and above-ground biomass is through remote sensing. Remote sensing: a) passively measures the absorption, transmission or reflection of sunlight (or energy) from the earth's surface within discrete electromagnetic wavelengths (or bands); or b) actively emit pulses of energy, which provide an estimate of the three-dimensional properties of the earth's surface. The Moderate Resolution Imaging Spectroradiometer (MODIS) is an example of a passive sensor and represents the current standard for operational remote sensing of the global terrestrial biosphere. MODIS sensors, onboard AQUA and TERRA satellite

platforms provides daily coverage of the entire earth's surface at resolutions of 250 m, 500 m, and 1000 m within up to 36 narrow spectral bands. However, pixels are prone to various influences (e.g. atmospheric scattering, mixed pixels, and illumination angle) which can lead to inaccuracies in measured canopy structure (e.g. Sun and Ranson, 2000; Fernandes et al. 2004; Xu et al. 2004; Eriksson et al. 2006; Jin et al. 2007). Airborne scanning light detection and ranging (lidar) is an example of an active sensor used to map the three-dimensional characteristics of tree canopies and the ground surface using one discrete waveband at 1064 nm (near infrared) (Wehr and Lohr, 1999). Discrete return lidar systems rapidly emit laser pulses towards the earth's surface at rates between 5 kHz to 160 kHz. Laser pulses can reflect (or "return") from canopy surfaces twice before reflecting from the ground. Airborne lidar provides very high resolution irregular point data ranging from approximately 35 cm (between returns) to 5 m. Lidar data can also be expensive to obtain, and therefore may only be collected once or possibly a few times per site.

Understanding the average reflectance of low resolution pixels (e.g. MODIS) used to estimate biomass and CO_2 fluxes using remote sensing, requires measurements of canopy structure for validation purposes. However, ground-based measurements of the canopy are difficult, time consuming, and expensive. Measurements are often limited to small areas and can be difficult to repeat within exact locations (Heinsch et al. 2006). The EC system provides some means for evaluating MODIS estimates of vegetation productivity (for example gross primary production (GPP) and net primary production (NPP)), but is limited in spatial extent. Airborne lidar may provide another means for evaluating MODIS products over large areas, thereby reducing the need for extensive ground validation. There is currently very little research on the use of lidar for validation of remote sensing products.

In this dissertation, CO_2 was measured at a jack pine chronosequence of four stands located in Saskatchewan, Canada. These included: a) a recently clearcut site scarified in 2002; b) a site harvested in 1994; c) an immature site harvested in 1975; and d) a mature forest of approximately 90 years old. The EC system was used at each site to measure CO_2 fluxes from the surrounding ecosystem at temporal rates of 10 and 20 Hz for periods of seconds up to years. CO_2 flux and meteorology were used to understand better the carbon cycle within a jack pine chronosequence during dry and wet years. CO_2 flux measurements were then integrated with airborne lidar data for the purposes of evaluating MODIS vegetation products. Four research objectives are discussed in the following sections.

1.2 Thesis Objectives

1.2.1 Objective 1: Investigation of LUE

1.2.1.1 Problem Statement

The influence of meteorological driving mechanisms on the variability of CO_2 uptake and respiration in previously disturbed forests, and during abnormally dry and wet years, is not well understood. Understanding these processes is critical as northern climates continue to warm. Light use efficiency (LUE), defined as the ability of vegetation to use absorbed light for photosynthesis, can be used to understand resource limitations affecting light use and CO_2 uptake. It is not clear if within- and between-site differences in LUE are more important than inter-annual variability and if this varies with site age (Gu et al. 2002). There are also various ways to calculate LUE, which leads to incompatible results within the literature (Schwalm et al. 2006). This is especially important because remote sensing models use LUE to estimate regional to global CO_2 uptake (Running et al. 1999; Running et al. 2004). Remote sensing models currently employ simplistic estimates of LUE, based on the idea of functional convergence of LUE

between ecosystems (Monteith, 1972). Numerous studies have found that LUE varies with changes in atmospheric driving mechanisms, depending on vegetation type, age, and structure (e.g. Turner et al. 2003; Schwalm et al. 2006; Leuning et al. 2005). These results indicate that functional convergence of LUE likely does not exist, and therefore the accuracy of remote sensing models that use biome-specific LUE may be in question (e.g. Turner et al. 2002; Turner et al. 2003; Heinsch et al. 2006). Examination of LUE, therefore, is very important, especially within forest stands that have been previously disturbed.

1.2.1.2 Objectives

Light use efficiency (LUE) (g $C \cdot MJ^{-1}$ of APAR), can be estimated at the ecosystem level as the ratio of gross primary production (GPP) (g $C \cdot m^{-2} \cdot d^{-1}$) to absorbed photosynthetically active radiation (APAR) ($MJ \cdot m^{-2} \cdot d^{-1}$). The purpose of this study was to determine how LUE varied within a jack pine chronosequence during different radiation conditions (cloudy, partly cloudy, and sunny). Up to four years have also been examined per site during dry and wet periods. The influences of meteorological driving mechanisms and different methods for estimating LUE, including those used in remote sensing-based models, were also discussed. It is well understood that stand age, radiation regime, and interannual variability will affect net ecosystem exchange (NEE) and ecosystem respiration (Re), however, the importance of these influences on LUE are not well understood.

1.2.1.3 Brief Methodology:

The period of study (2002-2005) experienced large differences in yearly cumulative precipitation, providing a unique opportunity to study LUE over a range of soil moisture conditions. In this study, meteorological driving mechanisms were related to LUE to determine their interaction at different sites. The varying influences of cloudy, partly sunny, and sunny days on LUE have also

been examined on a daily basis, per growing season to determine if different canopy structural characteristics and stand age impacted LUE differently during these periods.

1.2.1.4 Contribution to Knowledge:

In this study, canopy structure and age are shown to have significant and varying influences on LUE. This has implications for remote sensing-based LUE models used in the estimation of regional GPP. By improving the resolution of land-cover products and structural attributes, as well as inclusion of diffuse radiation and cloud cover, improvements to MODIS GPP and NPP products can be made.

1.2.2 Objective 2: Vegetation Structure and Ground Elevation Influences on CO_2 Exchanges

1.2.2.1 Problem Statement

Variability in vegetation structural characteristics and ground surface elevation has an important influence on vegetation production and available resources (e.g. moisture and nutrient regimes). For example, the variability in leaf area within and between vegetated ecosystems affects significantly, energy exchanges and mass fluxes (e.g. Baldocchi and Meyers, 1998; Gower et al. 1999). Increases in foliage result in increased photosynthesis, reduced energy absorbed by the soil surface, decreased soil warming, and decreased soil respiration (Griffis et al. 2003; Baldocchi and Meyers, 1998). However, few studies have examined the influence of structural and ground elevation heterogeneity on fluxes. This is due, in part, to our inability to map the variability of forest structure and elevation at high resolutions and in three dimensions. Airborne lidar provides the ability to develop new techniques for sampling various canopy structural attributes, including foliage cover, canopy height, and canopy depth variability throughout an ecosystem. Understanding the influences of vegetation structural and elevation heterogeneity on the

magnitude of CO_2 fluxes is important because these: a) provide a means for assessing the influence of leaf area and canopy height on flux variability; b) may be important factors within increasingly more structurally and topographically heterogeneous ecosystems; and c) can be used to develop and/or evaluate ecosystem models that incorporate ground surface elevational influences on fluxes.

1.2.2.2 Objectives:

In this study, vegetation structure and elevation were characterised using lidar within the contours of half-hourly flux footprint maximum area probability density functions (PDFs) (approximately 80% of the probability of flux) from Kljun et al. (2004). The objective was to quantify the influences of vegetation structure and elevation on CO_2 concentrations measured by the EC system, specifically net ecosystem production (NEP) and GPP. Three growing season periods were examined in 2002 at a fairly homogeneous mature jack pine site in Saskatchewan, Canada.

1.2.2.3 Brief Methodology:

The footprint parameterization is applied operationally to average 30-minute measurements of CO_2 fluxes. The combined influences of meteorological variables, incoming PAR, relative humidity, soil moisture, and soil temperature on NEP and GPP were examined using Landberg light response curves and a multiple linear regression. Structural vegetation characteristics and ground surface topography were then extracted from airborne lidar. The fraction of vegetation cover and elevation were combined within a second multiple regression to determine if they significantly affected fluxes during the three periods studied.

1.2.2.4 Contribution to Knowledge:

Meteorological driving variables account for a significant component of the variability in fluxes. Fractional cover can also influence NEP and GPP, and can be more important that some

meteorological driving variables at certain times during the year. This study provides new methodologies for extracting and understanding the sensitivity of fluxes to variations in the environment surrounding the EC system. It may also be used as a test to determine if the EC system is spatially representing the ecosystem in question.

1.2.3 Objective 3: Using Airborne Lidar for the Assessment of MODIS fPAR

1.2.3.1 Problem Statement

Leaf area is particularly important, affecting energy and mass exchanges between the terrestrial biosphere and the atmosphere (e.g. Chen et al. 2005). Accurate spatial and temporal estimates of leaf area index (LAI) and the fraction of photosynthetically active radiation absorbed by the canopy (fPAR) are required as inputs into ecosystem/atmosphere models (e.g. Gower et al. 1999; Chen et al. 2007). Remote sensing can be used to estimate spatial and temporal changes in leaf area; however sensors are often not able to resolve the complexity of the vegetation canopy within averaged pixels (e.g. Xu et al. 2004; Eriksson et al. 2006; Jin et al. 2007). Accurate spatial and temporal methods of collecting fPAR and LAI would therefore be beneficial and cost-effective for scaling from radiation sensors to wider area coverage (and lower resolutions). Lidar data collection and availability is also wide-spread throughout North America and Europe (e.g. U.S. Geological Survey (via the CLICK project: http://lidar.cr.usgs.gov/)) enabling alternative uses, such as satellite validation, for the data.

1.2.3.2 Objectives:

This study introduces the concept of using airborne lidar for the validation of MODIS vegetation indices and land cover products. Objectives of this study are to:

1. Provide a model to estimate spatial variability of fPAR from lidar using the return ratio of canopy fractional cover.

2. Compare model results with fPAR estimated from PAR radiation sensors and digital hemispherical photography (DHP);
3. Evaluate the differences between MODIS estimates of fPAR and lidar fPAR at the 1 km x 1 km pixel level within a jack pine chronosequence (three sites) and over the lower part of the White Gull River watershed.

The goal was to provide a simple and robust model that can be used to evaluate MODIS vegetation indices using airborne lidar and locally measured incoming PAR radiation.

1.2.3.3 Brief Methodology:

Airborne lidar is used to estimate the fraction of vegetation cover based on a ratio of the total number of laser pulses returned from the canopy to the total number of returns (or all returns) within a 1 m x 1 m x height column. Lidar fractional cover was then compared with fPAR estimated from DHP and PAR sensors to determine the accuracy of the lidar model. The fPAR model was then used to examine differences between MODIS fPAR and lidar-fPAR. These were determined by subtracting average 1 km resolution lidar fPAR pixels from MODIS fPAR within a watershed containing 99 MODIS pixels.

1.2.3.4 Contribution to Knowledge:

The ability to map fPAR accurately using airborne lidar has many applications. Scaling of fPAR from individual radiation sensors and DHP to large heterogeneous areas using lidar provides a direct link to MODIS vegetation products and reduces the need for expensive field validation. Lidar can also provide an estimate of within-pixel variability, which will enable assessment of the accuracy and validity of MODIS pixels within heterogeneous environments, such as those which have been previously disturbed. The spatial distribution of fPAR derived from lidar data may be used to validate MODIS fPAR, and may be especially useful for modelling GPP at high spatial

and temporal resolutions as explored in the final chapter. The use of lidar as a validation tool for lower resolution remote sensing products has not been previously examined (to the authors' knowledge).

1.2.4 Objective 4: Validation of MODIS GPP using the EC system and airborne lidar

1.2.4.1 Problem Statement

The influences of within-pixel heterogeneity in canopy cover on MODIS products are also not well known because MODIS pixels may or may not capture localized variability (Milne and Cohen, 1999). Within-pixel land-cover heterogeneity plays an important role on the extrapolation of CO_2 exchanges from the local to regional scales. Therefore, within-pixel patterns of CO_2 uptake as a result of variability in canopy structure, especially leaf area, may create further discrepancies within lower spatial resolution remote sensing-based modeling schemes. The ability to estimate GPP across a range of species types, ages, and scales using airborne lidar will aid in the validation of the MODIS GPP product beyond the EC system. It will also provide important information on the organization of within-pixel patches and their influence on individual pixels. Several validation schemes are currently underway. These include the Accelerated Canopy Chemistry Program (ACCP) (Aber, 1994); Bigfoot (e.g. Cohen and Goward, 2004; Turner et al. 2006); Fluxnet (e.g. Heinsch et al. 2006); and the Prototype Validation Exercise (PROVE) (e.g. Havstad et al. 2000). However, few studies have been able to quantify the influences of mixed pixels on MODIS GPP. There have been no studies that have used airborne lidar to model GPP for the evaluation of the MODIS GPP products.

1.2.4.2 Objectives:

Three objectives were examined in this study. The first objective related average plot measured canopy height and fractional cover to inputs used in Landsberg light response curves during the growing season of 2004. Inputs such as the maximum average GPP, light compensation point and the scaling factor were directly related to canopy height and fractional cover at these sites. Relationships based on canopy structure were then substituted for Landsberg inputs to predict daily cumulative GPP with incoming PAR during the growing season of 2005. The second objective was to compare cumulative eight-day observed GPP estimated from the EC system, the MODIS GPP product and a lidar-derived canopy structure model based on the Landsberg approach applied within 1 km x 1 km MODIS pixel areas. The third objective examined the influences of within-pixel vegetation heterogeneity on an average daily estimate of GPP at varying pixel resolutions.

1.2.4.3 Brief Methodology

Inputs used in site-specific Landsberg light response curves were compared with canopy height and foliage fractional cover estimated from airborne lidar and measured in the field. Relationships between inputs and canopy structure were used to create models of GPP on a per site basis during the growing season of 2004 and tested in 2005. Lidar-Landsberg models of GPP were then compared at the site level and with MODIS estimates of GPP. The last part of this study examined the influence of scaling and within-pixel heterogeneity on estimates of GPP. Individual MODIS pixel areas of lidar-derived GPP were aggregated from 1 m resolution to 25 m (typical of a Landsat pixel), 250 m, 500 m and 1000 m (typical of MODIS vegetation products). Biases were determined by subtracting each lower resolution product from the 1 m^2 GPP from lidar.

1.2.4.4 Contribution to Knowledge:

The results of this study indicate that airborne scanning lidar is an especially useful tool for scaling between EC measurements and lower resolution satellite products. This is the first study to use lidar to scale between EC system estimates of GPP and MODIS products. The ability to accurately estimate canopy fractional cover and leaf area from lidar within one to many MODIS pixels for GPP estimation has many benefits. These include continuous scaling of leaf area over varying pixel resolutions, significantly reduced time and costs associated with extensive LAI measurement within and beyond pixels, and the ability to map and discretize the three-dimensional foliage area with depth into the canopy.

1.3 Thesis Organisation

Following this introduction, the thesis has been organized into a set of four chapters that follow the typical conventions and style required for manuscripts to be submitted to academic journals. Each chapter builds upon the previous chapter(s) and refers to published literature. This provides a consistent flow of ideas, objectives, and methodologies throughout the thesis. References cited are also provided at the end of each chapter. A discussion follows the research and analysis chapters, which ties together important results and discusses future research. The final Summary and Conclusions chapter briefly summarizes the thesis and discusses important conclusions. One appendix chapter provides a discussion on terms used in the thesis (Appendix 1). This is included at the end of the thesis for reference.

1.4 References

Aber, 1994. Accelerated canopy chemistry program. Final Report to NASA EOS-IWG.

Amiro, B.D., A.L. Orchansky, A.G. Barr, T.A. Black, S.D. Chambers, F.S. Chapin III, M.L. Goulden, M. Litvak, H.P. Liu, J.H. McCaughey, A. McMillan, and J.T. Randerson, 2006. *Agricultural and Forest Meteorology.* 140:41-50.

Arain, A., and N. Restrepo-Coupe, 2005. Net ecosystem production in a temperate pine plantation in southeastern Canada. *Agricultural and Forest Meteorology.* 128:223-241.

Baldocchi, D., 2008. Turner Review No. 15: 'Breathing' of the terrestrial biosphere: lessons learned from a global network of carbon dioxide flux measurement systems. *Australian Journal of Botany.* 56:1-26.

Baldocchi, D., and T. Meyers, 1998. On using eco-physiological, micrometeorological and biogeochemical theory to evaluate carbon dioxide, water vapor and trace gas fluxes over vegetation: a perspective. *Agricultural and Forest Meteorology*. 90:1-25.

Chen, J. M., X. Chen and W. Ju, X. Geng, 2005. A remote sensing-driven distributed hydrological model: mapping evapotranspiration in a forested watershed. *Journal of Hydrology*. 305:15-39.

Chen, B., J. M. Chen, G. Mo, K. Yuan, K. Higuchi, and D. Chan. 2007. Modeling and scaling coupled energy, water, and carbon fluxes based on remote sensing: An application to Canada's landmass. *Journal of Hydrometeorology*, 8: 123-143.

Cohen, W.B., T.A. Spies, and M. Fiorella, 1995. Estimating the age and structure of forests in a multi-ownership landscape of western Oregon, USA. *International Journal of Remote Sensing.* 16:721-746.

Cohen, W. and S. Goward, 2004, Landsat's role in ecological application of remote sensing. *Bioscience.*54:573-584.

Dewar, R.C., B.E. Medlyn, and R.E. McMurtrie, 1998. A mechanistic analysis of light and carbon use efficiencies. *Plant, Cell and Environment.* 21:573-588.

Eriksson, H.M., L. Eklundh, A. Kuusk, and T. Nilson, 2006. Impact of understory vegetation on canopy reflectance and remotely sensed LAI estimates. *Remote Sensing of Environment*. 103:408-418.

Fernandes, R. A., J. R. Miller, J. M. Chen, and I. G. Rubinstein, 2004. Evaluating Image Based Estimates of Leaf Area Index in Boreal Conifer Stands over a Range of Scales using High-Resolution CASI Imagery. *Remote Sensing of Environment*, 89: 200-216.

Giasson, M.-A., C. Coursolle, and H. Margolis, 2006. Ecosystem-level CO_2 fluxes from a boreal cutover in eastern Canada before and after scarification. *Agricultural and Forest Meteorology.* 140:23-40.

Gower, S.T., C. J. Kucharik, and J.M. Norman, 1999. Direct and indirect estimation of leaf area index, f_{APAR}, and net primary production of terrestrial ecosystems. *Remote Sensing of Environment.*70:29-51.

Griffis, T.J., T.A. Black, K. Morgenstern, A.G. Barr, Z. Nesic, G.B. Drewitt, D. Gaumont-Guay, and J.H. McCaughey, 2003. Ecophysiological controls on the carbon balances of three southern boreal forests. *Agricultural and Forest Meteorology.* 117:53-71.

Gu, L., D. Baldocchi, S. Verma, T.A. Black, T. Vesala, E. Falge, and P. Dowty, 2002. Advantages of diffuse radiation for terrestrial ecosystem productivity. *Journal of Geophysical Research.* 107(D6):4050.

Havstad, K.M., W. Kustas, A. Rango, J.C. Ritchie, and T.J. Schmugge, 2000. Jornada experimental range: A unique arid land location for experiments to validate satellite systems. *Remote Sensing of Environment.* 74(1):13-25.

Heinsch, F.A., M. Zhao, S.W. Running, J.S. Kimball, R.R. Nemani, K.J. Davis, P.V. Bolstad, B.D. Cook, A.R. Desai, D.M. Ricciuto, B.E. Law, W.C. Oechel, H.Luo, S.C. Wofsy, A.L. Dunn, J.W. Munger, D.D. Baldocchi, L. Xu, D.Y. Hollinger, A.D. Richardson, P.C. Stoy, M.B.S. Siqueira, R.K. Monson, S.P. Burns, and L.B. Flanagan, 2006. Evaluation of remote sensing based terrestrial productivity from MODIS using regional tower eddy flux network observations. *IEEE Transactions on Geoscience and Remote Sensing.* 44(7):1908-1925.

Humphreys, E.R., T.A. Black, K. Morgenstern, T. Cai, G.B. Drewitt, Z. Nesic, and J.A. Trofymow, 2006. Carbon dioxide fluxes in coastal Douglas-fir stands at different stages of development after clearcut harvesting. *Agricultural and Forest Meteorology.* 140:6-22.

IPCC, 2007. Climate Change 2007: The Physical Science Basis, Summary for Policymakers. Contribution of Working Group 1 to the Fourth Assessment Report of the Intergovernmental Panel on Climate Change.

Jin, Z, Q. Tian, J. M. Chen, and M. Chen, 2007. Spatial scaling between leaf area index maps of different resolutions. *Journal of Environmental Management.* 85: 628-637.

Law, B.E., E. Falge, L. Gu, D. Baldocchi, P. Bakwin, P. Berbigier, K. Davis, A. Dolman, M. Falk, J. Fuentes, A. Goldstein, A. Granier, A. Grelle, D. Hollinger, I. Janssenss, P. Jarvis, N. Jensen, G. Katul, Y. Mahli, G. Matteucci, T. Meyers, R. Monson, W. Munger, W. Oechel, R. Olson, K. Pilegaard, K.T. Paw U, H. Thorgeirsson, R. Valentini, S. Verma, T. Lesala, K. Wilson, S. Wofsy, 2002. Environmental controls over carbon dioxide and water vapor exchange of terrestrial vegetation. *Agricultural and Forest Meteorology.* 113:97-120.

Leuning, R., M. Raupach, P. Coppin, H. Cleugh, P. Isaac, O. Denmead, F. Dunin, S. Zegelin, and J. Hacker, 2004. Spatial and temporal variations in fluxes of energy, water vapour and carbon dioxide during Oasis 1994 and 1995. *Boundary-Layer Meteorology*. 110:3-38.

Massman, W.J., and X. Lee, 2002. Eddy covariance flux corrections and uncertainties in long-term studies of carbon and energy exchanges. *Agricultural and Forest Meteorology*. 113:121-144.

Milne, B.T., and W. B. Cohen, 1999. Multiscale assessment of binary and continuous landcover variables for MODIS validation, mapping, and modeling applications. *Remote Sensing of Environment.* 70:82-98.

Monteith, J.L. 1972. Solar radiation and productivity in tropical ecosystems. *Journal of Applied Ecology.* 9:747-766.

Morgenstern, K., T.A. Black, E. R. Humphreys, T.J. Griffis, G. B. Drewitt, T. Cai, Z. Nesic, D. L. Spittlehouse, and N.J. Livingston, 2004. Sensitivity and uncertainty of the carbon balance of a Pacific Northwest Douglas-fir forest during an El Niño/La Niña cycle. *Agricultural and Forest Meteorology.* 123:201-219.

Peichl, M., and M. A. Arain, 2006. Above- and belowground ecosystem biomass and carbon pools in an age-sequence of temperate pine plantation forests. *Agricultural and Forest Meteorology.* 140:51-63.

Running, S.W., R. Nemani, J. Glassy, P. Thornton, 1999. MODIS daily photosynthesis (Psn) and annual net primary production (NPP) product (MOD17). Theoretical basis document, Version 3. NASA Goddard Space Flight Center, Greenbelt, MD 20771, USA. Available online: http://modis.gsfc.nasa.gov/data/atbd/atbd_mod17.pdf.

Running, S.W., R. Nemani, F.A. Heinsch, M. Zhao, M. Reeves, and H. Hashimoto, 2004. A continuous satellite-derived measure of global terrestrial primary production. *BioScience*. 54(6):547-560.

Schwalm, C.R., T.A. Black, B.D. Amiro, M.A. Arain, A.G. Barr, C.P.-A. Bourque, A.L. Dunn, L.B. Flanagan, M.-A. Giasson, P.M. Lafleur, H.A. Margolis, J.H. McCaughey, A.L. Orchansky, and S.C. Wofsy, 2006. *Agricultural and Forest Meteorology.* 140:269-286.

Sun, G.Q. and K. Ranson, 2000. Modelling lidar returns from forest canopies. *IEEE Transactions on Geoscience and Remote Sensing*. 38:2617-2626.

Turner, D.P., S.T. Gower, W.B. Cohen, M. Gregory, T.K. Maiersperger, 2002. Effects of spatial variability in light use efficiency on satellite-based NPP monitoring. *Remote Sensing of Environment.* 80:397-405.

Turner, D.P., S. Urbanski, D. Bremer, S.C. Wofsy, T. Meyers, S.T. Gower, and M. Gregory, 2003. A cross-biome comparison of daily light use efficiency for gross primary production. *Global Change Biology.* 9:383-395.

Turner, D.P., W.D. Ritts, W.B. Cohen, S.T. Gower, S. W. Running, M. Zhao, M. H. Costa, A. A. Kirschbaum, J.M. Ham, S.R. Saleska, D.E. Ahl, 2006. Evaluation of MODIS NPP and GPP products across multiple biomes. *Remote Sensing of Environment.* 102:282-292.

Wehr, A., and U. Lohr, 1999. Airborne laser scanning: an introduction and overview. *ISPRS Journal of Photogrammetry and Remote Sensing*. 54(2-3):68-82.

Xu, S. J. M. Chen, R. Fernandes and J. Cihlar. 2004. Effects of subpixel water area fraction on mapping leaf area index and net primary productivity in Canada. *Canadian Journal for Remote Sensing*, 30: 797-804.

Chapter 2

Investigating Light Use Efficiency (LUE) Across A Jack Pine Chronosequence during Dry and Wet Years

2.1 Abstract

Light use efficiency (LUE) is the ability in which vegetated canopies use light for photosynthesis. It also provides a physical basis for scaling carbon uptake processes from the stand to global scales using remote sensing estimates of canopy cover as well as meteorological inputs. A better understanding of the factors that control LUE will result in improved global estimates of carbon uptake from the terrestrial biosphere. Several recent studies have examined meteorological and species-related factors controlling LUE. However few studies have compared LUE variability within stands of different ages, and during normal and anomalous soil moisture conditions, which may become more prevalent with climate change. This study presents on LUE observations made at a jack pine chronosequence (4 stands: recent clearcut (age: 1-3), regenerating (age: 8-9), immature (age: 29-30), and mature (~90 years old)) during one normal (2002), one very dry (2003), and two very wet (2004, 2005) growing seasons in Saskatchewan, Canada. The objective of this study was to examine factors that control variability in LUE within stands of different ages during drought and wet conditions.

Cumulative CO_2 fluxes decreased significantly at all sites during the drought year of 2003, as did average LUE. Canopy foliage at the recently regenerating jack pine site increased by 19% between 2002 and 2003. Foliage growth rate was reduced by 6% between 2003 and 2004, and foliage decreased by 6% from 2004 to 2005. Over the four years studied, LUE was greatest at the

mature jack pine site and lower, but similar at the other three sites. Growing season average LUE varied with average soil moisture at each site, except at the newly regenerating site where soil moisture had little influence. Daily average vapour pressure deficit (VPD) typically had the greatest influence on the variability in LUE at all sites. Diffuse vs. direct radiation conditions also had a significant but varying affects on LUE within jack pine stands of different ages.

2.2 Introduction

Light use efficiency (LUE) (g $C \cdot MJ^{-1}$ of APAR), defined as the ratio of gross primary production (GPP) (g $C \cdot m^{-2} \cdot d^{-1}$) to absorbed photosynthetically active radiation (APAR) ($MJ \cdot m^{-2} \cdot d^{-1}$), describes the ability of vegetation to use light for photosynthesis. LUE varies instantly with changes in GPP and radiation conditions, but is typically estimated over averaging periods of 30-minutes or individual days. Dewar et al. (1998) summarize three generalizations from the literature with respect to ecosystem LUE: a) LUE is constant during vegetation growth when water supply is non-limiting; b) the use of carbon for gross photosynthesis (carbon use efficiency [CUE]) is constant across species; and c) APAR is positively correlated with increased leaf nitrogen. These generalizations enable aggregation of LUE and vegetation productivity (for example, net primary production [NPP] and GPP) from local to global scales using remote sensing-based land-cover types and ecosystem models (Turner et al. 2002, Running et al. 2004, Drolet et al. 2005).

The eddy-covariance (EC) method provides a direct measurement of net ecosystem exchange (NEE), where –NEE is equal to net ecosystem production (NEP). This can be used to estimate GPP and ecosystem respiration (Re) used in calculations of LUE. Numerous studies have shown that LUE varies both linearly and non-linearly with changes in air temperature (T_{air}), and/or vapour pressure deficit (VPD), and soil moisture (θ), depending on vegetation type, age, and

structure (e.g. Turner et al. 2003, Schwalm et al. 2006, Leuning et al. 2005). This indicates that LUE is not a simple function of meteorological driving mechanisms, or species type, and therefore functional convergence between many species is unlikely. Lack of functional convergence of LUE will affect model accuracy of vegetation productivity. Further, the use of varying definitions and methods for calculating LUE has led to mixed and non-comparable results within the literature (Gower et al. 1999, Schwalm et al. 2006).

Few studies have examined controls on the variability of LUE within different ages of the same species or during anomalous meteorological conditions. The purpose of this study was to determine how LUE varied within different ages of jack pine stands, during different radiation conditions (cloudy, partly cloudy, and sunny) and very dry and wet periods over up to four years per site. The influences of meteorological driving mechanisms and different methods for estimating LUE, including those used in remote sensing-based models, were also discussed.

2.3 Study Area

A chronosequence of four jack pine (*Pinus banksiana* Lamb.) stands have been examined during the growing season (June 1st to September 30th) over a period of four years (2002 to 2005), where data were available. Stands include: a mature jack pine forest of ~90 years of age (OJP) (examined years 2002-2005); an immature jack pine forest (HJP75) (examined years 2004-2005, age 29-30); a rapidly regenerating young jack pine forest (HJP94) (examined years 2002-2003, age 8-9); and a recently clearcut and scarified site with jack pine seedlings (HJP02) (examined years 2003-2005, age 1-3). The jack pine sites are located within 6 km of each other in the lower part of the White Gull watershed, north of Prince Albert, Saskatchewan, Canada. OJP and HJP75 were studied extensively during the Boreal Ecosystem-Atmosphere Study (BOREAS) (e.g. Baldocchi et al. 1997a, Baldocchi et al. 1997b, Gower et al. 1997). In this study, all sites were

operating as part of Fluxnet-Canada (Barr et al. 2006, Coursolle et al. 2006), under the Boreal Ecosystem Research and Monitoring Sites (BERMS) project. The BERMS research project concentrates on species and disturbance-induced differences in carbon and water exchanges within the same climatic region (e.g. Kljun et al. 2006, Barr et al. 2006). Individual sites tend to be relatively flat, varying by less than 12 m in elevation (Chasmer et al. *accepted*). Soils are sandy, coarse-textured and well-drained (Baldocchi et al. 1997b). Each site contains extensive meteorological and CO_2, water, and energy flux measuring equipment in accordance with Fluxnet-Canada protocols (www.fluxnet-canada.ca) as well as mensuration information, site characteristics, and temporal and high-resolution remote sensing data.

Forest stand characteristics are described in Table 2.1 (OJP, HJP75, and HJP94), based on measured forest stand data from eight, eight, and six forest mensuration plots per site, respectively. At OJP, HJP75 and HJP94, forest mensuration plots were 11.3 m in radius, and were located 100 and 500 m from the EC flux station (OJP and HJP75), and within 250 m at HJP94. Foliage gap fraction estimates were made at individual plots during diffuse conditions using digital hemispherical photography (DHP) set to two F-stops below default exposure (Zhang et al. 2005). Gap fraction was measured during May and August 2005 and was converted to leaf area index (LAI) using thresholding methods of Leblanc et al. (2005). DHP was set up at five photos (four each at 11.3 m distances from the centre photo) per plot. LAI was adjusted to account for canopy clumping, woody:total area ratios and needle:shoot area ratios for sites (Chen et al. 2006). LAI estimates were slightly lower than those of Chen et al. (2006) at OJP, although comparisons with effective LAI were almost the same, indicating possible differences in allometric woody:total and needle:shoot area ratios used. Differences in DHP-estimated LAI may also be due to instrumentation, heterogeneity in leaf area, and structural variability throughout the site.

Table 2.2 contains mensuration information from four 2-m-wide x 25-m-long transects of 1 m^2 plots (50 plots per transect) measured in late May, 2005 at HJP02.

Table 2.1. Average vegetation characteristics at OJP, HJP75, and HJP94 for 22 plots. The values in parentheses represent standard deviation (stdev).

Site	Number of trees sampled	Average stem density (stdev) (stems m^{-2})	Average tree height (stdev) (m)	Average DBH* (stdev) (cm)	Average LAI (stdev) ($m^2 \cdot m^{-2}$)	Average canopy depth (stdev) (m)	Average crown diameter (stdev) (m)	Other species
OJP	381	0.11 (0.001)	14.2 (3.5)	9.33 (4.55)	1.6 (0.1)**	8.3 (2.7)	2.0 (1.0)	Alder, bearberry, reindeer lichen, blueberry, cranberry
HJP75	1447	0.59 (0.19)	6.3 (1.6)	5.69 (3.49)	2.8 (0.42)	3.5 (1.3)	0.9 (0.4)	Grasses, reindeer lichen, bearberry
HJP94	2081	0.86 (0.56)	1.6 (0.7)	2.31 (1.05)	1.1 (0.2)	1.6 (0.7)	0.7 (1.1)	Grass, blueberry, alder, raspberry, bearberry, reindeer lichen

* DBH refers to tree bole diameter at breast height (1.3 m above the ground).
** LAI measurements from Chen et al. (2006) differ from LAI observed in this study.

Table 2.2. Average vegetation characteristics at HJP02 for 200 1m x 1m plots along four transects. Average percent cover does not add up to 100% (averaged between four transects) because some plots have more or less amounts of individual coverage types. The values in parentheses represent standard deviation (stdev).

Number of trees (in 200 1m plots)	Average tree height (stdev) (m)	Average % tree cover (stdev)	Average % grass cover (stdev)	Average % reindeer lichen cover (stdev)	Average % soil cover (stdev)	Average % wood debris cover (stdev)	Average % herb cover (stdev)	Average estimated LAI ($m^2 \cdot m^{-2}$)
37	0.19 (0.12)	9 (11)	21 (18)	23 (30)	32 (18)	26 (24)	8 (15)	0.29

The period of study (2002-2005) saw large differences in yearly cumulative precipitation, providing a unique opportunity to study LUE over a range of soil moisture (i.e. dry to wet) conditions. Figure 2.1 illustrates cumulative precipitation measured at OJP from 2001 to 2005. The year 2001 is included because drought conditions occurred during and prior to 2001 and lasted until 2003, leading to significant water shortages for periods of greater than one year (e.g. Kljun et al. 2006).

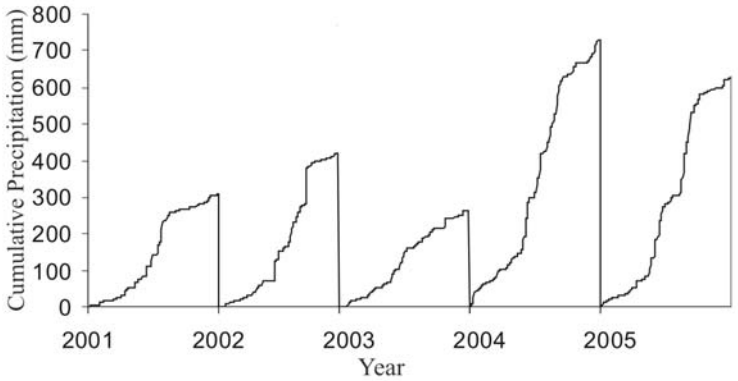

Figure 2.1. Cumulative precipitation measured at OJP for 2001 to 2005 illustrating dry (i.e. 2001 and 2003), and wet conditions (i.e. 2004 through 2005). 2002 may be considered normal because the cumulative precipitation approximates the 30-year normal yearly cumulative precipitation (~450 mm) measured by Environment Canada at a nearby weather station (Waskesiu, Saskatchewan).

2.4 Site Instrumentation

Site instrumentation has been discussed in Coursolle et al. (2006), Kljun et al. (2006), and Barr et al. (2006). Briefly, the EC method was used at all sites throughout the growing season to measure CO_2 fluxes averaged over 30-minute periods. NEP ($\mu mol \cdot m^{-2} \cdot s^{-1}$) was measured by the EC system where NEP = -NEE ($\mu mol \cdot m^{-2} \cdot s^{-1}$). Positive NEP indicates that CO_2 from the atmosphere was used for photosynthesis, whereas negative NEP indicates that the site was releasing more CO_2 into the atmosphere than it was using for photosynthesis. Each site has undergone the same measurement and data processing protocol whereby daily Re ($\mu mol \cdot m^{-2} \cdot s^{-1}$) was modeled using the relationship between nighttime Re and soil temperature (Barr et al. 2004). GPP ($\mu mol \cdot m^{-2} \cdot s^{-1}$), defined as the uptake of CO_2 by the ecosystem through photosynthesis, was estimated from measured NEP and modeled Re: GPP = NEP + Re. CO_2, H_2O and friction velocity were measured using a sonic anemometer (CSAT3, Campbell Scientific Inc. Edmonton, Alberta, Canada at OJP and HJP02; Gill R3-50, Gill Instruments Ltd., England at HJP75; SAT-550, Kaijo

Co., Tokyo, Japan at HJP94) combined with a closed path infrared gas analyzer (LI 6262, LI-COR Inc., Lincoln, NE, USA) (Barr et al. 2006). EC systems have been installed above the canopy at heights of approximately 28 m, 17 m, 3 m, and 2 m above the ground surface at OJP, HJP75, HJP94, and HJP02 respectively. The 30-minute average CO_2 fluxes were determined from 20 Hz, 20 Hz, 10 Hz, and 20 Hz measurements at the OJP, HJP75, HJP94, and HJP02 using block averaging. Any gaps in the 30-minute fluxes were filled using a moving-window regression approach (Barr et al. 2006, Kljun et al. 2006). Despite the inherent problems with the EC technique (e.g. Massman and Lee, 2002), data were quality controlled using a minimal surface friction velocity of 0.35 m s^{-1}. Inaccuracies in Re and GPP may exist within this analysis, but are beyond the scope of this study. Averaging over longer periods also minimizes the influence of errors within the data. Further processing of EC data are discussed in Kljun et al. (2006) and Barr et al. (2006).

LUE was determined for daytime periods, defined as the period of time for which daytime incoming above-canopy shortwave radiation exceeded 1.0 $W \cdot m^{-2}$. Net radiation (Rn) was measured using a four-component net radiometer ($W \cdot m^{-2}$) (CNR1, Kipp and Zonen USA Inc. Bohemia, NY), and has been used with above canopy PAR to estimate variations in foliage growth at HJP94 and HJP02 (discussed below). Above- and below-canopy PAR ($\mu mol\ m^{-2} \cdot s^{-1}$) was converted into $MJ \cdot m^{-2}$ per half hour and per day using a conversion of 0.25 and adjusted for daytime minutes. PAR was measured using LI-COR model LI190 at OJP and HJP75 (LI-COR Biosciences, Nebraska, USA); and Eko model ML-020P (Eko Instruments, Co. Ltd., Japan) at HJP94 and HJP02. Above canopy incident and reflected PAR sensors were installed on booms at heights of 28 m, 17 m, 3 m and 2 m above the ground at OJP, HJP75, HJP94, and HJP02. Below

canopy incident PAR measurements were made at OJP and HJP75 at a height of ~1 m. Below-canopy PAR measurements were not available at HJP94 or HJP02.

In this study, meteorological driving mechanisms were related to LUE to determine their interaction at different sites. Daily average T_{air} and VPD were measured using top-of-canopy air temperature and relative humidity sensors (model HMP45C, Vaisala by Campbell Scientific Inc. Edmonton Alberta, Canada). Soil volumetric moisture content (θ) ($m^3 \cdot m^{-3}$) was measured at equal depths, (0 to 15cm, 15 to 30cm, 30 to 60cm, 60 to 90cm, 90 to 120cm, and 120 to 150 cm) at each location using soil moisture probes (CS615, Campbell Scientific Inc., Edmonton, Alberta). Soil temperature was measured using soil temperature probes (CS107b, Campbell Scientific Inc., Edmonton, Alberta) placed at depths (2 cm, 5 cm, 10 cm, 20 cm, 50 cm, and 100 cm) within the soil column. Soil moisture was examined at depths of 30 to 60 cm, and soil temperature was examined at depths of 10 cm.

2.5 Methodology

2.5.1 Calculation of Light Use Efficiency

APAR was used in the estimation of LUE, with GPP, and can be calculated from PAR sensors as:

$$APAR = (PAR_{AC\downarrow} - PAR_{AC\uparrow}) - (PAR_{BC\downarrow} - PAR_{BC\uparrow}), \quad [1]$$

where $PAR_{AC\downarrow}$ is above canopy incoming PAR, $PAR_{AC\uparrow}$ is above canopy reflected PAR, $PAR_{BC\downarrow}$ is incoming below canopy PAR after interception with branches and leaves, and $PAR_{BC\uparrow}$ is the reflected PAR from the ground surface (Gower et al. 1999). In this study $PAR_{BC\uparrow}$ was not measured at any of the sites, therefore it has not been included in the estimation of APAR.

Reflected ground surface PAR albedo ($PAR_{BC\uparrow}$) is 6% at OJP and HJP75 (Chen, 1996), and does not contribute greatly to the reduction of APAR at these sites.

There was only one PAR sensor measuring $PAR_{BC\downarrow}$ at OJP and HJP75. Each sensor was compared with 40 DHPs per site at 100 m and 500 m locations from each tower to assess the representivity of the OJP and HJP75 $PAR_{BC\downarrow}$ sensors. Average fPAR measured by PAR sensors was 0.61 (OJP) and 0.70 (HJP75) in 2005. Average fPAR from DHP was 0.54 (stdev. = 0.06) (OJP) and 0.55 (stdev = 0.06) (HJP75). Green fPAR estimates of Chen et al. (2006) in 2005 were 0.49 (OJP) and 0.54 (HJP75) using TRAC (fractional cover was not provided). Results of Chen et al. (2006) were slightly lower than our estimates of fractional cover because Chen et al. (2006) removed the fraction of wood observed by the sensor as well as $PAR_{AC\uparrow}$ and $PAR_{BC\uparrow}$. Average difference between DHP and PAR sensors at OJP was 11%, and at HJP75 it was 21%. This indicates that $PAR_{BC\downarrow}$ at OJP and HJP75 may have been located in areas that had slightly greater foliage than the rest of the stand, on average. DHP methods are also prone to measurement errors and have been found to underestimate gap fraction by 8%, on average, at a number of sites when compared with other optical methods (Chen et al. 2006). Despite slight overestimation of fPAR by PAR sensors at HJP75, fPAR estimates were reasonable approximations of DHP measurements throughout the stand.

APAR was not directly measured at HJP94 and HJP02 because of the lack of $PAR_{BC\downarrow}$, therefore APAR was modeled at HJP94 and HJP02 based on Beer's Law:

$$APAR = \alpha_s \cdot PAR_{AC\downarrow} (1 - e^{-kL^*}), \qquad [2]$$

where α_s is the canopy absorptivity ($1 - PAR_{AC\uparrow} / PAR_{AC\downarrow}$), and k is the extinction coefficient estimated as a constant 0.45 for simplicity (Chen et al. 2006). LAI (L) likely varies within the growing season and between years at HJP94 and HJP02. Unfortunately, monthly measurements of LAI were not made at these sites. To rectify this, NDVI was used at both sites to estimate monthly average LAI following methods discussed in Wilson and Meyers (2007). Monthly mean NDVI values were calculated from 30-minute global shortwave radiation and incoming and reflected PAR between 09:00 and 15:00 local time. Only clear days were used in the averaging procedure where above-canopy incoming shortwave radiation was greater than 200 $W \cdot m^{-2}$. LAI was estimated per month following Wilson and Meyers (2007):

$$LAI = -K \log\left(\frac{NDVI_{\max} - NDVI}{NDVI_{\max} - NDVI_{\min}}\right) \qquad [3]$$

$NDVI_{max}$ is the maximum NDVI with dense vegetation, NDVI is measured for the month, $NDVI_{min}$ is the minimum NDVI with no vegetation, and K is a scaling constant based on measured LAI (Tables 2.1 and 2.2). Table 2.3 provides minimum and maximum NDVI measurements and estimated LAI minimum and maximum from 2002 (2003 at HJP02) to 2005.

Table 2.3. NDVI, LAI, and the scaling constant, K. Minimum and maximum growing season average estimates are shown based on *in situ* measured LAI (Tables 2.1 and 2.2) during the last year of study (2005).

Site	Year	Minimum Summer NDVI	Maximum Summer NDVI	K	Minimum LAI	Maximum LAI
HJP02	2003	0.16	0.49	0.9	0.20	0.21
	2004	0.29	0.50	0.9	0.25	0.31
	2005	0.37	0.57	0.9	0.24	0.31
HJP94	2002	0.14	0.56	3.9	0.64	0.73
	2003	0.29	0.57	3.9	0.97	1.07
	2004	0.33	0.59	3.9	1.03	1.14
	2005	0.31	0.56	3.9	1.01	1.06

Beer's Law was also used to model APAR at OJP for comparison with measured APAR (as an example). Figure 2.2 provides a comparison between APAR derived using radiation sensors and modeled results from [2] at OJP. High correlation between the Beer's Law method for estimating APAR and measured APAR at OJP indicate that results will be comparable to measured methods at HJP94 and HJP02.

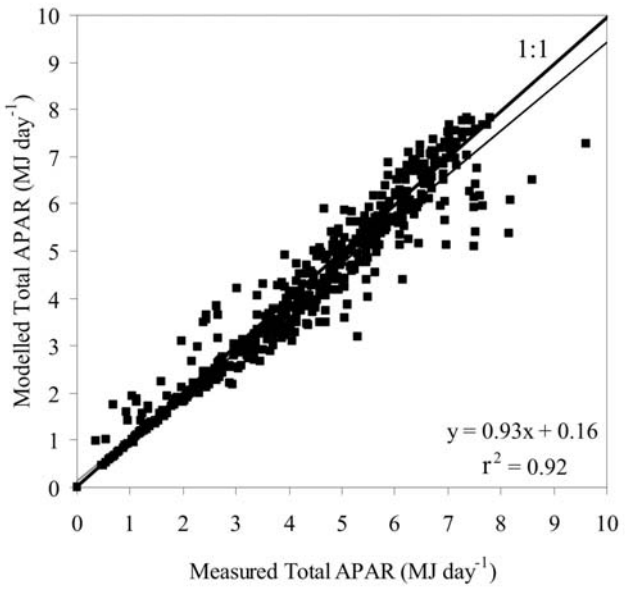

Figure 2.2. Relationship (thin line) between measured total daytime APAR and modeled APAR at OJP during the four years of study (n = 488). The relationship tends to follow the 1:1 line for most days.

Cloudy, partly sunny, and sunny days have been examined on a daily basis, per growing season, based on the ratio of measured incoming shortwave radiation (K_{in}) to the modelled ground surface shortwave radiation (K_{mod}). Modelled incoming shortwave radiation was determined using the clear sky model of Bird and Hulstrom (1991) (http://rredc.nrel.gov/solar/models/clearsky/) adjusted for latitude, longitude, and time zone of the sites. The influences of solar zenith angle and leaf angle/area effects have been reduced by averaging K_{in}/K_{mod} between 1000 and 1400,

local sun time. Daily ratios of K_{in}/K_{mod} were used to define cloudy (< 0.33), partly sunny (> 0.33 and < 0.66), and sunny (> 0.66) days.

2.5.2 Statistical Analysis

Statistical analyses used in this study were done using MiniTab Software, v. 15 (State College, Pennsylvania). Comparisons were made to determine the influence of site age, radiation conditions, and drought vs. wet years on LUE using an Analysis of Variance (ANOVA) (Ebdon 1992). In all cases, the description of how the ANOVA was employed (e.g. multiple factor vs. single factor) was described along with the results. An ANOVA requires that: 1) all data examined are normally distributed; 2) variances are equal; and 3) data do not co-vary. We have analyzed and discussed data limitations within the ANOVA test. As part of the ANOVA we implicitly state where significant differences exist ($p \leq 0.05$), but do not use this method to test hypotheses. Least squares (quadratic) regression methods were used to determine the relationships between LUE and meteorological driving mechanisms.

2.6 Results

2.6.1 Influences of Dry, Normal and Wet Years on LUE at Individual Sites

In this study, strong differences in meteorological driving mechanisms, and CO_2 fluxes, GPP, NEP, and Re were found during dry, normal and wet years and between the sites studied (Table 2.4). The drought year of 2003 had a strong influence on meteorological conditions measured at each site, resulting in higher average growing season APAR, T_{air} and stronger VPD. Average θ was reduced by up to 40% at all sites. The wet years of 2004 and 2005 had greater than normal cumulative annual precipitation (~760 mm and 640 mm as opposed to 290 mm in 2003), increased θ, and lower growing season average T_{air}, APAR and VPD. 2002 had normal amounts of precipitation, and average meteorology was similar to 2004 and 2005.

Table 2.4 presents cumulative totals of CO_2 fluxes and average meteorological conditions during the growing season at each site from 2002 to 2005. Cumulative growing season increases in GPP, NEP, and Re are shown in Figure 2.3 for each site. NEP did not vary greatly at OJP despite large average differences in soil moisture (varying by as much as 40%). Average growing season GPP and Re at OJP were found to decrease from 2002 to 2003 by 9% and 8%, despite an early peak in GPP from June to early August. This was caused by a warm spring and leaf flush of approximately three weeks earlier than in 2002 (Kljun et al. 2006). Cumulative mid-growing season (July and August 2004) GPP remained low compared with 2002 and 2005 (Figure 2.3a). Re fluxes decreased by 8% in 2003 and increased slightly in 2004 and 2005. Kljun et al. (2006) found that fluxes were significantly reduced during prolonged drought (2000 to 2003) at a mature aspen (OA) site located within approximately 100 kms of the jack pine forests studied. The authors also found that fluxes at OJP and a mature black spruce stand (OBS) were not greatly affected, as has also been observed here. Low θ was also found to negatively affect photosynthesis in Euskirchen et al. (2006) for jack pine forests in Michigan. Further, Baldocchi et al. (1997b) suggest that the OJP forest will continue to gain water via deeper sources, although after years of drought, it is not clear if water will continue to be available. HJP75, measured in 2004 and 2005 were also very similar, although mid-season CO_2 fluxes, GPP and Re were lower in 2004 than in 2005 (Figure 2.3b). GPP comparisons during the drought were not made at HJP75 due to lack of data collection. At HJP94, average growing season GPP decreased by 5% and NEP increased by 12%, in proportion with significant decrease in Re by 17% in 2003. GPP was significantly greater in June and July 2003, than at the same time in 2004, likely due increased air temperatures and an early spring (Kljun et al. 2006). By the end of the growing season, NEP was only slightly greater in 2003 than 2002 at HJP94. Fluxes at HJP02 were not measured in 2002,

but became a greater source of CO_2 to the atmosphere from 2003 to 2004. -NEP increased by 14% between 2003 and 2004, GPP increased by 30%, as did Re (24%). Increases in GPP by 22% and decreases in Re by 16% from 2004 to 2005 resulted in a reduction in –NEP by 66%.

Table 2.4. Growing season average meteorological conditions, annual variability in canopy structure, and CO_2 flux totals per site and for up to four years of study.

Site	*Year*	*Ave. T_{air} °C*	*Ave. VPD Pa*	*Ave. T_{soil} °C*	*Ave. θ $m^3 \cdot m^{-3}$*	*fPAR*	*Ave. Total APAR $MJ \cdot d^{-1}$*	*Ave. Total IPAR $MJ \cdot d^{-1}$*	*Ave. LUE g $C \cdot MJ^{-1}$ APAR*	*Ave. LUE g $C \cdot MJ^{-1}$ IPAR*	*Total GPP g $C \cdot m^{-2}$, June to Sept.*	*Total NEP g $C \cdot m^{-2}$, June to Sept.*	**Total Re g $C \cdot m^{-2}$, June to Sept.**
OJP	2002	14.95	1.69	12.68	0.10	0.55	4.12	4.47	1.06	1.00	475	166	299
	2003	16.59	1.70	13.02	0.06	0.55	4.23	4.60	0.87	0.82	432	164	274
	2004	14.00	1.22	11.40	0.09	0.55	3.75	4.08	1.09	1.01	450	173	278
	2005	14.95	1.31	12.42	0.09	0.56	3.96	4.29	1.06	0.98	463	184	280
HJP 75	2002	-	-	-	-		-	-	-	-	-	-	-
	2003	-	-	-	-		-	-	-	-	-	-	-
	2004	14.10	1.22	12.68	0.13	0.70	3.70	3.50	0.85	0.81	459	195	256
	2005	14.89	2.65	13.68	0.12	0.69	4.05	4.29	0.77	0.75	463	198	259
HJP 94	2002	14.98	1.65	14.80	0.08	0.25	2.34	2.51	0.82	0.77	208	45	162
	2003	15.24	1.70	15.26	0.07	0.35	3.27	3.50	0.58	0.54	197	51	135
	2004	-	-	-	-	0.38	-	-	-	-	-	-	-
	2005	-	-	-	-	0.36	-	-	-	-	-	-	-
HJP 02	2002	-	-	-	-		-	-	-	-	-	-	-
	2003	16.63	1.66	15.41	0.12	0.08	0.87	0.94	0.72	0.66	45	-51	100
	2004	13.93	1.21	14.19	0.14	0.18	0.94	1.01	0.73	0.68	65	-59	132
	2005	14.39	1.26	13.87	0.11	0.20	0.84	0.92	0.85	0.79	84	-20	111

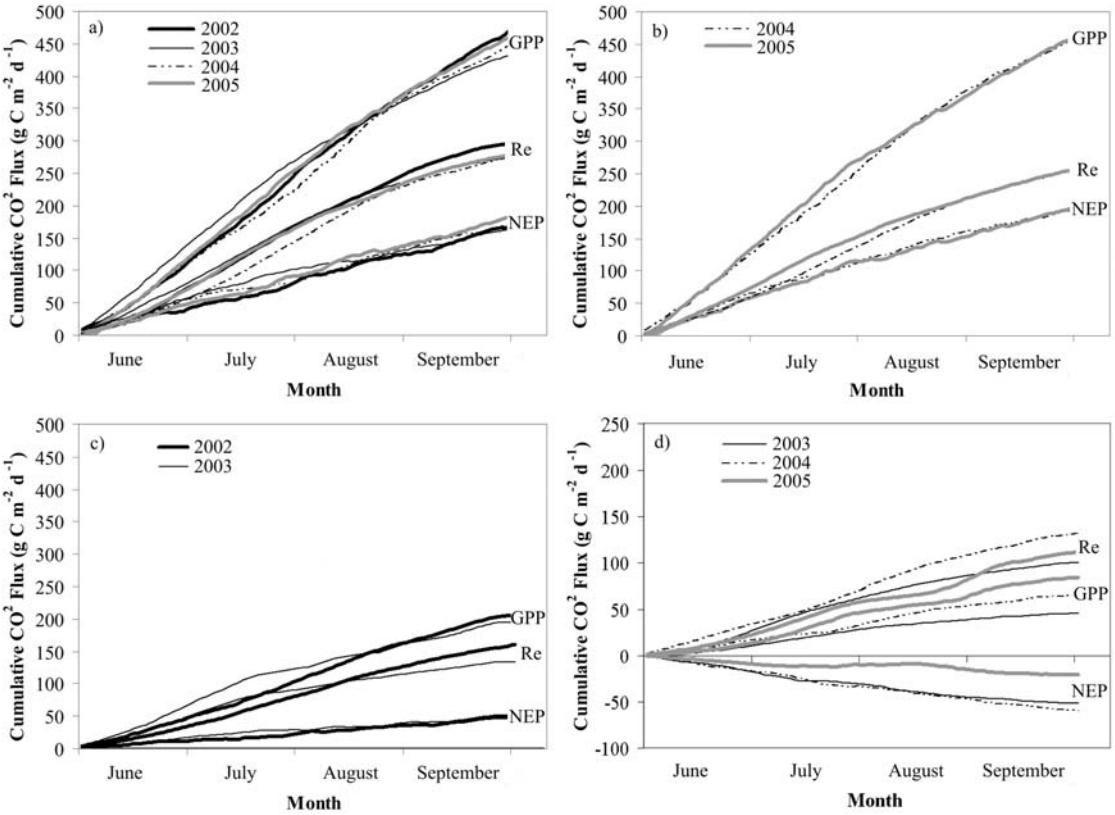

Figure 2.3. Cumulative growing season CO_2 fluxes estimated at a) OJP; b) HJP75; c) HJP94; and d) HJP02. Early spring temperatures in 2003 increased fluxes near the beginning of the growing season (June).

Did the drought of 2003 reduce the efficiency at which jack pine at varying stages of growth use light for photosynthesis? LUE was lower at all sites in 2003 (Table 2.4), in comparison with growing season average θ (Figure 2.4). Strong correspondence between rising and falling LUE and average θ per year was observed for most sites except HJP02, which tended to increase in LUE, regardless of changes in average θ. Changes in LUE were also a function of average changes in APAR, especially during the drought year when both APAR and IPAR were greater than other years, resulting in lower LUE. APAR was 11% greater in 2003 than 2004 at OJP corresponding with the 20% decrease in LUE. APAR was 28% greater at HJP94 in 2003 than

2002, corresponding with a 29% decrease in LUE. However, at HJP02, APAR was reduced by only 7% in 2003 when compared with 2004.

Comparisons between LUE in 2003 vs. 2005 were made using a single factor ANOVA at OJP and HJP02. HJP75 and HJP94 were not included due to lack of data during these years. LUE was normally distributed in all cases, and variances between LUE in 2003 and 2005 were approximately the same at OJP. However, variance in HJP02 LUE data for 2003 and 2005 varied by 30%. Average daily LUE varied significantly between the drought of 2003 and the wet period of 2005 at OJP ($p = 0.000$, $F = 11.75$, $F_{critical} = 3.88$), however, at HJP02, LUE remained relatively the same regardless of dry and wet conditions ($p = 0.27$, $F = 1.23$, $F_{critical} = 3.91$). If we compare during the years that were studied at HJP75 and HJP94, LUE at HJP75 decreased slightly with soil moisture from 2004 to 2005, as did HJP94 from 2002 to 2003 (Figure 2.4).

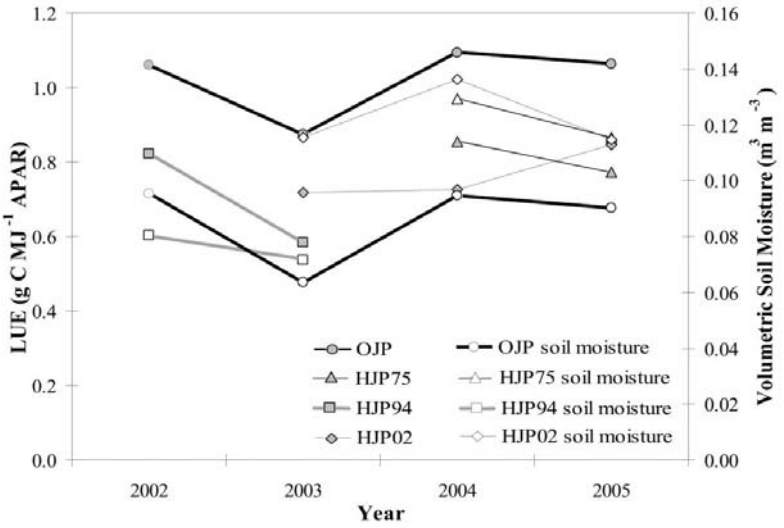

Figure 2.4. Growing season average LUE per year and average θ at each site.

2.6.2 Meteorological Influences on GPP and LUE

Meteorological drivers and the amount of solar radiation available for photosynthesis play important roles on the variability GPP and LUE per growing season year and per site (Figure 2.5). For all years studied, approximately 50% of the variability in VPD occurred because of changes in T_{air} (p=0.000). T_{air} and T_{soil} were also autocorrelated (r^2 = 0.35, p = 0.000), whereas T_{air} and VPD had lesser influences on θ at all sites. Incoming PAR had the largest control on GPP at OJP and HJP75 (Figure 2.5a and b), accounting for approximately (r^2) 28 and 36 percent (p = 0.000) of the variability in carbon uptake over the four year period. Total daily GPP increased with total incoming PAR to a saturation level of approximately 4.2 g $C \cdot m^{-2} \cdot d^{-1}$ and 8 MJ of PAR at OJP and did not vary greatly from year to year. Turner et al. (2003) found that GPP tended to saturate at high levels of solar radiation due to low leaf area and maximum photosynthetic capacity within boreal conifers, as was also found at OJP. VPD and T_{air} had less influence on GPP at OJP (VPD r^2 = 0.21, p<0.001, T_{air} r^2 = 0.14, p < 0.01) using a quadratic least squares regression (Figure 2.5a). Optimal photosynthesis at OJP occurred at VPD of 200 Pa and T_{air} of 18°C. Similar relationships were also found at HJP75, where GPP saturated at approximately 4 g $C \cdot m^{-2} \cdot d^{-1}$ but could withstand higher levels of incoming PAR of 10 MJ, on average. VPD and T_{air} had the greatest influence on GPP at HJP75 (VPD r^2 = 0.20, p < 0.001; T_{air} r^2 = 0.20, p < 0.001). Optimal levels of photosynthesis occurred at 350 Pa and at T_{air} of 18°C. Lagergren et al. (2005) found that VPD had a strong relationship with NPP, where maximum photosynthesis tended to saturate at approximately 600 to 800 Pa within a mixed conifer site in Sweden. They state that stomata will close at high VPD levels, limiting photosynthesis. Similar results were found by Jenkins et al. (2007) at a northern hardwood forest where incoming PAR had the greatest influence on gross carbon exchanges, however, VPD and T_{air} were only weakly correlated with CO_2 concentration.

Variability in daily θ at OJP and HJP75 was small and did not correlate well with GPP on a daily basis.

LUE was also strongly affected by meteorological driving mechanisms at OJP and HJP75 (Figure 2.5). LUE at OJP decreased to 0.6 g C·MJ^{-1} APAR with increasing VPD to a maximum of 400 Pa when examined over all four growing seasons (r^2 = 0.33, p = 0.000). LUE also decreased with increasing T_{air} and was positively correlated with changes in θ. HJP75 tended to be only weakly correlated with daily average T_{air} (r^2 = 0.13, p < 0.01) in 2002 and 2003 and decreased with T_{air} greater than 20°C (Figure 2.5a and b). Jenkins et al. (2007) found that a maximum bound of VPD had a strong influence on maximum LUE, despite a lack of correlation with high frequency data. Lagergren et al. (2005) also found that LUE tended to increase with increasing VPD up to approximately 600 Pa before decreasing to approximately half at maximum VPD within a mixed conifer forest in Sweden. They suggest that a linear decrease in LUE from 100% to 50% will occur between VPDs of 50 and 150 Pa per day, whereas Waring et al. (1995) assume this decrease to occur between 150 and 250 Pa.

At the two younger sites, HJP94 and HJP02, daily average meteorological driving mechanisms had weak (non-significant) influences on GPP (Figure 2.5c and d). Incoming PAR had the greatest influence on GPP at HJP94 (r^2 ~ 0.10, p = 0.1), where GPP tended to saturate at 2 g C·m^{-2}·d^{-1}, approximately 12 MJ of PAR. GPP also increased to 2 g C·m^{-2}·d^{-1} and then decreased with T_{air} > 15°C and VPD > 200 Pa. LUE was strongly influenced by VPD at HJP94 (r^2 = 0.47, p = 0.000) where LUE decreased to below 0.5 g C·MJ^{-1} of APAR at VPDs of approximately 400 Pa. LUE was greatest at $T_{air,}$ = 10°C, but decreased almost linearly beyond 10°C. $T_{air,}$ and VPD were

strongly autocorrelated at HJP94 (r^2 = 0.68), therefore relationships between LUE and T_{air} and VPD were similar. T_{soil} and θ had minimal influences on LUE at HJP94 on a daily basis. No significant relationships between GPP and driving mechanisms were found at HJP02. However, LUE at HJP02 decreased with increasing VPD (r^2 = 0.19, p = 0.000) to LUE levels of approximately 0.5 g $C \cdot m^{-2} \cdot d^{-1}$ at approximately 350 Pa. Strong controls by VPD at these sites may be due to low soil moisture content and limits to stomatal conductance (e.g. Jenkins et al. 2007).

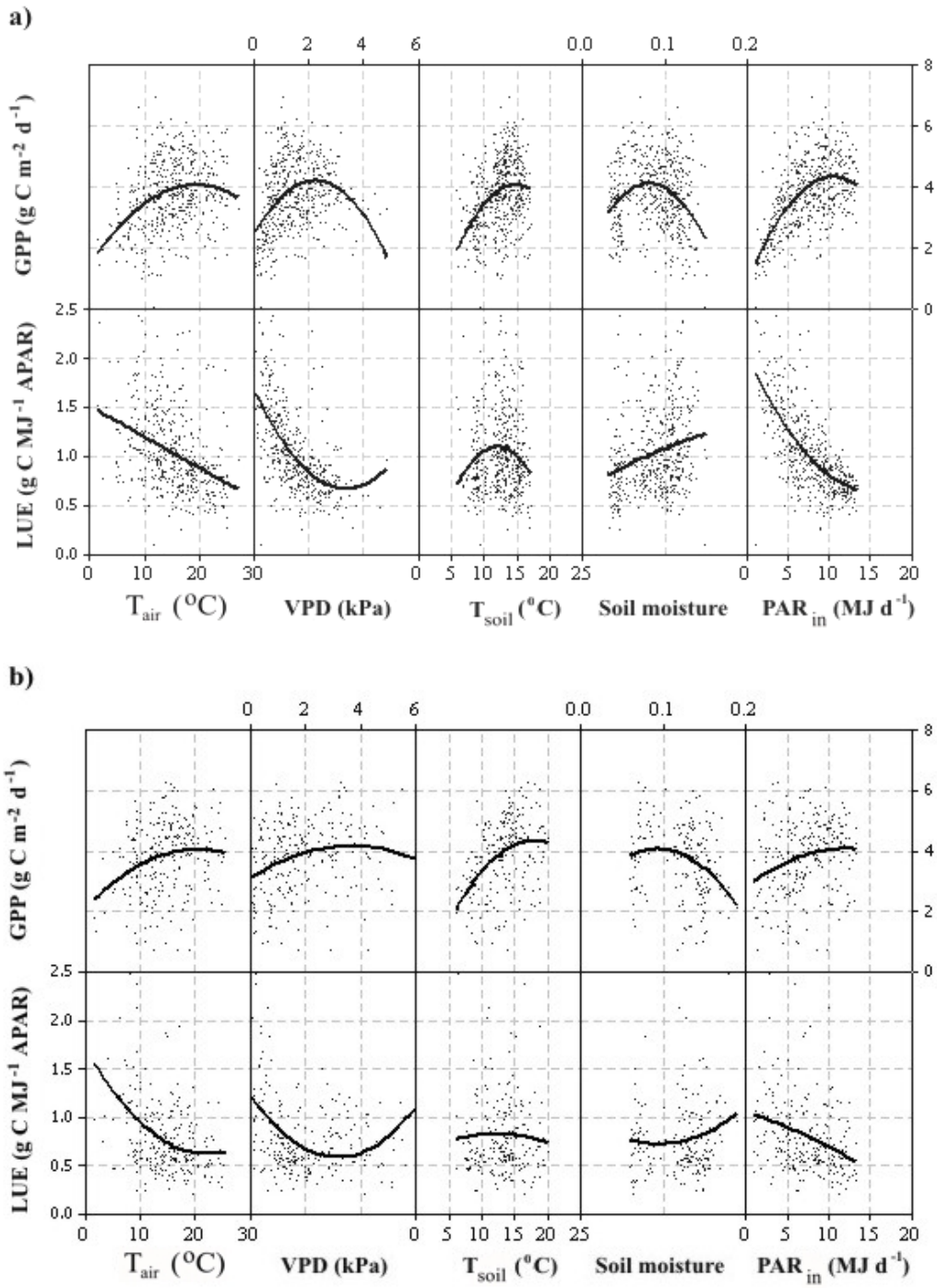

Figure 2.5. Daily average meteorological influences on total daily GPP and average LUE at a) OJP and b) HJP75 for the 2002 to 2005 combined growing seasons (where data exist). Quadratic regression lines ($y=b_0+b_1x+b_2x^2$) are provided to illustrate relationships between driving mechanisms and GPP and LUE.

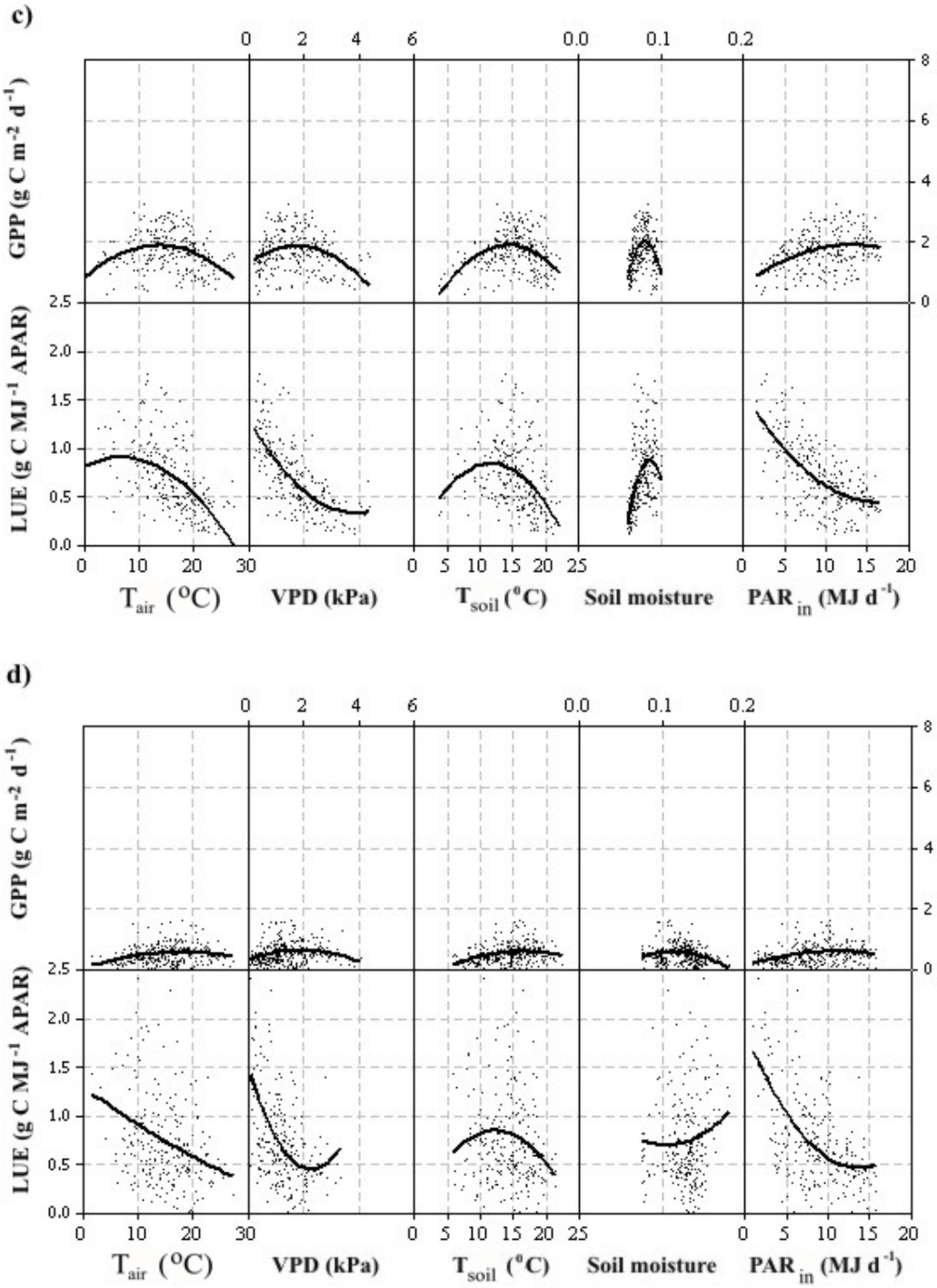

Figure 2.5 cont. Daily average meteorological influences on total daily GPP and average LUE at c) HJP94 and d) HJP02 for the 2002 to 2005 combined growing seasons (where data exist).

2.6.3 LUE Differences between Jack Pine Ages

Functional convergence of LUE between species and age classes was first discussed in Monteith (1972) and has been examined in numerous studies since (e.g. Ruimy et al. 1994, Ruimy et al. 1999, Goetz and Prince, 1996, Green et al. 2001, Green et al. 2003, Ahl et al. 2004, Schwalm et al. 2006). There is a general consensus that LUE varies strongly as a result of species type, age, and environment, therefore, there tends to be little evidence of functional convergence (e.g. McCrady and Jokela, 1998, Lagergren et al. 2005, Schwalm et al. 2006). Does this assumption hold over longer periods of time and within different ages of trees? In this study, a multiple factor ANOVA was set up to examine daily average LUE from all growing seasons at all four sites, simultaneously. LUE at each site was normally distributed. However, all sites had some interdependence, with correlations (r^2) of 0.27 (HJP02), 0.43 (HJP94) and 0.55 (HJP75) when compared with OJP for the entire four year (growing season only) period. HJP75, HJP94, and HJP02 were more independent, with correlations ranging between 0.10 and 0.15 (r^2). Significant differences in LUE existed between OJP ($p = 0.000$, $F = 48.79$, $F_{critical} = 2.61$), and the other three sites (HJP75, HJP94 and HJP02). Differences between HJP75 and HJP94 were less significant (OJP: $p = 0.07$, $F = 2.71$, $F_{critical} = 3.01$). The second factor, drought effects on LUE within species, was also found to have a significant influence on LUE per species between the drought year of 2003 and other years examined ($p = 0.000$, $F = 11.75$, $F_{critical} = 3.88$).

Differences in average LUE between HJP94 and HJP02, and to a lesser extent, HJP75 were not significant (Figure 2.6). These results were also biased because HJP75 included only the two wet years (2004 and 2005), whereas HJP94 included one normal (2002) and one drought (2003) year. Assuming that LUE is greater during wet years than dry ones (as was found for OJP), LUE at

HJP75 could be biased towards slightly higher values, and HJP94 could be biased towards slightly lower values. This may increase similarity in average LUE estimates per site.

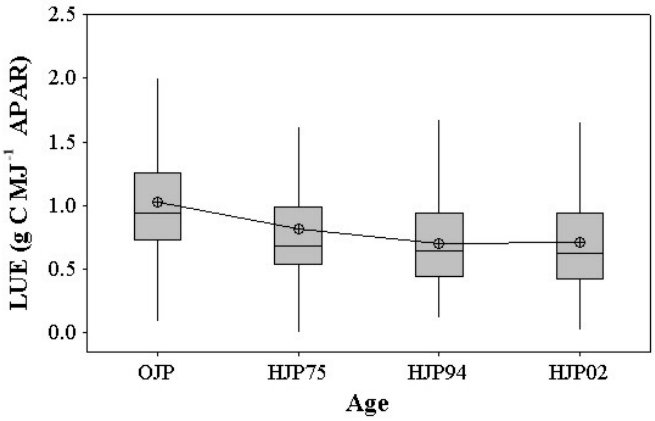

Figure 2.6. Box plot of daily average LUE over four growing seasons (June to September). Circle with cross hairs represent mean LUE, whereas the central line represents the median LUE. The top portion of the box is the top 75th percentile, and bottom portion of the box is the lower 25th percentile. Upper and lower whisker lines extend to the maximum and minimum limits of LUE.

2.6.4 Influences of Radiation on LUE at Individual Sites

Radiation conditions have a large influence on LUE within many species (e.g. Roderick et al. 2001, Green et al. 2003, Gu et al. 2002, Still et al. 2004, Schwalm et al. 2006, Jenkins et al. 2007). However it is not known to what extent radiation conditions affect LUE within different ages of the same species. To what extent does LUE vary due to radiation conditions within different ages of jack pine trees? Does site age or canopy structure affect LUE at the jack pine sites?

Figure 2.7 presents box plots of LUE during sunny, partly sunny and cloudy radiation conditions for each individual site. A multiple factor ANOVA has been used to test differences in age-specific daily average LUE for up to four growing seasons based on: 1) radiation conditions; and

2) dry vs. wet years (as these are inherent factors within all datasets). Significant differences in LUE were found at each site due to varying radiation conditions; however, drought vs. wet years did not have a significant affect on the use of diffuse vs. direct radiation for photosynthesis. The largest differences in LUE occurred between cloudy and partly sunny, and to a lesser extent partly sunny and sunny conditions at all sites. This study found that differences in LUE between cloudy and partly sunny conditions were greatest at HJP02 (p = 0.000, F = 40.86, $F_{critical}$ = 3.03) where average daily LUE during cloudy conditions was 0.55 g C·MJ^{-1} APAR greater than during partly sunny conditions. Similar average LUE differences of 0.49 and 0.47 g C·MJ^{-1} APAR were found between cloudy and partly sunny conditions at HJP75 (p = 0.000, F = 62.86, $F_{critical}$ = 3.03) and OJP (p = 0.000, F = 141.94, $F_{critical}$ = 3.01). Finally HJP94 had the least difference in average daily LUE (0.39 g C·MJ^{-1} APAR) between cloudy and partly sunny conditions (p = 0.000, F = 58.22, $F_{critical}$ = 3.03).

Smaller differences in average LUE were found between partly sunny and sunny radiation conditions. OJP had the greatest difference in average LUE between partly sunny and sunny conditions (0.25 g C·MJ^{-1} APAR). HJP75 and HJP02 had the same difference in average LUE between partly sunny and sunny conditions (0.19 g C·MJ^{-1} APAR), whereas HJP94 had the least difference (0.15 g C·MJ^{-1} APAR). These results indicate that site age and/or canopy structure exhibit some influence on LUE, although results tend to be somewhat confounding. We might expect that the greatest effects of diffuse vs. direct conditions would occur at OJP and HJP75 due to a reduction of shadow (e.g. Gu et al. 2002), but it appears that these differences were strongest at the youngest site.

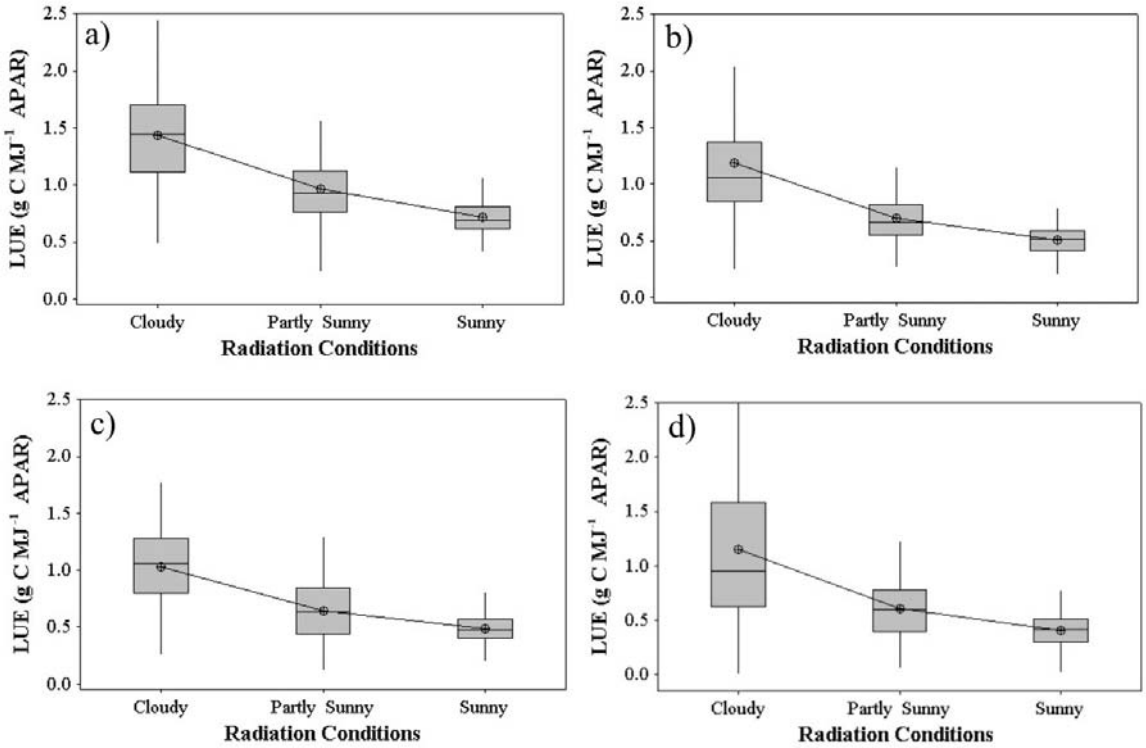

Figure 2.7. Box plots of daily average LUE over four growing seasons (June to September) studied for a) OJP, b) HJP75, c) HJP94, and d) HJP02. Each growing season has been divided into cloudy, partly sunny, and sunny days. Circles with cross hairs represent mean LUE, whereas the central line represents the median LUE. The top portion of the box is the top 75th percentile, and bottom portion of the box is the 25th percentile. Upper and lower whisker lines extend to the maximum and minimum limits of LUE.

2.6.5 A Comparison of Methods for Estimating LUE

Several methods used for estimating LUE have been discussed within the literature. Popular methods include: 1) LUE = GPP(or NPP)/APAR (Ruimy et al. 1999, Gu et al. 2002, O'Connell et al. 2003, Green et al. 2003, Ahl et al. 2004, Still et al. 2004, Lagergren et al. 2005, Schwalm et al. 2006, Jenkins et al. 2007); 2) LUE = GPP(or NPP)/IPAR (Nichol et al. 2000, Green et al. 2001, Turner et al. 2002, Turner et al. 2003, Martin and Jokela, 2004, Coursolle et al. 2006, Pereira et al. 2007); 3) LUE = GPP/total intercepted solar radiation (K_{in}) (Gu et al. 2002, Allen et al. 2005, discussed); and 4) a biome-specific maximum LUE (1.058 g C·MJ^{-1} IPAR for evergreen needle

leaf forests) linearly reduced with VPD and/or T_{air} within remote-sensing based production efficiency models (e.g. MODIS) (Running et al. 1999, Running et al. 2004, Bradford et al. 2005, Heinsch et al. 2006, Yuan et al. 2007). The problem with using one or many different methods for estimating LUE is that there may be an inconsistency between reported LUE estimates within the literature. For example, the use of GPP or NPP may not result in vastly different LUE estimates, because GPP includes the removal of Re, whereas NPP includes the removal of autotrophic respiration (Ra) only (Lovett et al. 2006, Kljun et al. 2006). LUE based on GPP or NPP will likely be similar. However, using IPAR as opposed to APAR may result larger in differences in LUE, especially within open canopies (e.g. Gower et al. 1999).

The term, APAR also tends to vary within the literature. It is defined according to [1], but in much of the literature, it does not include the $PAR_{BC\uparrow}$ component (e.g. this study), or the $PAR_{AC\uparrow}$ component (e.g. Coursolle et al. 2006, Schwalm et al. 2006, for some sites). Coursolle et al. (2006), as in numerous other studies, use IPAR = $PAR_{AC\downarrow} - PAR_{BC\downarrow}$ and may be modeled from Beer's Law if the $PAR_{BC\downarrow}$ is not included. Therefore, LUE depends on how IPAR and APAR are estimated. Do varying definitions of APAR or IPAR greatly affect LUE?

Examples of four different methods for estimating average growing season LUE (from daily averages) are illustrated for the jack pine sites over four years of study (Figure 2.8). In the first example (a), APAR is defined as: APAR = $(PAR_{AC\downarrow} - PAR_{AC\uparrow}) - (PAR_{BC\downarrow})$ at OJP and HJP75, but was modeled using Beer's Law at HJP94 and HJP02, with the inclusion of $PAR_{AC\uparrow}$. In b) IPAR was estimated as $PAR_{AC\downarrow}$-$PAR_{BC\downarrow}$, and was modeled using Beer's Law at HJP94 and HJP02. The example in c) used incoming shortwave radiation (K_{in}) only at all sites. The LUE example in d) was used within the MODIS GPP remote sensing context. It incorporates a constant

maximum LUE (1.058 g C·MJ^{-1} IPAR) determined per classified biome type and is linearly reduced when VPD exceeds 2500 Pa, and T_{air} freezes stomata closed (-8°C) (Heinsch et al. 2006). LUE estimates in d) are typically driven using meteorology from general circulation model (GCM) reanalysis, but in this case maximum LUE has been reduced using measured T_{air} and VPD at the tower.

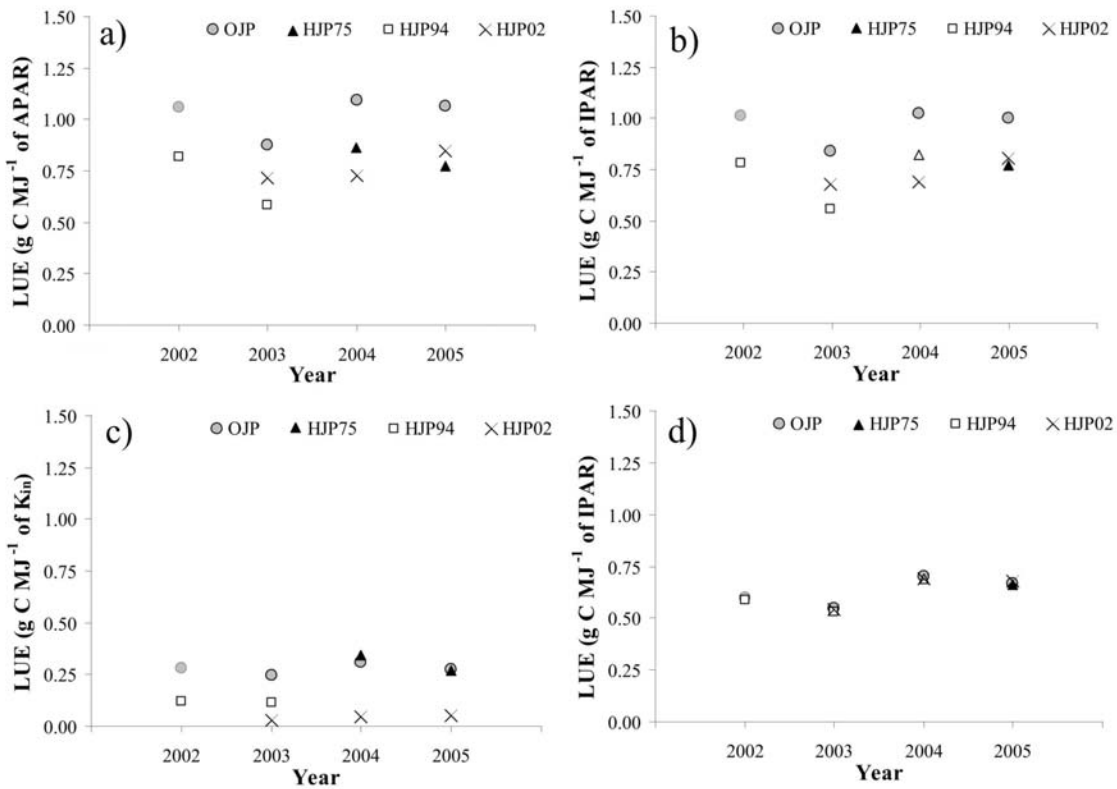

Figure 2.8. A comparison of four separate methods commonly used to estimate LUE: a) LUE = GPP/APAR; b) LUE = GPP/IPAR; c) LUE = GPP/total intercepted solar radiation; d) LUE = 1.058 g C·MJ^{-1} IPAR linearly reduced with VPD > 2500 Pa, and T_{air} < -8°C. Each has been averaged from daily estimates per growing season per year.

The results in Figure 2.8 illustrate little difference between LUE estimated using APAR (Figure 2.8a) as opposed to the IPAR (Figure 2.8b), even as canopies increase in openness. The above canopy reflected component is approximately 3% to 7%. Ground surface PAR albedo was measured by Chen (1996) at OJP and HJP75, and was approximately 6% of incoming above

canopy PAR. Inclusion of reflected PAR from the ground surface would increase LUE_{APAR} by an additional 6% in comparison with LUE_{IPAR}. Use of incoming shortwave radiation only (Figure 2.8c), without removal of incident radiation below the canopy resulted in an overestimation of light and a strong decrease in LUE at all sites. Shortwave solar radiation is problematic because much of the near infrared portion of the spectrum is strongly scattered and is not used in photosynthesis (Gower et al. 1999).

The final method (Figure 2.8d), based on a biome-specific maximum LUE, follows growing season average trends of LUE observed at each site. The maximum LUE approximately matches average LUE of OJP. This includes a reduction of LUE in 2003 followed by increased LUE in 2004 and 2005. Average growing season LUE used by MODIS to estimate GPP (with the inclusion of fPAR from MODIS) was underestimated by approximately 40% (OJP), 15% (HJP75), 14% (HJP94), and 16% (HJP02), on average. MODIS often overestimates fPAR (e.g. Heinsch et al. 2006) which is multiplied by LUE to estimate GPP. Low biome-specific LUE may be used to offset overestimates of fPAR by MODIS when used to calculate global GPP products (e.g. Zhao et al. 2003, Turner et al. 2006, Heinsch et al. 2006). Inclusion of varying degrees of diffuse and direct radiation measured on a global basis per day using remote sensing satellites may also improve LUE estimates per biome-type applied to fPAR to estimate cumulative GPP.

2.7 Discussion

2.7.1 Drought and Wet Growing Season Influences on LUE

Average LUE per site was approximately double those of Schwalm et al. (2006) for the growing season of 2004 at the same sites. Schwalm et al. estimate average growing season LUE 0.5 g C·MJ^{-1} of APAR (OJP) 0.48 g C·MJ^{-1} of APAR (HJP75) and 0.11 g C·MJ^{-1} of APAR (HJP02),

where APAR is estimated from measured LAI and the MODIS-based LAI product (HJP02) using Beer's Law. LAI measurements in Schwalm et al. (2006) were approximately 25% to 35% greater at OJP and HJP75 and 75% greater at HJP02 when compared with Chen et al. (2006) and this study. MODIS typically overestimates LAI at HJP02 because of mixed pixel influences within the site (Chasmer et al. *accepted*). Overestimates of LAI would result in underestimates of LUE if using a Beer's Law approach. Results of Turner et al. (2003) are similar to ours, where LUE varied from between 0.8 and 1.2 g $C \cdot MJ^{-1}$ of APAR between June and September at a northern boreal black spruce stand. Green et al. (2003) found that annual average LUE for a jack pine forest was 0.71 g $C \cdot MJ^{-1}$ of IPAR, also in the range of results found in this study. The same result 0.71 g $C \cdot MJ^{-1}$ of IPAR was also found in Lagergren et al. (2005) for a mixed conifer forest in Sweden.

The results of this study indicate that variability in LUE can be strongly affected by severe drought and wet years within jack pine of varying ages (Figure 2.4). Similar results have been found in Pereira et al. (2007) within Mediterranean ecosystems (oak, eucalyptus, and grassland) and Allen et al. (2004) within irrigated and non-irrigated sweetgum and sycamore stands. Pereira et al. (2007) found that drought caused reduction in photosynthesis as a result of seasonal water deficits and elevated light and T_{air}. They also mention that ground plants with shallow root systems die during droughts, and Re is less affected than carbon uptake. Phillips and Riha (1993) suggest that drought might cause increased partitioning of biomass to roots, thereby causing a reduction in LUE within older ecosystems. When GPP and Re were compared at the jack pine sites, during drought and wet years, we found that the magnitude of GPP and Re reductions were dependent on age. For example, at OJP, GPP in 2003 is reduced by 8% and Re by 7% from 2002

cumulative values. However, in HJP94, GPP was reduced by 5% and Re by 17% between years 2002 and 2003.

2.7.2 Environmental Influences on LUE

The influences of diffuse vs. direct radiation had clear but varied influences on LUE at jack pine stands of different ages. Other studies have found that diffuse radiation and the lack of within canopy shadows significantly increased LUE (e.g. Roderick et al. 2001, Gu et al. 2002, Still et al. 2004, Turner et al. 2003, Schwalm et al. 2006, Jenkins et al. 2007, Pereira et al. 2007). Positive relationships between LUE and increased diffuse vs. direct radiation have not been examined within different ages of the same species. Increased LUE occurs during cloudy conditions because more light is scattered and distributed within the canopy (Gu et al. 2002). Direct illumination of the canopy results in saturation of photosynthesis, whereas the remaining portion of the canopy (not saturated by sun flecks) is in shadow and is not able to photosynthesize efficiently (Gu et al. 2002). In this study, we have shown that the decrease of LUE between cloudy (diffuse) to partly cloudy radiation conditions is greater than from partly cloudy to sunny (direct) conditions at different ages of jack pine sites studied. This result agrees with that of Jenkins et al. (2007) who state that when the ratio of diffuse to total radiation is high, the efficiency for photosynthesis will also be great, and will increase linearly to a point where the sky is diffuse, but bright (before direct sunlight breaks through the clouds). However, as uniform cloud cover decreases and direct radiation conditions increase, LUE will decrease and the rate of photosynthesis will peak (Gu et al. 2002, Turner et al. 2003, Schwalm et al. 2006).

The transition of LUE from diffuse to direct light conditions tended to be great at OJP and HJP75, possibly due to slight shadowing within these open and low LAI canopies. LUE at HJP94 was

less influenced by direct and diffuse radiation conditions than at OJP and HJP75, although light conditions did have a significant influence on LUE. By observation, the canopy at HJP94 does not intersect in many parts of the site and trees often had branches extending to the ground surface. Needles were located on the outer envelope of individual trees. HJP02 tended to be most affected by diffuse vs. direct conditions out of all sites studied, and also had the greatest variability in LUE. In 2005, HJP02 consisted of small jack pine seedlings, alder (*Alnus crispa* Ait.) shrubs and a ground cover of herbs and grasses. Without any shadows, saturation of photosynthesis in combination with increased T_{air} and VPD occurred almost immediately with direct radiation. The linear increase of GPP with APAR, described by a light response curve, was almost non-existent (Figure 2.5d), possibly resulting in strong differences between LUE during cloudy as opposed to partly cloudy conditions.

Meteorological driving mechanism influences on LUE also varied between different jack pine sites and ages. VPD tended to have the greatest influence on LUE at most sites studied but was less important at HJP75. This may be due to increased leaf area, tree density, and increased within canopy shadowing, as well as decreased roughness. Gu et al. (2002) found that VPD and T_{air} tended to have varying influences on vegetation photosynthesis during different radiation conditions, possibly as a result of upper canopy as opposed to lower canopy leaf temperature. For example, during direct radiation conditions, upper leaves may have higher temperatures and may experience greater VPD than lower leaves, which are in shadow. These results also correspond with those of Turner et al. (2003) within several biomes; a mixed conifer forest in Lagergren et al. (2005); and within several forest types in Gu et al. (2002). VPD also co-varied with T_{air}, relative humidity (RH), and latent energy exchanges (LE), which explained much of the variability in LUE at numerous sites in Schwalm et al. (2006). Jenkins et al. (2007) found a lack of

correspondence between LUE and VPD and T_{air} at a northern hardwood stand. VPD and/or T_{air} influences on LUE may become more important within moisture deficient forest such as the boreal jack pine forests used in this study. Average daily θ had little influence on daily estimates of LUE (except at HJP94, where it has a stronger influence, r^2 = 0.20). When averaged over the growing season at each site, θ tends to have a strong influence on the seasonal variability of LUE. Schwalm et al. (2006) found that soil moisture had a moderate influence on LUE at three mature deciduous sites and two regenerating forests, including HJP02, whereas Kljun et al. (2006) found almost an immediate response of CO_2 fluxes to θ at a mature aspen site.

The use of LUE, especially within remote sensing-based production efficiency models, would benefit from the inclusion of daily diffuse and direct LUE. Currently MODIS GPP algorithms estimate eight-day cumulative GPP from average fPAR multiplied by a maximum LUE term that is adjusted based on very high VPD and low T_{air}. Over the four years of study, 29% of days were cloudy, 50% were partly sunny, and 21% of days were sunny, resulting in large differences in LUE during those days. The use of an average biome-specific LUE may improve estimates of GPP by either increasing or decreasing LUE relative to the amount of cloud cover and diffuse radiation on a per day basis, and cumulated over the eight-day composited period.

2.8 Conclusions

In this study, CO_2 fluxes and LUE were examined over a unique period of drought, normal and wet conditions within a jack pine chronosequence in Saskatchewan, Canada. The purpose of the study was to determine meteorological and site-specific controls on LUE during years of severe drought and wet conditions. The efficiency at which vegetation uses light may change with increased air temperatures and drying, which may be one outcome of climatic change within the

Canadian boreal forest (Kljun et al. 2006). The ability to characterize changes in LUE and vegetation productivity, especially using remote sensing-based production efficiency models, is of importance. This study found that significant differences in LUE occurred at OJP, HJP75 and HJP94 during the drought of 2003, likely as a result of decreased average θ. LUE was not greatly affected by drought and wet conditions at HJP02, but NEP did vary between the years studied. Cumulative CO_2 fluxes (GPP, NEP, and Re) did not vary greatly at OJP between drought and wet years. Despite this, an early spring in 2003 resulted in early leaf flush and increased productivity before the effects of mid-summer soil drying were felt. Similar variability in fluxes were also found at HJP94, where GPP tended to be greater in 2003 during the early part of the growing season, but was reduced compared with other years towards the end of the growing season. GPP and Re tended to be lower at all sites in 2004, perhaps in response to the previous years drought, as well cooler growing season T_{air}. During 2004, leaf growth rates were significantly reduced at HJP94, and in 2005, leaf foliage cover was less than in 2004, despite typical rapid regeneration of this young site. Daily average VPD had the greatest influence on the variability of LUE at all sites, whereas daily θ did not greatly affect LUE. Diffuse vs. direct radiation conditions also had large but varying influences on LUE at different sites, depending on canopy structural characteristics. Differences between cloudy and partly sunny/sunny conditions were greatest at HJP02, possibly due to almost immediate saturation of GPP with increased PAR. OJP and HJP75 were also subject to large differences LUE during cloudy and partly sunny conditions, likely as a result of some within-canopy shadowing. These results suggest that the inclusion of radiation conditions (e.g. diffuse vs. direct) in the calculation of LUE would improve remote-sensing estimates of GPP from MODIS.

2.9 Acknowledgements

We would like to thank the Fluxnet-Canada Research Network and the Boreal Ecosystem Research and Monitoring Sites (BERMS) Project and all those individuals involved for collection and processing of flux data. Field data collection was performed with the aid of Chris Hopkinson, Bruce Davison, Chris Beasy, and Jordan Erker. Also, thank-you to the late Werner Bauer (site manager) for his help and support. Two anonymous reviewers are thanked for their comments and help on the manuscript, and Sonia Wharton is acknowledged for her suggestions. Funding for this project has been provided by CFCAS, NSERC, the BIOCAP Canada Foundation, and the Climate Research Division of Environment Canada. Laura has been generously supported by graduate student scholarships from NSERC and OGSST.

2.10 References

Ahl, D.E., S. Gower, D.S. Mackay, S. N. Burrows, J. M. Norman and G.R. Diak. 2004. Heterogeneity of light use efficiency in a northern Wisconsin forest: implications for modeling net primary production with remote sensing. *Remote Sensing of Environment.* 93:168-178.

Allen, C.B., R. Will, R. McGarvey, D. Coyle and M. Coleman. 2004. Radiation-use efficiency and gas exchange responses to water and nutrient availability in irrigated and fertilized stands of sweetgum and sycamore. *Tree Physiology.* 25:191-200.

Baldocchi, D.D., C.A. Vogel and B. Hall 1997a. Seasonal variation of energy and water vapor exchange rates above and below a boreal jack pine forest canopy. *Journal of Geophysical Research.* 102(D24):28,939-28,951.

Baldocchi, D.D., C.A. Vogel and B. Hall. 1997b. Seasonal variation of carbon dioxide exchange rates above and below a boreal jack pine forest. *Agricultural and Forest Meteorology.* 83:147-170.

Barr, A.G. K. Morgenstern, T.A. Black, J.H. McCaughey and Z. Nesic. 2006. Surface energy balance closure by the eddy-covariance method above three boreal forest stands and implications for the measurement of the CO_2 flux. *Agricultural and Forest Meteorology.* 140:322-337.

Barr, A.G., T.A. Black, E.H. Hogg, N. Kljun, K. Morgenstern and Z. Nesic. 2004. Inter-annual variability in the leaf area index of a boreal aspen-hazelnut forest in relation to net ecosystem production. *Agricultural and Forest Meteorology.* 126:237-255.

Bird, R.E. and R.L Hulstrom. 1991. A simplified clear sky model for direct and diffuse insolation on horizontal surfaces. *SERI Technical Report SERI/TR-642-761*, February, Solar Energy Research Institute, Golden CO.

Bradford, J.B., J.A. Hicke. and W.K. Lauenroth. 2005. The relative importance of light-use efficiency modifications from environmental conditions and cultivation for estimation of large-scale net primary productivity. *Remote Sensing of Environment.* 96:246-255.

Chasmer, L., N. Kljun, A. Barr, A. Black, C. Hopkinson, H. McCaughey and P. Treitz. Vegetation structural and elevation influences on CO_2 uptake and respiration within a mature jack pine forest in Saskatchewan, Canada. *Canadian Journal of Forest Research (accepted).*

Chen, J.M., A. Govind, O. Sonnentag, Y. Zhang, A. Barr and B. Amiro. 2006. Leaf area index measurements at Fluxnet-Canada forest sites. *Agricultural and Forest Meteorology*. 140:257-268.

Chen, J.M. 1996. Canopy architecture and remote sensing of the fraction of photosynthetically active radiation absorbed by boreal conifer forests. *IEEE Transactions on Geoscience and Remote Sensing*. 34(6):1353-1368.

Coursolle, C., H.A. Margolis, A.G. Barr, T.A. Black, B.D. Amiro, J.H. McCaughey, L.B. Flanagan, P.M. Lafleur, N.T. Roulet, C. P.-A. Bourque, M.A. Arain, S.C. Wofsy, A. Dunn, K. Morgenstern, A.L. Orchansky, P.Y. Bernier, J.M. Chen, J. Kidston, N. Saigusa and N. Hedstrom. 2006. Late-summer carbon fluxes from Canadian forests and peatlands along an east-west continental transect. *Canadian Journal of Forest Research.* 36:783-800.

Dewar, R.C., B.E. Medlyn and R.E. McMurtrie. 1998. A mechanistic analysis of light and carbon use efficiencies. *Plant, Cell and Environment.* 21:573-588.

Drolet, G.G., K.F. Huemmrich, F.G. Hall, E.M. Middleton, T.A. Black, A.G. Barr and H.A. Margolis. 2005. A MODIS-derived photochemical reflectance index to detect inter-annual variations in the photosynthetic light-use efficiency of a boreal deciduous forest. *Remote Sensing of Environment.* 98:212-224.

Ebdon, D. 1992. Statistics in Geography, 2nd Edition, Oxford, Alden Press. 232 pgs.

Euskirchen, E.S., K. Pregitzer and J. Chen. 2006. Carbon fluxes in a young, naturally regenerating jack pine ecosystem. *Journal of Geophysical Research.* 111:D01101.

Goetz S.J. and S.D. Prince. 1996. Remote sensing of net primary production in boreal forest stands. *Agricultural and Forest Meteorology.* 78:149-179.

Gower, S.T., J.G. Vogel, J.M. Norman, C.J. Kucharik, S.J. Stelle and T.K. Stow. 1997. Carbon distribution and aboveground net primary production in aspen, jack pine, and black spruce stands in Saskatchewan and Manitoba, Canada. *Journal of Geophysical Research.* 102(D24):29,029-29,041.

Gower, S.T., C. J. Kucharik and J.M. Norman. 1999. Direct and indirect estimation of leaf area index, f_{APAR}, and net primary production of terrestrial ecosystems. *Remote Sensing of Environment.*70:29-51.

Green, S.D., E. Kruger, G. Stanosz and G. Isebrands. 2001. Light-use efficiency of native and hybrid poplar genotypes at high levels of intracanopy competition. *Canadian Journal of Forest Research.* 31:1030-1037.

Green, S.D., J.E. Erickson and E. Kruger. 2003. Foliar morphology and canopy nitrogen as predictors of light-use efficiency in terrestrial vegetation. *Agricultural and Forest Meteorology.* 115:163-171.

Gu, L., D. Baldocchi, S. Verma, T.A. Black, T. Vesala, E. Falge and P. Dowty. 2002. Advantages of diffuse radiation for terrestrial ecosystem productivity. *Journal of Geophysical Reseearch.* 107(D6), 4050.

Heinsch, F.A., M. Zhao, S.W. Running, J.S. Kimball, R.R. Nemani, K.J. Davis, P.V. Bolstad, B.D. Cook, A.R. Desai, D.M. Ricciuto, B.E. Law, W.C. Oechel, H.Luo, S.C. Wofsy, A.L. Dunn, J.W. Munger, D.D. Baldocchi, L. Xu, D.Y. Hollinger, A.D. Richardson, P.C. Stoy, M.B.S. Siqueira, R.K. Monson, S.P. Burns and L.B. Flanagan. 2006. Evaluation of remote sensing based terrestrial productivity from MODIS using regional tower eddy flux network observations. *IEEE Transactions on Geoscience and Remote Sensing.* 44(7):1908-1925.

Jenkins, J.P., A.D. Richardson, B.H. Braswell, S.V. Ollinger, D.Y. Hollinger and M.-L. Smith. 2007. Refining light-use efficiency calculations for a deciduous forest canopy using simultaneous tower-based carbon flux and radiometric measurements. *Agricultural and Forest Meteorology.* 143-64-79.

Kljun, N., T.A. Black, T.J. Griffis, A.G. Barr, D. Gaumont-Guay, K. Morgenstern, J.H. McCaughey and Z. Nesic. 2006. Response of net ecosystem productivity of three boreal forest stands to drought, 2006. *Ecosystems*. 9:1128-1144.

Lagergren, F., L. Eklundh, A. Grelle, M. Lundblad, M. Molder, H. Lankreijer and A. Lindroth. 2005. Net primary production and light use efficiency in a mixed conifer forest in Sweden. *Plant, Cell, and Environment.* 28:412-423.

Leblanc, S. G., J. M. Chen, R. Fernandes, D. W. Deering and A. Conley. 2005. Methodology comparison for canopy structure parameters extraction from digital hemispherical photography in boreal forests. *Agricultural and Forest Meteorology*, 129:187-207.

Leuning, R., H.A. Cleugh, S.J. Zegelin and D. Hughes. 2005. Carbon and water fluxes over a temperate *Eucalyptus* forest and a tropical wet/dry savanna in Australia: measurements and comparison with MODIS remote sensing estimates. *Agricultural and Forest Meteorology.* 129:151-173.

Lovett, G.M., J. Cole and M. Pace. 2006. Is net ecosystem production equal to ecosystem carbon accumulation? *Ecosystems*. 9:1-4.

Martin, T.A. and E.J. Jokela. 2004. Developmental patterns and nutrition impact radiation use efficiency components in southern pine stands. *Ecological Applications.* 14(6):1839-1854.

Massman, W.J. and X. Lee. 2002. Eddy covariance flux corrections and uncertainties in long term studies of carbon and energy exchange. *Agricultural and Forest Meteorology.* 113:121-144.

McCrady, R.L. and E. Jokela. 1998. Canopy dynamics, light interception and radiation use efficiency of selected loblolly pine families. *Forest Science.* 44:64-72.

Monteith, J.L. 1972. Solar radiation and productivity in tropical ecosystems. *Jounal of Applied Ecology.* 9:747-766.

Nichol, C.J., K. F. Huemmrich, T.A. Black, P. G. Jarvis, C.L. Walthall, J. Grace, and F.G. Hall. 2000. Remote sensing of photosynthetic-light-use efficiency of boreal forest. *Agricultural and Forest Meteorology.* 101:131-142.

O'Connell, K.E., S. Gower and J. Norman. 2003. Comparison of net primary production and light-use dynamics of two boreal black spruce forest communities. *Ecosystems.* 6:236-247.

Pereira, J.S., J.A. Mateus, L.M. Aires, G. Pita, C. Pio, J.S. David, V. Andrade, J. Banza, T.S. David. T.A. Paco and A. Rodrigues. 2007. Net ecosystem carbon exchange in three contrasting Mediterranean ecosystems – the effect of drought. *Biogeosciences.* 4:791-802.

Phillips, J.G. and S.J Riha. 1993. Canopy development and solar conversion efficiency in *Acadia auriculiformis* under drought stress. *Tree Physiology.* 12:137-149.

Roderick, M.L., G.D. Farquhar, S.L. Berry and I.R. Noble. 2001. On the direct effect of clouds and atmospheric particles on the productivity and structure of vegetation. *Oecologia*. 129:21-30.

Ruimy, A., G. Dedieu and B. Saugier. 1994. Methodology of the estimation of terrestrial net primary production from remotely sensed data. *Journal of Geophysical Research.* 99:5263-5283.

Ruimy, A., L. Kergoat, A. Bondeau and participants of the Potsdam NPP model intercomparison. 1999. Comparing global models of terrestrial net primary productivity (NPP): analysis of differences in light absorption and light-use efficiency. *Global Change Biology.* 5(51):56-64.

Running, S.W., R. Nemani, J. Glassy and P. Thornton. 1999. MODIS daily photosynthesis (Psn) and annual net primary production (NPP) product (MOD17). Theoretical basis document, Version 3. NASA Goddard Space Flight Center, Greenbelt, MD 20771, USA. Available online: http://modis.gsfc.nasa.gov/data/atbd/atbd_mod17.pdf.

Running, S. W., R. R. Nemani, F. A. Heinsch, M. Zhao, M.C. Reeves and H. Hashimoto. 2004. A continuous satellite-derived measure of global terrestrial primary production. *BioScience.* 54:547-560.

Schwalm, C.R., T.A. Black, B.D. Amiro, M.A. Arain, A.G. Barr, C.P.-A. Bourque, A.L. Dunn, L.B. Flanagan, M.-A. Giasson, P.M. Lafleur, H.A. Margolis, J.H. McCaughey, A.L. Orchansky and S.C. Wofsy. 2006. Photosynthetic light use efficiency of three biomes across an east-west continental-scale transect in Canada. *Agricultural and Forest Meteorology.* 140:269-286.

Still, C.J., J. Randerson and I. Fung. 2004. Large-scale plant light-use efficiency inferred from the seasonal cycle of atmospheric CO_2. *Global Change Biology.* 10:1240-1252.

Turner, D.P., S.T. Gower, W.B. Cohen, M. Gregory and T.K. Maiersperger. 2002. Effects of spatial variability in light use efficiency on satellite-based NPP monitoring. *Remote Sensing of Environment.* 80:397-405.

Turner, D.P., S. Urbanski, D. Bremer, S.C. Wofsy, T. Meyers, S.T. Gower and M. Gregory. 2003. A cross-biome comparison of daily light use efficiency for gross primary production. *Global Change Biology.* 9:383-395

Turner, D.P., W.D. Ritts, W.B. Cohen, S.T. Gower, S. W. Running, M. Zhao, M. H. Costa, A. A. Kirschbaum, J.M. Ham, S.R. Saleska and D.E. Ahl. 2006. Evaluation of MODIS NPP and GPP products across multiple biomes. *Remote Sensing of Environment.* 102:282-292.

Waring, R.H., B.E. Law, M. Goulden, S. Bassow, R. McCreight, S. Wofsy and F. Bazzaz. 1995. Scaling gross ecosystem production at Harvard Forest with remote sensing: a comparison of estimates from a constrained quantum-use efficiency model and eddy correlation. *Plant, Cell and Environment*. 18:1201-1213.

Wilson, T.B., and T. P. Meyers. 2007. Determining vegetation indices from solar and photosynthetically active radiation fluxes. *Agricultural and Forest Meteorology*. 144:160-179.

Yuan, W., S. Liu, G. Zhou, G. Zhou, L. Tieszen, D. Baldocchi, C. Bernhofer, H. Gholz, A. Goldstein, M. Goulden, D. Hollinger, Y. Hu, B. Law, P. Stoy, T. Vesala, S. Wofsy and others. 2007. Deriving a light use efficiency model from eddy covariance flux data for predicting daily gross primary production across biomes. *Agricultural and Forest Meteorology*. 143:189-207.

Zhang, Y., J. Chen and J. Miller. 2005. Determining digital hemispherical photograph exposure for leaf area index estimation. *Agricultural and Forest Meteorology*. 133:166-181.

Zhao, M., F.A. Heinsch, R. Nemani and S.W. Running. 2005. Improvements of the MODIS terrestrial gross and net primary production global data set. *Remote Sensing of Environment*. 95:164-176.

Chapter 3

Vegetation Structural and Ground Elevation Influences on CO_2 Uptake within a Mature Jack Pine Forest in Saskatchewan, Canada

3.1 Abstract

Carbon dioxide, water vapour, and energy fluxes vary spatially and temporally within forested environments. However, it is not clear to what extent they vary as a result of variability in biomass and elevation gradients. The following study presents a new methodology for extracting structural vegetation characteristics and elevation changes within footprints, for direct comparison with eddy covariance (EC) CO_2 flux concentrations. The purpose was to determine if within-site canopy structure and local elevation influenced CO_2 fluxes in a mature jack pine forest located in Saskatchewan, Canada. Airborne light detection and ranging (lidar) was used to extract tree height, canopy depth, foliage cover and elevation within 30-minute flux footprints. Within-footprint average structural components and elevation were related to 30-minute average net ecosystem productivity (NEP) and gross ecosystem production (GEP).

NEP and GEP were modeled using multiple regression and, when compared with measured fluxes, almost all periods showed improvements in the prediction of flux concentration when canopy structure and elevation were included. Increased biomass was related to increased NEP and GEP in June and August when the ecosystem was not limited by soil moisture. On a daily basis, fractional cover and elevation had varying but significant influences on CO_2 fluxes.

3.2 Introduction

The eddy covariance (EC) method is commonly used to measure the direction and movement of energy and trace gas (e.g. water, CO_2) concentrations throughout ecosystems (Baldocchi, 2008). Networks of EC systems have been set up at local, biome, continental and global scales based loosely on the idea that individual nodes are representative of larger ecosystems. These are then sometimes combined with remote sensing data and ecosystem models to determine spatial and temporal variability of CO_2 exchanges within areas that have undergone some prior disturbance (e.g. land management, extreme weather, insect infestation, fire, etc.), and within different stand ages, species types, and in areas of complex terrain (e.g. Heinsch et al. 2006).

Spatial heterogeneity in canopy structure and elevation may be an important consideration when measuring CO_2 and water fluxes, especially if wind directions do not vary. If the ecosystem is homogeneous, apart from other driving mechanisms, the location of the flux origin should not be important because it would not matter where the winds were originating from. There would be little variability in flux concentration resulting from the relatively similar characteristics of the ecosystem in all directions. However, if the ecosystem is spatially variable, then flux concentrations may vary depending on spatial location and winds originating from dominant directions (Rahman et al. 2001; Chen et al. 2008). In many ecosystems, spatial variations in the availability of soil nutrients and moisture are manifested in the variability of above-ground biomass and exchanges measured by EC (Baldocchi and Meyers, 1998; Griffis et al. 2003). If differences in the amount of CO_2 sequestration can be found between ecosystems, then is it true that areas of greater and lesser amounts of biomass may also affect CO_2 and water exchanges within a single ecosystem?

Few studies have directly examined the influence of structural and elevation heterogeneity on fluxes within a single ecosystem (Kim et al. 2006; Chen et al. 2008). Until recently, it has been difficult to spatially measure three-dimensional vegetation structure and ground surface elevation at high resolutions. Airborne light detection and ranging (lidar) is an active remote sensing technology that is used to measure canopy structure and ground surface elevation at high resolution. A footprint model may then be used to discretize the variability in canopy biomass and elevation at a particular place and time, which can then be correlated with trace gas exchanges measured by EC. The footprint model determines the probability that fluxes originated from a particular place within the ecosystem based on measured atmospheric turbulence (e.g., Foken and Leclerc, 2004; Vesala et al. 2008). Each footprint, therefore, contains the extent in x and y coordinates of the source/sink area and a probability (probability density function [PDF]) that the CO_2 source/sink at x/y will be measured at the sensor.

In this study, vegetation structure and elevation were characterized using lidar within the contours of half-hourly flux footprint areas (approximately 80% of the probability of flux) from Kljun et al. (2004). The objective was to quantify the influences of vegetation structure and elevation on CO_2 concentrations measured by EC, specifically net ecosystem production (NEP) and gross ecosystem production (GEP). Three growing season periods were examined in 2002 at a mature jack pine site in Saskatchewan, Canada.

3.3 Methods

3.3.1 Study Area and Site Characteristics

The study area consists of a mature jack pine (*Pinus banksiana* Lamb.) (OJP) forest of approximately 90 years old (Baldocchi et al. 1997) located near the southern edge of the boreal

forest (520230 E, 5974262 N), Saskatchewan Canada. The ground elevation varies between 482 m and 494 m throughout the 1000 m radius surrounding the EC flux measurement tower, and tree heights vary by up to 6 m (Figure 3.1a and b). The understory is comprised of lichens (*Cladina* spp.), bearberry (*Arctostaphylos uva-ursi* L.), cranberry (*Vaccinium vitisideae* L.) and sparse groupings of alder (*Alnus crispa* Ait.). Soils within the site are coarse and well-drained sand with low nitrogen content (Baldocchi et al. 1997). Measurements of forest structure (e.g. canopy height) within eight geo-located forest mensuration plots were used to validate lidar canopy structural attributes within the ecosystem (Table 3.1).

Table 3.1. Average structural vegetation characteristics measured at eight plots surrounding the flux measurement station at the jack pine site.

Plot #	Northing Coordinate (Zone 13) (m)	Easting Coordinate (m)	Elevation (m)	DBH* (cm)	Tree height (m)	Canopy depth = height – base (m)	LAIe** (m^2m^{-2})	Stem density (m^{-1})	Alder density (m^{-1})
1	520238.8	5974368.1	494.3	15.9	15.0	6.3	1.50	0.12	0.03
2	520224.5	5974155.5	495.1	14.6	13.6	6.1	1.45	0.08	0
3	520130.9	5974261.7	494.1	11.7	13.0	5.9	1.49	0.17	0
4	520365.4	5974259.0	492.5	12.9	13.3	5.2	1.55	0.15	0
5	520623.3	5974564.0	489.5	17.5	15.7	8.8	1.82	0.09	0.03
6	519813.4	5973981.9	491.9	16.1	14.9	8.1	1.52	0.10	0.02
7	520430.5	5973784.2	487.0	11.8	11.4	6.2	1.21	0.14	0
8	520012.7	5974728.1	492.4	23.6	16.4	11.2	1.49	0.04	0.47

*DBH = diameter at breast height; ** LAIe = effective leaf area index

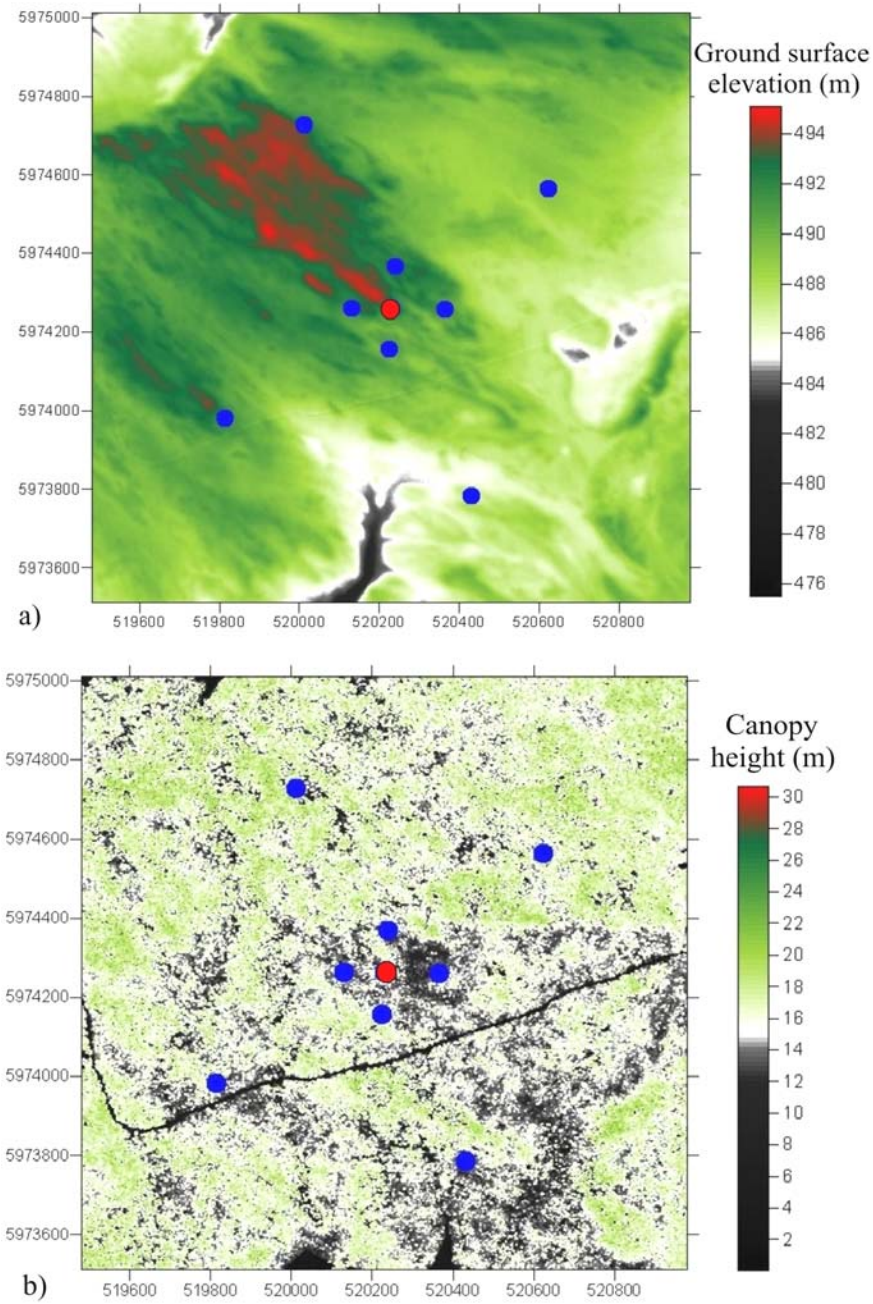

Figure 3.1. a) Lidar measured ground surface elevation within 750 m of the flux station with removal of understory and canopy vegetation. b) Lidar measured canopy heights within 750 m of the flux station after removal of topographical influences. Blue circles represent the location of 11.3 m radius measurement plots and the red circle represents the location of the EC flux tower (centre). Laser returns have been rasterized to produce a continuous surface digital elevation model (DEM) (a) of the ground returns and a canopy height model (CHM) of the maximum z returns (b).

3.3.2 Canopy Structure Measurements

Mensuration data (Table 3.1) were collected over two periods, May 9 to 16 and July 25 to August 15, 2005. Plot locations were selected for spatial representation according to compass cardinal directions at distances of 100 m (May field campaign), and 500 m (July/August field campaign) from the flux measurement station. Each plot has a radius of 11.3 m and follows Fluxnet-Canada protocols for measurements (Fluxnet-Canada, 2003). Plot location, tree height, base of live crown height, diameter at breast height, gap fraction, and effective LAI (LAIe) were measured at each plot. Alder were also counted and measured for height and crown diameter in each cardinal direction. Plots were located at the centre using survey-grade, differentially corrected global positioning system (GPS) receivers (Leica SR530, Leica Geosystems Inc. Switzerland; Ashtec Locus, Ashtec Inc., Hicksville, NY) with the same base station coordinate as was used for the lidar survey. Geo-location accuracies varied from 1 cm to 1 m depending on the canopy cover density at time of GPS data collection. Plots were geo-located so that lidar data could be directly compared with plot averages and individual tree measurements.

Canopy gap fraction was determined from digital hemispherical photography (DHP) at five locations within each plot (north, south, east, west, and centre), at distances of 11.3 m apart. All photographs were taken during either diffuse daytime conditions, or 30 minutes before dawn or after dusk to reduce the influence of sun brightness and apparent leaf reduction within the photograph (Zhang et al. 2005). Photographs were exposed to two f-stops below automatic exposure (normally set between one and four exposure settings and with larger aperture) (Chen et al. 2006). Each individual photograph was processed following sky and vegetation thresholding methods of Leblanc et al. (2005) to obtain estimates of gap fraction and fractional cover (1-gap

fraction). DHP version 1.6.1 software was used to process all photographs (S. Leblanc, Canada Centre for Remote Sensing provided to the Fluxnet-Canada Research Network).

Average DHP measurements slightly underestimated LAIe by 14% and 11% when compared with TRAC and LiCOR LAI-2000 transect methods in Chen et al. (2006) at the same site. It is likely that ecosystem heterogeneity, and technological differences between optical measurements of Chen et al. (2006) and DHP resulted in variability between LAIe estimates. Despite differences in LAIe when compared with Chen et al. (2006), our estimates provide reasonably close approximation of LAIe and, more importantly, are indicative of relative differences in canopy fractional cover using lidar.

3.3.3 Flux Measurements

Meteorological, CO_2 and H_2O flux measurements at OJP have been collected for 30-minute periods each day since 1999 (Griffis et al. 2003; Barr et al. 2006) and previously in 1994 during the Boreal Ecosystem-Atmosphere Study (BOREAS) (Middleton et al. 1997; Goetz et al. 1999). Three periods of five, nine, and seven days of flux and meteorological data were examined during the 2002 growing season when EC data were available. The selected periods occurred from June 10 to 15 (P1), July 5 to 13 (P2) and August 7 to 13 (P3), shown in Figure 3.2 with precipitation. These periods (and numbers of days) were chosen a) to coincide with dry periods during which little to no rainfall occurred; and b) so that the influence of three varying soil moisture regimes could be examined. Average tree height growth since BOREAS (1994 to 1996) was approximately 1 m over an 11-year period from measurements made during field campaigns in 1994 and those made in 2005 (Gower et al. 1997). Differences in canopy height between summer 2002 (flux measurements) and summer 2005 (field campaigns and lidar data collection) varied by less than 30 cm and were within the range of error of the lidar system.

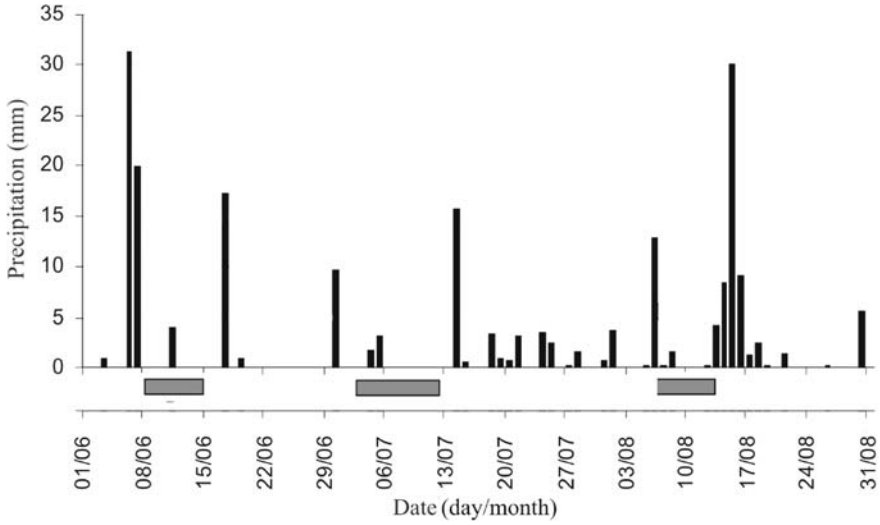

Figure 3.2. Precipitation (mm) recorded at OJP and during the growing season, 2002. Grey rectangles mark the duration of the three periods of study. Total cumulative precipitation in 2002 is ~410 mm, which is the 30-year normal precipitation for this area, but is the second consecutive drought year in western Canada (Kljun et al. 2006).

Meteorological and flux measurements made at OJP are described in detail in Barr et al. (2006) and Kljun et al. (2006). Briefly, above-canopy CO_2 fluxes were measured at approximately 28 m above the ground surface using the EC method at 20 Hz and aggregated over 30-minute periods. A sonic anemometer (CSAT3, Campbell Scientific Inc. Edmonton, Alberta, Canada) and closed-path infrared gas analyzer (LI-6262, LI-COR Biosciences Inc., Lincoln, Nebraska) were used to measure friction velocity and atmospheric CO_2. Net ecosystem exchange (NEE) ($\mu mol \cdot m^{-2} \cdot s^{-1}$) was measured by EC, where –NEE was equal to positive NEP ($\mu mol \cdot m^{-2} \cdot s^{-1}$). Positive NEP indicates that greater amounts of CO_2 were used in photosynthesis than were released via ecosystem respiration (Re). Daytime Re ($\mu mol \cdot m^{-2} \cdot s^{-1}$) was modeled from the relationship between nighttime Re and soil temperature (Barr et al. 2006). GEP ($\mu mol \cdot m^{-2} \cdot s^{-1}$), defined as the uptake of CO_2 by the ecosystem through photosynthesis, was estimated from measured NEP and modeled Re, where GEP = NEP + Re. A friction velocity threshold of greater than 0.35 m s^{-1} was

used to filter out periods when wind speeds were too low for accurate estimates of flux concentration.

Uncertainties in measuring CO_2 fluxes occur because, during calm and stable conditions, the transfer of CO_2 by non-turbulent exchanges are not detected by the EC system (Massman and Lee, 2002; Griffis et al. 2003). Early morning (before 0900 LST) and late afternoon (after 1700 LST) periods were not compared with canopy structure and site elevation because of the difficulty of measuring CO_2 storage in the air column below the EC sensors at that time (Yang et al. 1999). Nighttime fluxes have also been excluded because, during often stable nocturnal conditions, the footprint source area sometimes extended beyond the extent of the lidar dataset. Other issues associated with the accuracy of EC measurements include flux concentration loss due to a) instrument set up limitations, b) assumption of near neutral atmospheric stability; c) inability to consider the full complexity of EC equations; and d) 2D and 3D terrain influences (Massman and Lee, 2002). Average 24-hour energy balance closure for each day and each period was determined using the energy balance ratio method (e.g. Wilson et al. 2002). Average energy balance closure was ~88% (P1) (standard deviation (SD) = ~10%), ~83% (P2) (SD = ~8%), and ~85% (P3) (SD =~14%), calculated from net radiation (Rn), latent heat flux (Le), sensible heat flux (H), and soil heat flux (G). Barr et al. (2006) suggest that an energy balance correction may be applied to CO_2 fluxes, so that they are increased relative to the percentage that is under-estimated when unable to close the energy balance. This assumes that underestimation of energy fluxes are representative of underestimation of CO_2 fluxes. Based on this assumption, CO_2 fluxes have been corrected for underestimated energy fluxes and an inability to close the energy balance at OJP and other mature forest sites operated by Fluxnet-Canada (Canadian Carbon Program) at BERMS.

Meteorological variables were also examined to determine the influence of meteorology on flux exchanges prior to examining canopy structure and elevation effects. Measurements included above canopy incoming photosynthetically active radiation, PAR (μmol m^{-2} s^{-1}), relative humidity, RH (%), and air temperature, T_{air} (^{o}C) (model HMP45C, Vaisala by Campbell Scientific Inc. Edmonton Alberta, Canada), soil temperature, T_{soil} (^{o}C) (CS107b, Campbell Scientific Inc., Edmonton, Alberta), and volumetric soil moisture, θ (m^3 m^{-3}) (CS615, Campbell Scientific Inc., Edmonton, Alberta). Above canopy incoming and reflected PAR (μmol m^{-2} s^{-1}) and below-canopy incoming PAR (μmol m^{-2} s^{-1}) were measured using LI-COR model LI190 (LI-COR Biosciences, Nebraska, USA). θ was examined at depths of 30 to 60 cm, and T_{soil} was examined at depths of 10 cm. RH and T_{air} were examined above the canopy at a height of 16 m.

3.3.4 Lidar Data Collection and Processing

Lidar data were obtained at OJP on August 12, 2005 (Figure 3.1) using a scanning discrete pulse return system (ALTM3100, Optech Inc. North York, Ontario). The ALTM3100 is owned and operated by the Applied Geomatics Research Group, Nova Scotia. Up to four laser pulse reflections or "returns" were obtained per laser pulse emitted, at a rate of 71 kHz and at a flying height of 950 m above ground level (a.g.l.). The scan angle was set at ± 19° with 50% overlap of adjacent flight lines. This enabled penetration of laser pulses through to the base of the canopy, whilst also obtaining returns on all sides of individual trees (Chasmer et al. 2006). Cross-track and down-track resolutions, with 50 percent overlap of scans, were 35 cm ("post spacing", the distance between returns).

Percentile distributions were used to approximate average tree heights, base of live crown height and canopy depth (e.g. Lim and Treitz, 2004; Chasmer et al. 2006) within footprint PDF contour lines. Height and live canopy base height percentile distributions were calculated on individual

returns greater than or equal to 1.3 m above the ground surface so that returns from the ground surface would not influence and shift the percentiles downwards. Percentile distributions were also compared at mensuration plots to determine the most accurate and descriptive percentiles to adopt. The 90th and 8th percentiles were most appropriate for determining average tree heights and base of live crown height at the plot level. The resulting heights underestimated measured canopy heights by up to 0.94 m and overestimated the base of the live crown by up to 0.77 m when compared with plot-level averages. Canopy fractional cover (*f*cover) (where 1 = full canopy cover and 0 = no canopy cover) was determined from laser returns based on the ratio of the number of canopy returns to canopy and ground returns:

$$f\,\mathrm{cov}\,er = \left(\frac{\sum P_{canopy}}{\sum P_{all}} \right) \qquad [1]$$

where P_{canopy} is the total frequency of laser pulse returns within the canopy (≥ 1.3 m a.g.l.) and P_{all} is the total frequency of all laser pulse returns from the canopy and ground surface within each 1 m x 1 m x 30 m column. 1.3 m heights were chosen to capture the base of the canopy without inclusion of the understory, and also, because of the inability of the lidar to record multiple returns at heights within approximately 1.3 m of the ground. Morsdorf et al. (2006) indicate that *f*cover is an effective proxy indicator of variations in foliage density. A schematic diagram of the lidar structure classification is provided in Figure 3.3.

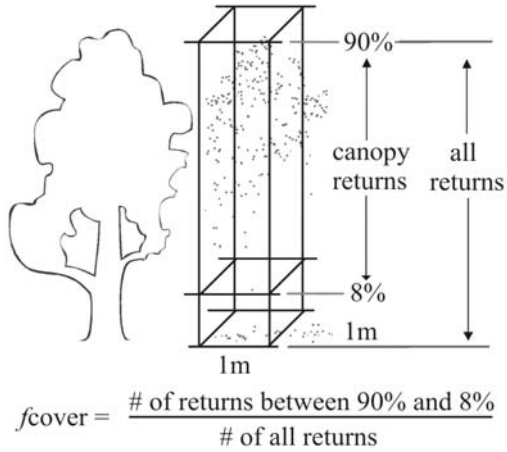

Figure 3.3. A schematic diagram of the distribution of laser returns within a tree and the methods used to differentiate canopy height (90th percentile), canopy base height (8th percentile), canopy depth (canopy height – canopy base height), and *f*cover within a 1 m x 1 m x z (height) column.

3.3.5 Footprint Data Analysis

The footprint parameterization used in this study follows that of Kljun et al. (2004). This parameterization was chosen because a) it is based on variables that are easy to derive from measurements obtained from EC; b) it is neither computationally difficult nor time-intensive; and c) it has been thoroughly applied and tested using a variety of meteorological (e.g. varying stability, roughness length, etc.) and technological (instrument measurement height) applications (Kljun et al. 2004).

The footprint parameterization allows for the derivation of the crosswind-integrated footprint ($\overline{f^y}$) based on the along-wind distance from the EC (x), the EC height (z_m), roughness length (z_0), and the height of the planetary boundary layer (H). Directionality and origin of the flux was determined from wind direction. Trace gas advection and diffusion was accounted for in the surface friction velocity (u_*), whereas buoyancy and the formation and size of eddies within the

planetary boundary layer were determined using the standard deviation of the vertical velocity (σ_w). Dispersion in the y direction (the cross-wind distance from the centre-line) was calculated using a Gaussian function (Amiro, 1998). Roughness length (z_0) at OJP has been estimated from Choudhury and Monteith, (1998) as:

$$z_0 = \begin{cases} z_{0s} + 0.28hX^{1/2} \ \ for\ 0 \le X \le 0.2 \\ 0.3h(1 - d/h)\ for\ 0.2 \le X \le 2 \end{cases} \qquad [2]$$

and

$$d = h\left[\ln\left(1 + X^{1/6}\right) + 0.031\ln\left(1 + X^{6}\right)\right], \qquad [3]$$

where $X = 0.2$ LAI (1.5 m^2 m^{-2} on average at OJP), h is the average height of the canopy, and z_{0s} is the soil surface roughness = ($0.10h_s$). h_s is the height of the understory (Shuttleworth and Wallace, 1985; Monteith and Unsworth, 1990), consisting mainly of sporadic and infrequently occurring alder and in many cases, footprints contained little to no understory. Therefore, h_s was assigned a value of zero. Finally, d is zero plane displacement. Therefore z_0 for OJP, using an average measured tree height of 14.2 m was 1.9 m, varied between 1.6 m and 2.2 m for shortest and tallest trees within measured plots (11.4 and 16.4 m, respectively). The location of maximum daytime flux varied between 176 m and 200 m from the flux tower for areas of smaller z_0 vs. areas of higher z_0 respectively, whereas the along wind distance may vary by as much as 50 m. Due to these slight variations in roughness length and minimal impact on footprint size, average z_0 for the entire site was based on average tree height.

Variable wind speed and boundary layer height also affect the length of the footprint (not shown), where increased u_* and decreased H results in footprints located nearer to the EC. Richardson

number (Ri) was used to determine approximate stability of the atmosphere (Monteith and Unsworth, 1990) based on air temperature and windspeed at 30-minute periods during relatively unstable conditions when u_* was >0.35 ms^{-1}:

$$Ri = (gT^{-1}\partial T_{air} / \partial z)/(\partial u / \partial z)^2, \qquad [4]$$

T is absolute temperature (K), g is gravitational acceleration (9.8 $m \cdot s^{-1}$), u is windspeed, and z is height. The generalized stability factor is calculated as:

$$F = (1 - 5Ri)^2 \qquad -0.1 \leq \mathrm{Ri} \leq 1 \qquad [5]$$

and

$$F = (1 - 16Ri)^{0.75} \qquad \mathrm{Ri} < -0.1. \qquad [6]$$

F was used to approximate H following tables in Gryning et al. (1987). The maximum along-wind and cross wind distances were used to estimate the area of the footprint and within footprint average canopy structure and elevation characteristics. Canopy structure and elevation were then correlated with 30-minute average CO_2 flux concentrations measured by EC.

3.3.6 Statistical Analysis

To determine if vegetation structure and elevation affect NEP and GEP, the combined influence of meteorological variables were first examined. Meteorological variables included incoming PAR, RH, T_{air}, T_{soil}, and θ. A Landsberg light response curve (Landsberg and Waring, 1997; Chen et al. 2002) was used to examine the relationship between incoming PAR and NEP (GEP) during individual periods:

$$NEP = P_{\max}(1 - e^{-a(PAR - I_{comp})}), \quad [7]$$

where $P_{\max}$ is the maximum average NEP (or GEP) at saturation, α is the slope of NEP (GEP) as it increases with incoming PAR, and I_{comp} is the light compensation point. The residuals of the measured vs. modeled flux ($NEP_{measured} - NEP_{modelled}$) were then examined to determine the remaining contribution of the most important meteorological variables (RH, T_{soil}, and θ) to the variability in the flux. This was done using a multiple linear regression (Chen et al. 2002). A linear regression was chosen because it was best able to describe the variability in the residuals. A second multiple linear regression was also performed to examine the combined influences of meteorological variables and the most important canopy structure (*f*cover) and elevation influences on the flux. Both multiple regression analyses were added (separately) to the $NEP_{modelled}$ and $GEP_{modelled}$ and compared with the measured NEP and GEP for each time period. Pearson's r correlation was used to determine the relative correspondence between flux concentration and meteorological driving variables, canopy structure, and elevation as a correlation matrix.

The influence of local meteorology was also assessed by relating wind direction to meteorological driving mechanisms during the periods of study. It could be argued that winds originating from particular directions may bring specific meteorological conditions (e.g. a north originating wind bringing cold air, a southern originating wind bringing warm air, changes in humidity from nearby lakes, etc.). These could affect the local meteorological driving mechanisms and photosynthesis. During the periods of study, it was found that wind direction had no influence on local meteorology. T_{air} ranged from ~5°C to 30°C, and a two-sample t-test confirms that T_{air} was un-related to the origin of wind ($r^2 = 0.04$, $p = 0.8$). Similarly, RH also had no relationship to wind direction (based on a two-sample t-test), and varied between ~20% and

100%, regardless of wind origin ($r^2 = 0.05$, $p = 0.72$). Therefore, it can be concluded that local weather conditions were not dependent on wind direction during the periods studied.

3.4 Results

3.4.1 Footprint Climatologies

Half-hourly filled footprint contour lines during three periods of study have been "overlaid" onto the CHM derived from lidar (Figure 3.4) to illustrate footprint directionality and location within the ecosystem. The main part of the footprint (containing 80% probability of flux) occurred within 500 m of the EC whereas footprint areas often extended to 1 km and beyond during stable conditions. Figure 3.5 illustrates the frequency of wind directions and flux origins throughout 2002 and during three periods of study. During 2002, approximately 45% of fluxes originated from areas northwest of the EC system. These areas are characterized by higher elevations, taller trees, and greater leaf area than the averages of the site (Table 3.2). Fluxes from the south-west (20%) and from the north-east (18%) originated from areas of average vegetation structure and elevation. 17% of winds originate from south-east quadrants, which typically have lower elevations, shorter trees, and lower leaf area. If winds originate from some directions more than others, the EC system may not be adequately sampling all of the within-site heterogeneity in fluxes. By comparison, during the three periods studied (Figure 3.5b), fluxes tended to come from fairly representative wind directions found in 2002. Sampling from most directions allowed for comparisons to be made from most parts of the ecosystem, bearing in mind that fluxes throughout the year most frequently originated from the northwest.

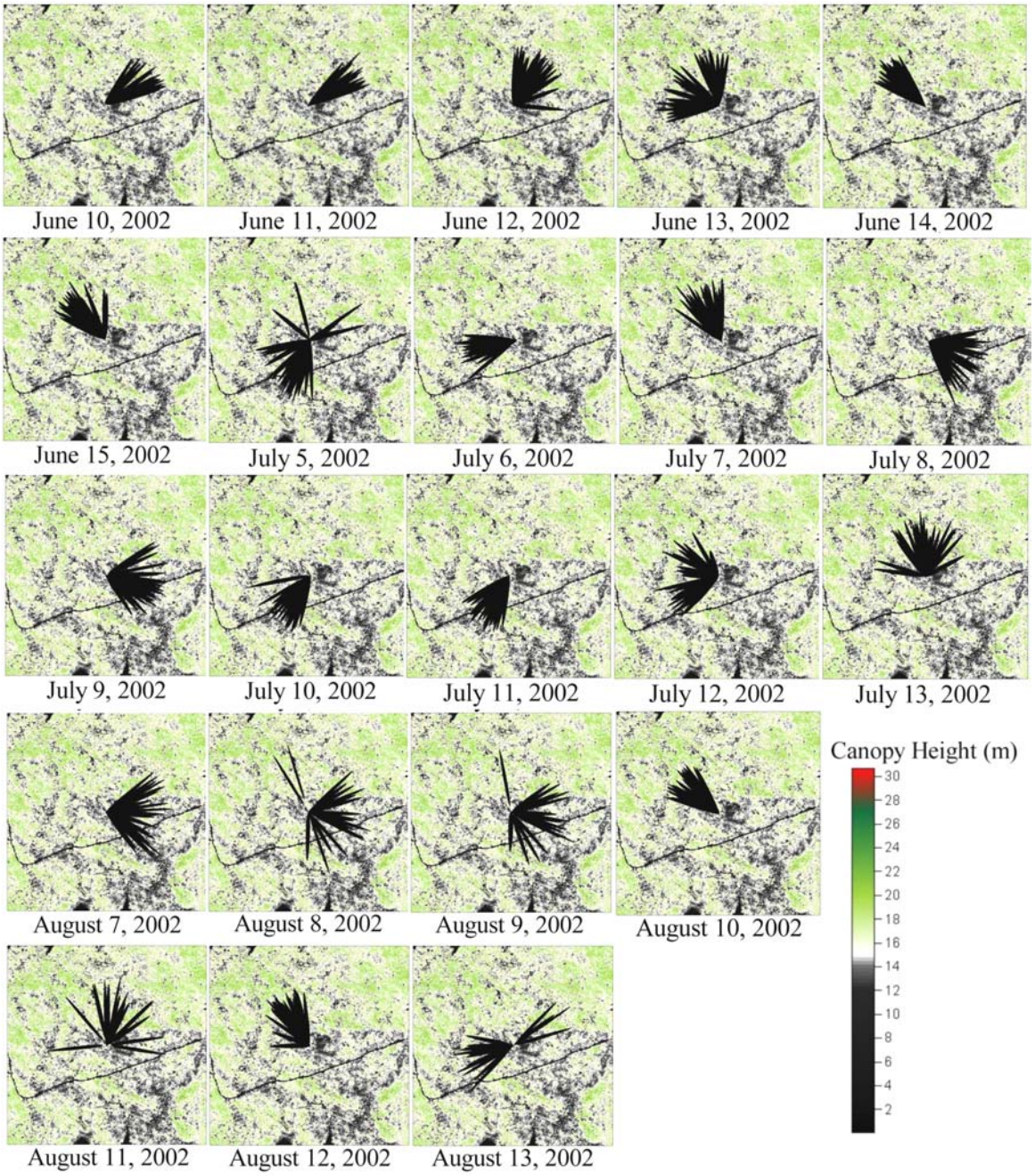

Figure 3.4. Daily 30-minute footprint extent (80% contour lines) and wind direction for the three periods of study are over-laid onto the OJP CHM (shown in Figure 3.1b) to illustrate variability in canopy height and associated footprint locations for daytime periods (0900 to 1700) (approximately 17 ½ hourly periods or 8.5 hours per day).

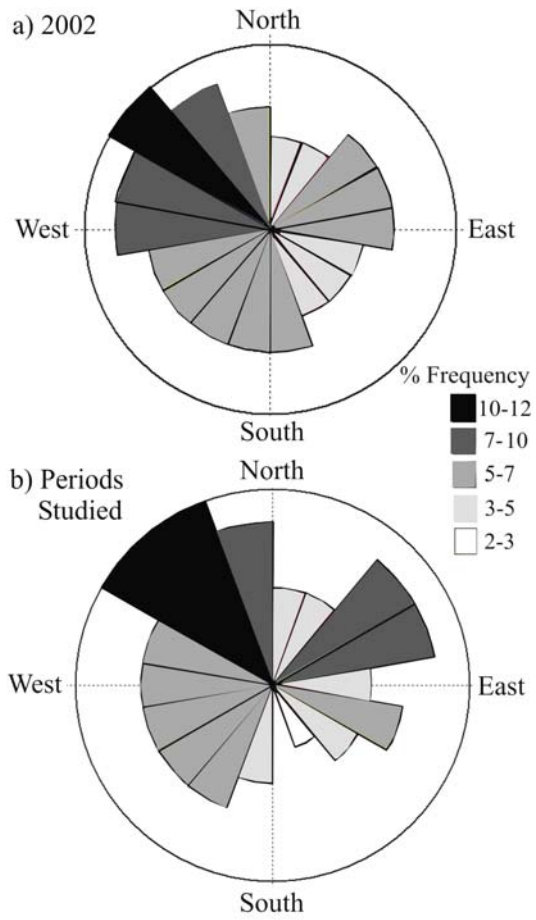

Figure 3.5. Wind roses of the percent frequency of wind directions at OJP during the year 2002 (a) and for the three periods studied (b).

Table 3.2. Average canopy structure and elevation characteristics surrounding the EC sensor. Source of flux areas may be influenced differently depending on wind direction, canopy structure and elevation.

Wind direction quadrants	Frequency of wind origin during periods studied	Average tree height (m) per wind direction quadrant	Average *f*cover per wind direction quadrant	Average elevation (m) per wind direction quadrant
North-west	45%	16.4	0.74	495
South-west	20%	14.9	0.55	491
North-east	18%	15.2	0.67	490
South-east	17%	11.6	0.43	487
Site Average	**-**	**14.8**	**0.63**	**4.91**

3.4.2 Dominant Meteorological Driving Mechanisms

To make comparisons between fluxes and spatial variability in biomass and elevation, the influence of meteorological variables on CO_2 uptake needs to first be determined. This divides structural and spatial influences from changing meteorological conditions. During all three periods, meteorological variables had varying influences on CO_2 fluxes. Landsberg light response curves indicate that NEP and GEP saturated at different levels of PAR depending on the time period within the growing season and available θ (Figure 3.6). P1 and P3 had higher amounts of precipitation preceding them than P2, and P2 had higher T_{air} than the other two periods. Saturation of NEP and GEP was more pronounced during P1 and P2, and was increasingly linear during P3. Table 3.3 provides information on average meteorological conditions per period, incoming PAR (PARin), θ, T_{air}, and VPD, which likely affected NEP and GEP light response curves during the three periods of study.

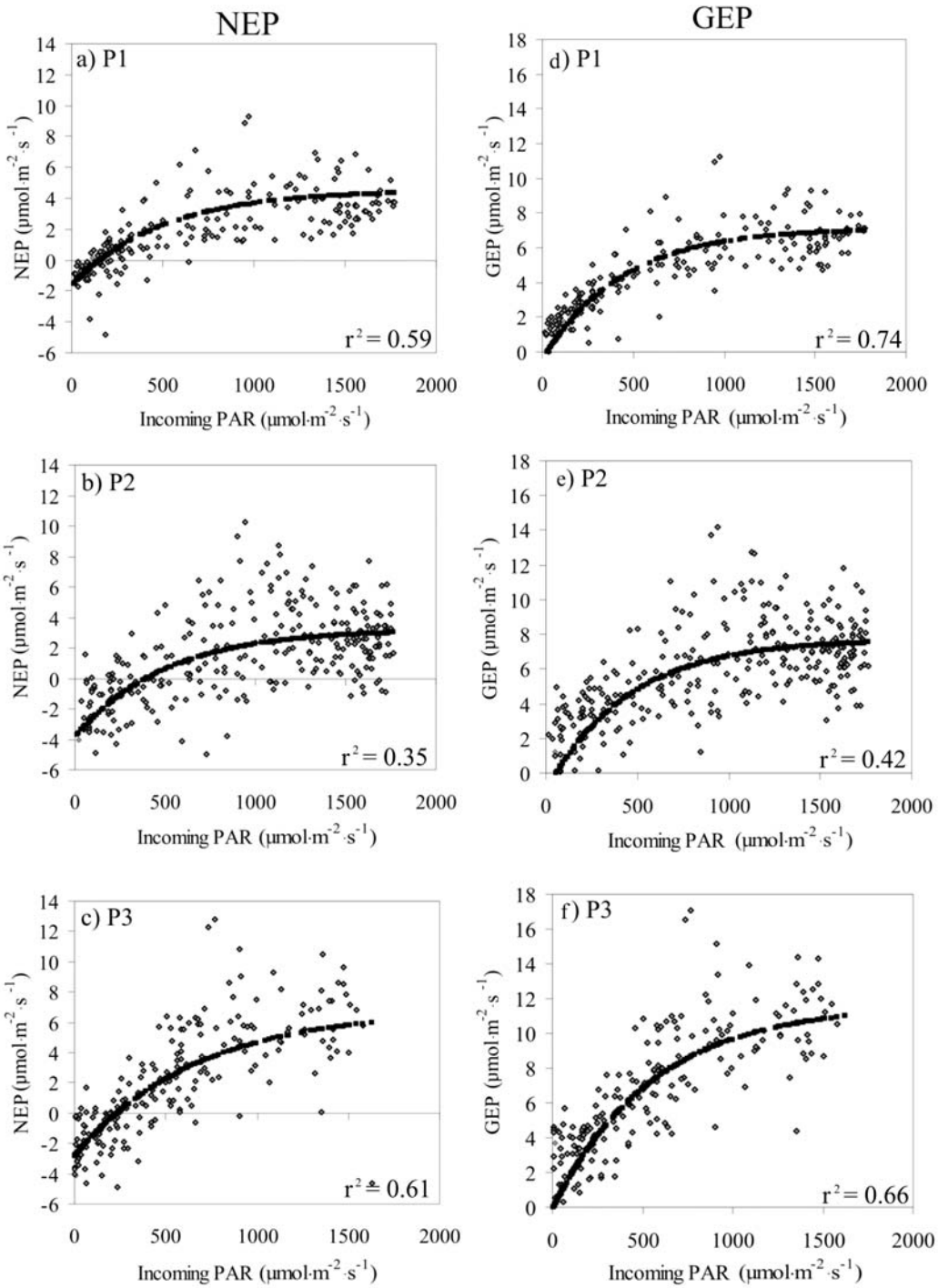

Figure 3.6. Relationships between NEP (a, b, and c) and GEP (d, e, and f) and PAR represented by Landsberg light response curves at OJP during the three periods of study: June 10 – 15, 2002 (a and d), July 5 – 13, 2002 (b and e), and August 7 – 13, 2002 (c and f). Relationships are shown for entire days when incoming PAR exceeded 0.1 µmol m^{-2} s^{-1}.

Table 3.3. Average meteorological conditions and NEP (GEP) P_{max} during three periods studied.

Periods	NEP P_{max} (μmol m^{-2} s^{-1})	GEP P_{max} (μmol m^{-2} s^{-1})	Average θ (m^3 m^{-3})	Average T_{air} (^{o}C)	Average T_{soil} (^{o}C)	Average VPD (Pa)	Average PARin (μmol m^{-2} s^{-1})
P1	4.5	7.1	0.82	16.8	9.2	132	767
P2	3.2	7.7	0.54	23.7	14.4	299	955
P3	6.8	11.6	0.068	19.0	14.3	154	523

Saturation of photosynthesis at OJP was consistent with the results of Turner et al. (2003). They found that two forests (one conifer and one deciduous) tended to saturate at high levels of absorbed PAR because of the low photosynthetic capacity of shade leaves and possible inhibition of photosynthesis of sunlit leaves during the afternoon. Within season influences of incoming PAR on CO_2 uptake and lower rates of saturation during P3 (as opposed to P1 and P2) were also found in Hollinger et al. (1999) within a mixed forest. Middleton et al. (1997) found that lower water use efficiency, reduced evapotranspiration and reduced CO_2 uptake at OJP in June and July 1994, were caused by low soil moisture and stomatal limitations to photosynthesis. They also observed a late summer and early autumn peak in photosynthesis at OJP and attributed this to the maturing of new needles. New needles commence growth in June and are fully developed by mid-July enabling increased photosynthesis in August (Middleton et al. 1997).

Incoming PAR accounted for the greatest variability in NEP and GEP during the three periods studied (Table 3.4) but had the least influence during P2 when NEP and GEP were highly variable. After removing the influence of PAR on NEP and GEP using the Landsberg equation, the residuals of the variance of NEP and GEP were affected by T_{air}, RH, θ, and T_{soil} to varying degrees. Table 3.4 summarizes the relationships and significance between the driving variables and NEP and GEP, respectively, during the three periods studied.

Table 3.4. Pearson's correlation coefficients for the relationships between NEP and GEP, and PAR using the Landsberg light response curve. Dominant meteorological variables affecting the residuals of NEP and GEP after accounting for PAR are also included. The *p*-value, the percentage when NEP and GEP were not affected by driving mechanisms, is shown in brackets. Number of observations = 192 (P1); 288 (P2); and 224 (P3).

Period		Incoming PAR	T_{air}	RH	T_{soil}	θ
NEP	P1	0.77 (0.000)	-0.59 (0.000)	0.54 (0.000)	-0.63(0.000)	0.22 (0.02)
	P2	0.59 (0.000)	-0.66 (0.000)	0.57 (0.000)	-0.49 (0.000)	0.30 (0.000)
	P3	0.78 (0.000)	-0.25 (0.004)	-0.072 (0.41)	-0.20 (0.03)	0.02 (0.79)
GEP	P1	0.86 (0.000)	-0.45 (0.000)	0.46 (0.000)	-0.38 (0.000)	0.007 (0.94)
	P2	0.65 (0.000)	-0.63 (0.000)	0.58 (0.000)	-0.42 (0.000)	0.30 (0.000)
	P3	0.81 (0.000)	-0.25 (0.004)	0.03 (0.74)	-0.12 (0.19)	-0.02 (0.86)

Interacting influences between meteorological variables and CO_2 fluxes cannot be ignored (Chen et al. 2002). Incoming PAR, T_{air}, RH, T_{soil} and θ each covaried to some degree, resulting in similar combined influences on NEP and GEP, as described in a correlation matrix during the three periods in Table 3.5. Incoming PAR correlated strongly with RH and to a lesser extent with T_{air} and very little with T_{soil} and θ. T_{air} also correlated strongly with RH and T_{soil}, whereas RH correlated less strongly with T_{soil}. If each is assessed individually with the residuals of NEP and GEP, after removing the influence of incoming PAR, we find that T_{air} and RH typically have similar but opposite influences on the residuals (Table 3.4). This suggests that T_{air} was typically low and RH was high when NEP and GEP residuals were positive (i.e. when the Landsberg equation underestimated NEP and GEP). T_{soil} and θ also had similar relationships with NEP and GEP residuals, but to a lesser extent than T_{air} and RH (Table 3.4). T_{soil} was similar to T_{air}, and was negatively related to increases in NEP and GEP residuals during all periods, whereas θ had the opposite relationship (i.e T_{soil} was low, and θ had greater water content during periods of increased CO_2 uptake). Similar results were also found at three Douglas-fir sites of varying ages in Chen et al. (2002), where T_{soil} and T_{air} were also negatively related to increases in the residuals of NEP (increased temperature equals decreased NEP).

Table 3.5. Pearson's r correlation matrix of interacting meteorological driving mechanisms and *p-values* (in brackets).

Period	Meteorological Parameter	Incoming PAR	T_{air}	RH	T_{soil}	θ
P1	Incoming PAR	-	0.59 (0.000)	-0.60 (0.000)	0.09 (0.19)	-0.23 (0.002)
	T_{air}	0.59 (0.000)	-	-0.94 (0.000)	0.65 (0.000)	-0.42 (0.000)
	RH	-0.60 (0.000)	-0.94 (0.000)	-	-0.62 (0.000)	0.34 (0.000)
	T_{soil}	0.09 (0.19)	0.65 (0.000)	-0.62 (0.000)	-	-0.67 (0.000)
	θ	-0.23 (0.002)	-0.42 (0.000)	0.34 (0.000)	-0.67 (0.000)	-
P2	Incoming PAR	-	0.42 (0.000)	-0.51 (0.000)	-0.13 (0.03)	0.09 (0.1)
	T_{air}	0.42 (0.000)	-	-0.69 (0.000)	0.68 (0.000)	-0.46 (0.000)
	RH	-0.51 (0.000)	-0.69 (0.000)	-	-0.15 (0.01)	-0.08 (0.18)
	T_{soil}	-0.13 (0.03)	0.68 (0.000)	-0.15 (0.01)	-	-0.80 (0.000)
	θ	0.09 (0.1)	-0.46 (0.000)	-0.08 (0.18)	-0.80 (0.000)	-
P3	Incoming PAR	-	0.50 (0.000)	-0.59 (0.000)	-0.10 (0.16)	0.33 (0.000)
	T_{air}	0.50 (0.000)	-	-0.56 (0.000)	0.45 (0.000)	0.22 (0.001)
	RH	-0.59 (0.000)	-0.56 (0.000)	-	-0.50 (0.000)	-0.61 (0.000)
	T_{soil}	-0.10 (0.16)	0.45 (0.000)	-0.50 (0.000)	-	0.18 (0.007)
	θ	0.33 (0.000)	0.22 (0.001)	-0.61 (0.000)	0.18 (0.007)	-

Meteorological variables, RH, T_{soil} and θ were combined using a multiple linear regression with the residuals of incoming PAR from the Landsberg approach (Table 3.6). These variables were used because there was the least interaction between them and they described the greatest combined variability in CO_2 flux. RH was able to describe much of the variability in T_{air}, resulting in the exclusion of T_{air} from the analysis. T_{soil} has been included, despite being used to derive GEP, it did not greatly covary with GEP during the periods examined (r = -0.02, P1; -0.36, P2; -0.18, P3). The multiple regressions were performed on the residuals of PAR vs. NEP and GEP for each time period because the Landsberg curve provided the best description of the relationship (Table 3.6). Regression equations were then added to the Landsberg equation for each period and were plotted against measured NEP and GEP in Figure 3.7. In all cases, inclusion of meteorological driving mechanisms (apart from incoming PAR) improved the prediction of NEP and GEP.

Table 3.6. Landsberg and multiple regression equations used to predict NEP and GEP using meteorological variables. Relative importance of each contribution is indicated by the *p-value.* Number of observations = 111 (P1); 166 (P2); and 126 (P3).

Period		Landsberg Equation	Multiple Regression Equations	*p-value* of Contribution		
				RH	T_{soil}	θ
NEP	P1	$y = 4.5(1 - e^{-0.002(PAR-160)})$	NEP_r = 23.9 + (0.016 RH) - (1.55 T_{soil}) - (129 θ)	0.001	0.000	0.000
	P2	$y = 3.2(1 - e^{-0.002(PAR-400)})$	NEP_r = -14.8 - (0.04 RH) + (0.92 T_{soil}) + (58.9 θ)	0.000	0.000	0.390
	P3	$y = 6.8(1 - e^{-0.0015(PAR-235)})$	NEP_r = -22.8 + (0.02 RH) - (1.06 T_{soil}) - (85 θ)	0.039	0.005	0.816
GEP	P1	$y = 7.1(1 - e^{-0.0023(PAR-32)})$	GEP_r = 3.10 + (0.01 RH) - (0.23 T_{soil}) - (17.7 θ)	0.006	0.439	0.202
	P2	$y = 7.7(1 - e^{-0.0022(PAR-60)})$	GEP_r = -8.4 + (0.05 RH) - (0.06 T_{soil}) + (139 θ)	0.000	0.769	0.051
	P3	$y = 11.6(1 - e^{-0.0018(PAR-10)})$	GEP_r = 16.7 + (0.005 RH) - (0.49 T_{soil}) - (140 θ)	0.687	0.183	0.656

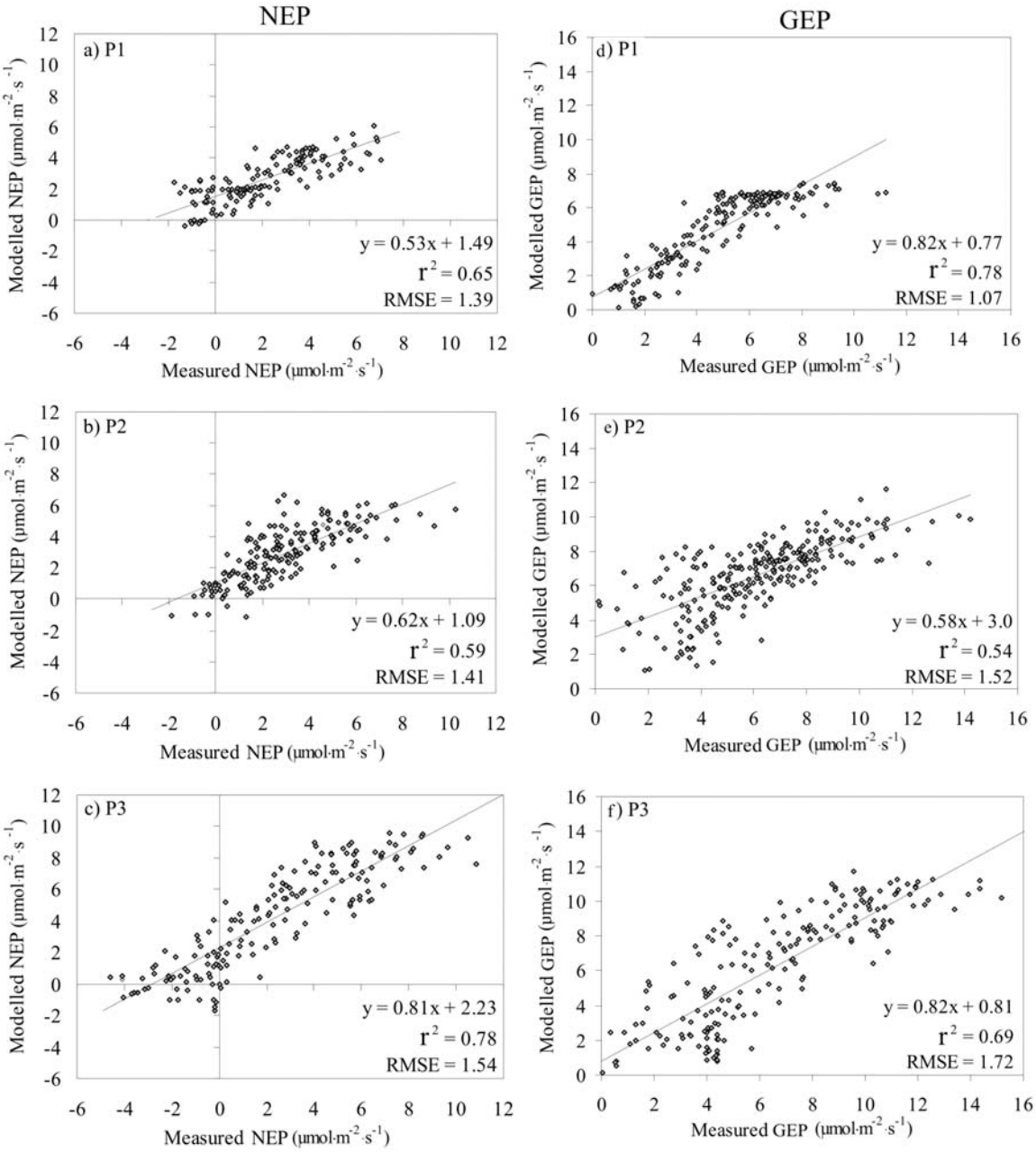

Figure 3.7. Relationships (adjusted r^2) between NEP (a, b, and c), GEP (d, e, and f), and modeled estimates of the same using Landsberg + multiple regression of the residuals presented in Table 3.6 during the three periods of study: June 10 – 15, 2002 (a and d), July 5 – 13, 2002 (b and e), and August 7 – 13, 2002 (c and f). Relationships are shown for entire days when incoming PAR exceeded 0.1 µmol m^{-2} s^{-1}.

3.4.3 Within Footprint Vegetation Structural and Ground Elevation Influences on Fluxes

We hypothesize that the inclusion of canopy structure and ground elevation will improve estimates of NEP and GPP when compared with meteorological variables. In other words, canopy structure and ground elevation will have some influence on the variability of CO_2 fluxes. *f*cover and elevation were combined within a multiple linear regression with meteorological driving variables, RH, T_{soil}, and θ and incoming PAR (Landsberg approach) for each of the periods studied (Table 3.7). Canopy structure indicators and elevation co-vary to some degree. Average canopy height was strongly positively correlated with average canopy depth (r = 0.94, p = 0.000), and *f*cover (r = 0.64, p = 0.000) and canopy depth was correlated with *f*cover (r = 0.71, p = 0.000). Canopy height was not significantly correlated with elevation (r = 0.16, p = 0.07), but *f*cover tended to be negatively correlated with elevation (r = -0.38, p = 0.000). *f*cover best described the variability in NEP and GEP when compared with other structural attributes. Modelled NEP and GEP, based on the multiple regression with the inclusion of meteorological variables, *f*cover and elevation were compared with measured in Figure 3.8.

Table 3.7. Multiple regression equations used to predict NEP and GEP using meteorological variables, *f*cover and elevation, added to Landsberg results (Table 3.6). Relative importance of each contribution is indicated by the *p-value.* Number of observations = 111 (P1); 166 (P2); and 126 (P3).

Period		Multiple Regression Equations	*p-value* of Contribution				
			RH	T_{soil}	θ	*f*cov.	Elev.
NEP	P1	NEP_r = 158 + (0.01 RH) - (1.54 T_{soil}) - (224 θ) + (0.27 Elev.) + (9.95 *f*cover)	0.23	0.000	0.001	0.041	0.21
	P2	NEP_r = -1.9 + (0.08 RH) - (1.44 T_{soil}) -(153 θ) + (0.041 Elev.) + (8.36 *f*cover)	0.000	0.000	0.05	0.10	0.63
	P3	NEP_r = 0.7 - (0.02 RH) - (1.60 T_{soil}) -(1091 θ) + (0.17 Elev.) + (18.5 *f*cover)	0.25	0.004	0.36	0.020	0.32
GEP	P1	GEP_r = 167 + (0.009 RH) - (0.84 T_{soil}) - (224 θ) -(0.30 Elev.) + (10.45 *f*cover)	0.15	0.000	0.000	0.025	0.15
	P2	GEP_r = -22.3 + (0.08 RH) - (0.88 T_{soil}) - (20.6 θ) -(0.05 Elev.) + (8.88 *f*cover)	0.000	0.000	0.79	0.071	0.53
	P3	GEP_r = 19.6 + (0.003 RH) – (0.84 T_{soil}) - (826 θ) - (0.075 Elev.) + (16.4 *f*cover)	0.85	0.15	0.11	0.032	0.66

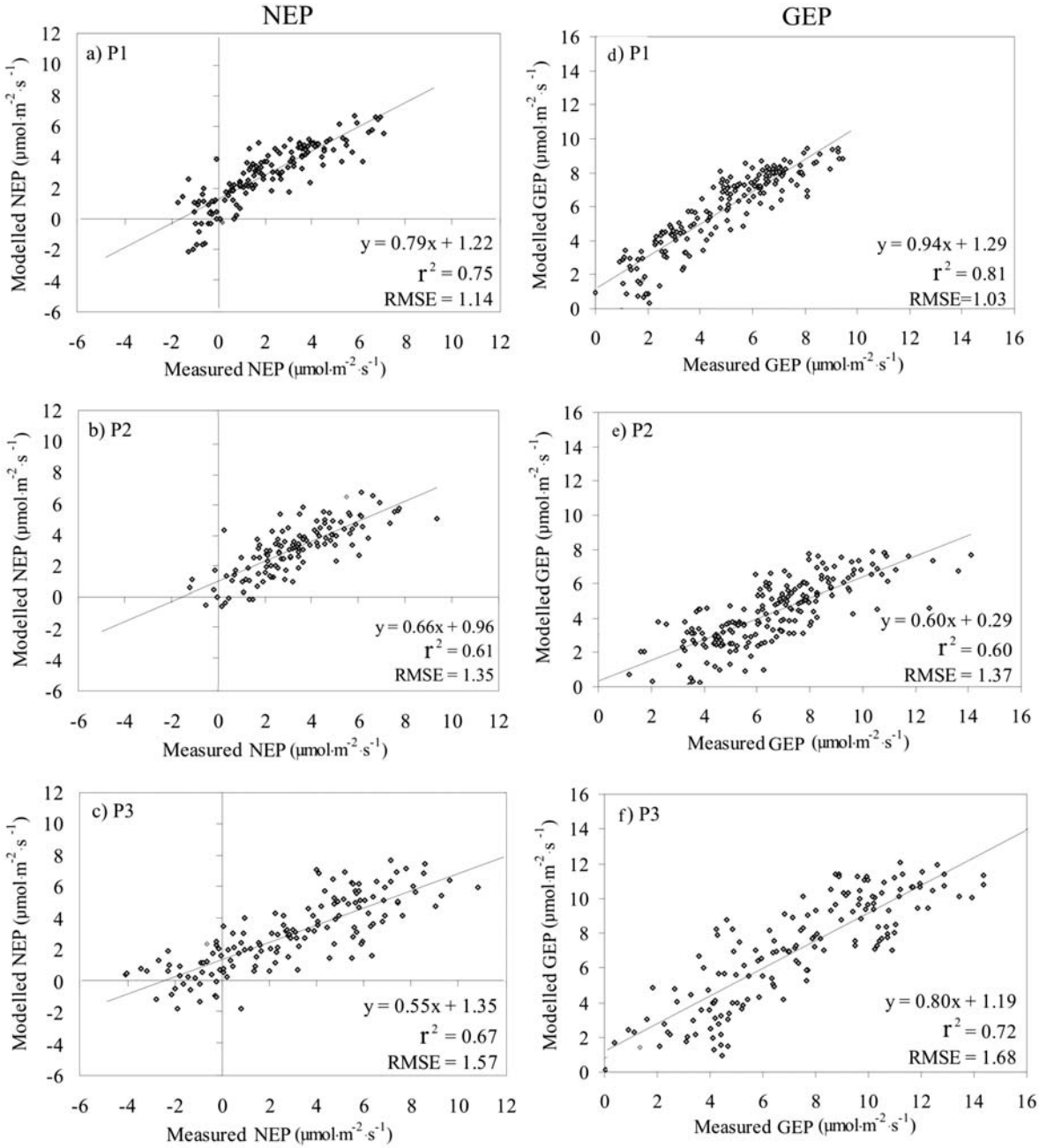

Figure 3.8. Relationships (adjusted r^2) between NEP (a, b, and c), GEP (d, e, and f), and modeled estimates of the same using Landsberg + multiple regression of the residuals presented in Table 3.6 (including fcover and elevation) during three periods of study: June 10 – 15, 2002 (a and d), July 5 – 13, 2002 (b and e), and August 7 – 13, 2002 (c and f). Relationships are shown for periods between 0900 and 1700 local time.

The inclusion of *f*cover was sometimes a more important component of the flux than daily variability in θ (P3, and to a certain extent P2) and RH (P1 and P3) (Table 3.7). Elevation, however, was not an important part of the combined influence on fluxes, demonstrated by *p-values* in Table 3.7. *f*cover improved prediction of NEP and GEP during most periods studied (when comparing r^2 and RMSE of Figures 3.8 and 3.9). During P1, prediction of NEP and GEP was improved by 10% and 5% when meteorological variables were included, and an additional 15% and 4% when *f*cover and elevation were included. Meteorological influences (apart from incoming PAR) had the least importance during P1 when compared with the other two periods. *f*cover had a larger influence on NEP than meteorological driving mechanisms (15% vs. 10%), and a slightly less important influence on GEP (4% vs. 5%). Smaller improvements were found during P2, apart from meteorological variables, which improved the Landsberg predicted NEP and GEP by 68% and 29% (NEP and GEP). Meteorological variables had a dominant influence on fluxes during P2, whereas *f*cover and elevation had relatively minor influences, improving modelled NEP and GEP by an additional 3% and 11%, respectively. Much of the variability in fluxes during P2 remained unexplained, even after inclusion of meteorological variables and canopy structure and elevation. During P3, *f*cover and elevation worsened the prediction of NEP by 16% when compared with that modeled using driving mechanisms alone (which improved NEP and GEP prediction by 28% and 4%), whereas GEP was only slightly improved by 4% when *f*cover was included. Small improvements to modeled NEP and GEP from *f*cover and elevation also resulted in lower root mean squared error (RMSE).

On a daily basis rather than by study periods, canopy structure and elevation had varying correspondence with measured NEP and GEP (Figure 3.9), perhaps due to sensitivity of fluxes to the vegetation characteristics of the maximum source area and available resources. We expect

that areas with more biomass (e.g. foliage amounts) would be positively related to increased CO_2 uptake by vegetation because increased numbers of leaves would be photosynthesizing. An assessment of light response curves during four days of similar meteorological conditions (July 7 and 8 and August 9 and 10), when fluxes came from opposite directions within the ecosystem yield direct evidence of the influences of canopy structure and elevation on fluxes. On July 7th and August 10th fluxes originated from the north-west part of the ecosystem: areas of relatively high leaf area, tall trees, and higher elevation. On July 8th and August 9th fluxes originated from the east and south east parts of the ecosystem: areas of relatively low leaf area, shorter trees, and low elevation. Light response curves for NEP and GEP on July 7th and August 10th (not shown) indicate that areas with greater amounts of biomass, located at higher elevations had greater ability to photosynthesize than areas with lesser amounts of biomass. A t-test confirms that significant differences in light response curves exist between dates where fluxes originated from high biomass as opposed to low biomass areas ($p < 0.01$). Differences in Landsberg curve descriptors P_{max} and I_{comp} are demonstrated in Table 3.8 for specific dates.

Table 3.8. NEP and GEP light response curve characteristics for four days of similar meteorological conditions when footprints originated from opposite parts of the ecosystem (high biomass vs. low biomass (fcover, tree height), and higher elevation (upland) vs. lower elevation (lowland)).

Date	P_{max} (μmol m^{-2} s^{-1})		I_{comp} (μmol m^{-2} s^{-1})		Daily total flux (μmol m^{-2} s^{-1})		Average Footprint Characteristics
	NEP	GEP	NEP	GEP	NEP	GEP	
July 7, 2002	3.1	7.5	450	273	44.9	166.8	High biomass, upland
July 8, 2002	2.3	6.7	470	350	40.1	151.7	Low biomass, lowland
August 9, 2002	5.8	9.7	390	125	87.3	194.4	Low biomass, lowland
August 10, 2002	8.5	11.8	310	50	92.4	199.6	High biomass, upland

Of the 22 days studied, 13 (59%) and 9 (41%) of the days showed significant ($p < 0.01$) positive relationships between increased biomass and increased NEP and GEP, respectively. Four and five additional days were also positively correlated with NEP and GEP, but did not have a significant influence. The opposite relationships were found on five and eight days (NEP, GEP), where increased biomass was also related to increased atmospheric CO_2 concentrations, but only two and three days were significant ($p < 0.01$). The best correspondence between CO_2 uptake and increased biomass occurred during P1 and P3 when photosynthesis was not limited by θ, high average T_{air}, and incoming PAR.

NEP and GEP were also significantly negatively affected by increased elevation (or vice versa) for 10 and 8 of 22 days, respectively (where $p < 0.01$) (Figure 3.9). Negative relationships occurred mostly during P2 and P3, corresponding with high average T_{air} and T_{soil}. For example, on June 13 2002, GEP (and NEP) were negatively affected by fluxes originating from areas of higher elevation (Figure 3.4). June 13th was also the warmest day of the week, having an average T_{air} = 21.8^{o}C as opposed to days previous and following (average T_{air} = 13.5 ^{o}C; 19.2^{o}C). Warmer days with increased T_{soil} typically resulted in negative correspondence between elevation and CO_2 fluxes. In this case T_{soil} provides a general estimate of ecosystem T_{soil} variability over time because it is only measured in one location. Average T_{air} and T_{soil} were greatest during P2 (T_{air} = 23.7 ^{o}C, T_{soil} = 14.4 ^{o}C) and P3 (T_{air} = 19.0 ^{o}C, T_{soil} = 14.3 ^{o}C) on days when elevation and NEP and GEP were significantly related. Cooler and wetter periods during P1 showed limited correspondence between CO_2 fluxes and elevation.

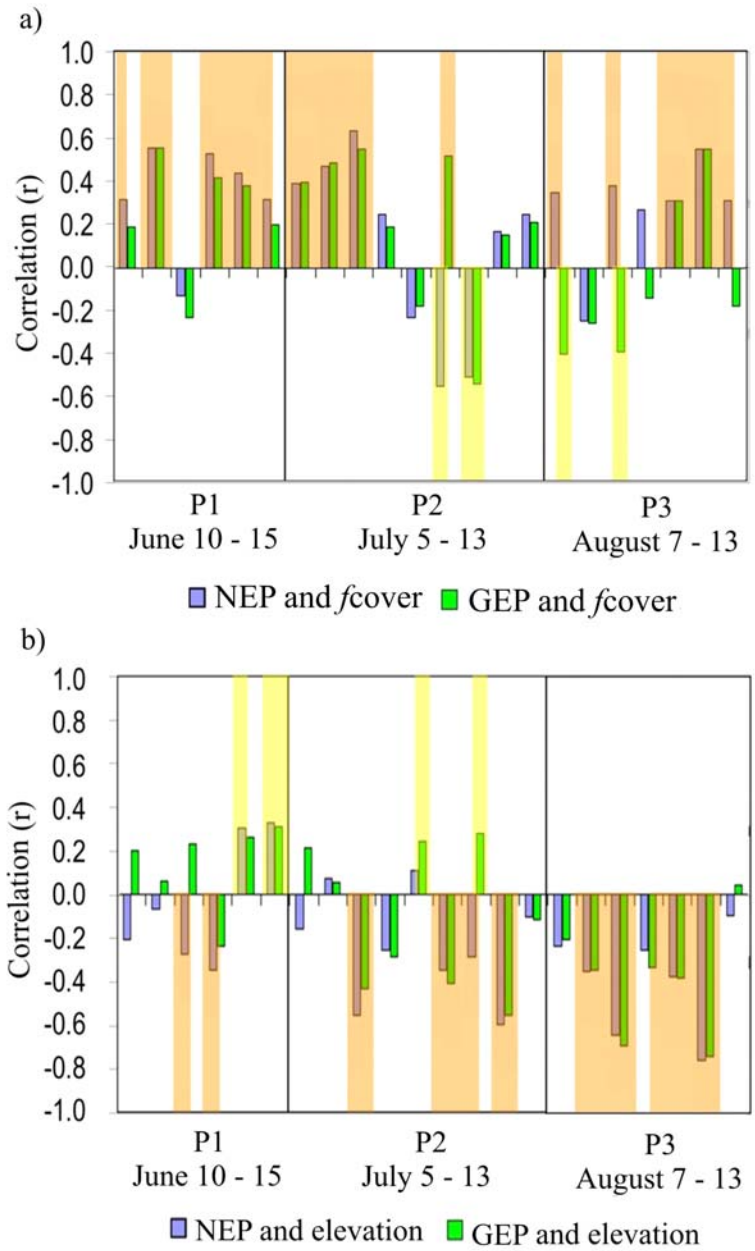

Figure 3.9. Bar graph of Pearson's r correlations between daily NEP and GEP and a) fcover and b) elevation influence (n = ~17 per day but may vary due to low u_*). Orange and yellow bars represent p-values < 0.01. In a) 13 of 22 (NEP) and 9 of 22 (GEP) days are significantly correlated with areas of increased fcover, whereas the opposite is found on 2 of 22 (NEP) and 3 of 22 (GEP) days. In b) 2 of 22 (NEP) and 3 of 22 (GEP) days are significantly correlated with areas of higher elevations, whereas 10 of 22 (NEP) and 8 of 22 (GEP) days are significantly correlated with areas of lower elevations. Increases in biomass (e.g. greater foliage) should be positively correlated with increased NEP and GEP.

3.5 Discussion and Conclusions

In this study, we found that CO_2 fluxes varied spatially and temporally due to variations in meteorological variables, canopy biomass and elevation gradients within a jack pine ecosystem. Why does the relative importance of interactions between CO_2 fluxes, and canopy structure and elevation vary on a daily basis and throughout each period? This may be due, in part, to sensitivity of fluxes to the characteristics of vegetation within the maximum source location of the fluxes and available resources. Footprint estimates indicate that the greatest contribution of measured fluxes typically originated from up to 150 m to 300 m from the tower. Trees were typically shorter within 150 m east and south-east of the EC system (average canopy height = 13.6 m) whereas trees were taller west and north-west of the tower (average canopy height =15.2 m) (Figure 3.1). Canopy *f*cover was also low, ranging from 0.36 to 0.45 in all directions within 150 m of the EC.

At distances of 150 m to 350 m of the EC, the ecosystem becomes more spatially variable. Average tree heights ranged from 12.5 m (south east of the EC) to 18.4 m (north west of the EC), resulting in ~32% difference in average tree height within two parts of the ecosystem from which CO_2 fluxes likely originated. *f*cover also varied significantly, ranging between 0.36 and 0.81 at spatial resolutions of 1 m. High average foliage fractional cover was located north-east and north-west of the EC, and lower foliage amounts were found to the south-east and south-west of the site (Table 3.2). Even on a daily basis, the amount of biomass sampled by eddy covariance can vary greatly at OJP, depending on the source location of fluxes. Variable maximum source area locations can vary over space, as do vegetation and elevation characteristics. When combined with meteorological variables, the effects of these (meteorology and biomass) on fluxes can also differ (Figure 3.9). At OJP, Baldocchi et al. (2000) found that between 25% and 35% of incoming

solar radiation reached the forest floor. Similarly, Griffis et al. (2003) suggest that approximately 70% of solar radiation is absorbed by the canopy at this site. In our study, spatial mapping of *f*cover by airborne lidar at 1 m resolution shows that the light penetration to the ground surface can be as little as 19%, in areas of high *f*cover and as great as 64% in areas of low *f*cover. These relatively large differences in the spatial variability of light absorption by canopies and penetration to the ground may explain the variable influences on CO_2 exchanges from different parts of the ecosystem. Future studies should examine the area extent of classified *f*cover, tree height and elevation within footprints, not only footprint averages examined in this study.

Over the course of several days, canopy structure and elevation exhibited strong influences on CO_2 fluxes during P1 and to a lesser extent in P3, but had relatively little influence during P2. This was perhaps because of limited availability of resources and saturation of photosynthesis by high amounts of average incoming PAR. Canopy structural influences on CO_2 fluxes were typically less important than meteorological variables, but during many days canopy structure, especially *f*cover, explained a comparatively large proportion of the variance of NEP and GEP.

In this study, assessment of average elevation within footprints was simplistic. For example, CO_2 fluxes may be affected by slope curvature leading to either wetting or drying of soils, thereby affecting tree growth, photosynthesis, and Re (e.g. Baldocchi et al. 1997; Baldocchi and Meyers, 1998). Elevation height is not necessarily indicative of micro-topographic features affecting fluxes of CO_2 within the landscape because micro-topography is also dependent on the spatial distribution of small hills and valleys, slope and aspect. This could be improved by incorporating local ground morphology, slope curvature (concave vs. convex) and aspect to properly classify upland and lowland areas and their attributes.

Based on this limited analysis and the variability in wind directions illustrated in Figure 3.4 for the entire year of 2002, flux measurements at this site may not be equally measuring fluxes from all parts of the ecosystem surrounding the EC flux station. Winds typically originate from upland areas which have slightly different canopy structural characteristics than low lying areas. Differences in the variability in NEP could be influenced, to some degree, by differences in canopy and ground surface characteristics in one part of the site as opposed to another. Rahman et al. (2001) found that EC underestimated gross CO_2 fluxes by 5% at OJP because biomass tended to be lower within the immediate vicinity of the EC as opposed to areas of higher biomass surrounding the ecosystem (also found here). Fluxes at more heterogeneous sites may have increased dependency on canopy structure and elevation. Along with meteorology, these may be a deciding factor on whether the annual carbon balance of a vegetated ecosystem is a net annual source or sink. Further research over extended (e.g. annual) periods is needed to determine if this is the case.

3.6 Acknowledgements

We would like to thank the Fluxnet-Canada Research Network and the Boreal Ecosystem Research and Monitoring Sites (BERMS) Project and all those individuals involved for collection and processing of flux data. We appreciate the efforts of the Applied Geomatics Research Group and C-CLEAR for collecting and processing at-cost lidar data and the National Water Research Institute (NWRI) for financially supporting part of the survey. Field data collection was performed with the aid of Bruce Davison, Chris Beasy, and Jordan Erker, and their efforts are appreciated. Jessika Töyra is acknowledged for her assistance with field validation and logistics and Sonia Wharton for advice. Also, thank-you to the late Werner Bauer (site manager) for his help and support. Funding for this project has been provided by CFCAS, NSERC, the BIOCAP

Canada Foundation, and the Climate Research Division of Environment Canada. Laura has been generously supported by graduate student scholarships from NSERC and OGSST.

3.7 References

Amiro, B. D., 1998. Footprint climatologies for evapotranspiration in a boreal catchment. Agricultural and Forest Meteorology. 90:195-201.

Baldocchi, D. D., C. A. Vogel, and B. Hall, 1997. Seasonal variation of carbon dioxide exchange rates above and below a boreal jack pine forest. Agricultural and Forest Meteorology. 83:147-170.

Baldocchi, D., and T. Meyers, 1998. On using eco-physiological, micrometeorological and biogeochemical theory to evaluate carbon dioxide, water vapor and trace gas fluxes over vegetation: a perspective. Agricultural and Forest Meteorology. 90:1-25.

Baldocchi, D., F. Kelliher, T. A. Black, and P. Jarvis, 2000. Climate and vegetation controls on boreal zone energy exchange. Global Change Biology. 6:69-83.

Baldocchi, D., 2008. Turner Review No. 15: 'Breathing' of the terrestrial biosphere: lessons learned from a global network of carbon dioxide flux measurement systems. Australian Journal of Botany. 56:1-26.

Barr, A.G., K. Morgenstern, T.A. Black, J.H. McCaughey, and Z. Nesic, 2006. Surface energy balance closure by the eddy-covariance method above three boreal forest stands and implications for the measurement of the CO_2 flux. Agricultural and Forest Meteorology. 140:322-337.

Chasmer, L., C. Hopkinson, B. Smith, and P. Treitz, 2006. Examining the influence of changing laser pulse repetition frequencies on conifer forest canopy returns. Photogrammetric Engineering and Remote Sensing. 72(12):1359-1367.

Chen, J., M. Falk, E. Euskirchen, K. Tha Paw U., T. Suchanek, S. Ustin, B. Bond, K. Brosofske, N. Phillips, and R. Bi, 2002. Biophysical controls of carbon flows in three successional Douglas-fir stands based on eddy-covariance measurements. Tree Physiology. 22:169-177.

Chen, J.M., A. Govind, O. Sonnentag, Y. Zhang, A. Barr, and B. Amiro, 2006. Leaf area index measurements at Fluxnet-Canada forest sites. Agricultural and Forest Meteorology. 140:257-268.

Chen, B., J. Chen, G. Mo, T.A. Black and D.E. Worthy, 2008. Comparison of regional carbon flux estimates from CO_2 concentration measurement and remote sensing based footprint integration. Global Biogeochemical Cycles. 22(GB2012).

Choudhury, B., and J. Monteith, 1988. A four-layer model for the heat budget of homogeneous land surfaces. Quarterly Journal of the Royal Meteorological Society. 114:373-398.

Fluxnet-Canada, 2003. Fluxnet-Canada measurement protocols. Working draft version 1.3. Fluxnet-Canada Network Management Office, Laval, Quebec. Available online: http://www.fluxnet-canada.ca.

Foken, T., and M. Y. Leclerc, 2004. Methods and limitations in validation of footprint models. Agricultural and Forest Meteorology. 127:223-234.

Goetz, S., S. Prince, S. Goward, M. Thawley, J. Small, and A. Johnston, 1999. Mapping net primary production and related biophysical variables with remote sensing: Application to the BOREAS region. Journal of Geophysical Research. 104(D22):27,719-27,734.

Gower, S., V. Vogel, J. Norman, C. Kucharik, S. Steele, and T. Stow, 1997. Carbon distribution and aboveground net primary production of aspen, jack pine, and black spruce stands in Saskatchewan and Manitoba, Canada. Journal of Geophysical Research. 102(2):29,029 – 29,041.

Griffis, T. J., T. A. Black, K. Morgenstern, A. G. Barr, Z. Nesic, G. B. Drewitt, D. Gaumont-Guay, J. H. McCaughey, 2003. Ecophysiological controls on the carbon balances of three southern boreal forests. Agricultural and Forest Meteorology. 117:53-71.

Gryning, S. E., A. Holtslag, J. S. Irwin, and B. Silvertsen, 1987. Applied dispersion modeling based on meteorological scaling parameters. Atmospheric Environment. 21(1):79-89.

Heinsch, F.A., M. Zhao, S. Running, J. Kimball, R. Nemani, K. Davis, P. Bolstad, B. Cook, A. Desai, D. Ricciuto, B. Law, W. Oechel, H. Kwon, H. Luo, S. Wofsy, A. Dunn, J. W. Munger, D. Baldocchi, L. Xu, D. Hollinger, A. Richardson, P. Stoy, M. Siqueira, R. Monson, S. Burns, and L. Flanagan, 2006. Evaluation of remote sensing based terrestrial productivity from MODIS using regional tower eddy flux network observations. IEEE Transactions on Geoscience and Remote Sensing. 44(7):1908-1925.

Hollinger, D.Y., S.M. Goltz, E.A. Davidson, J.T. Lee, K. Tu, and H.T. Valentine, 1999. Seasonal patterns and environmental control of carbon dioxide and water vapour exchange in an ecotonal boreal forest. Global Change Biology. 5:891-902.

Kim, J., Q. Guo, D. Baldocchi, M. Leclerc, L. Xu, and H. Schmid, 2006. Upscaling fluxes from tower to landscape: Overlaying flux footprints on high-resolution (IKONOS) images of vegetation cover. Agricultural and Forest Meteorology. 136:132-146.

Kljun, N., P. Calanca, M. Rotach, H. Schmid, 2004. A simple parameterisation for flux footprint predictions. Boundary-Layer Meteorology. 112:503-523.

Kljun, N., T. A. Black, T. J. Griffis, A. G. Barr, D. Gaumont-Guay, K. Morgenstern, J. H. McCaughey, and Z. Nesic, 2006. Response of Net Ecosystem Productivity of Three Boreal Forest Stands to Drought. Ecosystems, 9:1128-1144.

Landsberg, J.J., and R.H. Waring, 1997. A generalized model of forest productivity using simplified concepts of radiation-use efficiency, carbon balance and partitioning. Forest Ecology and Management.95:209-228.

Leblanc, S., J. Chen, R. Fernandes, D. Deering, and A. Conley, 2005. Methodology comparison for canopy structure parameters extraction from digital hemispherical photography in boreal forests. Agricultural and Forest Meteorology. 129:187-207.

Lim, K., and P. Treitz, 2004. Estimation of aboveground forest biomass from airborne discrete return laser scanner data using canopy-based quantile estimators. Scandinavian Journal of Forest Research. 19(6):558-570.

Massman, W.J. and X. Lee, 2002. Eddy covariance flux corrections and uncertainties in long term studies of carbon and energy exchange. Agricultural and Forest Meteorology. 113:121-144.

Middleton, E. M., J. Sullivan, B. Bovard, A. Deluca, S. Chan, and T. Cannon, 1997. Seasonal variability in foliar characteristics and physiology for boreal forest species at five Saskatchewan tower sites during the 1994 Boreal Ecosystem-Atmosphere Study. Journal of Geophysical Research. 102(D24):28831-28844.

Monteith, J., and M. Unsworth, 1990. Principles of Environmental Physics. 2nd ed. Edward Arnold, New York. 291 pgs.

Morsdorf, F., B. Kötz, E. Meier, K. Itten, and B. Allgöwer, 2006. Estimation of LAI and fractional cover from small footprint airborne laser scanning data based on gap fraction. Sensing of Environment. 104:50-61.

Rahman, A., J. Gamon, D. Fuentes, D. Roberts, and D. Prentiss, 2001. Modeling spatially distributed ecosystem flux of boreal forest using hyperspectral indices from AVIRIS imagery. Journal of Geophysical Research. 106(D24):33579-33591.

Shuttleworth, W., and J. Wallace, 1985. Evaporation from sparse crops – An energy combination theory. Quarterly Journal of the Royal Meteorological Society. 111:839-855.

Turner, D.P., S. Urbanski, D. Bremer, S. Wofsy, T. Meyers, S. Gower, and M. Gregory, 2003. A cross-biome comparison of daily light use efficiency for gross primary production. Global Change Biology. 9:383-395.

Vesala, T., N. Kljun, U. Rannik, J. Rinne, A. Sogachev, T. Markkanen, K. Sabelfeld, Th. Foken, M.Y. Leclerc, 2008. Flux and concentration footprint modelling: State of the art. Environmental Pollution, 152:653;666.

Wilson, K.B., A. Goldstein, E. Falge, M. Aubinet, D. Baldocchi, P. Berbigier, C. Bernhofer, R. Ceulemans, H. Dolman, C. Field, A. Grelle, A. Ibrom, B.E. Law, A. Kowalski, T. Meyers, J. Moncrieff, R. Monson, W. Oechel, J. Tenhunen, R. Valentini, and S. Verma, 2002. Energy balance closure at FLUXNET sites. Agricultural and Forest Meteorology. 113:223-243.

Yang, P.C., T.A. Black, H.H. Neumann, M.D. Novak and P.D. Blanken. 1999. Spatial and temporal variability of CO_2 concentration and flux in a boreal aspen forest. J Geophys Res. 104:27,653-27,661.

Zhang, Y., J. Chen, and J. Miller, 2005. Determining digital hemispherical photograph exposure for leaf area index estimation. Agricultural and Forest Meteorology. 133:166-181.

Chapter 4

Using Airborne Lidar for the Assessment of MODIS fPAR

4.1 Abstract

Airborne light detection and ranging (lidar) data were compared with coincident digital hemispherical photography (DHP) and radiation sensors within a jack pine chronosequence of three sites. The purpose of the study was to compare a simple lidar model of the fraction of photosynthetically active radiation absorbed by the canopy (fPAR) with DHP and PAR estimates of fPAR, and then, to scale lidar fPAR to MODIS pixels. Average DHP fPAR was estimated at 40 locations per site and compared with fPAR estimated using PAR sensors located at the centre of mature and immature jack pine forests, old jack pine and a jack pine site harvested in 1975 (OJP and HJP75, respectively). DHP under-estimated average fPAR by 11% and 21% at OJP and HJP75 when compared with PAR sensors. This was attributed to differences in canopy foliage cover throughout the stand and, as reported in the literature, underestimation by the DHP method. A fractional-cover ratio (*f*cover) based on the number of canopy lidar returns to the total number of returns was then compared with fPAR estimated from DHP at 110 geographically located photographs. *f*cover compared well with DHP-derived fPAR using annulus rings 1-9 at mature, immature, and regenerating sites (r^2 = 0.84, RMSE = 0.01) and to a lesser extent using rings 1-5 (r^2 = 0.66, RMSE = 0.11). When compared with DHP, *f*cover was underestimated by ~3% (rings 1-9) and overestimated by ~16% (rings 1-5). Using the relationship between *f*cover and DHP (rings 1-9), lidar-derived fPAR was then averaged and compared to ~1 km resolution Moderate Resolution Imaging Spectroradiometer (MODIS) pixels throughout a watershed. MODIS fPAR was within 10% of lidar fPAR for approximately 1/4 of the area (24 pixels).

4.2 Introduction

Covering approximately 76 percent of the global land surface area, vegetation plays a key role in the functioning of local ecosystems and can affect processes at scales as large as global weather patterns (Pielke et al. 1998). Leaf area is particularly important, affecting energy and mass exchanges between the terrestrial biosphere and the atmosphere (e.g. Chen et al. 2005). Accurate spatial and temporal estimates of measurable leaf attributes, e.g., leaf area index (LAI) and/or the fraction of photosynthetically active radiation absorbed by the canopy (fPAR), are required as inputs into ecosystem/atmosphere models (e.g. Gower et al. 1999; Chen et al. 2007).

LAI is defined as one-half the total leaf area per unit ground surface area (m^2 m^{-2}) (Chen et al. 2006) whereas fPAR can be estimated from radiation sensors based on the ratio:

$$fPAR = ((PAR_{AC\downarrow} - PAR_{AC\uparrow}) - (PAR_{BC\downarrow} - PAR_{BC\uparrow}))/PAR_{AC\downarrow} \quad [1]$$

where $PAR_{AC\downarrow}$ is the incident photosynthetically active radiation (PAR) above the canopy, $PAR_{AC\uparrow}$ is the reflected PAR above the canopy, $PAR_{BC\downarrow}$ is the incident below-canopy PAR after interception by branches and leaves, and $PAR_{BC\uparrow}$ is the reflected PAR from the ground surface (Gower et al. 1999). Despite their importance, LAI and fPAR are difficult and time consuming to measure spatially and temporally within representative ecosystems. Both require measurement of canopy fractional cover and light transmission (optical methods) (Gower et al. 1999; Huemmrich et al. 1999; Leblanc et al. 2005; Schwalm et al. 2006; Chen et al. 2006; Sonnentag et al. 2007), or alternative approaches involving destructive sampling of leaves and branches. Optical methods are less time consuming than destructive sampling, and are more frequently used (Jonckheere et al. 2004). These rely on temporal measurements from radiation sensors located above and below the canopy on a meteorological tower (e.g. Schwalm et al. 2006; Gower et al. 1999; Huemmrich

et al. 1999; [1]). They can also be collected spatially below the canopy via incident hemispherical radiation measurement units such as the LiCOR LAI-2000 Plant Canopy Analyzer, Tracing Radiation and Architecture of Canopies (TRAC), and digital hemispherical photography (DHP) (e.g. Leblanc et al. 2005; Chen et al. 2006; Sonnentag et al. 2007). Optical methods are inexpensive to operate, but remote study locations often make it difficult to measure changes frequently throughout the growing season (Heinsch et al. 2006).

Other methods used for estimating LAI and fPAR include measurements of reflected light collected using remote sensing satellite and airborne platforms (e.g., the Moderate Resolution Imaging Spectroradiometer (MODIS)) (Gamon et al. 2004). Remote sensing methods using spectral reflectance alone are not able to resolve the complexity of the vegetation canopy within averaged pixels of fPAR and LAI (e.g. Xu et al. 2004; Eriksson et al. 2006; Jin et al. 2007). Radiative transfer models often improve spectral reflectance measurements by incorporating species-based three-dimensional canopy structure, leaf and stem geometry, and foliage density at the tree to canopy level (e.g. Myneni et al. 1997; Goel and Thompson, 2000; Sun and Ranson, 2000; Fernandes et al. 2004). These can be directly related to variability in canopy reflectance measured using remote sensing methods. Accurate spatial and temporal methods of collecting fPAR and LAI would therefore be beneficial and cost-effective for scaling from radiation sensors at a local scale to landscape and regional scales (at lower resolutions).

The fractional cover of vegetation (where 1 = full canopy cover and 0 = no canopy cover) may be estimated from airborne light detection and ranging (lidar) using a combination of the ratio of the number of canopy laser returns (single and multiple) to all returns (e.g. Morsdorf et al. 2006; Hopkinson and Chasmer, 2007):

$$f\,\mathrm{cover} = \left(\frac{\sum P_{canopy}}{\sum P_{all}} \right). \qquad [2]$$

P_{canopy} is the total frequency of laser pulse returns within the canopy and P_{all} is the total frequency of all laser pulse returns. These ratios are calculated within a specified resolution or grid (e.g. 1 m x 1 m). Morsdorf et al. (2006) examined numerous laser pulse ratios and DHP annulus ring configurations, and found that central rings combined with first pulse returns provided the strongest correlations. Also, the extraction of lidar data within a circular area mimicked by DHP ("data traps", Lovell et al. 2003; Morsdorf et al. 2006) were found to be most appropriate when radii of up to 2 m were used (Morsdorf et al. 2006). Hopkinson and Chasmer (2007) extend the waveform lidar approaches of Lefsky et al. (1999) and Parker et al. (2001) and use laser pulse intensity as an indicator of transmission losses through the canopy. In their study, the Beer-Lambert Law was modified to include the ratio of lidar intensity-based ground return power to the total return power.

Current studies that use lidar to estimate effective LAI (L_e), fractional cover, and fPAR tend to concentrate on one or a couple of different forest types within a specified location (e.g. Thomas et al. 2006) and often with controlled lidar survey configurations (e.g. Hopkinson and Chasmer, 2007). It is not known how well the return ratio (i.e., *fcover*) will work given different tree heights and canopy closure. Further, the use of lidar as a validation tool for lower resolution remote sensing products has not been examined (to the authors' knowledge). This study reports on the application of the return ratio described in [2] (i.e., *fcover*) at a jack pine chronosequence for the evaluation of MODIS fPAR across a watershed.

Relationships between mixed pixels, land cover type, and canopy structural characteristics found in lidar data may be used to better understand inconsistencies in MODIS fPAR/LAI products without the need for extensive field validation. Inexpensive and sometimes free lidar data are available through a number of website and contact listings (e.g. the United States Geological Survey CLICK program). This simple lidar methodology for estimating fPAR could be an important step towards improving ecosystem models and validating remote sensing products, such as those derived from MODIS.

4.3 Methodology

4.3.1 Study Areas

In this study, three jack pine (*Pinus banksiana* Lamb.) sites of different stand ages were examined during the 2005 growing season (June 1 to September 31). All sites are located in close proximity to each other (~6 km) within the White Gull River watershed, located north of Prince Albert, Saskatchewan, Canada. The three sites consist of (i) a mature (i.e., old) jack pine (OJP) forest, approximately 90 years old (520230 E, 5974262 N, UTM zone 13); (ii) an immature jack pine forested harvested in 1975 (HJP75) (523326 E, 5969765 N); and (iii) a regenerating jack pine forest harvested in 1994 (HJP94) (522606 E, 5973386 N). The canopy structure and species characteristics of the sites are described in Table 4.1. The area extent of the forests are approximately 3 km x 3 km (OJP and HJP75), covering approximately three MODIS pixels each. The homogeneous area representative of HJP94 is 700 m along the narrowest part (east to west) and extends up to 1 km along the longest edge. The site falls within one MODIS pixel, which also contains a mixture of older jack pine trees.

Table 4.1. Average vegetation characteristics at OJP, HJP75, and HJP94 for 22 plots. The values in parentheses represent standard deviation (stdev).

Site	Number of trees sampled	Average stem density (stdev) (stems m^{-2})	Average tree height (stdev) (m)	Average DBH* (stdev) (cm)	Average LAI (stdev) ($m^2 \cdot m^{-2}$)	Average canopy depth (stdev) (m)	Average crown diameter (stdev) (m)	Other species
OJP	381	0.11 (0.001)	14.2 (3.5)	9.33 (4.55)	1.6 (0.1)**	8.3 (2.7)	2.0 (1.0)	Alder, bearberry, reindeer lichen, blueberry, cranberry
HJP75	1447	0.59 (0.19)	6.3 (1.6)	5.69 (3.49)	2.8 (0.4)	3.5 (1.3)	0.9 (0.4)	Grasses, reindeer lichen, bearberry
HJP94	2081	0.86 (0.56)	1.6 (0.7)	2.31 (1.05)	1.1 (0.2)	1.6 (0.7)	0.7 (1.1)	Grass, blueberry, alder, raspberry, bearberry, reindeer lichen

* DBH refers to tree bole diameter at breast height (1.3 m above the ground).
** LAI measurements from Chen et al. (2006) differ from LAI observed in this study.

4.3.2 DHP Data Collection and Analysis

In this study, DHP was used to validate lidar estimates of *f*cover at plots throughout each site. If lidar provides *f*cover estimates that can be related to DHP fPAR, then lidar may be used to evaluate MODIS fPAR. Canopy gap fraction was collected using DHP (Nikon Coolpix 8.0 mega pixel, with a Nikon FC-E9 180° fisheye converter; Nikon Inc. Tokyo, Japan) at geo-located plots within each study area. One photograph was taken at the centre of the plot, and four were located 11.3 m from the centre, along cardinal (N, S, E, and W) directions determined using a compass bearing and measuring tape (Fluxnet-Canada, 2003). Photographs were located at the centre of the plot using differentially corrected data obtained from survey-grade global positioning systems (GPS) (Leica SR530, Leica Geosystems Inc. Switzerland; Ashtec Locus, Ashtec Inc., Hicksville, NY). Geo-location accuracies vary from 1 cm to 1 m depending on the canopy cover density at the time of GPS data collection. Photographs were taken at a height of ~1.3 m at OJP and HJP75 and at a height of 0.7 m at HJP94. The heights of the trees within HJP94 (i.e.,a regenerating stand) were often less than 2 m. All photographs were taken during either diffuse daytime

conditions, or at dawn or dusk at two F-stops below normal exposure to reduce the influence of sun brightness and apparent leaf reduction within the photograph (Zhang et al. 2005). Individual photographs were processed following sky and vegetation thresholding methods of Leblanc et al. (2005) to obtain estimates of gap fraction (Ω). DHP version 1.6.1 software was used to process all photographs (S. Leblanc, Canada Centre for Remote Sensing provided to L. Chasmer through the Fluxnet-Canada Research Network).

Estimates of fPAR were determined from DHP based on Ω from annulus rings 1 – 5 (0-50°) and 1 – 9 (0 - 81°) from individual photographs (Gower et al. 1999), and including albedo (Chen et al. 2006):

$$fPAR = (1-\rho_a) - (1-\rho_u)e^{-0.45(1-\alpha)L_e/\cos\theta} \qquad [3]$$

where ρ_a is the PAR albedo of the stand (i.e., above-canopy), ρ_u is the PAR albedo of the ground, and θ is the solar zenith angle at 12:00 local standard time on the date of the lidar survey. ρ_a was estimated from Chen et al. (2006) as 0.05 at OJP and HJP75, and 0.08 at HJP94. ρ_u was estimated as 0.06 at OJP and HJP75 and 0.15 at HJP94 (Chen 2006). An extinction coefficient (k) of 0.45 was used to estimate global PAR (Chen et al. 2006). L_e was multiplied by a scaling factor of 1.16 (Chen et al. 2006) prior to calculation of fPAR in [3]. It is expected that lidar *f*cover should be highly correlated with DHP fPAR, because L_e was estimated directly from Ω (1-fractional cover) and k, where $L_e = -\ln(\Omega)/k$. In this study, allometric estimates of wood fraction (α) were not removed from L_e, or fPAR.

4.3.3 Validation of DHP Using PAR Sensors

PAR was measured using LI-COR model LI190 at OJP and HJP75 (LI-COR Biosciences, Nebraska, USA); and Eko model ML-020P (Eko Instruments, Co. Ltd., Japan) at HJP94. Above canopy incident and reflected PAR sensors were installed on booms at heights of 28 m, 17 m, and 3 m above the ground at OJP, HJP75, and HJP94, respectively. Below canopy incident PAR measurements were made at OJP and HJP75 at a height of ~1 m, but $PAR_{BC\uparrow}$ measurements were not made. Below-canopy PAR measurements were also not available at HJP94. Therefore, the use of HJP94 PAR sensor measurements for validation of DHP was excluded in this study. Measurements at OJP and HJP75 were examined specifically from June 1st to September 30th, 2005 over 30-minute average periods at each site.

One below-canopy PAR sensor was examined per site. These were located within 10 m of towers containing above-canopy PAR. Towers were located at the centre of the sites and between photo plots (located 100 and 500 m from the tower), and therefore location-specific and varying canopy heterogeneity within DHP plots was not captured by PAR sensors. Although DHP was not obtained directly below PAR sensors, we felt it was important to compare photographic methods with PAR sensors to determine if: a) DHP provides a reasonable estimate of fPAR when compared with PAR measurements; and b) PAR sensors were representative of the canopy characteristics throughout each site.

Diffuse PAR (Model BF3, Delta-T Inc. Cambridge, UK) was also measured during the 2005 growing season at OJP at a height of 28 m to determine the ratio of diffuse to direct PAR days. fPAR should be examined during diffuse days because estimates are more consistent than during direct radiation days (Gower et al. 1999). fPAR measurements were then compared during diffuse

conditions at both OJP and HJP75. Despite being approximately 6 kms apart, we assumed that diffuse radiation conditions did not vary greatly between the two sites. fPAR measured during diffuse vs. direct PAR conditions were averaged between 1000 and 1400 local sun time (LST) so that fPAR was not affected by low diurnal solar zenith angles.

4.3.4 Lidar Data Collection and Processing

Lidar data were obtained on August 12, 2005 for the entire watershed using a scanning discrete pulse return system (ALTM3100, Optech Inc. North York, Ontario) owned and operated by the Applied Geomatics Research Group (AGRG), Nova Scotia. Up to four laser pulse reflections or "returns" were obtained per laser pulse emitted, at a rate of 71 kHz and at a flying height of 950 m above ground level (a.g.l). The scan angle was set at ± 19° with 50% overlap of adjacent flight lines. This enabled penetration of laser pulses through to the base of the canopy, whilst also obtaining returns on all sides of individual trees (Chasmer et al. 2006). Cross-track and along-track resolutions, with 50 percent overlap of scans, were 35 cm ("post spacing", the distance between returns) or ~8 returns per m^2.

Laser pulse ranges, aircraft movement/attitude (i.e., pitch, roll and heading) and ground and airborne GPS trajectories were combined within REALM (Optech Inc. Toronto, Ontario) and POSPAC (Applanix Inc., Toronto, Ontario) proprietary software processing packages at the AGRG. POSPAC was used to extract positional GPS and attitude information from an inertial measurement unit and position orientation system within the laser head to create a forward and reverse trajectory of aircraft position. This information was then combined in REALM with the laser timing information to create an x, y, z coordinate of laser reflection at the point where the laser pulse intercepts a feature on, or near the ground surface.

After the initial processing of lidar range files and GPS data, location (i.e. *x, y, z*) and intensity data were imported into Terrascan (Terrasolid, Finland) for classification and subsetting. Each larger area dataset was first filtered for outlying (far above and below ground) returns. Returns were then classified into "ground" returns. All returns, including those from the ground, were kept in a separate "all" file (P_{all} [2]). Ground classification was required to provide a digital terrain model (DTM) from which all other returns may be normalized relative to the ground surface. This enabled classification of canopy returns located at heights ≥1.3 m (0.7 m at HJP94) above the ground surface (P_{canopy}) and P_{all} (all returns including ground, those above the ground but below 1.3 (0.7) m, and canopy returns ≥1.3 m (0.7 m at HJP94)). Normalization of P_{all} and P_{canopy} returns was performed in Surfer (Golden Software Inc. Golden, CO). The DTM was interpolated from lidar point data at 2 m resolution to avoid "holes" where returns have been effectively blocked from reaching the ground. The DTM was rasterised using an inverse distance weighting procedure (IDW) where each return within 2 m x 2 m cells is used to create a generalized grid of the ground surface. This method provides accurate estimates of elevation from high resolution lidar data and rapid processing when compared with other methods (e.g. kriging) (Wise, 2000). Figure 4.1 illustrates how the *f*cover return ratio is calculated from lidar.

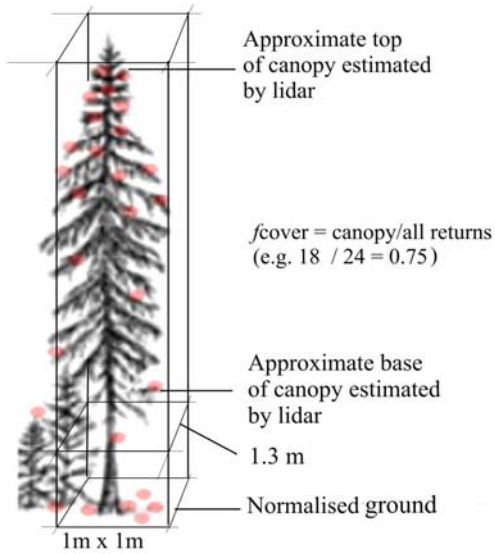

Figure 4.1. A schematic diagram of the distribution of laser returns within a conifer tree (represented by red circles) and calculation of the *f*cover ratio within a 1 m x 1 m x z (height) column. The ratio in [2] is estimated for every 1 m x 1 m of ground area within each site.

4.3.5 MODIS Data

The MODIS fPAR product (MOD15A2 Collection 4.0) was obtained for the lower part of the White Gull River watershed during cumulative 8-day periods (www.modis.ornl.gov/modis/index.cfm). MODIS fPAR was averaged during July and August 2005 to provide a single estimate of fPAR ($fPAR_{MODIS}$) and to reduce the influence of pixels that did not meet quality control (~75% of the area over the growing season). Averaged dates included: July 12, 2005; July 28, 2005; August 5, 2005; and August 29, 2005. The four days were selected because pixel fPAR did not vary greatly (i.e., less than 15%) and also centered on the time of the lidar survey. fPAR estimated from lidar at 1 m resolution was averaged within each geo-referenced MODIS pixel ($fPAR_{lidar}$) and subtracted from MODIS fPAR ($fPAR_{MODIS}$) to provide an estimate of the differences between lidar and MODIS.

4.4 Results

4.4.1 Validating fPAR from DHP using Radiation Sensors

Differences between measured fPAR and diffuse to direct PAR are shown in Figure 4.2 at OJP and HJP75 throughout the growing season. Diffuse days have been classified as being equal to, or greater than 1 when compared with direct PAR. Days when the diffuse to direct PAR ratio was between 0.5 and 1 were excluded in Figure 4.2 so that only clear sky and diffuse sky differences were examined. fPAR was more variable during direct (sunny) days at OJP and HJP75 than during diffuse days (Gower et al. 1999). fPAR varied by less than 5% over the growing season at these sites, indicating that accurate fPAR estimates at a single "snap-shot" in time may be adequate for vegetation photosynthesis modeling when foliage is not changing.

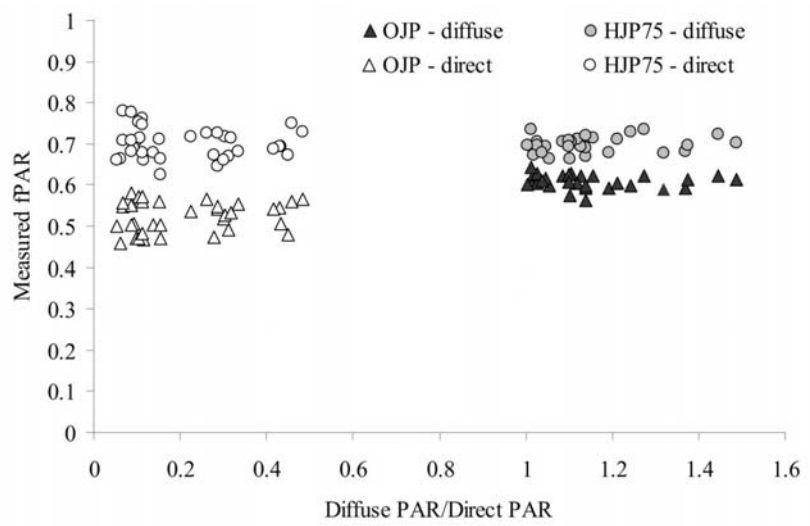

Figure 4.2. Comparison of fPAR on days with high and low ratios of diffuse to direct PAR days throughout the growing season at OJP and HJP75.

Average fPAR comparisons between DHP, radiation sensors, and lidar *f*cover are shown in Table 4.2. Results of Chen et al. (2006) were slightly lower than our estimates because they removed

the fraction of wood observed by the sensor. Average fPAR from DHP underestimated that measured by PAR sensors by 11% (OJP) and 21% (HJP75). This indicates that $PAR_{BC\downarrow}$ at OJP and HJP75 may have been located in areas that had slightly greater foliage than the rest of the stand, on average. Alternatively, DHP may have slightly underestimated the amount of foliage observed. DHP methods have been found to underestimate L_e by approximately 8%, on average, at a number of sites when compared with the LAI-2000 (Chen et al. 2006).

Table 4.2. Comparisons between 2005 average fPAR estimates at OJP and HJP75 from: Chen et al. (2006); diffuse and direct PAR; average fPAR measured from DHP (annulus rings 1-5 and 1-9); and average photo plot-level *f*cover from lidar.

Site	Transect green fPAR at noon Aug. 15, 2005 (Chen et al. 2006)	Average Measured fPAR (diffuse days)	Average Measured fPAR (direct days)	Average fPAR from DHP (rings 1-5)	Average fPAR from DHP (rings 1-9)	Average *f*cover from Lidar
OJP	0.49	0.61	0.52	0.46	0.54	0.46
HJP75	0.54	0.69	0.70	0.45	0.55	0.47

4.4.2 Relationship between fPAR from DHP and Lidar *f*cover

A strong relationship ($r^2 = 0.84$ $p = 0.000$; Figure 4.3a) was found between lidar *f*cover and DHP fPAR using annulus rings 1-9 (and $r^2 = 0.66$ $p = 0.01$, rings 1-5; Figure 4.3b) as a result of two clusters of data along the 1:1 line. These clusters were grouped into OJP and HJP75, and HJP94. The individual relationships between *f*cover and DHP fPAR per site are not significant ($r^2 = 0.28$, OJP; 0.14, HJP75; and 0.15, HJP94) due to relatively small variability in *f*cover and fPAR between plots within individual stands. Despite poor relationships within individual stands, the *f*cover method does work well over a broad range of stand types and fractional covers (Chasmer et al. *accepted*). In Figure 4.3a airborne lidar *f*cover slightly underestimated fPAR when compared with each photograph using annulus rings 1-9. fPAR estimated from DHP typically includes more wood biomass than lidar, because DHP collects information from below the canopy, whereas lidar collects information from above the canopy. Therefore fPAR from DHP is slightly greater than fPAR from lidar because of the inclusion of wood biomass. Lidar

overestimated DHP fPAR by approximately 16%, which is close to the woody:total ratio at OJP (0.20) and HJP75 (0.15). Lidar *f*cover was typically over-estimated at HJP94 because, unlike at OJP and HJP75, much of the foliage is located near the ground surface and was measured by lidar (where *f*cover beneath trees = 100%). Rings 1-5 greatly underestimated fPAR because only the top parts of the trees were observed within photographs. At OJP and HJP75, it is suggested that local gaps within the canopy had greater influences on average fPAR estimates using 5 rings as opposed to 9. The two outliers (Figure 4.3b), where fPAR was significantly greater than *f*cover (i.e., for HJP94) were likely due to the location of photographs in close proximity to tree branches.

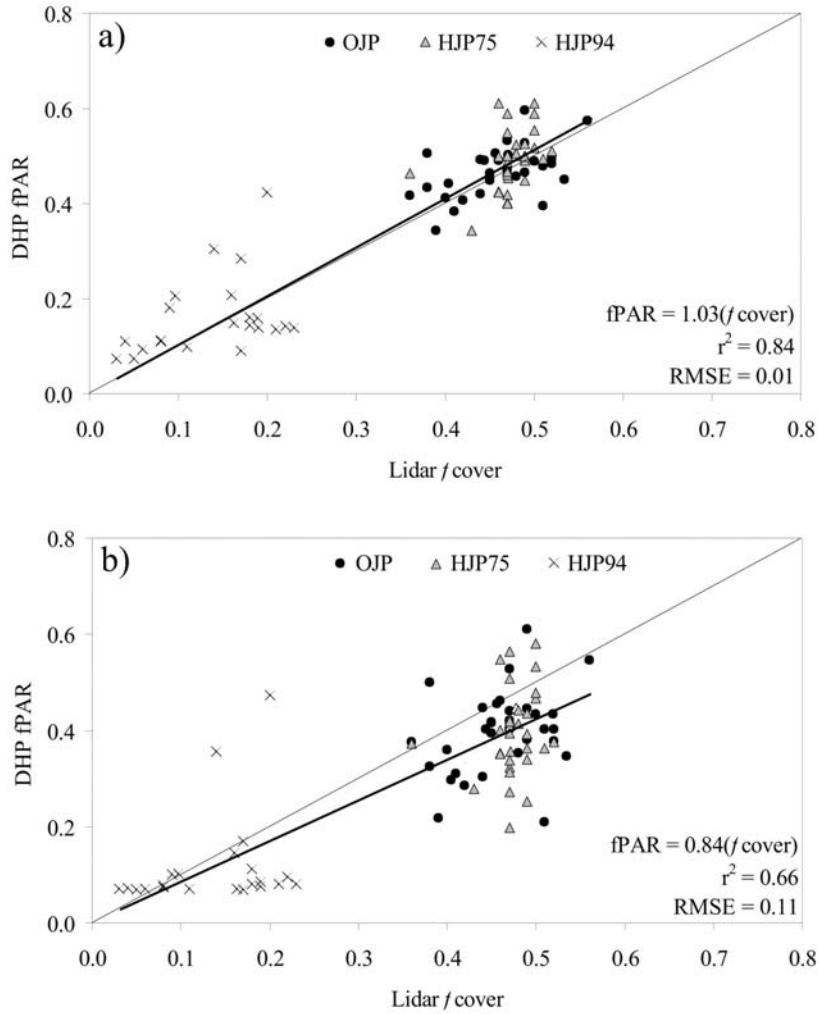

Figure 4.3. Comparisons between lidar fcover and DHP fPAR using annulus rings 1-9 (a) and 1-5 (b).

4.4.3 Using Lidar to Assess MODIS fPAR within a Watershed

A 1 m x 1 m $fPAR_{lidar}$ image map, based on the relationship between *f*cover and DHP fPAR (Figure 4.3a) for the White Gull River watershed is presented in Figure 4.4. This watershed contains OJP, HJP75 and HJP94 as well as two other eddy covariance flux stations operated by the Canadian Carbon Program (CCP). The relationship assumes that all vegetation types within the watershed are treated similarly to jack pine. An examination of 486 sites located across

Canada, containing 11 different species and up to four different classes of forest regeneration demonstrates that the relationship varied by less than 8% when compared with the jack pine sites examined here (Chasmer et al. *accepted*).

The area covered by lidar is up to 7 km wide x 18 km in length, providing 99 MODIS fPAR comparison pixels (~1 km resolution), over five biome types (evergreen needle leaf forest, deciduous broadleaf forest, mixed forest, grassland, permanent wetlands). Subset areas in Figure 4.4 illustrate spatial patterns of vegetation cover within the watershed. The watershed is partly managed and contains a mixture of heterogeneous land cover types typical of the Canadian boreal forest. Heterogeneous areas are also problematic for MODIS fPAR product accuracy due to the fragmentation of the landscape.

The evaluation of MODIS vegetation products using optical LAI and fPAR methods has been underway since the satellites were launched (i.e., 1999 (Terra) and 2001 (Aqua)), resulting in a number of improved leaf area products (e.g. Turner et al. 2003; Zhao et al. 2005; Heinsch et al. 2006; Pisek and Chen, 2007). Validation of MODIS vegetation products is essential but difficult because of vegetation heterogeneity and scaling influences over areas contained within MODIS pixels (Fernandes et al. 2004; Xu et al. 2004; Turner et al. 2006).

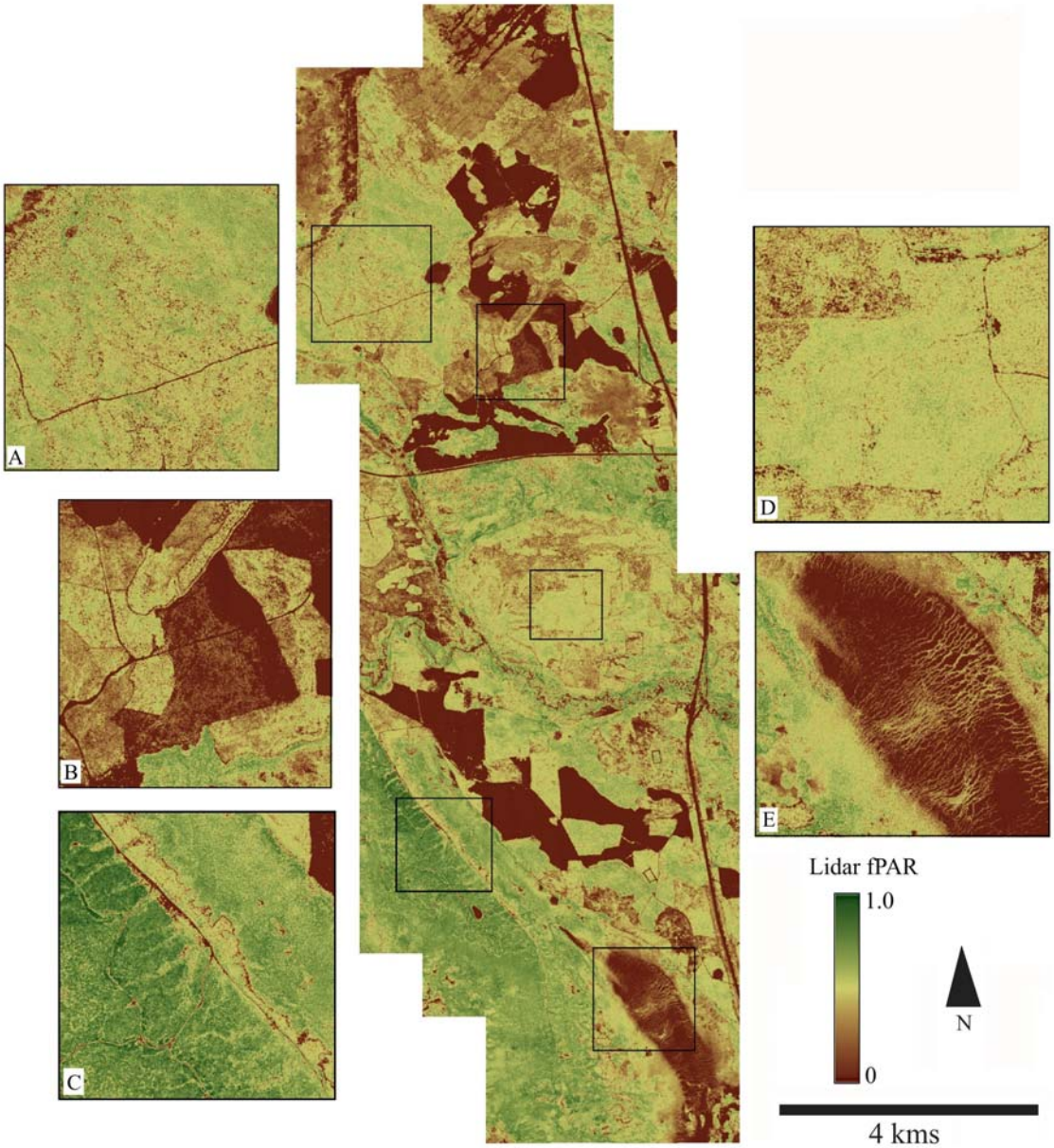

Figure 4.4. fPAR estimated from airborne lidar using the ratio of the number of canopy returns to total returns [2], and the regression model for all species (annulus rings 1-9) at a spatial resolution of 1 m. Subset areas have been expanded to show details in the spatial heterogeneity of fPAR. These include A) OJP, B) HJP94, C) riparian zone of the White Gull River, D) HJP75, and E) fen site, also monitored by the Canadian Carbon Program (CCP). Recent clear cuts have fPAR values close to zero, whereas low-lying shrub and grass vegetation near the White Gull River have fPAR values approaching one.

Comparisons between lidar fPAR and MODIS fPAR are shown visually in Figure 4.5. $fPAR_{lidar}$ was averaged within each geo-referenced MODIS pixel ($fPAR_{MODIS}$) and subtracted from $fPAR_{MODIS}$. The difference image has been superimposed as a translucent layer (1 km x 1 km pixels) over the $fPAR_{lidar}$ image (Figure 4.4). The purpose of Figure 4.5 is to demonstrate differences between $fPAR_{lidar}$ and $fPAR_{MODIS}$ across the watershed, and also, to show spatial vegetation heterogeneity within the landscape that might affect the accuracy of $fPAR_{MODIS}$ within some pixels.

Average $fPAR_{MODIS}$ for the watershed was 0.73 (stdev. = 0.07), whereas average $fPAR_{lidar}$ was 0.40 (stdev. = 0.24). MODIS pixels that were overestimated when compared with $fPAR_{lidar}$ contained recently clear cut areas and a fen. Approximately 22% of pixels within the watershed were in this category. MODIS did provide good estimates of fPAR (within 10% of $fPAR_{lidar}$) within pixels that were relatively homogeneous. These contribute to approximately 24% of the watershed. The remaining pixels were over-estimated by up to 30%, even in some areas where homogeneous pixels exist.

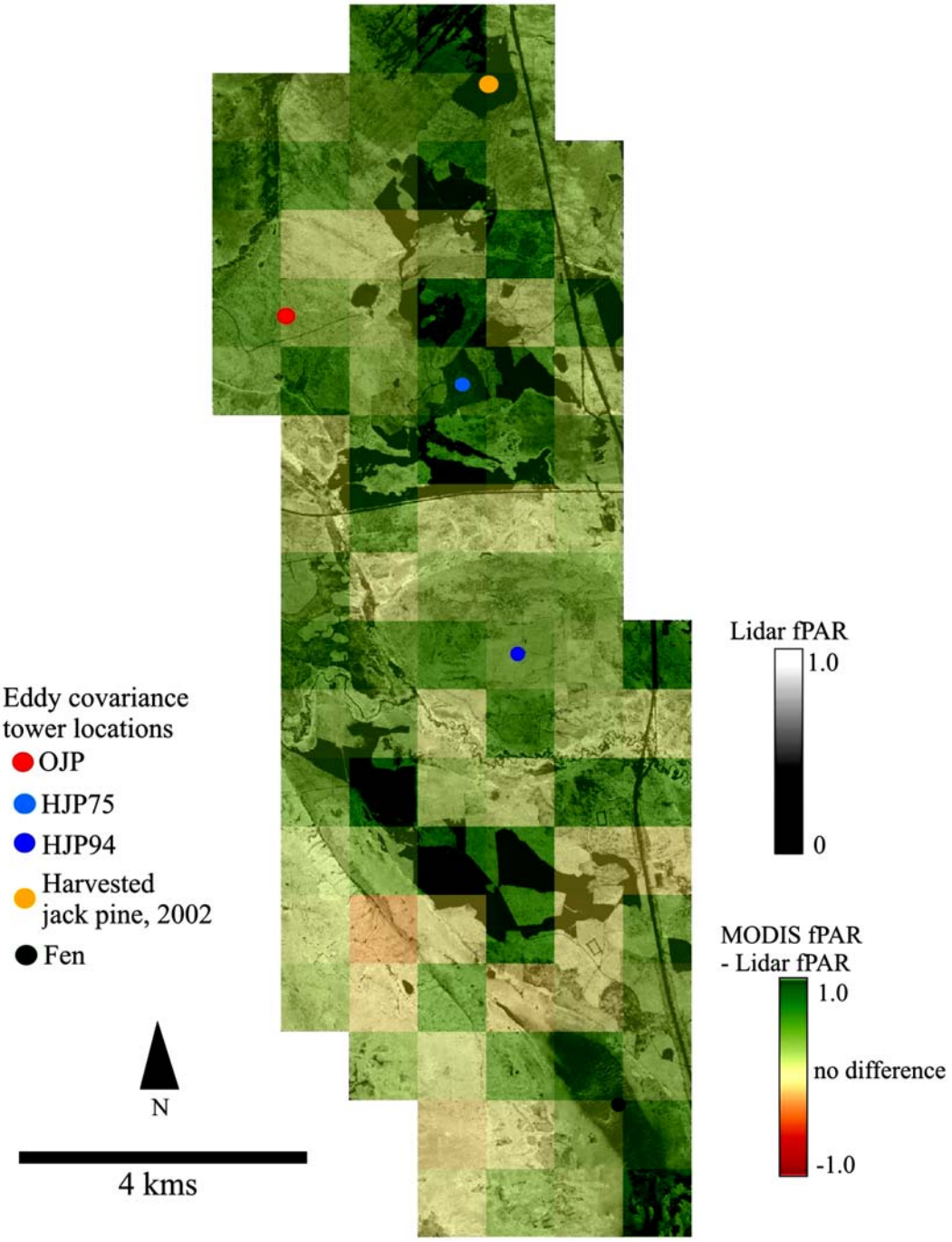

Figure 4.5. Two image maps are illustrated in this figure. The first (illustrated in dark to light tones) shows $fPAR_{lidar}$ at 1 m resolution. Overlaid on top of the $fPAR_{lidar}$ image is the difference between average 1 km x 1 km $fPAR_{lidar}$ and $fPAR_{MODIS}$ shown as transparent pixels. Shades of green indicate that $fPAR_{MODIS}$ was overestimated when compared $fPAR_{lidar}$. Shades of red indicate $fPAR_{MODIS}$ underestimates $fPAR_{lidar}$.

4.5 Discussion

There are a number of possible reasons for the differences found between some $fPAR_{MODIS}$ pixels and average $fPAR_{lidar}$. These may stem from inaccuracies associated with the lidar approach, or problems within the MODIS fPAR product.

The lidar algorithm [2] does not take into account the fractional coverage of grass vegetation because of the inability to separate pulses between short grasses/understory and the ground below ~1.3 m a.g.l. (Hopkinson et al. 2005). $fPAR_{lidar}$ within grassland and recently cleared forests were close to zero, resulting in apparently large over-estimates by $fPAR_{MODIS}$ when these may or may not exist.

When collecting DHP and PAR sensor measures of fPAR, sensors are usually located at heights above the understory so that only the dominant canopy is included. However, the MODIS fPAR product observes both understory and canopy greenness, and therefore appears to overestimate fPAR when compared with DHP and PAR sensors, when this may not be the case (Wang et al. 2004; Heinsch et al. 2006). Wang et al. (2004) and Heinsch et al. (2006) found that MODIS greatly overestimated fPAR at evergreen needle leaf sites with an open canopy and significant understory. They suggest that sites with open canopies should consider the understory contribution to fPAR and LAI. We also found that MODIS slightly overestimated fPAR at OJP when compared with $fPAR_{lidar}$. This site has an alder understory located within some parts of the ecosystem that were not included in either the $fPAR_{lidar}$ or DHP fPAR estimates. The alder understory will likely increase $fPAR_{MODIS}$ due to increased foliage cover within pixels. MODIS is similar to lidar because it receives information vertically, from both the canopy and understory, as well as horizontally over the entire pixel. We suggest that lidar may be used to define understory

vegetation below the base height of the canopy, but above the ground surface. This assumes that the understory has a fractional cover of 100 percent (per return resolution, e.g. 1 m) due to the 1.3 m "blind distance" of lidar. This would increase fPAR estimates of lidar relative to MODIS and may provide more comparable estimates of fPAR within a MODIS pixel. Further research should focus on this topic.

Another issue that occurs in MODIS fPAR products is caused as a result of the fPAR retrieval algorithm every eight days. Coops et al. (2007) found that MODIS accurately estimated fPAR (without referring to a back-up algorithm) only 20% of the time over a five year period at a forest site in British Columbia. The majority of the fPAR datasets observed in Coops et al. (2007) were noisy and failed to use directionally-corrected reflectance required by best quality controlled pixels (Knyazikhin et al. 1999). Further, geolocation issues within cumulative datasets can reduce the locational accuracy of MODIS pixels by ~10% (or 100 m) in any direction (Wolf et al. 2002). This could affect the differences between $fPAR_{MODIS}$ and $fPAR_{lidar}$, where MODIS reflectance may come from areas beyond the pixel, but were not accounted for by lidar. Geolocation errors may also be increased when data are converted from the native Integerized Sinusoidal Projection (Turner et al. 2004).

Finally, land cover mis-classification resulted in over-estimation of $fPAR_{MODIS}$ when compared with measured fPAR in Cohen et al. (2003), Hill et al. (2006), and Turner et al. (2006). The organization of within pixel heterogeneity or "patches" of vegetation vs. clear cut may affect $fPAR_{MODIS}$ within mixed pixels if these are not classified correctly. In this study, differences between $fPAR_{MODIS}$ and $fPAR_{lidar}$ exist within open canopies that show significant pixel fractions containing bare earth (also found in Huemmrich et al. 2005; Turner et al. 2006). Hansen et al.

(2000) found that the global vegetation classification scheme is approximately 85% correct. In this study, 21% of pixels were mis-classified as either woody savanna, instead of evergreen needle leaf forest or evergreen needle leaf forest instead of open grassland (determined from 76 handheld GPS measurements taken throughout the watershed (data not shown)). Pixels that were evergreen needle leaf, but classified as woody savanna better approximated fPAR from lidar for the same pixels. These results show that the watershed area falls just outside of the average MODIS land classification accuracy.

4.6 Conclusions

In this study, a simple ratio of the number of canopy to total returns from airborne lidar was used to estimate fPAR at a jack pine chronosequence. The results of this study indicate that airborne lidar *f*cover is closely related to fPAR based on comparisons with digital hemispherical photography (DHP) and above and below-canopy PAR sensors. Lidar fPAR was then compared with MODIS fPAR across a watershed. The results of the analysis show that MODIS typically overestimated fPAR within recently clearcut areas, but was often within 10% of lidar fPAR when examined over homogeneous pixels. These results are important because they demonstrate that MODIS fPAR, currently validated using DHP and radiation sensors, may be spatially evaluated using lidar. Airborne lidar also provides the ability to assess within-pixel canopy structure, land-cover patterns, and fragmentation, as well as the potential impact of understory species. These have been cited as the most problematic issues affecting MODIS land cover products, apart from atmospheric contamination of pixels and meteorological inputs discussed within recent literature (Heinsch et al. 2006; Wang et al. 2004). The availability of lidar data will enable further development and research into the methods discussed, including application within sites of greater leaf area and adjustment for understory species.

4.7 Acknowledgements

We would like to thank the Fluxnet-Canada Research Network and the Boreal Ecosystem Research and Monitoring Sites (BERMS) Project and all those individuals involved for collection and processing of flux data. We appreciate the efforts of the Applied Geomatics Research Group and C-CLEAR for collecting and processing at-cost lidar data and the National Water Research Institute (NWRI) and the Climate Research Division, Atmospheric Sciences and Technology Directorate, Environment Canada for financial support for the lidar survey. Field data collection was performed with the aid of Bruce Davison, Chris Beasy, and Jordan Erker, and their efforts are appreciated. Jessika Töyra is acknowledged for her assistance with field validation and logistics. Also, thank-you to the late Werner Bauer (site manager) for his help and support. MODIS data were obtained with many thanks from the Oak Ridge National Laboratory Distributed Active Archive Center (ORNL DAAC). 2007 MODIS subset land products are available on-line [http://www.daac.ornl.gov/MODIS/modis.html] from ORNL DAAC, Oak Ridge, Tennessee, U.S.A. Funding for this project has been provided by CFCAS, NSERC, PREA, and the BIOCAP Canada Foundation. Laura has been generously supported by graduate student scholarships from NSERC and OGSST and research assistantships from CRESTech.

4.8 References

Chasmer, L., C. Hopkinson, B. Smith, and P. Treitz, 2006. Examining the influence of changing laser pulse repetition frequencies on conifer forest canopy returns. *Photogrammetric Engineering and Remote Sensing*. 17(12):1359-1367.

Chasmer, L., C. Hopkinson, P. Treitz, H. McCaughey, A. Barr, and A. Black, A lidar-based hierarchical approach to assessing MODIS fPAR. *Remote Sensing of Environment* (*accepted)*.

Chen, J.M., 1996. Canopy architecture and remote sensing of the fraction of photosynthetically active radiation absorbed by boreal conifer forests. *IEEE Transactions on Geoscience and Remote Sensing*. 34(6):1353-1368.

Chen, J. M., X. Chen and W. Ju, X. Geng, 2005. A remote sensing-driven distributed hydrological model: mapping evapotranspiration in a forested watershed. *Journal of Hydrology*. 305:15-39.

Chen, J.M., A. Govind, O. Sonnentag, Y. Zhang, A. Barr, and B. Amiro, 2006. Leaf area index measurements at Fluxnet-Canada forest sites. *Agricultural and Forest Meteorology*. 140:257-268.

Chen, B., J. M. Chen, G. Mo, K. Yuan, K. Higuchi, and D. Chan. 2007. Modeling and scaling coupled energy, water, and carbon fluxes based on remote sensing: An application to Canada's landmass. *Journal of Hydrometeorology*, 8: 123-143.

Cohen, W. B., T.K. Maiersperger, Z. Yahg, S. Gower, D. Turner, W. Ritts, M. Berterretche, and S. Running, 2003. Comparisons of land cover and LAI estimates derived from ETM+ and MODIS for four sites in North America: A quality assessment of 2000/2001 provisional MODIS products. *Remote Sensing of Environment*. 88:235-255.

Coops, N.C., T.A. Black, R.S. Jassal, J.A. Trofymow, and K. Morgenstern, 2007. Comparison of MODIS, eddy covariance determined and physiologically modelled gross primary production (GPP) in a Douglas-fir forest stand. *Remote Sensing of Environment*. 107:385-401.

Eriksson, H.M., L. Eklundh, A. Kuusk, and T. Nilson, 2006. Impact of understory vegetation on canopy reflectance and remotely sensed LAI estimates. *Remote Sensing of Environment*. 103:408-418.

Fernandes, R. A., J. R. Miller, J. M. Chen, and I. G. Rubinstein, 2004. Evaluating Image Based Estimates of Leaf Area Index in Boreal Conifer Stands over a Range of Scales using High-Resolution CASI Imagery. *Remote Sensing of Environment*, 89: 200-216.

Fluxnet-Canada, 2003. Fluxnet-Canada Measurement Protocols, Working Draft Version 1.3. Fluxnet-Canada Network Management Office, Laval, Quebec. Available online: http://www.fluxnet-canada.ca.

Gamon, J. A., K.F. Huemmrich, J. M. Chen, D. Fuentes, F.G. Hall, J.S. Kimball, S. Goetz, J. Gu, K.C. McDonald, J.R. Miller, M. Moghaddam, D.R. Peddle, A.F. Rahman, J.-L. Roujean, E. A. Smith, C.L. Walthall, P. Zarco-Tejada. 2004. Remote sensing in BOREAS: lessons learned. *Remote Sensing of Environment.* 89:139-162.

Goel, N. and R. Thompson, 2000. A snapshot of canopy reflectance models and a universal model for the radiation regime. *Remote Sensing Reviews*, 18:197-225.

Gower, S.T., C. J. Kucharik, and J.M. Norman, 1999. Direct and indirect estimation of leaf area index, f_{APAR}, and net primary production of terrestrial ecosystems. *Remote Sensing of Environment*.70:29-51.

Hansen, M.C., R. S. DeFries, K. Townshend, and R. Sohlberg, 2000. Global land cover classification at 1 km spatial resolution using a classification tree approach. *International Journal of Remote Sensing*. 21:1331-1364.

Heinsch, F.A., M. Zhao, S. Running, J. Kimball, R. Nemani, K. Davis, P. Bolstad, B. Cook, A. Desai, D. Ricciuto, B. Law, W. Oechel, H. Kwon, H. Luo, S. Wofsy, A. Dunn, J. W. Munger, D. Baldocchi, L. Xu, D. Hollinger, A. Richardson, P. Stoy, M. Siqueira, R. Monson, S. Burns, and L. Flanagan, 2006. Evaluation of remote sensing based terrestrial productivity from MODIS using regional tower eddy flux network observations. *IEEE Transactions on Geoscience and Remote Sensing*. 44(7):1908-1925.

Hill, M.J., U. Senarath, A. Lee, M. Zeppel, J. Nightingale, R. Williams, T. McVicar, 2006. Assessment of the MODIS LAI product for Australian ecosystems. *Remote Sensing of Environment*. 101:495-518.

Hopkinson, C., L. Chasmer, G. Sass, I. Creed, M. Sitar, W. Kalbfleisch, and P. Treitz 2005: Assessing vegetation height and canopy volume in a Boreal wetland complex using airborne scanning LiDAR. *Canadian Journal of Remote Sensing*. 31(2):191-206.

Hopkinson, C. and L. Chasmer, 2007. Using discrete laser pulse return intensity to model canopy transmittance. *The Photogrammetric Journal of Finland*. 20(2):16-26.

Huemmrich, K.F., Black, T.A., Jarvis, P.G., McCaughey, J.H. and Hall, F.G. 1999. High temporal resolution NDVI Phenology from micrometeorological radiation sensors. *Journal of Geophysical Research* (Special BOREAS Issue H, BOREAS in 1999) 104(D22): 27934-27944.

Huemmrich, K.F., J. Privette, M. Mukelabai, R. Myneni, and Y. Knyazikhin, 2005. Time-series validation of MODIS land biophysical products in a Kalahari woodland, Africa. *International Journal of Remote Sensing.* 26(19):4381-4398.

Jin, Z, Q. Tian, J. M. Chen, and M. Chen, 2007. Spatial scaling between leaf area index maps of different resolutions. *Journal of Environmental Management.* 85: 628-637.

Jonckheere, I., S. Fleck, K. Nackaerts, B. Muys, P. Coppin, M. Weiss, and F. Baret, 2004. Review of methods for in situ leaf area index determination Part 1. Theories, sensors and hemispherical photography. *Agricultural and Forest Meteorology*. 121:19-35.

Knyazikhin, Y., J. Glassy, J. Privette, Y. Tian, A. Lotsch, Y. Zhang, Y. Wang, J.T. Morisette, P. Votava, R.Myneni, R. Nemani, S. Running, 1999. MODIS leaf area index (LAI) and fraction of photosynthetically active radiation absorbed by vegetation (FPAR) product (MOD15) algorithm theoretical basis document, http://modis.gsfc.nasa.gov/data/atbd/ land_atbd.php.

Koetz, B., G. Sun, F. Morsdorf, K. Ranson, M. Kneubuhler, K. Itten, and B. Allgower, 2006. Fusion of imaging spectrometer and LIDAR data over combined radiative transfer models for forest canopy characterization. *Remote Sensing of Environment*, doi:10.1016/j.rse.2006.09.013.

Kotchenova, S., X. Song, N. Shabanov, C. Potter, Y. Knyazikhin and R. Myneni, 2004. Lidar remote sensing for modeling gross primary production of deciduous forests. *Remote Sensing of Environment*. 92:158-172.

Leblanc, S. G., J. M. Chen, R. Fernandes, D. W. Deering, and A. Conley, 2005. Methodology comparison for canopy structure parameters extraction from digital hemispherical photography in boreal forests. *Agricultural and Forest Meteorology*, 129:187-207.

Lefsky, M.A., W.B. Cohen, S.A. Acker, G.G. Parker, T.A. Spies, D. Harding, 1999. Lidar Remote Sensing of the Canopy Structure and Biophysical Properties of Douglas-Fir Western Hemlock Forests. *Remote Sensing of Environment*, 70: 339-361.

Lovell, J., D. Jupp, D. Culvenor, and N. Coops, 2003. Using airborne and groundbased ranging lidar to measure canopy structure in Australian forests. *Canadian Journal of Remote Sensing*. 29(5):607-622.

Morsdorf, F., B. Kotz, E. Meier, K. Itten and B. Allgower, 2006. Estimation of LAI and fractional cover from small footprint airborne laser scanning data based on gap fraction. *Remote Sensing of Environment*. 104:50-61.

Myneni, R.B., R. R. Nemani, and S.W. Running, 1997. Algorithm for the estimation of global land cover, LAI and FPAR based on radiative transfer models. *IEEE Transactions in Geoscience and Remote Sensing*. 35:1380-1393.

Parker, G.G., Lefsky, M.A., Harding. D.J. 2001. Light transmittance in forest canopies determined using airborne laser altimetry and in-canopy quantum measurements. *Remote Sensing of Environment*, 76: 298-309.

Pielke, R.A., R. Avissar, M. Raupach, A. Dolman, Y. Xeng, and S. Denning, 1998. Interactions between the atmosphere and terrestrial ecosystems. Influence on weather and climate. *Global Change Biology*. 4:461-475.

Pisek, J., and J. M. Chen, 2007. Comparison and validation of MODIS and VEGETATION global LAI products over four BigFoot sites in North America. *Remote Sensing of Environment*, 109: 81-94.

Schwalm, C.R., T.A. Black, B.D. Amiro, M. A. Arain, A.G. Barr, C. P.-A. Bourque, A. Dunn, L. Flanagan, M.-A. Giasson, P. M. Lafleur, H.A. Margolis, J.H. McCaughey, A.L. Orchansky, and S.C. Wofsy, 2006. Photosynthetic light use efficiency of three biomes across an east-west continental-scale transect in Canada. *Agricultural and Forest Meteorology*. 140:269-286.

Sonnentag, O., J. Talbot, J. M. Chen, T. N. Roulet, 2007. Using direct and indirect measurements of leaf area index to characterize the shrub canopy of an ombrotrophic peatland. *Agricultural and Forest Meteorology*, 144: 200-212.

Sun, G.Q. and K. Ranson, 2000. Modelling lidar returns from forest canopies. *IEEE Transactions on Geoscience and Remote Sensing*. 38:2617-2626.

Thomas, V., D.Finch, J.H. McCaughey, T. Noland, L. Rich, and P. Treitz, 2006. Spatial modeling of the fraction of photosynthetically active radiation absorbed by a boreal mixedwood forest using a lidar-hyperspectral approach. *Agricultural and Forest Meteorology*. 140:287-307.

Turner, D.P., W. Ritts, W. Cohen, S. Gower, M. Zhao, S. Running, S. Wofsy, S. Urbanski, A. Dunn, and J.W. Munger, 2003. Scaling gross primary production (GPP) over boreal and deciduous forest landscapes in support of MODIS GPP product validation. *Remote Sensing of Environment*. 88:256-270.

Turner, D.P., S. Ollinger, and J. Kimball. Integrating remote sensing and ecosystem process models for landscape- to regional-scale analysis of the carbon cycle. *BioScience*. 54(6):573-584.

Turner, D.P., W.D. Ritts, W.B. Cohen, S.T. Gower, S. W. Running, M. Zhao, M. H. Costa, A. A. Kirschbaum, J.M. Ham, S.R. Saleska, D.E. Ahl, 2006. Evaluation of MODIS NPP and GPP products across multiple biomes. *Remote Sensing of Environment.* 102:282-292.

Wang, Y., C. Woodcock, W. Buermann, P. Stenberg, P. Voipio, H. Smolander, T. Hame, Y. Tian, J. Hu, Y. Knyazikhin, and R. Myneni, 2004. Evaluation of the MODIS LAI algorithm at a coniferous forest site in Finland. *Remote Sensing of Environment*. 91:114-127.

Wise, S. 2000. Assessing the quality for hydrological applications of digital elevation models derived from contours. *Hydrological Processes.* 14:1909-1929.

Wolfe, R.E., M. Nishihama, A. Fleig, J. Kuyper, D. Roy, J. Storey, and F. Patt, 2002. Achieving sub-pixel geolocation accuracy in support of MODIS land science. *Remote Sensing of Environment.* 31-49.

Xu, S. J. M. Chen, R. Fernandes and J. Cihlar. 2004. Effects of subpixel water area fraction on mapping leaf area index and net primary productivity in Canada. *Canadian Journal for Remote Sensing*, 30: 797-804.

Zhang, Y., J. Chen, and J. Miller, 2005. Determining digital hemispherical photograph exposure for leaf area index estimation. *Agricultural and Forest Meteorology*. 133:166-181.

Zhao, M., F.A. Heinsch, R.R. Nemani, and S. Running, 2005. Improvements of the MODIS terrestrial gross and net primary production global data set. *Remote Sensing of Environment.* 95:164-176.

Chapter 5

Scaling and Assessment of GPP from MODIS Using a Combination of Airborne Lidar and Eddy Covariance Measurements over Jack Pine Forests

5.1 Abstract

Understanding the influence of within-pixel land cover heterogeneity is essential for the extrapolation of measured and modeled CO_2 fluxes from the canopy to regional scales using remote sensing. Airborne light detection and ranging (lidar) was used to estimate spatial and temporal variations of gross primary production (GPP) across a jack pine chronosequence of four sites in Saskatchewan, Canada for comparison with the Moderate Resolution Imaging Spectroradiometer (MODIS) GPP product. This study utilizes high resolution canopy structural information obtained from airborne lidar to bridge gaps in spatial representation between plot, eddy covariance (EC), and MODIS estimates of vegetation GPP. First we investigate linkages between canopy structure obtained from measurements and light response curves at a jack pine chronosequence during the growing season of 2004. Second, we use the measured canopy height and foliage cover inputs to create a structure-based GPP model ($GPP_{Landsberg}$) which was tested in 2005. The GPP model is then run using lidar data (GPP_{Lidar}) and compared with eight-day cumulative MODIS GPP (GPP_{MODIS}) and EC observations (GPP_{EC}). Finally, we apply the lidar GPP model at spatial resolutions of 1 m to 1000 m to examine the influence of within-pixel heterogeneity and scaling (or pixel aggregation) on GPP_{Lidar}. When compared over eight-day cumulative periods throughout the 2005 growing season, the standard deviation of differences between GPP_{lidar} and GPP_{MODIS} were less than differences between either of them and GPP_{EC} at all sites. As might be expected, the differences between pixel aggregated GPP estimates are most

pronounced at sites with the highest levels of spatial canopy heterogeneity. The results of this study demonstrate one method for using lidar to scale between eddy covariance flux towers and coarse resolution remote sensing pixels using a structure-based Landsberg light curve model.

5.2 Introduction

Ecosystem gross primary production (GPP) can be estimated at the flux footprint scale using eddy covariance (EC) methods (e.g. Barr et al. 2006) or over contiguous land cover types at the low resolution pixel scale using satellite-derived products from sensors such as the Moderate Resolution Imaging Spectroradiometer (MODIS) (e.g. Heinsch et al. 2006). However, reconciling local EC estimates of GPP from spatially and aerially variant flux footprints with fixed coverage satellite-based estimates poses a challenge that is a function of the disparate scales and methods of observation (e.g. Turner et al. 2002; Chen et al. 2008). In this paper, we aim to address part of this scaling problem by using canopy structural information extracted from airborne light detection and ranging (lidar) data to improve estimates of GPP both at the flux footprint and MODIS pixel scales.

A number of factors are known to lead to a level of incongruence between MODIS and site-specific (EC) estimates of GPP. These include: a) under-estimation of CO_2 exchanges by EC due to atmospheric stability, resulting in the apparent over-estimation of GPP by MODIS (e.g. Massman and Lee, 2002; Coops et al. 2007); b) scaling errors associated with comparing point measurements of GPP, leaf area index (LAI) and the fraction of photosynthetically active radiation absorbed by the canopy (fPAR) to large area remote sensing pixels (Tian et al. 2002; Turner et al. 2002; Turner et al. 2004; Heinsch et al. 2006); c) a limited ability to accurately represent the effects of three-dimensional canopy shadowing and ground surface reflectance on MODIS pixels (Xu et a. 2004; Erikson et al. 2006; Jin et al. 2007); and d) MODIS pixel

geolocation issues and the inclusion of land areas not represented by EC (Turner et al. 2004). Plot or transect measurements of vegetation characteristics, used to rectify these issues within large area MODIS pixels, are also often difficult and time-consuming to obtain, especially in remote locations (Heinsch et al. 2006).

We believe that some of the challenges associated with comparing EC estimates of GPP with fixed coverage MODIS pixel-based estimates can be addressed by scaling between these disparate observation methods using airborne lidar data. Lidar provides a very high resolution map of the three-dimensional characteristics of the vegetated canopy, understory, and ground surface. The interception of photosynthetically active radiation (PAR) by the canopy and understory directly impacts GPP and photosynthesis (e.g. Baldocchi and Meyers, 1998) through the convergence efficiency of intercepted PAR to GPP, also known as light use efficiency (LUE) (Turner et al. 2002; Schwalm et al. 2006). LUE can be estimated from the slope of a Landsberg light response curve, which is related to the saturation of photosynthesis beyond certain light levels (e.g. Turner et al. 2002; Turner et al. 2003). If LUE for an ecosystem is known or can be estimated from a look-up table, for example, then the Landsberg curve can be used to model GPP:

$$GPP_{Landsberg} = P_{\max}(1 - e^{-a(PAR - I_{comp})}), \qquad [1]$$

where $P_{\max}$ is the maximum average GPP at saturation (g C m^{-2}) (the point at which GPP plateaus with increased light levels), α is the slope or scaling factor of GPP as it increases with incoming PAR, and I_{comp} is the light compensation point at which GPP is zero. This then provides the context for scaling between EC and MODIS using airborne lidar. EC estimates of GPP are based on measures of flux from the ecosystem, and MODIS estimates of GPP are based on the

absorption and reflection of light from within ~1 km resolution pixels. However, actual canopy detail is not considered. In both cases (EC and MODIS) the canopy and understory structure is implicit in directly influencing the GPP estimate. Lidar enables this implicit treatment of canopy structure to be made explicit in both cases.

A hypothesis can be formulated as follows: Foliage density and canopy height, which can be estimated from lidar, may correspond with variability in LUE. LUE is also used in the MODIS algorithm to estimate GPP. To illustrate that LUE and GPP may be related to canopy structure, an example is provided: Papers by Schwalm et al. (2006) and Chen et al. (2006) have recorded LUE, canopy height and fractional cover (as fPAR) for the same 16 Fluxnet-Canada forest sites. Comparing the observations from both papers, we find that average growing season LUE for boreal conifer and deciduous forests, temperate rain forest, previously harvested stands, and previously burned stands is significantly related to average canopy height ($r^2 = 0.61$, $p = 0.001$, RMSE = 0.19 g C MJ^{-1} APAR (not shown)) (see Schwalm et al. 2006). Based on this comparison and results in Chasmer et al. (2008) and Chasmer et al. (accepted) it follows that (all else being equal) areas displaying taller canopy heights and/or fractional canopy cover will be positively related to gross photosynthesis and CO_2 uptake. Therefore, Landsberg input parameters, such as average maximum GPP, may be greater for canopies containing more biomass and taller trees. The light compensation point may also vary due to within canopy shadowing, fractional cover and vegetation height. For example, shorter vegetation with lower fractional cover will receive more radiation early in the morning than taller vegetation with greater fractional cover (due to long morning shadows), thereby increasing the level of light required for photosynthesis in forests of taller trees and greater leaf area. If this is the case, then GPP may be modeled using the Landsberg curve, canopy height and fractional cover estimates from airborne lidar.

The analysis presented first investigates linkages between field-based canopy structure measurements and Landsberg light response curves at a jack pine chronosequence during the growing season of 2004 and tested in 2005 ($GPP_{Landsberg}$). Second, we use the lidar inputs (fractional cover and canopy height) to create a structure-based GPP model (GPP_{lidar}) (also tested in 2005). GPP_{lidar} is then compared with eight-day cumulative MODIS GPP (GPP_{MODIS}) and EC observations (GPP_{EC}). Finally, we apply GPP_{lidar} at spatial resolutions of 1 m to 1000 m at three jack pine sites to examine the influence of within-pixel heterogeneity and scaling (or pixel aggregation) on modeled GPP.

5.3 Data Collection

5.3.1 Site Characteristics

Four jack pine sites, forming a post-harvest chronosequence, were examined during the growing seasons (June 1st to September 31st) of 2004 and 2005. The jack pine stands included a mature jack pine forest of ~90 years of age (OJP); an immature jack pine forest harvested in 1975 (HJP75); a regenerating jack pine forest harvested in 1994 (HJP94); and a naturally regenerating jack pine site harvested in 2000 and scarified in 2002 (HJP02). The forest stands are located within 6 km of each other near the southern edge of the boreal forest, north of Prince Albert, Saskatchewan, Canada. All sites examined in this study were operating as part of Fluxnet-Canada (Barr et al. 2006; Margolis et al. 2006), under the Boreal Ecosystem Research and Monitoring Sites (BERMS) project. Each site is relatively flat with coarse-textured and well-drained sandy soils (e.g., Baldocchi et al. 1997).

Forest stand characteristics are summarized in Tables 5.1 (OJP, HJP75, and HJP94) and 2 (HJP02). Measurements of canopy structure were made at eight (OJP), eight (HJP75), and six

(HJP94) geo-located 11.3 m radius plots located at distances of 100 m and 500 m (at OJP and HJP75) and within 250 m (HJP94) of EC towers in May and August, 2005. At HJP02, four 25 m x 2 m transects containing 50 1 m x 1 m plots were located at distances of 50 m to 75 m (N, S, E, and W) from the EC tower. The centre of plots, and the start and end of transects were located using survey-grade, differentially corrected global positioning system (GPS) receivers (Leica SR530, Leica Geosystems Inc. Switzerland; Ashtec Locus, Ashtec Inc., Hicksville, NY) with the same base station coordinate as was used for the lidar survey. Geo-location accuracies varied from 1 cm to 1 m depending on the canopy cover density at the time of GPS data collection.

Canopy gap fraction was obtained using digital hemispherical photography (DHP) at OJP, HJP75, and HJP94, and radiation sensors at HJP02 (Chasmer et al. 2008). One photograph was taken at the centre of the plot, and four were located 11.3 m from the centre along cardinal (N, S, E, and W) directions, determined using a compass bearing and measuring tape (Fluxnet-Canada, 2003). Photographs were taken at a height of ~1.3 m at OJP and HJP75, and 0.7 m at HJP94. Trees were often less than 2 m in height at HJP94; therefore a lower DHP height was chosen to capture more biomass. Photographs were taken during either diffuse daytime conditions, or 30 minutes before dawn or after dusk, at one F-stop below normal exposure. Under-exposure of photographs reduces the influence of sun brightness and under-estimation of leaf area (Zhang et al. 2005). Individual photographs were processed following sky and vegetation thresholding methods of Leblanc et al. (2005). Thresholds for sky and foliated pixels were used to obtain estimates of gap fraction (Ω) within the software, DHP version 1.6.1 (S. Leblanc, Canada Centre for Remote Sensing provided to L. Chasmer through the Fluxnet-Canada Research Network). Average canopy height, estimated using a Vertex sonic hypsometer (Haglof, Maddison), and vegetation

fractional cover (1- Ω) per site were compared with inputs used in light response curves, whereas plot level averages were compared with lidar estimates of the same.

Table 5.1. Average vegetation characteristics at OJP, HJP75, and HJP94 for 22 plots. The values in parentheses represent standard deviation (stdev).

Site	Number of trees sampled	Average stem density (stdev) (stems m^{-2})	Average tree height (stdev) (m)	Average DBH* (stdev) (cm)	Average LAI (stdev) ($m^2 \cdot m^{-2}$)	Average canopy depth (stdev) (m)	Average crown diameter (stdev) (m)	Other species
OJP	381	0.11 (0.001)	14.2 (3.5)	9.33 (4.55)	1.6 (0.1)**	8.3 (2.7)	2.0 (1.0)	Alder, bearberry, reindeer lichen, blueberry, cranberry
HJP75	1447	0.59 (0.19)	6.3 (1.6)	5.69 (3.49)	2.8 (0.4)	3.5 (1.3)	0.9 (0.4)	Grasses, reindeer lichen, bearberry
HJP94	2081	0.86 (0.56)	1.6 (0.7)	2.31 (1.05)	1.1 (0.2)	1.6 (0.7)	0.7 (1.1)	Grass, blueberry, alder, raspberry, bearberry, reindeer lichen

* DBH refers to tree bole diameter at breast height (1.3 m above the ground).
** LAI measurements from Chen et al. (2006) differ from LAI observed in this study.

Table 5.2. Average vegetation characteristics at HJP02 for 200 1m x 1m plots along four transects. Average percent cover does not add up to 100% (averaged between four transects) due to varying amounts of vegetation coverage per plot.

Number of trees (in 200 1m plots)	Average tree height (stdev) (m)	Average % tree cover (stdev)	Average % grass cover (stdev)	Average % reindeer lichen cover (stdev)	Average % soil cover (stdev)	Average % wood debris cover (stdev)	Average % herb cover (stdev)	Average estimated LAI ($m^2 \cdot m^{-2}$)
37	0.19 (0.12)	9 (11)	21 (18)	23 (30)	32 (18)	26 (24)	8 (15)	0.29

5.3.2 Site Instrumentation

Measurement and processing of eddy covariance (EC) data has been discussed in Kljun et al. (2006) and Barr et al. (2006) and follow Fluxnet-Canada procedures for standardization between sites. Briefly, EC was used at all sites to measure CO_2 fluxes averaged over 30-minute periods and then aggregated on a daily basis and again, over eight day periods for comparison with MODIS. The plot measurement-based GPP model ($GPP_{Landsberg}$) was developed using EC data

collected during the growing season (June 1st to September 31st) of 2004 and was then tested and compared with GPP_{EC} and GPP_{MODIS} in 2005.

GPP (used interchangeably with gross ecosystem production, GEP) was estimated from EC-measured net ecosystem production (NEP) ($\mu mol \cdot m^{-2} \cdot s^{-1}$) and modeled ecosystem respiration (Re) ($\mu mol \cdot m^{-2} \cdot s^{-1}$). Re was estimated based on the relationship between nighttime Re and soil temperature (Barr et al. 2004). Cumulative daily estimates of GPP_{EC} have been expressed in units of g $C \cdot m^{-2} \cdot day^{-1}$ for direct comparison with GPP_{MODIS} (kg $C \cdot m^{-2} \cdot 8\text{-days}^{-1}$ converted to g $C \cdot m^{-2} \cdot 8\text{-days}^{-1}$). CO_2, H_2O and friction velocity were measured using a sonic anemometer (CSAT3, Campbell Scientific Inc. Edmonton, Alberta, Canada at OJP and HJP02; Gill R3-50, Gill Instruments Ltd., England at HJP75; SAT-550, Kaijo Co., Tokyo, Japan at HJP94) combined with a closed path infrared gas analyzer (LI 6262, LI-COR Inc., Lincoln, NE, USA). EC systems have been installed above the canopy at heights of approximately 28 m, 17 m, 3 m, and 2 m at OJP, HJP75, HJP94, and HJP02 respectively. Any gaps in the 30-minute fluxes were filled using a moving-window regression approach (Barr et al. 2006; Kljun et al. 2006). EC data were quality controlled using a minimal surface friction velocity of 0.35 m s^{-1} at all sites, and an energy balance closure correction was applied to reduce under-estimates of measured net ecosystem exchange (NEE) by EC (Barr et al 2006).

Above-canopy incoming and reflected PAR (400 to 700 nm) and below-canopy incoming PAR were measured using quantum sensors LI-COR model LI190 at OJP and HJP75 (LI-COR Biosciences, Nebraska, USA); and Eko model ML-020P (Eko Instruments, Co. Ltd., Japan) at HJP94 and HJP02. Above canopy incident and reflected PAR sensors were installed on booms at heights of 28 m, 12 m, 3 m and 2 m above the ground at OJP, HJP75, HJP94, and HJP02. Below

canopy incident PAR measurements were made at OJP and HJP75 at a height of ~1 m. Below-canopy PAR measurements were not available at HJP94 and HJP02.

5.3.3 Lidar Data Collection and Analysis

Airborne lidar data were obtained throughout the entire White Gull River watershed, including jack pine chronosequence sites, on August 12, 2005. The lidar system is an Airborne Laser Terrain Mapper (ALTM) 3100 (Optech Inc. Toronto, Ontario, Canada) small-footprint discrete pulse return lidar. Data were collected in partnership with the Applied Geomatics Research Group (AGRG), Nova Scotia, Canada. The lidar was flown at a height of 950 m above the ground surface, and emitted laser pulses at a rate of 70 kHz. A $\pm 19^{o}$ scan angle was used with 50% overlap of scan lines, enabling penetration of laser pulses through to the base of the canopy and returns from all sides of individual trees (Chasmer et al. 2006). Up to four laser returns were obtained per laser pulse emitted resulting in cross- and down-track resolutions of ~35 cm.

After initial processing of GPS trajectories and range files at the AGRG, lidar data were imported into the software package Terrascan (Terrasolid, Finland) for area subsetting and laser return classification. The larger lidar dataset was subset into 1 km x 1 km areas containing EC flux stations within the same geographical area covered by one MODIS pixel. Circular 11.3 m radius mensuration plots were also extracted from the lidar for comparison with average plot-measured canopy height and fractional cover. Lidar datasets were then filtered for outlying returns greater than the height of the EC tower or lower than 1.5 m below the ground surface. Datasets were then classified into "ground" returns (P_{ground}), "canopy" returns (above 1.3 m at OJP and HJP75; and 0.7 m at HJP94) (P_{canopy}), and "all" returns (which included ground returns) (P_{all}). P_{ground} was used to create a 2 m x 2 m digital terrain model (DTM) from which P_{all} and P_{canopy} returns were normalized relative to the ground surface. The DTM was created by interpolating between ground

returns within 2 m resolution pixels using an inverse distance weighting procedure (IDW) (i.e. O'Sullivan and Unwin, 2003) and a search radius of 3 m. This method was chosen because it a) retains point values of the data; b) is a rapid interpolation method, which is important when dealing with large volumes of lidar data; and c) is appropriate for regularly spaced data (Myers, 1994). Although the resolution of the lidar dataset is greater than 2 m, areas of dense canopy foliage and individual alder bushes can reduce the density of ground returns. Therefore a 2 m resolution was used to avoid "holes" within the DTM.

Lidar canopy height models (CHM) were created from the normalized maximum z-height (m) at jack pine sites using IDW at 1 m x 1 m resolution. At HJP02, short vegetation and ground topography could not be resolved between first, intermediate, and last returns. This is due to the inability of lidar systems to distinguish between returns separated by less than 1.6 m, depending on the lidar systems used (Hopkinson et al. 2005). Therefore, comparisons at HJP02 were limited to measured data only and did not include any lidar data analysis. Fractional cover (*f*cover) (where 1 = full canopy cover and 0 = no canopy cover) was estimated based on the ratio of the number of canopy returns to the number of all returns within 1 m x 1 m x height columns throughout each site:

$$f\,\mathrm{cover} = \left(\frac{\sum P_{canopy}}{\sum P_{all}} \right). \qquad [2]$$

The *f*cover or "return ratio" method has been examined in various forms within numerous studies and closely approximates fractional cover when compared with DHP (Morsdorf et al. 2006; Solberg et al. 2006; Hopkinson and Chasmer, in review).

5.3.4 MODIS GPP Product

GPP_{MODIS} (Collection 5) data were obtained from the Oak Ridge National Laboratory (ORNL) Distributed Active Archive Center (DAAC) (http://www.modis.ornl.gov/modis/ index.cfm) and was subset into 3 km x 3 km areas (9 pixels) at OJP, HJP75, HJP94 and HJP02 flux tower sites. Eight-day cumulative periods were compared with the same cumulated GPP periods observed from EC. Only days that contained the best quality controlled MODIS data for all nine pixels were included. The estimation of GPP by MODIS is described in detail in Running et al. (1999); Zhao et al. (2005); and Heinsch et al. (2006).

5.4 Methods

In this study, four methods are used to estimate GPP. These include EC (GPP_{EC}), Landberg curves based on local plot measurements ($GPP_{Landsberg}$), Landsberg curves based on airborne lidar (surrounding the EC) within the area covered by one MODIS pixel (GPP_{lidar}), and MODIS pixel estimates containing the EC (GPP_{MODIS}). $GPP_{Landsberg}$ has been modeled in 2004 and tested and compared in 2005. Table 5.3 provides a summary of the four methods that are used. Further discussion of the methodologies used to define these estimates is found in the following sections.

Table 5.3. Summary of GPP methods estimated using EC, plot measurements, airborne lidar, and MODIS.

GPP Estimation Method	Description	Growing Season Examined	Data Inputs
GPP_{EC}	GPP estimated using EC	2004 and 2005. 2005 compared with all other GPP methods.	NEE, Re
$GPP_{Landsberg}$	GPP estimated using canopy structure inputs from forest plot measurements	Method developed in 2004, tested in 2005. 2005 compared with all other GPP methods.	Incoming PAR, average measured tree height and fractional cover
GPP_{lidar}	GPP estimated using area averaged canopy height and fractional cover from airborne lidar. Average areas include that within MODIS pixel area including the EC (1km x 1km)	2005 compared with all other GPP methods.	Incoming PAR, lidar average tree height and fractional cover
GPP_{MODIS}	GPP estimated from MODIS within the pixel containing the EC at each site.	2005 compared with all other GPP methods.	Incoming PAR, MODIS fPAR product, and LUE determined from a look-up table.

5.4.1 Landsberg Light Response Curve Analysis and Development of GPP Model

The first objective makes comparisons between Landsberg input variables used to predict GPP from light response curves and canopy structure attributes at the jack pine chronosequence during the growing season of 2004. The purpose is to first determine if there is a relationship between canopy structure and Landsberg input variables, and if there is, to then develop GPP models based on canopy structure and Landsberg principles.

The Landsberg equation [1] (e.g. Landsberg and Waring, 1997; Chen et al. 2002) was used to examine the relationships between daily average incoming PAR and GPP_{EC} per site during 2004. Fitted values for P_{max} and α were compared to canopy height across sites and the fitted value for I_{comp} was compared with average fractional cover across sites to estimate GPP ($GPP_{Landsberg}$). However, fractional cover was not actually measured in 2004. To estimate fractional cover in 2004, DHP plot measurements were adjusted based on percentage differences in fractional cover measurements made by PAR sensors between 2004 and 2005:

$$\text{Fractional cover} = (PAR_{AC\downarrow} - PAR_{BC\downarrow}) / PAR_{AC\downarrow}, \qquad [3]$$

and at HJP94 and HJP02:

$$\text{Fractional cover} = PAR_{AC\downarrow} (1 - e^{-kL^*}) / PAR_{AC\downarrow} \qquad [4]$$

where $PAR_{AC\downarrow}$ is above-canopy incoming PAR, and $PAR_{BC\downarrow}$ is incoming below-canopy PAR after interception with branches and leaves. L is LAI, and k is the extinction coefficient estimated

as a constant 0.45 for simplicity (Chen et al. 2006). Measured fractional cover [3, 4] was examined during diffuse radiation conditions only and then averaged throughout the growing season. Based on results of Middleton et al. (1997) we have assumed that canopy fractional cover did not vary at the jack pine sites within the growing seasons studied.

Measured below canopy PAR percent differences between the two years were used to vary site-averaged estimates of fractional cover between 2004 and DHP measurements in 2005. PAR adjusted DHP fractional cover was estimated as 0.57 (OJP), 0.73 (HJP75), 0.41 (HJP94), and 0.22 (HJP02) in 2004. Measurement of average fractional cover by DHP was 0.59 (OJP), 0.72 (HJP75), 0.39 (HJP94) and 0.29 (HJP02) in 2005. Meteorological conditions during 2004 were similar to 2005; however, a severe drought in 2003 and a late, cool spring in 2004 may have caused slight reduction in foliage cover at some sites (Chasmer et al. 2008).

Tree heights also were not measured in 2004 and were estimated based on jack pine forest growth rates in Manitoba and Saskatchewan (Burns and Honkala, 1990). Average growth rates are approximately 0.15 m from ages one to two, 0.23 m per year from ages five to eight years, 0.33 m per year at age 30, and 0.23 m per year at age 50. Canopy heights for 2004 were reverse estimated and averaged from the 2005 field plot data as 13.97 m (OJP), 5.64 m (HJP75), 1.37 m (HJP94), and 0.15 m (HJP02).

5.4.2 GPP Model Assessment

GPP was modeled based on the relationships between canopy height and fractional cover, and Landsberg curve inputs in 2004. To test the applicability of the model, the structure-based GPP model was run during the 2005 growing season by substituting 2005 measured canopy height and

fractional cover, and incoming PAR into the Landsberg equations ($GPP_{Landsberg}$). $GPP_{Landsberg}$ was then compared with GPP_{EC} in 2005.

Root mean square error (RMSE), systematic RMSE ($RMSE_s$) and unsystematic RMSE ($RMSE_u$) were used to evaluate the accuracy of $GPP_{Landsberg}$ when compared with GPP_{EC}. RMSE provides a measure of the average differences between observed and predicted GPP, whereas $RMSE_s$ and $RMSE_u$ provide measures of the systematic biases and unsystematic or random biases un-related to the model (Rymph, 2004). $RMSE_s$ and $RMSE_u$ were calculated as:

$$RMSE_s = \sqrt{\frac{\sum_{i=1}^{n}(\hat{P}_i - O_i)^2}{n}} \qquad [5]$$

and

$$RMSE_u = \sqrt{\frac{\sum_{i=1}^{n}(P_i - \hat{P}_i)^2}{n}} \qquad [6]$$

where O_i is the GPP_{EC}, P_i is the $GPP_{Landsberg}$, $\hat{P}_i = mO_i + b$, and m and b are the slope of the regression lines and Y-intercepts, respectively (from Rymph, 2004). Models that perform well have low RMSE, $RMSE_s$ should be close to zero and the $RMSE_u$ should be close to the RMSE. Low measurements of $RMSE_s$ indicate that the model is predicting at maximum accuracy and the sources of errors are random and not related to the model (Rymph, 2004).

5.4.3 Model Application and Comparison

The third objective uses airborne lidar to spatially model GPP (GPP_{lidar}) within the 1 km x 1 km area surrounding the EC station (equivalent to one MODIS pixel) at 1 m resolution during the

growing season of 2005. Average canopy height from the CHM and lidar fractional cover (*f*cover) are input into the Landsberg GPP model (Objective 1) to estimate GPP (GPP_{lidar}). GPP_{lidar} is compared with GPP_{MODIS} and GPP_{EC}, cumulated over 8-day periods during the growing season of 2005. The purpose is to compare GPP_{lidar} at the MODIS pixel scale with GPP_{EC} at the flux footprint scale and GPP_{MODIS} at 1 km resolution to determine if differences in GPP exist as a result of spatial variability in canopy structure beyond the footprint of the EC station. We hypothesize that GPP_{Lidar} and GPP_{MODIS} will be more similar than when compared with GPP_{EC} because the same area will be included in the estimation of GPP using remote sensing methods, whereas GPP_{EC} will sample a smaller area within the larger MODIS pixel. The maximum source area of the footprint extends to up to 1 km at OJP and HJP75, 250 m at HJP94, and 150 m at HJP02 during convective daytime periods (Chasmer et al. accepted).

5.4.4 GPP Scaling Analysis

The final objective aggregates GPP_{lidar} from 1 m to 25 m, 250 m, 500 m, and 1000 m resolutions to determine the influence of within pixel patches on GPP estimation. This is done by averaging from higher resolution pixels (i.e. 1 m) to lower resolutions in ArcGIS (ESRI, CA). When scaling from 1 m to 25 m resolution, for example, the mean of all 1 m resolution pixels within the 25 m x 25 m area are used to estimate a single value of GPP at 25 m resolution. This was repeated for all pixels within each MODIS pixel area (i.e. 1 km x 1 km). The same methodology was then applied to other resolutions by aggregating all 1 m x 1 m pixels within 250 m x 250 m, 500 m x 500 m, and 1000 m x 1000 m pixels by retaining the individual 1 m resolution cell values of GPP. The mean GPP_{lidar} of the lower resolution pixels was used following results of Woolard and Colby (2002). They found that the means of the aggregated pixels were statistically most appropriate when compared with other methods of aggregation (i.e. central pixel resampling, median, etc.)

and retained patterns in the landscape at varying scales. Comparisons between resolutions were then made by subtracting each lower resolution pixel from 1 m x 1 m pixels.

5.5 Results

5.5.1 Comparisons between Landsberg Inputs and Canopy Structure

Incoming PAR accounted for 60%, 54%, 61% and 8% of the variability of 30-minute average GPP_{EC} at OJP, HJP75, HJP94, and HJP02 (Table 5.4, Figure 5.1). Landsberg curve relationships between GPP_{EC} and incoming PAR indicate that saturation occurred at different levels of PAR depending on the forest age and the structural characteristics of the site. This indicates that canopy structure plays a role in the variability in CO_2 uptake per site, and the non-linearity of the Landsberg curves. GPP saturated at incoming PAR levels of approximately 800, 700 and 450 $\mu mol \cdot m^{-2} \cdot s^{-1}$ at OJP, HJP75, HJP94 and almost immediately at HJP02.

Table 5.4. Parameters (P_{max}, I_{comp}, and α) used in Landsberg curves and the correlation between incoming PAR and GPP described by the Landsberg curve. Landsberg input parameters have been determined from all 30-minute periods of PAR and GPP measured during the growing season of 2004.

Site	P_{max} ($\mu mol \cdot m^{-2} \cdot s^{-1}$)	α (scaling)	I_{comp} ($\mu mol \cdot m^{-2} \cdot s^{-1}$)	Correlation (r^2) between incoming PAR and GPP described by Landsberg curve
OJP	10.37	0.0048	12	0.60
HJP75	9.25	0.0035	14	0.54
HJP94	6.53	0.0028	10	0.61
HJP02	1.71	0.0011	8	0.08

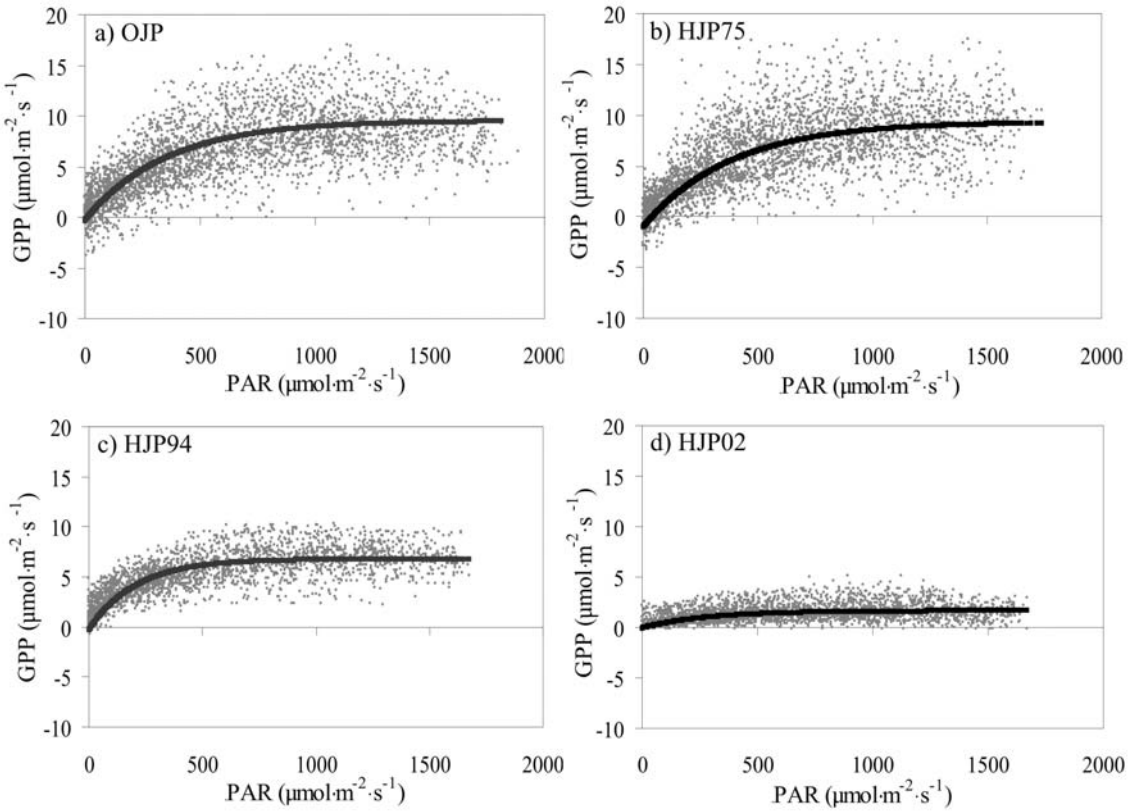

Figure 5.1. Landsberg model light response curves and relationships between observed 30-minute incoming PAR ($\mu mol \cdot m^{-2} \cdot s^{-1}$) and GPP ($\mu mol \cdot m^{-2} \cdot s^{-1}$) during the 2004 growing season.

Relationships between average measured tree heights, measured fractional cover and Landsberg input variables are shown in Figure 5.2 for 2004. P_{max} was positively related to average canopy height ($r^2 = 0.99$), where taller trees had greater average maximum GPP at saturation than shorter trees at the sites studied. The relationship was non-linear, where increases in P_{max} with height were greatest between HJP02 and HJP94, and leveled off between HJP75 and OJP. Relationships between P_{max} and fractional cover were lower, but still non-linear ($r^2 = 0.74$). I_{comp} was linearly related to the average fraction of foliage cover within each stand ($r^2 = 0.99$) and non-linearly related to canopy height ($r^2 = 0.80$). The scaling function (α) also varied with canopy structure (r^2

= 0.97, canopy height; 0.68, fractional cover). α was greatest at OJP and was slightly lower at HJP75 and HJP94. At HJP02, the scaling function was much lower than at other sites.

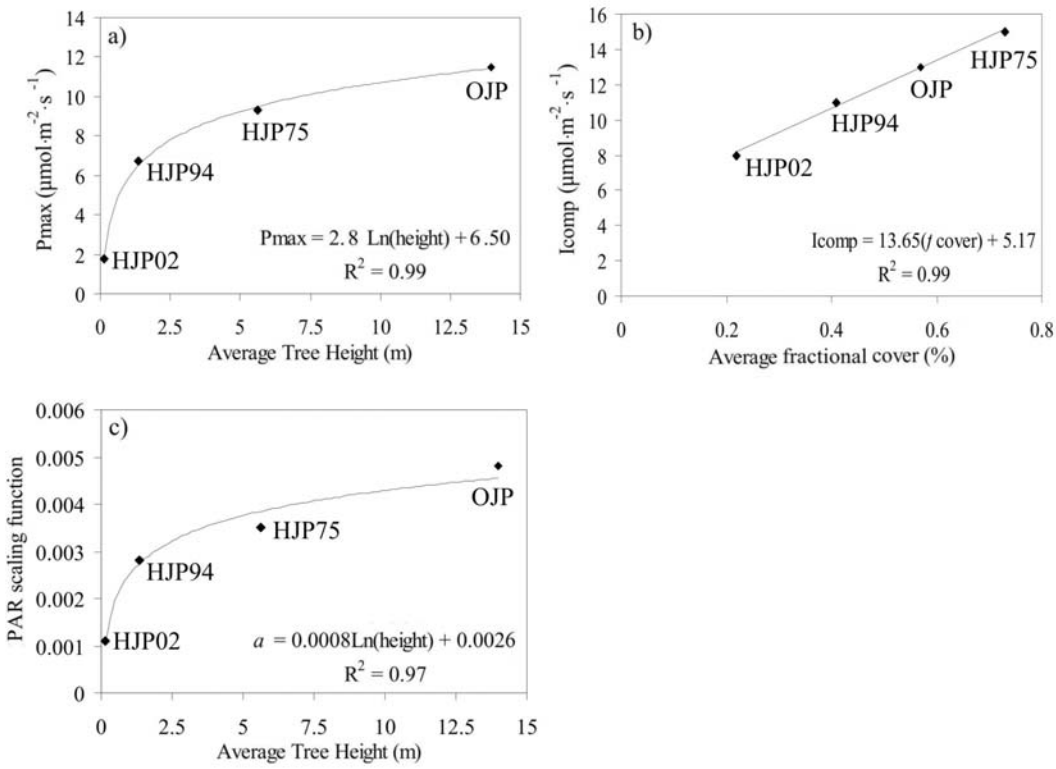

Figure 5.2. Site-level relationships between a) P_{max} and average measured tree height; b) I_{comp} and average measured fractional foliage cover from DHP; and c) α and average measured tree height estimated in 2004.

Based on the relationships between plot measured canopy structure (Table 5.1) and Landsberg input variables (Figure 5.2), canopy structure obtained either from plot measurements may be used to model GPP. P_{max}, I_{comp}, and α can be substituted into the Landsberg equation (including daily incoming PAR) based on logarithmic and linear relationships between sites as follows:

$$P_{max} = 2.8 \text{ x Ln(tree height)} + 6.50, \qquad [7]$$

$$I_{comp} = 13.7 \text{ x (fractional cover)} + 5.17, \quad [8]$$

and

$$\alpha = 0.0008 \text{ x Ln(tree height)} + 0.0026. \quad [9]$$

Application of these relationships is suitable only for the sites examined in this study. Relationships between measured canopy structure and Landsberg inputs should be examined at other sites.

5.5.2 Comparing GPP Predicted from Height and Fractional Cover with Observed GPP

In the second objective, $GPP_{Landsberg}$ [Eq. 7, 8, and 9], is tested and compared with GPP_{EC} during the 2005 growing season at each site. Average canopy cover and tree heights from plot measurements were used to estimate $GPP_{Landsberg}$ (Table 5.3; Figure 5.3).

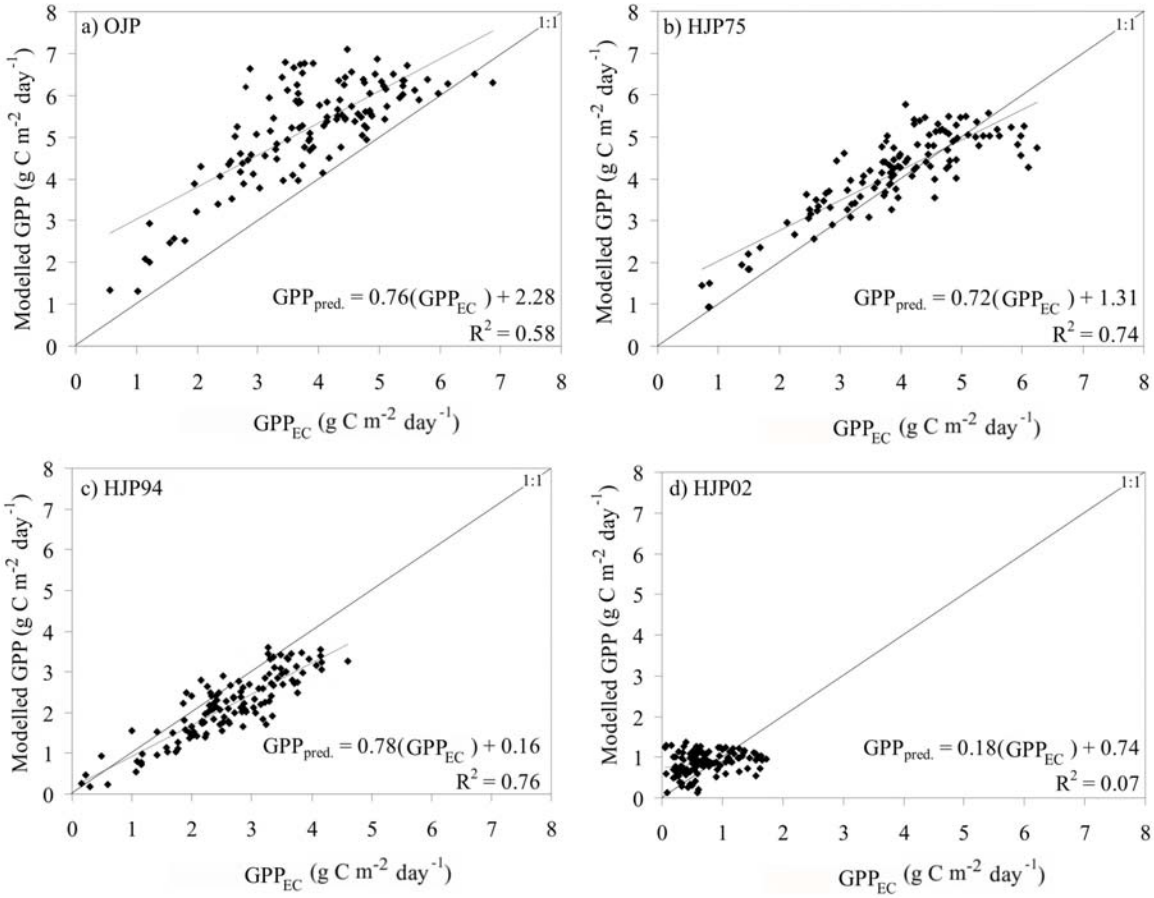

Figure 5.3. Comparisons between GPP_{EC} and $GPP_{Landsberg}$ with the inclusion of measured canopy height and fractional cover during the growing season of 2005.

$GPP_{Landsberg}$ (Table 5.5) compared well with GPP_{EC} at all sites but HJP02 in 2005. The slopes of the linear regression (ideally 1.00) were between 0.72 and 0.78 at OJP, HJP75, and HJP94. The Y-intercept was close to zero at HJP94 and HJP02, but high at OJP and HJP75 (2.28 g $C \cdot m^{-2} \cdot d^{-1}$, and 1.31 g $C \cdot m^{-2} \cdot d^{-1}$). This indicates that $GPP_{Landsberg}$ was over-estimated at OJP and HJP75 for low values of GPP_{EC}. Table 5.5 provides measures of $GPP_{Landsberg}$ model accuracy when compared with GPP_{EC}. Examination of daily GPP_{EC} using probability plots (not shown) indicate that OJP and HJP02 were normally distributed in 2004, whereas HJP75 and HJP94 were not normally distributed. In 2005, when the model was tested, OJP, HJP75, and HJP94 were normally distributed, whereas HJP02 was not. Either Pearson's r or Spearman's rank correlations are

shown for each site because Pearson's r correlation requires that data are normally distributed, whereas Spearman's rank does not. Daily RMSE was less than 10% of the mean daily GPP, and systematic errors varied by less than ~14% of the mean daily GPP at HJP75, HJP94, and HJP02. Unsystematic errors were lower than systematic errors at all sites, except HJP75, indicating that predicted GPP may have been influenced by other factors at this site. At OJP, however, the model did not perform as well, indicating that predicted GPP was prone to some systematic biases and could be further refined.

Table 5.5. Measurements of the accuracy of GPP_{EC} vs. $GPP_{Landsberg}$ (n = 122) during the growing season of 2005. *p-values* are included in brackets. Pearson's r correlation is appropriate for OJP, HJP75 and HJP94, whereas Spearman's rank correlation is appropriate for HJP02.

Site	RMSE ($g\ C \cdot m^{-2} \cdot d^{-1}$)	$RMSE_s$ ($g\ C \cdot m^{-2} \cdot d^{-1}$)	$RMSE_u$ ($g\ C \cdot m^{-2} \cdot d^{-1}$)	Pearson's correlation coefficient (r) (*p*)	Spearman's rank correlation (*p*)
OJP	1.59	1.38	0.75	0.76 (0.000)	-
HJP75	0.66	0.42	0.87	0.86 (0.000)	-
HJP94	0.63	0.46	0.39	0.87 (0.000)	-
HJP02	0.45	0.37	0.26	-	0.28 (0.002)

5.5.3 Comparing GPP_{EC} with GPP_{MODIS} and GPP_{lidar}

Airborne lidar provided reasonable estimates of canopy fractional cover (based on annulus rings 1-9) at 40, 40, and 30 DHP locations within OJP, HJP75, and HJP94, respectively. Correlations (r^2) between measured vs. lidar *f*cover were 0.86 for all DHP plots combined. Due to reduced variance for individual forest cover types, however, the site-specific (OJP, HJP75, and HJP94 (HJP02 has been excluded)) lidar and DHP fractional cover correlations were not as strong (r^2 = 0.22 (p = 0.01), 0.09 (p < 0.1), and 0.21 (p = 0.01), respectively). This indicates that the *f*cover method works well over variable canopy structures, but not as well within a single ecosystem of little variability. Average percent differences between measured and lidar-estimated *f*cover were 19% (standard deviation (stdev.) = 9%, OJP), 15% (stdev. = 9%, HJP75) and 36% (stdev. = 22%,

HJP94). Comparisons between plot-averaged measured tree height and lidar canopy heights, based on the 90th percentile of the return distribution, were strong (r^2 = 0.99) and followed an almost 1:1 relationship. Site-specific correlations were also strong at OJP (r^2 = 0.88) and HJP75 (r^2 = 0.83), but were weak at HJP94 (r^2 = 0.18, p = 0.32). This was due to the low height of the trees at HJP94 resulting in reduced probability of multiple returns and increased penetration of pulses into surrounding tall grasses and shrubs (Hopkinson et al. 2005). From the results presented here and elsewhere, lidar can provide a map of the spatial variability of canopy height (e.g. Hopkinson et al. 2005) and *f*cover (e.g. Morsdorf et al. 2006) for use in the Landsberg-based GPP model over large areas.

Direct comparisons between GPP_{EC}, GPP_{MODIS}, and GPP_{lidar} are shown in Figure 5.4. Adjacent MODIS pixels provide maximum and minimum ranges (as error bars) of GPP and were used as bounds for geo-location errors that occur as a result of sensor geometry, earth curvature, and ground surface topography (e.g. Wolfe et al. 2002; Turner et al. 2004).

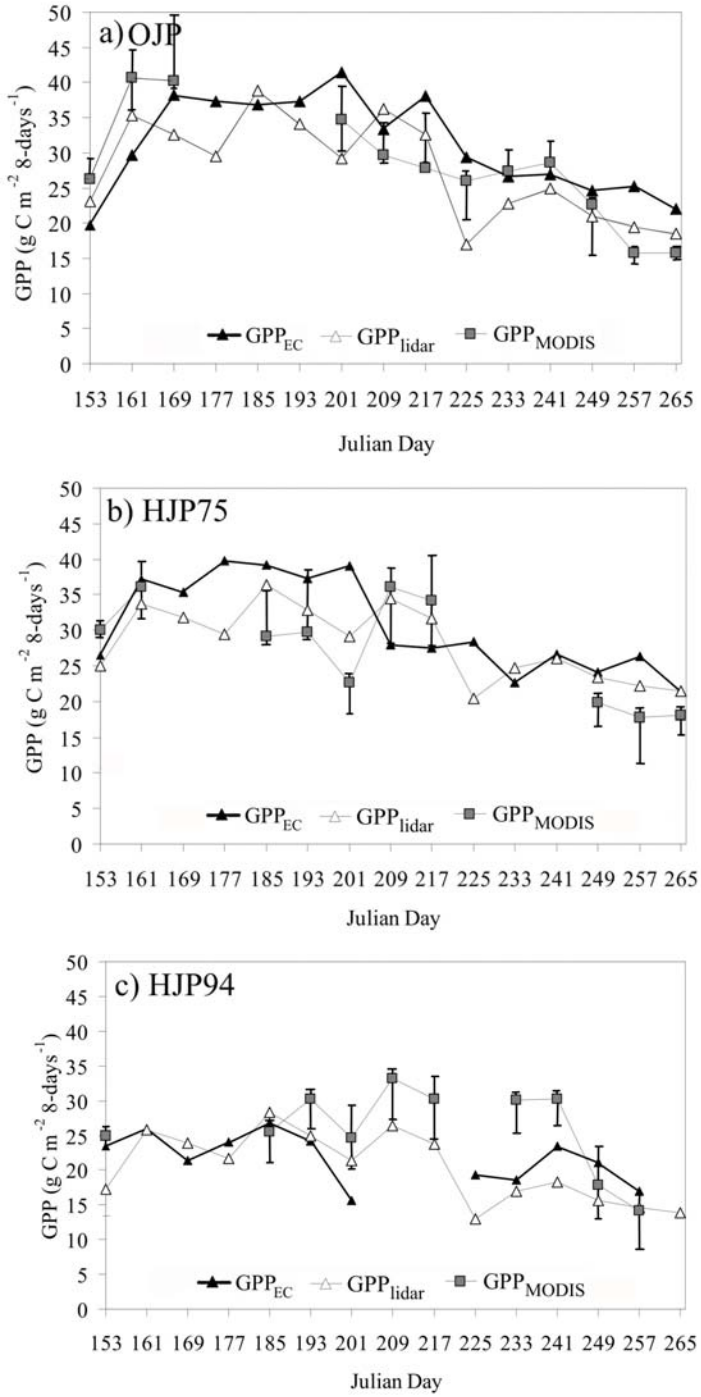

Figure 5.4. Eight-day cumulative average GPP comparisons between GPP_{EC}, GPP_{MODIS}, and GPP_{lidar} at a) OJP; b) HJP75; and c) HJP94. Error bars on MODIS data indicate the range of GPP recorded for eight adjacent pixels (to the centre one, nine in total).

Mixed pixels may have had some influence on the relationships between GPP_{EC}, GPP_{lidar}, and GPP_{MODIS} (Figure 5.4). Table 5.6 provides Pearson's r correlation coefficients between GPP_{EC}, GPP_{lidar} and GPP_{MODIS} and the average percent difference when compared with each other for all sites examined. OJP is relatively homogeneous throughout the entire MODIS pixel. Lidar estimated average (1 km x 1 km area surrounding the EC) *f*cover was 0.62 (slightly higher than measured, 0.59) and average canopy heights were much lower than that measured at plots (11.2 m) (Table 5.1). At OJP, GPP_{lidar} undestimated eight-day total GPP_{EC} by 11%, whereas GPP_{MODIS} underestimated eight-day total GPP_{EC} by 6%, on average (Figure 5.4, Table 5.6). The differences may have been due, in part, to shorter average vegetation heights within the larger MODIS pixel as opposed to taller trees within the footprint of the EC system.

At HJP75, average lidar canopy height and *f*cover (5.67 m, 0.47) were lower than plot measurements (Table 5.1), which may have caused some underestimation of GPP_{lidar} (6%) when compared with GPP_{EC} (Figure 5.4, Table 5.6). MODIS underestimated GPP_{EC} by 9%, on average. When GPP_{MODIS} was compared with GPP_{lidar}, average differences of 6% were found. The standard deviation of differences were greatest between GPP_{EC} and remote sensing estimates (GPP_{lidar}, and GPP_{MODIS}) (16% and 24%, respectively), but were less when comparing between GPP_{lidar} and GPP_{MODIS} (14%).

At HJP94, the footprint area of the EC covers approximately 50% of the MODIS pixel for the site. The remaining 20% and 30% of the pixel contains older jack pine stands with average tree heights of 12 m and 6.5 m, respectively. Tree heights and *f*cover within the MODIS pixel area were also greater (5.2 m, 0.32) than those measured within plots near the tower (Table 5.1). Average GPP_{lidar} underestimated GPP_{EC} by 6%, especially towards the end of the growing season,

whereas GPP_{MODIS} overestimated GPP_{EC} by 17% and GPP_{lidar} by 18% (Figure 5.4, Table 5.6). The standard deviation of the differences were also smallest when comparing GPP_{lidar} with GPP_{MODIS} (17%) but larger when comparing between GPP_{EC} and GPP_{MODIS} (31%).

Table 5.6. Pearson's r correlations between GPP_{EC}, GPP_{lidar}, and GPP_{MODIS} including *p-values* (in brackets). Average percent differences are shown for eight-day composite periods (where data were available) over the growing season, 2005.

Site	Pearson's r correlation GPP_{EC} and GPP_{lidar}	Average % difference = GPP_{EC} - GPP_{lidar}	Pearson's r correlation GPP_{EC} and GPP_{MODIS}	Average % difference = GPP_{EC} - GPP_{MODIS}	Pearson's r correlation GPP_{lidar} and GPP_{MODIS}	Average % difference: = GPP_{lidar} - GPP_{MODIS}
OJP	0.71 (0.003)	11%	0.64 (0.030)	6%	0.77 (0.003)	8%
HJP75	0.70 (0.004)	6%	0.39 (0.270)	9%	0.81 (0.004)	6%
HJP94	0.63 (0.280)	6%	0.64 (0.100)	-17%	0.59 (0.04)	-18%

5.5.4 Assessing the Influence of Site Heterogeneity - Scaling GPP from 1m to 1000m

From the results of the previous section, it is evident that differences between GPP_{Lidar}, GPP_{MODIS} and GPP_{EC} may depend, in part, on the location and distribution of "patches" of vegetation within mixed pixels. Individual MODIS pixels may include areas of diverse vegetation cover, ranging from recent clearcuts and grasslands, to older and/or more productive forests, wetlands, and agricultural areas (Milne and Cohen, 1999). It is not clear if within-pixel patches have influenced pixel average GPP_{lidar} and GPP_{MODIS} when compared with GPP_{EC}. To examine the influences of spatial heterogeneity in vegetation structure, 1 m resolution GPP_{lidar}, estimated for a single day, was aggregated by averaging to 25 m, 250 m, 500 m, and 1000 m pixel resolutions and then subtracted from 1 m pixels to demonstrate where GPP differences may exist between adjacent patches of vegetation types (Figure 5.5).

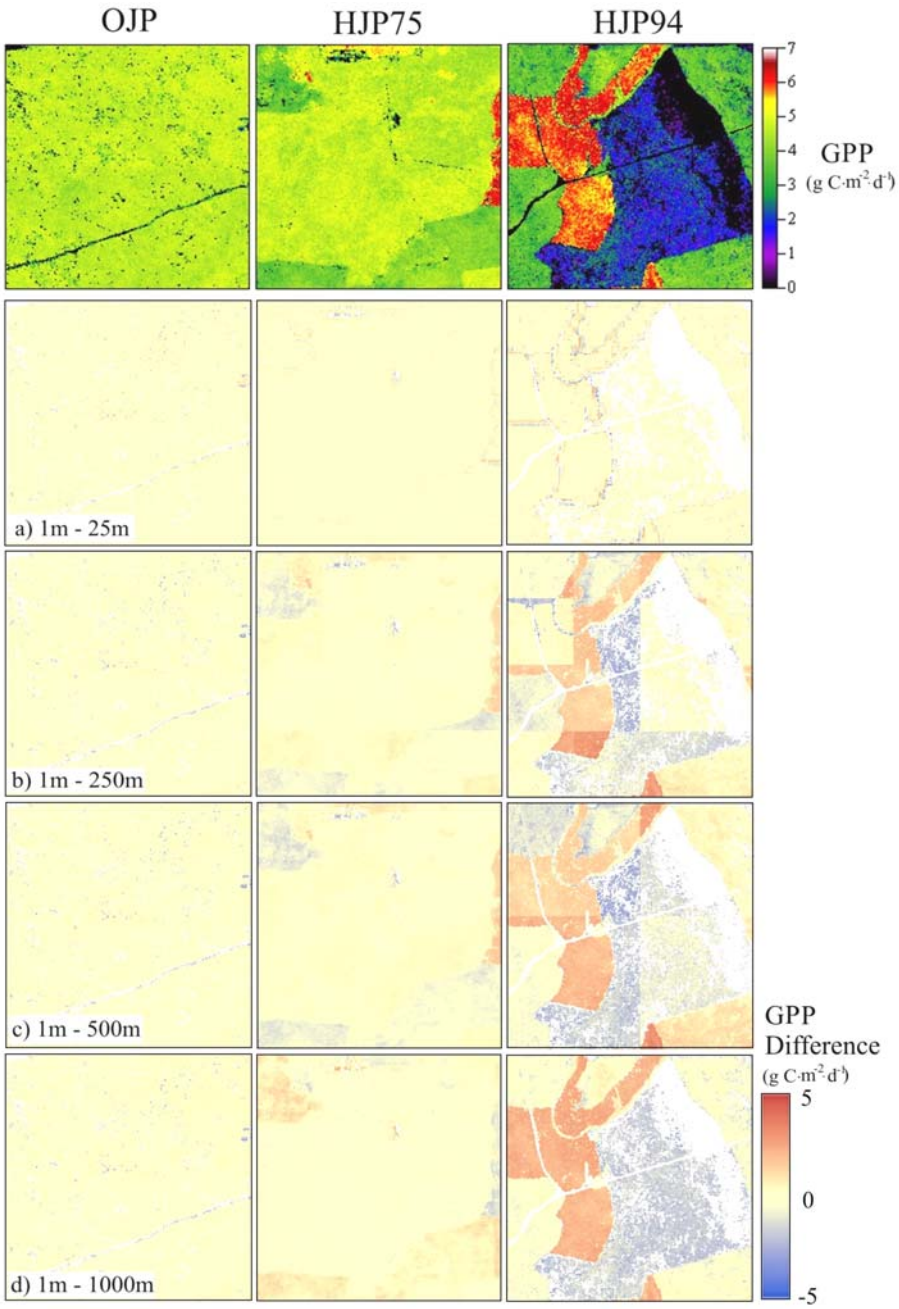

Figure 5.5. Differences between GPP_{lidar} on June 16, 2005 (as an example) at 1 m resolution and a) 25 m b) 250 m; c) 500 m; and d) 1000 m pixels. Maps of GPP_{lidar} illustrate more and less productive parts within 1 km x 1 km MODIS pixel areas. Low resolution pixels were subtracted from 1 m resolution pixels at each site. Positive differences indicate that lower resolutions underestimate GPP compared with 1 m resolution, whereas negative differences indicate that lower resolutions over-estimate GPP when compared with 1 m resolution. Gray areas equal missing data due to short vegetation.

After aggregating 1 m GPP_{lidar} to lower resolutions, and subtracting them from the original 1 m GPP_{lidar} dataset, GPP_{lidar} was found to vary by almost 10% at the heterogeneous HJP94 site when lower resolutions were used (Table 5.7). We can start to see the effects of aggregation in Figure 5.5a, (3rd panel) at HJP94. Differences between 1 m and 25 m resolutions along the outer edges of the HJP94 site (rectangular area located in the centre of the pixel) were over-estimated by 25 m resolution pixels compared with 1 m resolution pixels, due to edge effects and averaging between taller and shorter vegetation. A t-test confirms that significant differences between 1 m and 25 m resolution pixels exist at HJP94 ($p = 0.000$, n = 1600), and to a lesser extent between 1 m and 250 m resolutions ($p = 0.10$, n = 16). The greatest deviations were found at HJP94 at pixel resolutions between 25 m and 500 m, which underestimated average GPP (when compared with 1 m resolution) by up to 10% over the 1 km pixel, and by as much as 5 g C m^{-2} d^{-1} (140%) when compared with 1 m resolutions. These results exemplify the averaging of GPP that occurs as resolution decreases. At HJP75, as pixel resolution decreased to 500 m, pixel average GPP also decreased indicating that short vegetation surrounding the site had some influence on average GPP at lower (e.g. 500 m) resolutions. Slight edge effects at 25 m resolution can be found at HJP75 (Figure 5.5 a, 2nd panel) between shorter vegetation along the outer edges of the site, and taller vegetation within the site, however, differences between higher and lower pixel resolutions were not significant. Systematic over- and under-estimation of GPP_{lidar} was not found at OJP and average differences between high and low resolution pixels were less than 1.5%. Significant differences at OJP exist between 1 m and 25 m resolution pixels ($p = 0.05$, n = 1600), but not at lower resolutions. The effects of pixel averaging at OJP and HJP75 were not great as at HJP94 because these sites are relatively homogeneous and were not subject to large pixel differences as a result of structural heterogeneity. Similar observations have been found in Reich et al. (1999)

who show that differences in photosynthetic capacity of vegetation patches can affect the averaging of pixels at lower resolutions.

Table 5.7. Summary statistics (percent differences) between GPP estimated at 1 m spatial resolution and lower resolutions per site. Negative signs represent underestimation of GPP by lower resolution pixels.

Site	Difference statistics due to pixel resolution	Pixel Resolution (subtracted from 1 m)				
		1 m x 1 m	25 m x 25 m	250 m x 250 m	500 m x 500 m	1000 m x 1000 m
OJP	Average pixel GPP (g $C \cdot m^{-2} \cdot d^{-1}$)	4.22	4.21	4.27	4.26	4.22
	Mean % difference from 1 m	0	-0.2	1.2	0.9	0
	Pixel (GPP) standard deviation	0.30	0.24	0.19	0.17	0
HJP75	Average pixel GPP (g $C \cdot m^{-2} \cdot d^{-1}$)	4.54	4.55	4.55	4.41	4.54
	Mean % difference from 1 m	0	0.2	0.2	-2.8	0
	Pixel (GPP) standard deviation	0.44	0.46	0.59	0.57	0
HJP94	Average pixel GPP (g $C \cdot m^{-2} \cdot d^{-1}$)	3.65	3.29	3.31	3.31	3.56
	Mean % difference from 1 m	0	-9.9	-9.3	-9.3	-2.5
	Pixel (GPP) standard deviation	1.53	1.52	1.25	1.5	0

The results of Figure 5.5 and Table 5.7 provide a good rationale for using low resolution MODIS vegetation products within homogeneous sites, and higher resolution products (e.g. 25 m) within heterogeneous sites. Depending on the location of patches within pixels, the averaging that occurs within decreasing resolutions may be prone to large and compounding errors in GPP (e.g. Kimball et al. 1999).

5.6 Discussion

5.6.1 Influence of Site Heterogeneity

Low standard deviations in the range of differences between GPP_{lidar} and GPP_{MODIS} indicate the importance of comparing MODIS GPP products over homogeneous pixels where EC systems exist. HJP94 and to a lesser extent, HJP75 are considered “mixed pixels” because they contain

some areas of taller and shorter vegetation and variable canopy fractional cover. If applied over an entire MODIS pixel, we expect that GPP_{lidar} and GPP_{MODIS} would be similar because the same pixel area containing the same average vegetation characteristics was used to estimate GPP. In principle, greater differences should exist when comparing predicted GPP (MODIS or lidar) with GPP_{EC} because EC samples only part of the mixed pixel and, therefore, does not represent other landcover types within that pixel. If EC provides only partial coverage of the pixel, then it may be more appropriate to apply a lidar-based or ecosystem model approach over the entire pixel to reduce differences that may be caused by mixed pixels. Alternatively, the spatially variant footprint can be modeled and within footprint lidar-based canopy attributes extracted to scale from point to landscape scales (e.g. Chasmer et al. accepted).

5.6.2 Other Influences Affecting MODIS vs. EC GPP

Differences between EC, MODIS and lidar-modeled GPP may also be due to energy balance closure, and biome-specific estimates of LUE and fPAR used by MODIS. EC is prone to underestimating CO_2 fluxes, and differences between GPP_{EC} and GPP estimated using lidar and MODIS may be affected by this. Barr et al. (2006) found that energy balance closure at OJP was 0.86% (±0.003) for daytime periods when friction velocity was greater than 0.35 m s^{-1}. Lack of energy balance closure is sometimes believed to lead to deficits in measured fluxes (Barr et al. 2006; Baldocchi 2008). This uncertainty is minimized, in part, by applying an energy balance correction to the measured fluxes so that deficits are reduced. Baldocchi (2008) suggest that adjusting for energy balance closure may not be appropriate because underestimates in the energy balance may not be manifest in underestimates in CO_2 fluxes. Energy balance correction has been applied to all sites examined in this study (Barr et al. 2006), which may have also increased differences between GPP_{MODIS} and GPP_{EC}.

The use of LUE and estimation of fPAR by MODIS may also introduce additional errors. MODIS typically uses a biome-specific look-up table of LUE, varied with changes in air temperature (Tair) and vapour pressure deficit (VPD) (e.g. Heinsch et al. 2002). However, LUE between vegetation species, age classes, previous disturbance, and meteorological drivers tends to vary greatly (e.g. McCrady and Jokela, 1998; Lagergren et al. 2005; Jenkins et al. 2007; Pereira et al. 2007; Schwalm et al. 2006; Chasmer et al. 2008), despite the simple application of LUE in the MODIS GPP algorithm (Turner et al. 2003). With respect to meteorological driving mechanisms, Jenkins et al. (2007) found that PAR had the greatest influence on measured gross carbon exchanges, whereas Tair and VPD had only weak influences. Lagergren et al. (2005), on the other hand, found the opposite to be true. Chasmer et al. (2008) found that the importance of meteorological drivers on LUE varied with forest age, as did LUE. When applying the MODIS biome-specific estimate for LUE, linearly varied with measured Tair and VPD, Chasmer et al. (2008) found that average growing season LUE was underestimated by 40% at a mature jack pine forest, and between 14% and 16 % within younger jack pine stands when compared with measured LUE.

The estimation of fPAR by MODIS could also increase differences between EC-measured GPP and that of MODIS. For example, Turner et al. (2006) found that MODIS underestimated measured GPP in highly productive sites and overestimated measured GPP in low productivity sites. Heinsch et al. (2006) also found that MODIS often over-estimates fPAR, which is used as a multiplier with LUE to estimate GPP. Therefore, low biome-specific estimates of LUE may be used to offset over-estimates of fPAR by the MODIS algorithm (e.g. Zhao et al. 2003; Turner et al. 2006; Heinsch et al. 2006). When compared over an entire watershed (99 MODIS pixels), Chasmer et al. (accepted b) found that MODIS overestimated fPAR when compared with lidar

estimates of the same in approximately 22% of the watershed, especially where pixels contained mixed vegetation with low biomass (e.g. cleared areas). However, in 30% of the watershed, that which contained areas of high biomass, MODIS slightly underestimated fPAR when compared with lidar. These results may also have contributed to the differences between GPP_{MODIS} and GPP_{EC}.

5.6.3 Implications of Research

The results of this study indicate that airborne scanning lidar is a useful tool for scaling between EC measurements and lower resolution satellite products. Whilst it does not measure the reflective properties of the canopy, which may be directly applicable to MODIS, it does provide information on three-dimensional vegetation structure. The ability to accurately estimate canopy fractional cover and leaf area from lidar within one to many MODIS pixels has many benefits. These include, but are not limited to, continuous scaling of leaf area over varying pixel resolutions, significantly reduced time and costs associated with extensive LAI measurements within and beyond pixels, and the ability to map and discretize the three-dimensional foliage area with depth into the canopy. Running et al. (1999) provide a list of measurements that are useful for validating MODIS using ecosystem models. Several of these can be accurately obtained from airborne lidar and may be incorporated into ecosystem models. These include: a) light transmission (e.g. Solberg et al. 2006; Thomas et al. 2006; Hopkinson and Chasmer, 2007); b) above ground biomass (Patenaude et al. 2004; Omasa et al. 2007); c) leaf area index (Magnussen and Boudewyn, 1998; Morsdorf et al. 2006; Hopkinson and Chasmer, in review); d) canopy height (Naesset and Bjerknes, 2001; Hopkinson et al. 2005); e) aerodynamic roughness length and zero plane displacement (Chasmer et al. accepted); and f) above-ground growth increment (Yu et al. 2004; Hopkinson et al. 2007). The increasing popularity of lidar, and vast lidar data collection and archiving projects (e.g. the USGS CLICK project, and the Canadian LIMERIC

data archive) have made lidar an accessible tool for the evaluation of lower resolution remote sensing products. Repeat surveys and small-area monitoring strategies are also gaining focus (Hopkinson et al. 2007).

Lidar estimates of fractional cover at high resolutions may be combined with incoming PAR (e.g. in this study) and other meteorological driving mechanisms to produce spatial and temporal maps of GPP. If ecosystem production models (e.g. SVAT, Running et al. 1999; Biome BGC, Thornton et al. 2002; 3PGS, Coops et al. 2007), were combined with airborne lidar, the results may provide more appropriately scaled estimates of GPP for MODIS evaluation than EC within mixed pixels. In this study, differences between GPP_{MODIS} and GPP_{lidar} were not as large as differences between GPP_{EC}. This was due, in part, to the same area being compared between MODIS and lidar. Within mixed MODIS pixels, EC samples the ecosystem of interest, and may or may not provide an accurate description of GPP for the entire MODIS pixel (Rahman et al. 2002). If the forest is homogeneous and extends beyond the MODIS pixel, then comparisons between MODIS and EC should be similar, as was shown in this study.

5.7 Conclusions

In summary, this study describes the application of a canopy structure-based GPP model within both homogeneous and mixed pixels for comparison with the MODIS GPP product. First, canopy height and foliage fractional cover were compared with inputs used in Landsberg light response curves during the growing season of 2004. P_{max} was positively, but non-linearly, related to canopy height. Similar relationships were also found between the canopy structure and both the scaling factor (a) and I_{comp}. A GPP model was created based on the strong relationships found between canopy structure and Landsberg inputs. $GPP_{Landsberg}$ approximated GPP_{EC} at HJP75 and HJP94, but over-estimated GPP_{EC} at OJP and under-estimated GPP_{EC} at HJP02.

Second, we used lidar inputs into the $GPP_{Landsberg}$ model (instead of measured: i.e. GPP_{lidar}) with GPP_{EC} and the GPP_{MODIS} within 1 km x 1 km MODIS pixel areas surrounding the EC. When compared over eight-day cumulative periods throughout the 2005 growing season, the standard deviation of differences between GPP_{lidar} and GPP_{MODIS} were less than differences between GPP_{EC} at all sites. Although OJP and HJP75 were relatively homogeneous surrounding the EC system, lower canopy heights and leaf area may have resulted in lower estimates of GPP by lidar and MODIS than measured. At HJP94, MODIS overestimated GPP when compared with EC, possibly due to taller trees with higher leaf area surrounding the site, but outside of the fetch of the EC system. Differences in canopy cover and tree height within and beyond the site did not have the same affect on GPP_{lidar}, which was slightly underestimated towards the end of the growing season.

Finally, we examined the influence of coarser resolutions and within-pixel averaging on GPP_{lidar} at OJP, HJP75, and HJP94. We found that the largest differences occurred at HJP94, especially when aggregating pixels beyond 25 m. This provides a good rationale for using high resolution spatial data in heterogeneous environments. Further, the use of airborne scanning lidar greatly reduces the need for extensive field validation, and is an appropriate method for scaling between EC estimates of GPP and MODIS products.

5.8 Acknowledgements

We would like to thank the Fluxnet-Canada Research Network and the Boreal Ecosystem Research and Monitoring Sites (BERMS) Project and all those individuals involved for collection and processing of flux data. We appreciate all of the efforts of Dr. Chris Hopkinson, the Applied Geomatics Research Group, and C-CLEAR for collecting and processing at-cost lidar data. Also

we appreciate help from the National Water Research Institute (NWRI) and the Climate Research Division, Atmospheric Sciences and Technology Directorate, Environment Canada for financial support for the lidar survey. Field data collection was performed with the aid of Chris Hopkinson, Bruce Davison, Chris Beasy, and Jordan Erker, and their efforts are appreciated. Jessika Töyra is acknowledged for her assistance with field validation and logistics. Also, thank-you to the late Werner Bauer (site manager) for his help and support. MODIS data were obtained with many thanks from the Oak Ridge National Laboratory Distributed Active Archive Center (ORNL DAAC). 2005 MODIS subset land products are available on-line [http://www.daac.ornl.gov/ MODIS/modis.html] from ORNL DAAC, Oak Ridge, Tennessee, U.S.A. Funding for this project has been provided by CFCAS, NSERC, PREA, the BIOCAP Canada Foundation, and the Climate Research Division of Environment Canada. Laura has been generously supported by graduate student scholarships from NSERC and OGSST and research assistantships from CRESTech.

5.9 References

Arain, A., and N. Restrepo-Coupe, 2005. Net ecosystem production in a temperate pine plantation in southeastern Canada. *Agricultural and Forest Meteorology.* 128:223-241.

Baldocchi, D., 2008. Turner Review No. 15: 'Breathing' of the terrestrial biosphere: lessons learned from a global network of carbon dioxide flux measurement systems. *Australian Journal of Botany.* 56:1-26.

Baldocchi, D.D., C.A. Vogel, and B. Hall, 1997. Seasonal variation of carbon dioxide exchange rates above and below a boreal jack pine forest. *Agricultural and Forest Meteorology.* 83:147-170.

Baldocchi, D., and T. Meyers, 1998. On using eco-physiological, micrometeorological and biogeochemical theory to evaluate carbon dioxide, water vapor and trace gas fluxes over vegetation: a perspective. *Agricultural and Forest Meteorology*. 90:1-25.

Barr, A.G., T.A. Black, E.H. Hogg, N. Kljun, K. Morgenstern, and Z. Nesic, 2004. Inter-annual variability in the leaf area index of a boreal aspen-hazelnut forest in relation to net ecosystem production. *Agricultural and Forest Meteorology.* 126:237-255.

Barr, A.G., K. Morgenstern, T.A. Black, J.H. McCaughey, and Z. Nesic, 2006. Surface energy balance closure by the eddy-covariance method above three boreal forest stands and implications for the measurement of the CO_2 flux. *Agricultural and Forest Meteorology.* 140:322-337.

Burns, R. and B. Honkala, 1990. Silvics of Forest Trees of the United States Supersedes Agriculture Handbook 271. US Department of Agriculture, Forest Service, Washington DC. PDF copies available on website: http://na.fs.fed.us/pubs/

Chasmer, L., C. Hopkinson, B. Smith, and P. Treitz, 2006: Examining the influence of changing laser pulse repetition frequencies on conifer forest canopy returns. *Photogrammetric Engineering and Remote Sensing*. 17(12):1359-1367.

Chasmer, L., H. McCaughey, A. Barr., A. Black, A. Shashkov, P. Treitz, and T. Zha, 2008. Investigating light use efficiency (LUE) across a jack pine chronosequence during dry and wet years. *Tree Physiology.* 28 (9):1395-1406.

Chasmer L., A. Barr, A. Black, C. Hopkinson, N. Kljun, H. McCaughey, P. Treitz, (accepted) Vegetation structural and elevation influences on CO_2 uptake within a mature jack pine forest in Saskatchewan Canada. *Canadian Journal of Forest Research.*

Chasmer, L., C. Hopkinson, P. Treitz, H. McCaughey, A. Barr, A. Black, (accepted b). A lidar-based hierarchical approach for assessing MODIS fPAR. Submitted to *Remote Sensing of Environment.*

Chapin III, F.S., P. Matson, and H. Mooney, 2002. Principles of Terrestrial Ecosystem Ecology. Springer-Verlag New York, Inc. 436 pgs.

Chen, J., M. Falk, E. Euskirchen, K.T. Paw U., T.H. Suchanek, S. Ustin, B. J. Bond, K.D. Brosofske, N. Phillips, and R. Bi, 2002. Biophysical controls of carbon flows in three successional Douglas-fir stands based on eddy-covariance measurements. *Tree Physiology.* 22:169-177.

Chen, J.M., A. Govind, O. Sonnentag, Y. Zhang, A. Barr, and B. Amiro, 2006. Leaf area index measurements at Fluxnet-Canada forest sites. *Agricultural and Forest Meteorology*. 140:257-268.

Cohen W. B. and C. O. Justice, 1999. Validating MODIS terrestrial ecology products: Linking *in situ* and satellite measurements. *Remote Sensing of Environment.* 70:1-3.

Coops, N.C., T.A. Black, R. S. Jassal, J.A. Trofymow, and K. Morgenstern, 2007. Comparison of MODIS, eddy covariance determined and physiologically modeled gross primary production (GPP) in a Douglas-fir forest stand. *Remote Sensing of Environment*. 107:385-401.

Eriksson, H.M., L. Eklundh, A. Kuusk, and T. Nilson, 2006. Impact of understory vegetation on canopy reflectance and remotely sensed LAI estimates. *Remote Sensing of Environment*. 103:408-418.

Falge, E., D. Baldocchi, J. Tenhunen, M. Aubinet, P. Bakwin, P. Berbigier, C. Bernhofer, G. Burba, R. Clement, K. Davis, J. Elbers, A. Goldstein, A. Grelle, A. Granier, J. Guomundsson, D. Hollinger, A. Kowalski, G. Katul, B. Law, Y. Malhi, T. Meyers, R. Monson, J. W. Munger, W. Oechel, K. T. Paw U, K. Pilegaard, U. Rannik, C. Rebmann, A. Suyker, R. Valentini, K. Wilson, S. Wofsy, 2002. Seasonality of ecosystem respiration and gross primary production as derived from FLUXNET measurements. *Agricultural and Forest Meteorology*. 113:53-74.

Fluxnet-Canada, 2003. Fluxnet-Canada measurement protocols. Working draft version 1.3. Fluxnet-Canada Network Management Office, Laval, Quebec. Available online: http://www.fluxnet-canada.ca.

Griffis, T.J., T.A. Black, K. Morgenstern, A.G. Barr, Z. Nesic, G.B. Drewitt, D. Gaumont-Guay, and J.H. McCaughey, 2003. Ecophysiological controls on the carbon balances of three southern boreal forests. *Agricultural and Forest Meteorology.* 117:53-71.

Heinsch, F.A., M. Zhao, S.W. Running, J.S. Kimball, R.R. Nemani, K.J. Davis, P.V. Bolstad, B.D. Cook, A.R. Desai, D.M. Ricciuto, B.E. Law, W.C. Oechel, H.Luo, S.C. Wofsy, A.L. Dunn, J.W. Munger, D.D. Baldocchi, L. Xu, D.Y. Hollinger, A.D. Richardson, P.C. Stoy, M.B.S. Siqueira, R.K. Monson, S.P. Burns, and L.B. Flanagan, 2006. Evaluation of remote sensing based terrestrial productivity from MODIS using regional tower eddy flux network observations. *IEEE Transactions on Geoscience and Remote Sensing.* 44(7):1908-1925.

Hopkinson, C., L. Chasmer, G. Sass, I. Creed, M. Sitar, W. Kalbfleisch, and P. Tretiz, 2005. Vegetation class dependent errors in lidar ground elevation and canopy height estimates in a boreal wetland environment. *Canadian Journal of Remote Sensing.* 31(2):191-206.

Hopkinson, C. and L. Chasmer (in review). Testing a lidar intensity based model of canopy fractional cover across multiple forest ecozones. *Remote Sensing of Environment.*

Hopkinson, C. and L. Chasmer, 2007. Using discrete laser pulse return intensity to model canopy transmittance. *The Photogrammetric Journal of Finland*. 20(2):16-26.

Hopkinson, C., L. Chasmer, and R. Hall, 2007. Using airborne lidar to examine forest growth. *Remote Sensing of Environment.* 112(3):1168-1180.

Jenkins, J.P., A.D. Richardson, B.H. Braswell, S.V. Ollinger, D.Y. Hollinger, and L.-L. Smith, 2007. Refining light-use efficiency calculations for a deciduous forest canopy using simultaneous tower-based carbon flux and radiometric measurements. *Agricultrual and Forest Meteorology.* 143-64-79.

Jin, Z, Q. Tian, J. M. Chen, and M. Chen, 2007. Spatial scaling between leaf area index maps of different resolutions. *Journal of Environmental Management.* 85: 628-637.

Kljun, N., T.A. Black, T.J. Griffis, A.G. Barr, D. Gaumont-Guay, K. Morgenstern, J.H. McCaughey, and Z. Nesic, 2006. Response of net ecosystem productivity of three boreal forest stands to drought, 2006. *Ecosystems*.9:1128-1144.

Kimball, J.S., S.W. Running, and S.S. Saatchi, 1999. Sensitivity of boreal forest regional water flux and net pimary production simulations to sub-grid scale landcover complexity. *Journal of Geophysical Research.* 104:27789-27801.

Lagergren, F., L. Eklundh, A. Grelle, M. Lundblad, M. Molder, H. Lankreijer and A. Lindroth. 2005. Net primary production and light use efficiency in a mixed conifer forest in Sweden. *Plant, Cell, and Environment.* 28:412-423.

Landsberg, J.J., and R.H. Waring, 1997. A generalized model of forest productivity using simplified concepts of radiation-use efficiency, carbon balance and partitioning. *Forest Ecology and Management.* 95:209-228.

Law, B.E., E. Falge, L. Gu, D. Baldocchi, P. Bakwin, P. Berbigier, K. Davis, A. Dolman, M. Falk, J. Fuentes, A. Goldstein, A. Granier, A. Grelle, D. Hollinger, I. Janssenss, P. Jarvis, N. Jensen, G. Katul, Y. Mahli, G. Matteucci, T. Meyers, R. Monson, W. Munger, W. Oechel, R. Olson, K. Pilegaard, K.T. Paw U, H. Thorgeirsson, R. Valentini, S. Verma, T. Lesala, K. Wilson, S. Wofsy, 2002. Environmental controls over carbon dioxide and water vapor exchange of terrestrial vegetation. *Agricultural and Forest Meteorology.* 113:97-120.

Leblanc, S.G., J.M. Chen, R. Fernandes, D. Deering, and A. Conley, 2005. Methodology comparison for canopy structure parameters extraction from digital hemispherical photography in boreal forests. *Agricultural and Forest Meteorology*. 129:187-207.

Leuning, R., H.A. Cleugh, S.J. Zegelin, D. Hughes, 2005. Carbon and water fluxes over a temperate *Eucalyptus* forest and a tropical wet/dry savanna in Australia: measurements and

comparison with MODIS remote sensing estimates. *Agricultural and Forest Meteorology.* 129:151-173.

Magnussen, S. and P. Boudewyn, 1998. Derivations of stand heights from airborne laser scanner data with canopy-based quantile estimators. *Canadian Journal of Forest Research*. 28:1016-1031.

Margolis, H., L. Flanagan, and B. Amiro, 2006. The Fluxnet-Canada Research Network: Influence of climate and disturbance on carbon cycling in forests and peatlands. *Agricultural and Forest Meteorology.* 140:1-5.

Massman, W.J. and X. Lee, 2002. Eddy covariance flux corrections and uncertainties in long term studies of carbon and energy exchange. *Agricultural and Forest Meteorology.* 113:121-144.

McCrady, R.L. and E. Jokela. 1998. Canopy dynamics, light interception and radiation use efficiency of selected loblolly pine families. *Forest Science.* 44:64-72.

Milne, B.T., and W. B. Cohen, 1999. Multiscale assessment of binary and continuous landcover variables for MODIS validation, mapping, and modeling applications. *Remote Sensing of Environment.* 70:82-98.

Middleton, E. M., J. Sullivan, B. Bovard, A. Deluca, S. Chan, and T. Cannon, 1997. Seasonal variability in foliar characteristics and physiology for boreal forest species at five Saskatchewan tower sites during the 1994 Boreal Ecosystem-Atmosphere Study. *Journal of Geophysical Research*. 102(D24):28831-28844.

Morisette, J.T., J. L. Privette, and C. O. Justice, 2002. A framework for the validation of MODIS Land products. *Remote Sensing of Environment.* 83:77-96.

Morsdorf, F., B. Kötz, E. Meier, K. Itten, and B. Allgöwer, 2006. Estimation of LAI and fractional cover from small footprint airborne laser scanning data based on gap fraction. *Sensing of Environment.* 104:50-61.

Myers, D.E., 1994. Spatial interpolation: an overview. *Geoderma*. 62:17-28.

Naesset, E. and K-O Bjerknes, 2001: Estimating tree heights and number of stems in young forest stands using airborne laser scanner data. *Remote Sensing of Environment.* 78:328-340.

Omasa, K., F. Hosoi, and A. Konishi, 2007. 3D lidar imaging for detecting and understanding plant responses and canopy structure. *Journal of Experimental Botany.* 58(4):881-898.

O'Sullivan, D. and D. Unwin, 2003. Geographic Information Analysis. Wiley, New Jersey.

Patenaude, G., R.A. Hill, R. Milne, D. Gaveau, B. Briggs, and T. Dawson, 2004. Quantifying forest above ground carbon content using LiDAR remote sensing. *Remote Sensing of Environment.* 93:368-380.

Pereira, J.S., J.A. Mateus, L.M. Aires et al. 2007. Net ecosystem carbon exchange in three contrasting Meterranean ecosystems – the effect of drought. *Biogeosciences.* 4:791-802.

Rahman, A., J. Gamon, D. Fuentes, D. Roberts, and D. Prentiss, 2001. Modeling spatially distributed ecosystem flux of boreal forest using hyperspectral indices from AVIRIS imagery. *Journal of Geophysical Research.* 106(D24):33579-33591.

Reich, P.B., D. P. Turner, and P. Bolstad, 1999. An approach to spatially distributed modeling of net primary production (NPP) at the landscape scale and its application in validation of EOS NPP products. *Remote Sensing of Environment.* 70:69-81.

Running, S.W., R. Nemani, J. Glassy, P. Thornton, 1999. MODIS daily photosynthesis (Psn) and annual net primary production (NPP) product (MOD17). Theoretical basis document, Version 3. NASA Goddard Space Flight Center, Greenbelt, MD 20771, USA. Available online: http://modis.gsfc.nasa.gov/data/atbd/atbd_mod17.pdf

Running, S.W., R.R. Nemani, F.A. Heinsch, M. Zhao, M. Reeves, and H. Hashimoto, 2004. A continuous satellite-derived measure of global terrestrial primary production. *BioScience*. 54(6):547-560.

Rymph, S.J. 2004. Modeling growth and composition of perennial tropical forage grasses. Ph.D. Thesis, University of Florida. 330 pgs.

Schwalm, C.R., T.A. Black, B.D. Amiro, M.A. Arain, A.G. Barr, C.P.-A. Bourque, A.L. Dunn, L.B. Flanagan, M.-A. Giasson, P.M. Lafleur, H.A. Margolis, J.H. McCaughey, A.L. Orchansky, and S.C. Wofsy, 2006. *Agricultural and Forest Meteorology.* 140:269-286.

Solberg, S., E. Naesset, K. H. Hanssen, and E. Christiansen, 2006. Mapping defoliation during a severe insect attack on Scots pine using airborne laser scanning. *Remote Sensing of Environment*. 102:364-376.

Thomas, V., D.Finch, J.H. McCaughey, T. Noland, L. Rich, and P. Treitz, 2006. Spatial modeling of the fraction of photosynthetically active radiation absorbed by a boreal mixedwood forest using a lidar-hyperspectral approach. *Agricultural and Forest Meteorology*. 140:287-307.

Thornton, P., B.E. Law, H. Gholz, K. Clark E. Falge, D. Ellsworth, A. Goldstein, R. Monson, D. Hollinger, M. Falk, J. Chen, and J. Sparks, 2002. Modelling and measuring the effects of

disturbance history and climate on carbon and water budgets in evergreen needle leaf forests. *Agricultural and Forest Meteorology*. 113(1-2):185-222.

Tian, Y., C. Woodcock, Y. Wang, J. Privette, N. Shabanov, L. Zhou, Y. Zhang, W. Buermann, J. Dong, B. Veikkanen, T. Häme, K. Andersson, M. Ozdogan, Y. Knyazikhin, and R. Myneni, 2002. Multiscale analysis and validation of the MODIS LAI product 1. Uncertainty assessment. *Remote Sensing of Environment*. 83:414-430.

Turner, D.P., S.T. Gower, W.B. Cohen, M. Gregory, T.K. Maiersperger, 2002. Effects of spatial variability in light use efficiency on satellite-based NPP monitoring. *Remote Sensing of Environment.* 80:397-405.

Turner, D.P., S. Urbanski, D. Bremer, S.C. Wofsy, T. Meyers, S.T. Gower, and M. Gregory, 2003. A cross-biome comparison of daily light use efficiency for gross primary production. *Global Change Biology.* 9:383-395.

Turner, D.P., S. Ollinger, and J. Kimball, 2004. Integrating remote sensing and ecosystem process models for landscape- to regional-scale analysis of the carbon cycle. *BioScience*. 54(6):573-584.

Turner, D.P., W.D. Ritts, W.B. Cohen, S.T. Gower, S. W. Running, M. Zhao, M. H. Costa, A. A. Kirschbaum, J.M. Ham, S.R. Saleska, D.E. Ahl, 2006. Evaluation of MODIS NPP and GPP products across multiple biomes. *Remote Sensing of Environment.* 102:282-292.

Wolfe, R.E., M. Nishihama, A.J. Fleig, J.A. Kuyper, D.P. Roy, J.C. Storey and F.S. Patt, 2002. Achieving sub-pixel geolocation accuracy in support of MODIS land science. *Remote Sensing of Environment.* 83:31-49.

Woolard, J., and J. Colby, 2002. Spatial characterization, resolution, and volumetric change of coastal dunes using airborne lidar: Cape Hatteras, North Carolina. *Geomorphology.* 48(1-3):269-287.

Xu, S. J. M. Chen, R. Fernandes and J. Cihlar. 2004. Effects of subpixel water area fraction on mapping leaf area index and net primary productivity in Canada. *Canadian Journal for Remote Sensing*, 30: 797-804.

Yu, X., J. Hyyppä, H. Kaartinen, and M. Maltamo, 2004. Automatic detection of harvested trees and determination of forest growth using airborne laser scanning. *Remote Sensing of Environment.* 90451-462.

Zhang, Y., J. Chen, and J. Miller, 2005. Determining digital hemispherical photograph exposure for leaf area index estimation. *Agricultural and Forest Meteorology*. 133:166-181.

Zhao, M., F.A. Heinsch, R.R. Nemani, and S. Running, 2005. Improvements of the MODIS terrestrial gross and net primary production global data set. *Remote Sensing of Environment.* 95:164-176.

Chapter 6

Discussion

The research presented has provided new methodologies for using airborne lidar for MODIS product validation, and has improved understanding of ecosystem processes within a four-site jack pine chronosequence. This has been achieved through the integration of: (i) high temporal resolution micrometeorological and carbon cycle methods; (ii) high resolution three-dimensional lidar data; and (iii) low resolution 2-D spatial and temporal data from MODIS. The following discussion outlines the current state of knowledge and future research within the areas of remote sensing and CO_2 flux exchanges within ecosystems.

6.1 Observing LUE and the Ability of Chronosequence Jack Pine Forests to Sequester CO_2 During Dry and Wet Years

Light use efficiency (LUE) is an important parameter used in remote sensing to scale localized processes at the ecosystem level to larger regions (e.g. Turner et al. 2003; Heinsch et al. 2006). LUE can be described simply as the slope of the relationship between gross primary productivity (GPP) and absorbed photosynthetically active radiation (APAR) (e.g. Dewar et al. 1998; Turner et al. 2003). Despite its wide application for remote sensing-based vegetation production estimates (e.g. GPP and net primary production [NPP]), within-biome variability in LUE is not well understood. Some biases that currently exist within remote sensing GPP products are a function of the LUE multiplier, as well as the methods used to reduce biome-specific maximum LUE using meteorological variables (Zhao et al. 2005; 2006). The LUE term is also problematic because it is not a direct function of vegetation functional type, leaf area, or age (e.g. Schwalm et al. 2006). Therefore, it cannot easily be varied with leaf area or stand structural characteristics using remote sensing.

Although Chapter 2 focused mainly on variability of LUE within different ages of jack pine, much can be learned from this study when applying it within the context of remote sensing-based GPP models. In this study, comparisons were made using a variety of methods to estimate LUE, including a MODIS-based maximum LUE approach. When comparing between sites, LUE differences between stand ages can vary greatly, especially with changes in growing season average soil moisture and APAR (Schwalm et al. 2006; Chapter 2). Also, canopy structure, and the ability of jack pine to use light during diffuse and direct radiation conditions has a significant influence on average and daily LUE estimates. Hence, the proportion of diffuse versus direct radiation conditions (per day) should be incorporated within 8-day cumulative remote sensing-based GPP models.

When using a biome-specific maximum LUE (e.g. used in MODIS algorithms), the variability between stand age and species type is generalized. Biome-specific LUE is underestimated when compared with site averages in Chapter 2, and does not vary with age. However, MODIS also tends to over-estimate fPAR, which when multiplied by low estimates of LUE, typically provides GPP estimates that approximate those from EC within homogeneous pixels (Heinsch et al. 2006; Chapter 5). MODIS GPP products are not highly biased over large areas, but become problematic when compared over local areas. Combining remote sensing and other spatial datasets (e.g. airborne and space-borne lidar data, Landsat data, and forestry maps) can improve MODIS estimates of GPP by describing better and classifying species and biome types as well as heterogeneous areas in the landscape. This is important for the application of species-specific LUE estimates within ecosystem models.

The results of this study indicate that forest age-since-disturbance has a significant impact on LUE estimates used in scaling GPP over broader areas. LUE will affect the accuracy of remote sensing GPP and NPP models if a biome-specific maximum (e.g. that which is used in MODIS algorithms) is used instead of an age-based LUE. Sub-pixel characterization of forests could greatly improve remote sensing estimates of GPP and NPP within mixed pixels.

6.2 Investigating the Influence of Canopy Structure on CO_2 Fluxes within a Mature Jack Pine Forest

It has been demonstrated that canopy structure and elevation are important factors affecting CO_2 fluxes within ecosystems (e.g. Middleton, et al. 1997; Leuning, et al. 2004). Several studies have discussed how within-ecosystem variability in NEP, GPP, and Re have been influenced by variations in upland versus lowland areas (e.g. Baldocchi et al. 1996), leaf chemistry (e.g. Middleton et al. 1997) and canopy structure (Baldocchi and Meyers, 1998; Gower et al. 1999). Methods for examining the influences of vegetation biomass and elevation on mass exchanges (e.g. CO_2 and water) have not been well developed. A few studies have examined spatially variable influences on CO_2 fluxes using footprint model parameterizations. However, these studies were unable to resolve adequately the three-dimensional properties of the canopy (Amiro, 1998; Rahman et al. 2002; Kim et al. 2006). The objectives of Chapter 3 were to first characterize canopy structure and elevation using lidar within the contours of half-hourly flux footprint maximum area probability density functions (PDF's) and then to relate variability in canopy structure and elevation to NEP and GPP estimated from EC.

The results of this study indicate that vegetation structure, especially fractional cover and canopy height, play an important role in the variability in CO_2 concentrations. These results are not necessarily surprising, but the magnitudes and timing of influence of canopy structural

characteristics on the spatial variability of CO_2 had not been known previously. During some periods, meteorological variables played a more important role on CO_2 flux variability than the spatial distribution of biomass and elevation, whereas during other periods, they were not as important. The application of these methods over a variety of sites containing lidar data, and over periods of one or more years has interesting implications for future research. For example, these methods are especially useful for determining if EC is adequately representing the fluxes from all parts of the ecosystem, and also, if the ecosystem sampled by EC is spatially variable. Several EC flux stations within the Fluxnet-Canada Research Network and the Canadian Carbon Program currently have lidar data. These include: Old Jack Pine, Harvested-1975, -1994, and -2002 Jack Pine sites, Old Black Spruce, and the Fen site (BERMS, Saskatchewan); Groundhog River flux station (Ontario); Kennedy Siding (British Columbia); Clayoquot Sound flux station (British Columbia); and eastern boreal black spruce sites in Quebec. Application of the methods described may reveal interesting relationships between canopy structure, elevation, and CO_2 fluxes during specific times of the growing season and year.

The methodology developed may also be used to improve footprint model parameterizations. One of the shortcomings of the footprint model parameterization is that it is unable to account for the spatial heterogeneity in canopy structure or elevation affecting the vertical and horizontal location of footprints (Schmid, 2002). Current footprint models use an average roughness length, which affects the location and vertical extent of the footprint (Chapter 3). Improvements made to footprint models based on three-dimensional canopy structure and elevational variability may be used to further refine the flux source areas, and quantify structural and elevation influences, especially in areas of complex terrain. Franklin and Waring (1980) state that forests located along the Pacific Northwest, especially old growth forests found in mountainous environments, are one

of the greatest sinks for atmospheric CO_2 in the world. Despite their importance, the use of EC in mountain forest environments is problematic because of the influences of topography and the drainage flows of air from higher to lower elevations (Massman and Lee, 2002). The combined use of airborne lidar and footprint models may be used to improve the EC system methodology in these environments because spatial variability in canopy structure and elevation can be described more completely.

6.3 Using Airborne Lidar for the Assessment of MODIS fPAR

The validation of MODIS vegetation products is currently difficult because many of the products are not spatially or temporally measured beyond EC systems (Heinsch et al. 2006). A number of research programs have concentrated on the spatial validation of MODIS vegetation products. For example, Turner et al. (2003b; 2006) have examined MODIS vegetation products across a number of biomes and scales using a spatial sampling methodology within the Bigfoot Program. Studies in Australia and the United States (e.g. Hill et al. 2006; Heinsch et al. 2006; Coops et al. 2007) have used relatively homogeneous areas including EC systems and radiation measurements for spatially assessing MODIS products over multiple biomes. Many of the methodologies used for spatial sampling are expensive both in time and in human resources. Airborne lidar offers the potential for modeling the spatial distribution of fPAR (Chapter 4) and GPP (Chapter 5) if meteorological inputs such as incoming PAR are incorporated into the model. The use of lidar for validating remote sensing products has been discussed briefly in Hill et al. (2006) and applied to Landsat data in Lefsky et al. (2005).

In Chapter 4, spatial estimates of fPAR from airborne lidar were developed based on the ratio of canopy to total laser returns within three of four chronosequence jack pine sites studied (OJP, HJP75, and HJP94). Previous research on this and similar methods using airborne lidar have been

examined by Morsdorf et al. (2006) and Solberg and Naesset (2006). The methods presented here have not been examined over open canopies and varying vegetation heights. Further, lidar has not been used to evaluate the MODIS fPAR product. Results from Chapter 4 demonstrate that airborne lidar can be used to accurately estimate fPAR when compared with spatial estimates from digital hemispherical photography (DHP).

There are also some shortcomings for using lidar when evaluating MODIS products. Lidar is not able to characterize the fPAR within short vegetation environments. Discrete return lidar effectively samples near the top of grasses and shrubs (Hopkinson et al. 2005) but multiple returns are not recorded at distances of less than ~1.3 m. Therefore if a return is recorded within the understory vegetation (<1.3 m) a ground return will not be recorded, and fPAR will equal 100%. This results in either large under-estimates or over-estimates of fPAR by MODIS. There is also concern expressed within the literature that optical (field) measurements of fPAR and LAI do not account for understory vegetation, which is averaged within pixels (Heinsch et al. 2006). Airborne lidar, although unable to record multiple returns from within short understory canopies, may be used to map the existence of the understory within pixels and may provide more realistic estimates of fPAR observed by MODIS.

A second shortcoming of lidar is its use for multiple surveys due to the expensive nature of the technology and airborne operations. Airborne lidar is often used to survey an area once, and therefore, any models that use airborne lidar data need to assume a non-varying canopy. If the lidar survey was performed during maximum leaf conditions, MODIS data could be validated during the approximate time period for which the lidar data were collected. Research that has concentrated on the application of airborne lidar for forest studies are now contracting repeat

surveys (e.g. Hopkinson et al. 2008; Chasmer et al. 2006; Naesset 2004). Also, airborne lidar surveys have been flown over many U.S. states, as well as local to regional areas in Canada. Many of these datasets are now becoming freely available to the public (for example, the U.S. Geological Survey Center for Lidar Information Coordination and Knowledge (CLICK) program). These datasets may become important for validating MODIS and other remote sensing products using the methodologies developed in this thesis.

6.4 Modelling and Scaling GPP from Lidar in Comparison with MODIS Products

Land cover heterogeneity is a significant issue in remote sensing, especially when the resolution of pixels used to estimate vegetation productivity is unable to capture local variability (Turner et al. 2003b). This is certainly the case with MODIS pixels, which estimate approximately weekly cumulative GPP at resolutions of 1 km. A large and homogeneous ecosystem's GPP can be fairly accurately estimated on a weekly basis using MODIS remote sensing algorithms (Heinsch et al. 2006). However, the increased requirement for natural resources and the conversion of forests to other land cover types following both harvesting and natural disasters has led to fewer large patches of homogeneous vegetated areas (Chen et al. 2002).

In Chapter 5, GPP was estimated using site-specific empirical models of the relationship between GPP and incoming PAR. Landsberg light-response curves were used to estimate average GPP at each site based on measured canopy height and fractional cover. The same models were then applied at the MODIS pixel scale using canopy structure averages from airborne lidar. Vegetation fractional cover (*f*cover) and canopy height were strongly related to the light compensation point, the scaling factor, and maximum GPP at saturation at all sites. The GPP models developed in Chapter 5 were site-specific, and these methods require testing within a number of other

ecosystems. Testing of these relationships does not necessarily require lidar data, but spatial application of the GPP models for MODIS GPP product evaluation does. If lidar canopy structural metrics can be related to Landsberg model inputs over a variety of forest stand types and ages, then this method may be used in combination with incoming PAR to spatially estimate GPP.

In the second part of Chapter 5 and also in Chapters 2 and 4, it was found that mixed pixels could introduce significant biases into MODIS vegetation products. The influence of within-pixel heterogeneity on modeled GPP estimated from airborne lidar was assessed by subtracting lower resolution datasets from a 1 m resolution dataset. This was performed by rasterizing GPP estimates determined at 1 m resolutions to lower, 25 m, 100 m, 250 m, 500 m, and 1000 m using an inverse distance weighting approach. The results of the final analysis chapter show how errors in GPP can be compounded at coarse resolutions within heterogeneous environments. This provides important justification for using moderate-resolution satellites, such as Landsat, for landscape classification. The classification of landscapes using a decision criteria based on landscape heterogeneity offers the possibility for improved MODIS products using higher resolution remote sensing datasets. For example, in heterogeneous areas, higher resolution MODIS pixels could be used, whereas in homogeneous regions, lower resolution pixels could be used. This will reduce computer power and storage limitations, whilst improving the accuracy and the validity of MODIS products.

6.5 Future Research

The findings of the research presented and the new methodologies developed may be incorporated into a number of future studies.

6.5.1 Footprint Modelling, Parameterization, and Improvement within Complex Canopies

As demonstrated in Chapter 3, variability in the spatial distribution of vegetation heights, leaf area, elevation and other variables not examined (e.g. photosynthetic capacity) will influence the extent of the flux source/sink area. Geographic information systems (GIS) are both user-friendly and have great potential for spatial and temporal modeling. Footprint model parameterizations may be improved or developed to incorporate three-dimensional canopy structural variability and characteristics of the ground surface topography. They may also include a variety of other user-defined metrics and indices. For example, the estimation of roughness length used within footprint models may be improved by incorporating elevation, the spatial distribution of the understory, canopy height, and fractional cover. Other indices may also be examined to determine the probability of more or less water flux within footprints using elevation (e.g. by using a "topographic wetness index", slope, and/or aspect, concavity or convexity). Lower resolution soil type and distribution maps may also be included. These may be integrated to form more complete and possibly more accurate spatial parameterizations of the flux source and sink areas within individual sites.

The EC system is also prone to error when examining fluxes over heterogeneous areas (Baldocchi and Meyers, 1998; Massman and Lee, 2002). The methods developed here may lead to further insights on EC measurement measurement and theory. Current EC methodologies remove terms related to the structural and elevational heterogeneity of the ecosystem. Therefore, sites that use EC should be uniform and homogeneous so that fluxes originating from one part of the site are generally representative of all areas, so as not to introduce bias. Airborne lidar provides measured canopy structure and elevation within and beyond EC flux footprints and has the potential to

improve EC methods that currently avoid the influences of large elevation gradients. The EC system also often underestimates mass exchanges because homogeneity in wind speed and turbulence is assumed (e.g. Sun et al. 2007). Application of EC over relatively flat surfaces allows for simplifying assumptions of wind speed and turbulence to be made. In mountainous environments, the simplifying assumptions do not apply because the vertical (mean) advective CO_2 fluxes are not accounted for. In these cases, fluxes are pushed upward due to down slope drainage flows towards the tower and EC system (Sun et al. 2007; R. Monson, presentation at NCAR, June 2007). Perhaps lidar could be used to model or at least understand better the effects of down-slope drainage flows of cool mountain air and the influences on vegetation growth and CO_2 fluxes.

Finally, the methods developed in Chapter 3 could be applied over a series of sites and over periods of one or more years to determine how canopy structure and elevation affect fluxes for multiple species types and temporal periods. Comparisons between the influences of canopy structure and topography during specific periods of interest (e.g. shoulder periods versus growing season), could provide important insights for ecosystem models. For example, some parts of the ecosystem may commence photosynthesis earlier than other parts, depending on slope orientation, snow depth and thaw. These insights could be used to help validate models that include topographic influences on CO_2 fluxes (e.g. Biome-BGC) (Thorton and Running, 1999).

6.5.2 MODIS Vegetation Product Validation and Improvement

Lidar canopy structure metrics, such as canopy height and fractional cover, show promise for spatial prediction of GPP when used in Landsberg equations. Spatial estimates of GPP at high resolutions may be used additionally to EC systems to validate the MODIS GPP product beyond the footprint of the EC system. This would effectively scale between local measurements of the

EC system and the wider area covered by one to many MODIS pixels. However, relationships between canopy structure and Landsberg model inputs should be examined at other sites. The influences of meteorological driving mechanisms could also be incorporated into the model to make it more physically based and to reduce the variability in daily estimates.

The development of a national or international satellite validation project using available airborne lidar would add insight to many of the current problems faced by lower resolution remote sensing products. Simple extraction methodologies within specified study areas or pixels of individual vegetation types would provide a wealth of information whilst also being statistically relevant. These could be incorporated with field validation campaigns and EC systems.

6.5.3 Spatial Scaling and the Influences of Vegetation Patches on MODIS Product Biases

One of the greatest challenges facing MODIS algorithm and product development is within-pixel heterogeneity. Average radiances from a number of vegetation types, clearings, or water bodies within pixels can lead to large and mixed influences on vegetation products (Milne and Cohen, 1998). The results found in Chapter 5 show the importance of patch distribution and scaling on a variety of resolutions from 1 m up to 1 km. Patch location, size, and the influence of edges between patches may be used to assess their influences on spectral radiance. Incorporation of higher resolution datasets within the classification scheme used by MODIS will help to resolve patch distribution issues within pixels and will likely improve estimates of fPAR, LAI, and GPP. For example, if recent Landsat 25-m-resolution datasets were used within the land classification scheme, MODIS algorithms could be adjusted to account for the transmissive properties of pixels at 25 m as opposed to 250 m or 1 km. Improvements made to land cover classification and LUE would likely lead to an improved MODIS dataset, especially in heterogeneous areas.

The combined use of meteorological and hydrological measurements, CO_2, water, and energy fluxes, high resolution lidar data, and low resolution spectral remote sensing data has provided an excellent basis from which to understand local influences on fluxes. Methods used to scale results from local sites to the region using MODIS have also been developed. It is hoped that these activities will progress as there appears to be much scope for continued research into both an understanding of the roles that disturbed ecosystems have within the national and global carbon balance as well as the methodologies used to understand these processes.

6.6 References

Amiro, B. D., 1998. Footprint climatologies for evapotranspiration in a boreal catchment. *Agricultural and Forest Meteorology*. 90:195-201.

Baldocchi, D., C. A. Vogel, 1996. A comparative study of water vapor, energy and CO2 flux densities above and below a temperate broadleaf and boreal pine forest. *Tree Physiology*. 16:5-16.

Baldocchi, D., and T. Meyers, 1998. On using eco-physiological, micrometeorological and biogeochemical theory to evaluate carbon dioxide, water vapor and trace gas fluxes over vegetation: a perspective. *Agricultural and Forest Meteorology*. 90:1-25.

Chasmer, L., C. Hopkinson, B. Smith, and P. Treitz, 2006. Examining the influence of changing laser pulse repetition frequencies on conifer forest canopy returns. *Photogrammetric Engineering and Remote Sensing.* 72(12):1359-1367.

Chen, J., M. Falk, E. Euskirchen, K.T. Paw U., T.H. Suchanek, S. Ustin, B. J. Bond, K.D. Brosofske, N. Phillips, and R. Bi, 2002. Biophysical controls of carbon flows in three successional Douglas-fir stands based on eddy-covariance measurements. *Tree Physiology.* 22:169-177.

Coops, N.C., T.A. Black, R. S. Jassal, J.A. Trofymow, and K. Morgenstern, 2007. Comparison of MODIS, eddy covariance determined and physiologically modelled gross primary production (GPP) in a Douglas-fir forest stand. *Remote Sensing of Environment*. 107:385-401.

Franklin, J.F., and Waring, R.H. 1980. Distinctive features of the northwestern conifer forest: development, structure and function. In: Waring, R.H. (editor). Forests: fresh perspectives from ecosystem analysis. Corvallis: Oregon State University Press, p. 59-86.

Gower, S., C. Kucharik, and J. Norman, 1999. Direct and indirect estimation of leaf area index, f_{APAR}, and net primary production of terrestrial ecosystems. *Remote Sensing of Environment*. 70:29-51.

Heinsch, F.A., M. Zhao, S.W. Running, J.S. Kimball, R.R. Nemani, K.J. Davis, P.V. Bolstad, B.D. Cook, A.R. Desai, D.M. Ricciuto, B.E. Law, W.C. Oechel, H.Luo, S.C. Wofsy, A.L. Dunn, J.W. Munger, D.D. Baldocchi, L. Xu, D.Y. Hollinger, A.D. Richardson, P.C. Stoy, M.B.S. Siqueira, R.K. Monson, S.P. Burns, and L.B. Flanagan, 2006. Evaluation of remote sensing based terrestrial productivity from MODIS using regional tower eddy flux network observations. *IEEE Transactions on Geoscience and Remote Sensing*. 44(7):1908-1925.

Hill, M.J., U. Senarath, A. Lee, M. Zeppel, J. Nightingale, R. Williams, T. McVicar, 2006. Assessment of the MODIS LAI product for Australian ecosystems. *Remote Sensing of Environment*. 101:495-518.

Hopkinson, C., L. Chasmer, G. Sass, I. Creed, M. Sitar, W. Kalbfleisch, and P. Tretiz, 2005. Vegetation class dependent errors in lidar ground elevation and canopy height estimates in a boreal wetland environment. *Canadian Journal of Remote Sensing.* 31(2):191-206.

Hopkinson, C. and L. Chasmer, 2007. Using discrete laser pulse return intensity to model canopy transmittance. *The Photogrammetric Journal of Finland*. 20(2):16-26.

Hopkinson, C., L. Chasmer, and R. Hall, 2008. Using airborne lidar to examine forest growth. *Remote Sensing of Environment.* 112(3):1168-1180.

Kim, J., Q. Guo, D. Baldocchi, M. Leclerc, L. Xu, and H. Schmid, 2006. Upscaling fluxes from tower to landscape: Overlaying flux footprints on high-resolution (IKONOS) images of vegetation cover. *Agricultural and Forest Meteorology*. 136:132-146.

Kljun, N., T. A. Black, T. J. Griffis, A. G. Barr, D. Gaumont-Guay, K. Morgenstern, J. H. McCaughey, and Z. Nesic, 2006. Response of Net Ecosystem Productivity of Three Boreal Forest Stands to Drought. *Ecosystems*, 9:1128-1144.

Lefsky, M., D. Turner, M. Guzy, and W. Cohen, 2005: Combining lidar estimates of aboveground biomass and Landsat estimates of stand age for spatially extensive validation of modeled forest productivity. *Remote Sensing of Environment*. 95:549-558.

Leuning, R., M. Raupach, P. Coppin, H. Cleugh, P. Isaac, O. Denmead, F. Dunin, S. Zegelin, and J. Hacker, 2004. Spatial and temporal variations in fluxes of energy, water vapour and carbon dioxide during Oasis 1994 and 1995. *Boundary-Layer Meteorology*. 110:3-38.

Massman, W.J. and X. Lee, 2002. Eddy covariance flux corrections and uncertainties in long term studies of carbon and energy exchange. *Agricultural and Forest Meteorology.* 113:121-144.

Markkanen, T., U. Rannik, B. Marcolla, A. Cescatti, and T. Vesala, 2003. Footprints and fetches for fluxes over forest canopies with varying structure and density. *Boundary-Layer Meteorology*. 106:437-459.

Middleton, E. M., J. Sullivan, B. Bovard, A. Deluca, S. Chan, and T. Cannon, 1997. Seasonal variability in foliar characteristics and physiology for boreal forest species at five Saskatchewan tower sites during the 1994 Boreal Ecosystem-Atmosphere Study. *Journal of Geophysical Research*. 102(D24):28831-28844.

Milne, B.T., and W. B. Cohen, 1999. Multiscale assessment of binary and continuous landcover variables for MODIS validation, mapping, and modeling applications. *Remote Sensing of Environment.* 70:82-98.

Morsdorf, F., B. Kötz, E. Meier, K. Itten, and B. Allgöwer, 2006. Estimation of LAI and fractional cover from small footprint airborne laser scanning data based on gap fraction. *Sensing of Environment.* 104:50-61.

Naesset, E., 2004. Effects of different flying altitudes on biophysical stand properties estimated from canopy height and density measured with a small-footprint airborne scanning laser. *Remote Sensing of Environment*, 91(2):243-255.

Schmid, H.P., 2002. Footprint modeling for vegetation-atmosphere exchange studies: a review and perspective. *Agricultural and Forest Meteorology.* 113:159-183.

Solberg, S., E. Naesset, K. H. Hanssen, and E. Christiansen, 2006. Mapping defoliation during a severe insect attack on Scots pine using airborne laser scanning. *Remote Sensing of Environment*. 102:364-376.

Sun, J., Burns, S.P., Delany, A.C., Oncley, S.P., Turnipseed, A.A., Stephens, B.B., Lenschow, D.H. LeMone, M.A., Monson, R.K. and Anderson, D.E., 2007. CO_2 transport over complex terrain. *Agricultural and Forest Meteorology.* 145: 1-21.

Thorton, P. and S. Running, 1999. An improved algorithm for estimating incident daily solar radiation from measurements of temperature, humidity, and precipitation. *Agricultural and Forest Meteorology.* 93(4)211:228.

Turner, D.P., S.T. Gower, W.B. Cohen, M. Gregory, T.K. Maiersperger, 2002. Effects of spatial variability in light use efficiency on satellite-based NPP monitoring. *Remote Sensing of Environment.* 80:397-405.

Turner, D.P., S. Urbanski, D. Bremer, S.C. Wofsy, T. Meyers, S.T. Gower, and M. Gregory, 2003. A cross-biome comparison of daily light use efficiency for gross primary production. *Global Change Biology.* 9:383-395.

Turner, D.P., W.D. Ritts, W.B. Cohen, S.T. Gower, M. Zhao, S.W. Running, S.C. Wofsy, S. Urbanski, A.L. Dunn, and J.W. Munger, 2003b. Scaling gross primary production (GPP) over boreal and deciduous forest landscapes in support of MODIS GPP product validation. *Remote Sensing of Environment.* 88:256-270.

Turner, D.P., W.D. Ritts, W.B. Cohen, S.T. Gower, S. W. Running, M. Zhao, M. H. Costa, A. A. Kirschbaum, J.M. Ham, S.R. Saleska, D.E. Ahl, 2006. Evaluation of MODIS NPP and GPP products across multiple biomes. *Remote Sensing of Environment.* 102:282-292.

Zhao, M., F.A. Heinsch, R. Nemani, and S.W. Running, 2005. Improvements of the MODIS terrestrial gross and net primary production global data set. *Remote Sensing of Environment.* 95:164-176.

Zhao, M., S.W. Running, and R. Nemani, 2006. Sensitivity of Moderate Resolution Imaging Spectroradiometer (MODIS) terrestrial primary production to the accuracy of meteorological reanalysis. *Journal of Geophysical Research.* 111:G01002.

Chapter 7

Summary and Conclusions

In this thesis, four research objectives have been examined for the purposes of improving our understanding of canopy structure influences on light use efficiency (LUE) and CO_2 exchanges. LUE is especially of interest because it is used to aggregate CO_2 flux processes within the terrestrial biosphere from local to global scales using remote sensing. This thesis focused on four previously-harvested jack pine sites within the southern part of the Canadian boreal forest.

Disturbed and regenerating forests are an important part of the terrestrial biosphere. The ability to quantify changes in biomass, vegetation health and productivity, and then to map these accurately across space and through time is of great importance for understanding the effects of forests on atmospheric CO_2 concentrations and climate change. In this thesis, we have gained a better understanding of the influences of canopy structure and age on CO_2 fluxes and LUE. Observations were then used to improve remote sensing-based vegetation production models and to determine biases associated with mixed pixels. In order to achieve these goals, a combination of meteorological data, CO_2 flux measurements, plot level field mensuration data, high resolution airborne lidar data, and low resolution Moderate Resolution Imaging Spectroradiometer (MODIS) data were employed.

A number of key findings were presented. These key findings extend current research and knowledge regarding CO_2 flux exchanges within a boreal jack pine chronosequence subject to both average conditions (according to the World Meteorological Organization 30-year normal

average precipitation and air temperature) and extreme (above and below WMO normal) dry and wet conditions. What has been discovered here is that LUE varies both between different ages and structural characteristics of sites, and also as a result of unique dry and wet soil moisture conditions. Therefore, it is not appropriate to apply a single estimate of maximum LUE within specific biomes (as is used to estimate GPP from MODIS). It would be more appropriate to apply LUE within a range of forest stand ages, species types, and structural classifications determined from Landsat, for example. This would likely improve national and global GPP estimates from MODIS, especially within heterogeneous environments, and would reduce the uncertainty caused by low resolution remote sensing products and spatially discrete measurements made by EC.

The key findings of this thesis also push current remote sensing analysis methods forward, especially within the realm of airborne lidar and passive spectral remote sensing. The results presented are original and are based on a physical understanding of foliage cover and radiation penetration through the canopy rather than more typically applied empirical models examined within the literature. Observations and specific relationships were used to create models of fPAR from airborne lidar for the validation of MODIS vegetation products within and beyond sites. The feasibility of the models was tested using mensuration plots, digital hemispherical photography (DHP) of leaf area, and PAR data available at each site. The output from these models was then compared with MODIS estimates, for the first time using airborne lidar. The methods used provide a sound and simple methodology for accurately mapping the spatial and temporal variability in fPAR at individual sites and across larger areas using airborne lidar.

Canopy structure and ground surface elevation played a key role in this thesis, whereby direct comparisons were made between CO_2 fluxes and the structural and elevational characteristics of

the ecosystem (Chapter 3). This was then expanded to relate structural characteristics to inputs into Landsberg's light response curves used to estimate GPP in Chapter 5. These results provide an effective new methodology for evaluating MODIS vegetation products using a combination of airborne lidar and incoming PAR at the sites studied. Finally, the GPP model was applied at resolutions of 1 m to 1 km to examine the influence of within-pixel heterogeneity and aggregation on modelled GPP. Again, this was the first time that a model of GPP developed from high resolution three-dimensional lidar was used to estimate the influences of vegetation patches on low resolution pixels. The results of the final analysis indicated that MODIS estimates of GPP were similar to estimates made by EC within homogeneous ecosystems (Chapter 5), but require further refinement to 25 m resolutions within heterogeneous pixels.

It is likely that the combination of moderate resolution (e.g. Landsat) land classifications used to create detailed forest maps for the application of maximum LUE estimates will improve MODIS products in heterogeneous forests. The difficulties associated with evaluating remote sensing data products within heterogeneous environments has been emphasized, illustrating the importance of using combined EC and airborne lidar or moderate resolution remote sensing data for the evaluation of global low resolution products from MODIS and future satellite programs.

Appendix A

Definitions and Concepts

There are several definitions and concepts that require explanation within the context of this research. Concepts are defined for a) site level measurements of local fluxes observed using the eddy covariance method, and meteorology definitions; and for b) large area remote sensing and modelling.

A.1 Site-Level Eddy Covariance and Meteorology Definitions and Concepts

A.1.1 Eddy Covariance Method

The EC system can be used to measure the net ecosystem exchange (NEE) of CO_2, water and energy exchanges into and out of the ecosystem. EC systems combine flux measurements with post-processing of high frequency data. Typically, EC systems located on tall towers tend to have longer integration times and sample much larger source areas compared to systems located on shorter towers that have much faster measurement times and smaller source areas. EC systems are currently the standard method for measuring and understanding carbon, water, and energy cycles within terrestrial ecosystems (e.g. Barr et al. 2006). Inclusion of night-time air temperature or soil temperature allows for partitioning of NEE into ecosystem respiration and photosynthesis (e.g. Falge et al. 2002; Griffis et al. 2003), which aid in the validation of ecosystem and remote sensing-based top-down and bottom-up models. Despite widespread use, EC systems also have inherent errors, which lead to deficits in NEE (e.g. Massman and Lee, 2002). These tend to be related to a) differences between instrument types and limitations, b) deficits in NEE during periods of atmospheric stability (e.g. Goulden et al. 1996); c) differences in data processing

procedures, and d) land surface influences, such as advection and drainage. The reader is referred to Massman and Lee (2002) for a thorough discussion of these issues.

A.1.2 Net Ecosystem Exchange (NEE), Net Ecosystem Production (NEP) and Net Biome Production (NBP)

Net ecosystem exchange (NEE) is a direct measure of the exchange of CO_2 between the terrestrial biosphere and the atmosphere. NEE is measured using the EC system, and is approximately the integration of gross primary production (GPP) and ecosystem respiration (Re) (which includes heterotrophic and autotrophic respiration) (Chapin et al. 2002). NEE also makes up a large component of the net ecosystem production (NEP), where the inverse of NEE is approximately equal to NEP in ecosystems that are not prone to removal of CO_2 via leaching and disturbance (Chapin et al. 2002). At the regional scale, NEP incorporates more heterogeneous ecosystems, and is therefore termed net biome production (NBP) (Chapin et al. 2002; 2006). However, at the local scale, Chapin et al. (2006) suggest that NEP is not the net carbon accumulation rate, and therefore, NEP should equal the balance between GPP and Re. NEE is negative within the atmospheric literature, meaning that CO_2 is being removed from the atmosphere and is used by ecosystems for photosynthesis. Where NEE is positive, CO_2 is being transferred from the ecosystem to the atmosphere via Re. NEE's sign convention is reversed within the ecological literature. The units for NEE are $\mu mol \cdot m^{-2} \cdot s^{-1}$, but to be consistent with the remote sensing literature, in this thesis the units are g or kg of $C \cdot m^{-2} \cdot d^{-1}$.

A.1.3. Gross Primary Production (GPP) and Gross Ecosystem Production

Gross primary production (GPP) is the net accumulation of carbon by photosynthesis during daytime periods per unit area and per unit time. It can be approximately determined as GPP = NEP +Re. GPP is not measured, and is therefore estimated based on the relationship between Re and air temperature (Chapin et al. 2002). During daytime periods, GPP is often greater than Re in

many vegetated ecosystems (Chapin et al. 2006). GPP and gross ecosystem production (GEP) are often used interchangeably within the literature, however Hymus and Valentini (2007) note that they do vary slightly where GEP contains a photorespiratory component that GPP does not. In this thesis GEP is measured by eddy covariance. The units for GPP and GEP are typically $\mu mol \cdot m^{-2} \cdot s^{-1}$ but in the context of remote sensing, we have kept the naming conventions of GPP (e.g. interchanged GEP with GPP) and have converted units to g or kg of $C \cdot m^{-2} \cdot d^{-1}$ to remain consistent with the literature.

A.1.4 Net Primary Production (NPP)

Net primary production per unit area and per unit time is calculated from the difference between GPP and autotrophic (or plant) respiration (Chapin et al. 2006). Autotrophic respiration includes production via biomass growth, above- and below-ground turnover of tissues, and transfer of carbon beyond the plant to herbivores, root symbionts, etc. (e.g. Chapin et al. 2006). The units for NPP are typically $\mu mol \cdot m^{-2} \cdot s^{-1}$.

A.1.5 Ecosystem Respiration (Re), Autotrophic Respiration (Ra), and Heterotrophic Respiration (Rh)

Ecosystem respiration is the total integrated respiration throughout the ecosystem and includes both autotrophic respiration (Ra) and heterotrophic respiration (Rh). Ra is respiration associated with plant tissues, whereas Rh is the total respiration from animals and microbes. Re can be modeled from NEE during night-time periods where NEE = Re and during day-time periods as a function of air or soil temperature (e.g. Barr et al. 2004). All are cumulative over a specified area and period of time. The units for Re are typically $\mu mol \cdot m^{-2} \cdot s^{-1}$.

A.1.6 Photosynthetically Active Radiation (PAR), Absorbed PAR (APAR), the fraction of PAR absorbed by a plant canopy (fPAR), and Intercepted PAR (IPAR)

Photosynthetically active radiation (PAR) is shortwave radiation ranging from 400 to 700 nm, and is used by vegetation for photosynthesis (e.g. Schwalm et al. 2006). Chlorophyll is especially adapted to absorption of blue and red light within the PAR spectrum, whereas carotenoids and xanthophylls use some green light and reflect the remainder (e.g. Nichol et al. 2000). Longer wavelengths (e.g. in the near infrared and beyond) are reflected by many plants within the terrestrial biosphere to limit over-heating of the leaf. Plants are not able to respond to increasing levels of solar radiation because of resource limitations to chemical reactions, resulting in light saturation and reduced efficiency of photosynthesis (e.g. Chapin et al. 2002; Turner et al. 2003). The contrast in reflectance between PAR used for photosynthesis and longer wavelengths (i.e. shortwave infrared) is fundamental for remote sensing of vegetation health and change across large land areas. PAR is often measured along with meteorology and atmospheric CO_2, water, and/or sometimes other fluxes (e.g. methane) both above and below the canopy. The incoming and reflected (from canopy) PAR measured above the canopy, and the incoming and reflected (from ground) PAR measured below the canopy can be used to estimate the amount of PAR absorbed by the canopy (APAR) and the fraction of PAR absorbed when compared to total incoming PAR (fPAR) (Gower et al. 1999). The intercepted PAR (IPAR) is the ratio between incoming PAR above the canopy and incoming PAR below the canopy and is similar to APAR in closed canopies (Gower et al. 1999). The units for all terms related to PAR are typically in $\mu mol \cdot m^{-2} \cdot s^{-1}$ but in the context of remote sensing, have been converted to $MJ \cdot m^{-2} \cdot d^{-1}$.

A.1.7 Light Use Efficiency (LUE)

LUE (g C·MJ^{-1} of APAR), defined as the ratio of gross ecosystem productivity (GEP) (gC·m^{-2}·d^{-1}) to absorbed photosynthetically active radiation (APAR) (MJ·m^{-2}·day^{-1}), describes the ability of vegetation to use light in combination with atmospheric carbon dioxide (CO_2) for photosynthesis. LUE is generally constant during vegetation growth when water supply is non-limiting. Further, the amount of carbon used for gross photosynthesis tends to remain constant across vegetation species (Dewar et al. 1998). These observations enable aggregation of LUE and vegetation productivity (e.g. NPP and GPP) from local to global scales using remote sensing-based land-cover types or ecosystem models (Turner et al. 2002; Drolet et al. 2005).

A.1.8 Leaf Area Index (LAI), Effective LAI (LAIe), Plant Area Index (PAI), and fractional cover

LAI is defined as one half of the total leaf area per unit ground area (Chen and Black 1992; Chen et al. 2006) (m^2·m^{-2}) and is a key parameter for estimating CO_2, water, and energy exchanges between the terrestrial biosphere and the atmosphere. Other definitions pertaining to leaf area include the projected LAI, which is the leaf area projected onto a horizontal plane; and the total LAI, including both sides of the leaf (or the spherical surface of pine needles). LAIe and PAI appear to be used synonymously within the literature and include both the leaf and wood area (Leblanc et al. 2005; Chen et al. 2006). The specific leaf area (SLA) is the ratio of green foliage surface area to dry foliage mass (Gower et al. 1999). Leaf area indices are often estimated based on the probability that a beam of light will penetrate through the canopy. In the case where all light is incident on the ground surface, and no canopy is visible, the canopy gap fraction may be assumed to be one (1) (fractional cover = zero). On the other hand, the canopy gap fraction will have a maximum value of zero (0) for a completely closed canopy where all light is intercepted by the canopy (fractional cover = 1).

A.2 Remote Sensing Terms

A.2.1 Remote Sensing

Remote sensing is defined as the ability to obtain "…information about an object, area, or phenomenon through the analysis of data acquired by a device that is not in contact with the object, area, or phenomenon under investigation" (Lillesand and Kiefer, 1994). Remote sensing uses reflected or emitted radiation to collect information related to the surface properties of the object. Reflected or emitted radiation may be passively or actively observed, where variations in electromagnetic energy that are either reflected or emitted by features are recorded by a sensor (e.g., camera). On the other hand, active remote sensing involves the emission of electromagnetic energy towards the object of interest, and then recording a portion of the signal that is reflected back towards the sensor. Active remote sensing systems include sonar (sound navigation and ranging), radar (radio detection and ranging) and lidar (light detection and ranging).

A.2.2 The Moderate Resolution Imaging Spectroradiometer (MODIS)

MODIS is a passive remote sensing instrument that was launched by NASA in 1999 on the Terra satellite and again in 2002 on the Aqua satellite. MODIS is able to retrieve reflectance information in 36 narrow electromagnetic bands and at various resolutions ranging from 250 m to 500 m or 1000 m. The sensors are able to record spectral information over the entire earth surface every one to two days. The sensors are primarily used to understand variability in cloud cover, terrestrial ecosystem processes, radiation, land surface meteorology, and ocean processes (e.g. http://www.daac.ornl.gov/MODIS/modis.html; Running et al. 2004).

A.2.3 Airborne Lidar / Airborne Laser Scanning (ALS)

Lidar is a maturing remote sensing and surveying technology that illuminates actively the ground surface and any objects above the ground through the rapid emission and reception of laser pulses

across an angular field of view (AFOV) (e.g. Wehr and Lohr, 1999). Lidar systems typically record three-dimensional data (i.e., x,y,z) for the location where the laser pulse reflects from the intercepted surface. Lidar systems also collect multiple laser pulse reflections, or 'returns' per laser pulse emitted. This results in a highly accurate and high resolution (e.g. < 1 m) three-dimensional sampling of the vegetation canopy, understory, and ground surface characteristics.

A.2.4 Pixels and Laser Returns

Digital images of the land surface collected using remote sensing methods are comprised of two-dimensional arrays of pixels or discrete picture elements, making the image appear to be continuous and of varying amounts of brightness. Each pixel has an associated average radiance that is measured using the remote sensing device, corresponding to the area represented by the pixel. Most remote sensing datasets have a specified set of pixel rows and columns making up the image. In low resolution datasets, such as MODIS and AVHRR products, pixels cover much larger areas and therefore provide an average radiance of one or many different land cover types, which are not fully representative of one land cover, thereby increasing the inaccuracy of radiance measurements within pixels. Higher resolution datasets, such as Landsat and IKONOS collect average radiance information within pixels that are much smaller (e.g. 25 m to 1 m resolutions or less), and can therefore resolve ambiguities found in lower resolution products.

Active lidar remote sensing systems do not measure average radiance information within pixels, but instead, have discrete elliptical laser pulse "footprints" or "returns" that are formed via a Gaussian envelope of reflected radiation that is returned to the sensor optics. In other words, the laser pulse footprint is the point of contact of the pulse of laser light of the feature, where laser light is scattered from the object and is recorded by the sensor optics. The location of a laser return is determined as a range measurement, or the time from which the laser pulse is emitted to

the time when it (the back-scatter) is received. Laser returns therefore describe the three-dimensional surface and some information on the radiometric characteristics of the object (e.g. dry or wet, shiny or dull, white or black). They are also different from pixels because they are not evenly spaced in x and y directions, and therefore do not form a perfect grid of discrete returns. For example, as the aircraft speed changes, laser pulses will be placed either closer together (as the aircraft slows down) or further apart (as the aircraft speeds up).